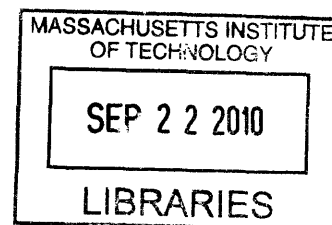


Design, Synthesis, and Characterization of Conjugated Polymers and Functional Paramagnetic Materials for Dynamic Nuclear Polarization

by
Eric Lawrence Dane

B.A. (High Honors) Chemistry
Michigan State University, 2001



ARCHIVES

SUBMITTED TO THE DEPARTMENT OF CHEMISTRY IN
PARTIAL FULFILLMENT OF THE REQUIREMENTS FOR THE DEGREE OF

DOCTOR OF PHILOSOPHY IN CHEMISTRY
AT
THE MASSACHUSETTS INSTITUTE OF TECHNOLOGY
SEPTEMBER 2010

© Massachusetts Institute of Technology, 2010. All Rights Reserved.

Signature of Author: _____

Department of Chemistry
June 22, 2010

Certified by: _____

Timothy M. Swager
Professor of Chemistry
Thesis Supervisor

Accepted by: _____

Robert W. Field
Professor of Chemistry
Chairman, Departmental Committee on Graduate Studies

This doctoral thesis has been examined by a Committee of the Department of Chemistry as follows:

Professor Rick L. Danheiser

Thesis Committee Chair

Professor Timothy M. Swager:

Thesis Supervisor

Professor Robert G. Griffin:

Department of Chemistry

**Design, Synthesis, and Characterization of Conjugated Polymers and
Functional Paramagnetic Materials for
Dynamic Nuclear Polarization**

by

Eric Lawrence Dane

SUBMITTED TO THE DEPARTMENT OF CHEMISTRY ON JUNE 22, 2010 IN PARTIAL FULFILLMENT OF
THE REQUIREMENTS FOR THE DEGREE OF DOCTOR OF PHILOSOPHY IN CHEMISTRY.

ABSTRACT

The design, synthesis, and characterization of a series of radicals and biradicals for use as dynamic nuclear polarization (DNP) agents is described. DNP is a method to enhance the S/N-ratio in solid-state nuclear magnetic resonance (SS-NMR) that involves transferring the polarization of electrons, which are more easily polarized due to their larger magnetic moment, to nuclei.

Two strategies to improve the performance of DNP-agents have been explored. The first involves combining a carbon-centered radical (1,3-bisdiphenylene-2-phenylallyl (BDPA) radical), which has a narrow line width at high field, with a nitroxide radical (2,2,6,6-tetramethylpiperidine-1-oxyl (TEMPO) radical), which has a broader line width at high field. The synthesis and characterization of a BDPA-TEMPO biradical is described and is a first step in testing whether polarization agents of this type will out perform the currently used biradicals. Additionally, the synthesis of a water-soluble derivative of BDPA is described. The second strategy involves designing dinitroxide biradicals that rigidly hold the radicals in an orthogonal geometry. The synthesis of dinitroxide radicals of this type is described, along with efforts to optimize aqueous solubility.

The design, synthesis, and characterization of thioether-containing poly(*paraphenylene-ethynylene*) (PPE) copolymers are reported. The polymers show a fluorescence turn-on response when exposed to oxidants in solution, and the oxidized polymers show desirable thin-film properties, such as high quantum yields and increased photostability. Work towards the synthesis of electroactive conjugated polymers based on the BDPA free radical is also reported.

Thesis Supervisor: Timothy M. Swager

Title: John D. MacArthur Professor and Head of Chemistry Department

CONTENTS

Title Page	1
Signature Page	3
Abstract	5
CHAPTER 1 - INTRODUCTION TO DYNAMIC NUCLEAR POLARIZATION WITH BIRADICALS	11
1.1 Introduction to Dynamic Nuclear Polarization (DNP)	12
1.2 Biradical Polarizing Agents for DNP	14
1.3 Strategies to Synthesize Improved Biradicals for DNP	15
1.4 References	19
CHAPTER 2 - SYNTHESIS OF A BDPA-TEMPO BIRADICAL	21
2.1 Introduction	22
2.2 Synthesis of a BDPA-TEMPO Biradical	23
2.3 EPR Characterization of Biradical	29
2.4 Conclusions	30
2.5 Experimental Section	31
2.6 References	36
2.7 NMR and EPR Spectra	38
CHAPTER 3 - SYNTHESIS OF A WATER-SOLUBLE BDPA RADICAL	57
3.1 Introduction	58
3.2 Synthesis	58
3.3 EPR studies	61
3.4 Experimental Section	63
3.5 References	66
3.6 NMR and EPR Spectra	68
CHAPTER 4 - RIGID ORTHOGONAL DINITROXIDE BIRADICALS WITH IMPROVED SOLUBILITY FOR DNP	81
4.1 Introduction	82
4.2 Synthesis	83
4.3 DNP results	89
4.4 Conclusions	89
4.6 References	92
4.7 Additional Figures	94
4.8 NMR spectra	99
CHAPTER 5 - CONJUGATED POLYMERS THAT RESPOND TO OXIDATION WITH INCREASED EMISSION	105
5.1 Introduction	106
5.2 Synthesis	109
5.3 Oxidation of Model Compounds	111
5.4 Optical and Photophysical Properties of the Model Compounds in Solution.	112
5.5 Oxidation of Polymers	115
5.6 Optical and Photophysical Properties of the Polymers in Solution.	118

5.8 Thin-film photophysics of polymers	121
5.9 Thin-film photobleaching studies	122
5.10 Understanding the Photophysical Behavior of the Model Compounds	123
5.11 Understanding the Photophysical Behavior of the Polymers	126
5.12 Understanding the behavior of the polymers in thin films	126
5.13 Blue-shifted versus red-shifted fluorescence turn-on response to H ₂ O ₂	127
5.14 Conclusions	127
5.15 Experimental Section	128
5.16 References	137
5.17 Additional Figures	141
5.18 NMR Spectra	150
CHAPTER 6 - WORK TOWARDS THE SYNTHESIS AND CHARACTERIZATION OF ELECTROACTIVE CONJUGATED POLYMERS BASED ON THE BDPA FREE RADICAL	165
6.1 Introduction	166
6.2 Synthesis	168
6.3 Electrochemistry	176
6.4 Conclusion	176
6.5 Experimental Section	178
6.6 References	190
6.7 NMR Spectra	192
CURRICULUM VITAE	225
ACKNOWLEDGEMENTS	227

CHAPTER 1

Introduction to Dynamic Nuclear Polarization (DNP) with Biradicals

1.1 Introduction to Dynamic Nuclear Polarization (DNP)

Nuclear magnetic resonance (NMR) is a powerful analytical technique for structural biology, and the closely related field of magnetic resonance imaging (MRI) has broad applicability in medical diagnostics ranging from sports injuries to cancer.¹ The capabilities of NMR are presently limited largely by sensitivity and contrast.² Improved methods that enhance the sensitivity of NMR as applied to biological and medical problems are therefore needed. A promising approach to greatly improve sensitivity is to incorporate dynamic nuclear polarization (DNP) into the NMR experiment.^{3,4,5,6}

DNP is a method used to increase the signal-to-noise ratio in NMR spectra by transferring the polarization of electrons to nuclei. In a contemporary DNP experiment, a diamagnetic sample, containing a small molecule or a polypeptide of interest, is doped with a paramagnetic polarization agent, which is often a stable organic radical. Microwave irradiation of the radical's electron paramagnetic resonance (EPR) spectrum transfers the large polarization of the electron spins to the nuclei.⁷ In this way, nuclear spin polarizations

can be theoretically enhanced by values approaching the ratio of the gyromagnetic ratios (γ) of the electron and nucleus, $(\gamma_e/\gamma_n) \sim 660$. DNP signal enhancements ranging from 50- to 400-fold are routinely observed depending on the details of the experiments (temperature, magnetic field, etc.).⁸ The largest signal enhancements are achieved in experiments where thermal mixing (TM) or cross

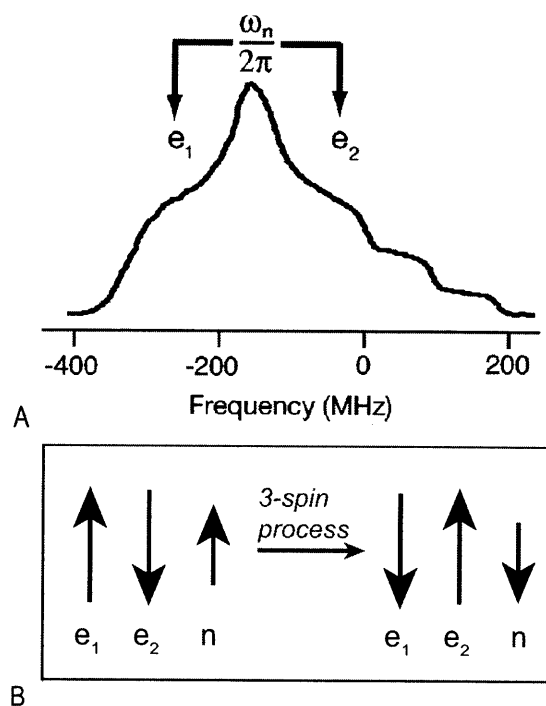


Figure 1. (a) EPR spectrum of a dinitroxide biradical in a solvent glass at 20 K. The spectrum is 600 MHz wide and is large compared to the ^1H -Larmor frequency (211 MHz) at the same magnetic field strength (as indicated by the arrows between e_1 and e_2). (b) Illustration of the microwave driven 3-spin process associated with TM or CE DNP, where a spin-flip involving two electrons causes a proton to become polarized. Adapted from reference 3.

effect (CE) mechanisms⁹ are operative. A detailed theoretical description of these polarization transfer mechanisms is available in the literature and will not be discussed.¹⁰ However, some general conceptual descriptions will be described to highlight the issues critical to the design of superior DNP agents.

The TM and CE mechanisms rely on a three spin process (Figure 1) that involves the coupling of two electrons ($S1$ and $S2$). For the process to occur, the Larmor frequencies of the electrons (ω_{oS1} and ω_{oS2} in the EPR spectrum of the polarizing agent) must be separated by a frequency difference that matches the nuclear Larmor frequency of a proton (I), ω_{oI} . When these electrons are sufficiently close in space to be dipolar coupled, irradiation at ω_{oS1} followed by a spin-flip with a radical at ω_{oS2} generates nuclear spin polarization, because the energy involved in this process matches the amount of energy required to polarize a proton.

DNP can be performed in samples containing a monomeric radical, such as 2,2,6,6-tetramethylpiperidine-1-oxyl (TEMPO) free radical. However, the efficiency of DNP depends strongly on the e^-e^- dipolar coupling between two radical centers giving rise to a spectral density that meets the frequency matching condition, $\omega_{oS1} - \omega_{oS2} = \omega_{oI}$. To satisfy this constraint, the concentration of monomeric radicals has to be sufficiently high to compensate for the $1/r^3$ distance dependence of the dipolar coupling, where r is the distance between the electron dipoles. High concentrations of TEMPO are undesirable for biomolecular structure determination, because the paramagnetic additive broadens the NMR signals and thereby attenuates the signal enhancement and decreases the resolution in the spectrum. To optimize the e^-e^- dipolar coupling between radicals for DNP, biradicals have been developed that constrain the distance between the two unpaired electrons.^{3,4,5} Studies using these biradicals have revealed that a careful balance of the distance and relative orientation of the radicals provides an approximate four-fold larger DNP enhancement (up to ~300-fold) at a four-fold lower electron concentration (~10 mM electrons). Thus, biradicals minimize the paramagnetic broadening of the NMR signals.

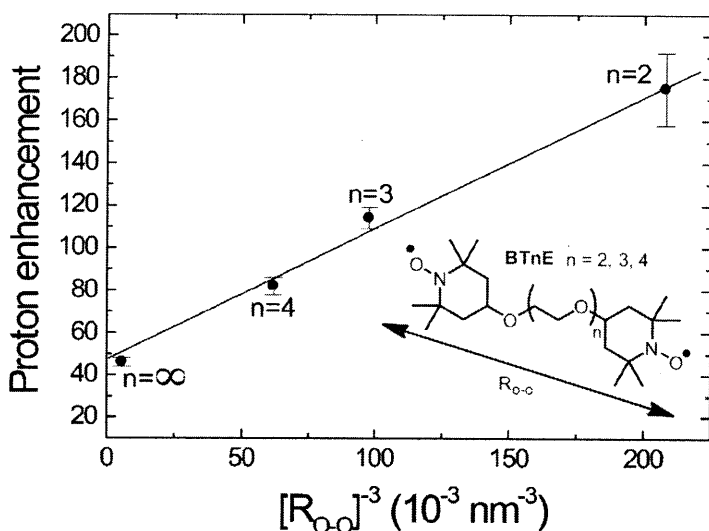


Figure 2.

The ^1H enhancement measured indirectly through the ^{13}C signal as a function of the approximate electron-to-electron dipolar coupling as measured by the distance, specifically $[R_{o-o}]^{-3}$. The data points show the DNP enhancements obtained from molecules corresponding to monomeric TEMPO ($n = \infty$) and BTnE ($n = 2-4$). Adapted from reference 3.

1.2 Biradical Polarizing Agents for DNP

The use of biradicals in DNP was pioneered at MIT through a collaboration between the research groups of Professor Robert G. Griffin and Professor Timothy M. Swager. Initial studies investigated a series of *bis*-TEMPO *n*-ethyleneglycol (BTnE) biradical polarizing agents (Figure 2, red). These biradicals were prepared from 4-hydroxy-TEMPO and di-, tri-, or tetra-ethyleneglycol-di-tosylate,¹¹ with a distance between the terminal radicals of R_{o-o} . Solution EPR spectra of BTnE ($n = 2, 3, \text{ or } 4$) (1 mM in ethanol) showed the expected 5 lines, indicating a strong exchange interaction (larger than the ^{14}N hyperfine interaction) between the electrons.¹² Samples for the DNP experiments consisted of 5 mM biradical and 2 M ^{13}C -urea dispersed in a 60:40 d_6 -DMSO/ H_2O (90% $^2\text{H}_2\text{O}$) glass-forming mixture. A control sample of 10 mM 4-hydroxy-TEMPO was also examined. The samples were contained in 4 mm sapphire rotors and a series of solid state (DNP/CPMAS) ^{13}C NMR spectra were recorded as a function of the microwave irradiation time using a 140 GHz gyrotron source and a low-temperature MAS probe operating at 90 K at $\beta_r/2\beta = 3.5$ kHz.¹³

Figure 3 illustrates a typical build up curve obtained with a sample of BT2E. Note that in the absence of microwave irradiation the ^{13}C signal from urea is not visible on the vertical scale used. However, with 3-15 seconds of microwave irradiation, the signal grows dramatically, reaching a plateau after ~15 seconds where an enhancement of ~175-fold was measured. The depen-

dence of the ^1H enhancement on the length of the ethylene glycol linker is shown in Figure 2. As the linker is shortened from $n = 4$ to $n = 2$, the enhancement increases from 80 to 175. For comparison, the monomeric TEMPO gave an enhancement of 45 in this solvent system. Thus, tethering the two TEMPO radicals increases enhancements by a factor of 3.9.

Based on this work, a biradical with a shorter R_{o-o} was pursued in order to increase the dipolar coupling between the unpaired electrons.

Additionally, the biradical was designed to be soluble in aqueous cosolvents. These constraints led to the synthesis of the improved biradical 1-(TEMPO-4-oxy)-3-(TEMPO-4-amino)-propan-2-ol (TOTAPOL) (see Figure 4 for structure).⁴ TOTAPOL has a spacing equivalent to 1.5 ethylene oxide groups when compared to BTnE-series. The vicinal hydroxyl and secondary amine provide improved water solubility as compared to the BTnE-series.

The DNP from TOTAPOL exceeded what would be expected from a direct extrapolation of the plot in Figure 2. Figure 4 shows the ^{13}C signal enhancement (~ 240 -fold) in a solid state NMR experiment using TOTAPOL (blue). Griffin and co-workers have used TOTAPOL to conduct 2-D solid-state NMR experiments on amyloid peptide nanocrystals. These experiments demonstrate the efficient transfer of DNP-enhanced ^1H polarization from an aqueous, radical-containing solvent matrix into peptide crystals via ^1H - ^1H spin diffusion across the matrix-crystal interface.^{14a} Investigating the structure of amyloid peptides is important to better understanding the role of such structures in a wide range of diseases.^{14b}

1.3 Strategies to Synthesize Improved Biradicals for DNP

I have explored two strategies to improve the performance of DNP-agents during my graduate work, which I will discuss in Chapters 2-4. The first strategy involves combining a carbon-

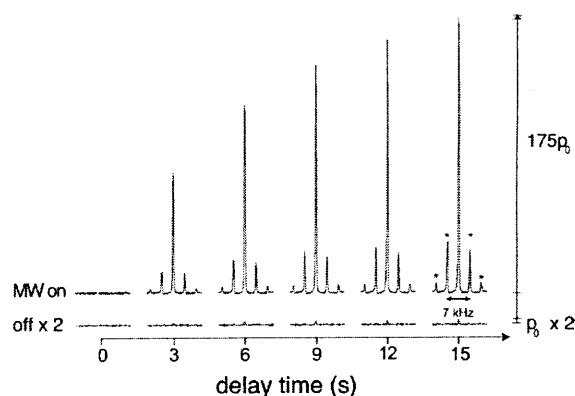


Figure 3. ^{13}C DNP-MAS spectra illustrating the growth of the ^{13}C -urea signal as the irradiation time is increased. The polarizing agent was BT2E and the observed enhancement was 175. Adapted from reference 3.

centered radical (1,3-bisdiphenylene-2-phenylallyl (BDPA) radical), which has a narrow line width at high fields, with a nitroxide radical (2,2,6,6-tetramethylpiperidine-1-oxyl (TEMPO) radical), which has a broader line width at high fields. This idea was first proposed by Griffin based on experiments using a water-soluble trityl derivative and 4-amino-TEMPO.¹⁵ Figure 5 displays the integrated EPR signal (top) and the ¹H-enhancement profile (bottom) for three polarization conditions. In each situation, the EPR spectrum was acquired from a sample with a radical concentration of 1 mM at 20 K in *d*₆-DMSO/D₂O and the ¹H-enhancement profile was acquired from a sample with a total radical concentration of 40 mM at 90 K in *d*₆-DMSO/D₂O/H₂O.

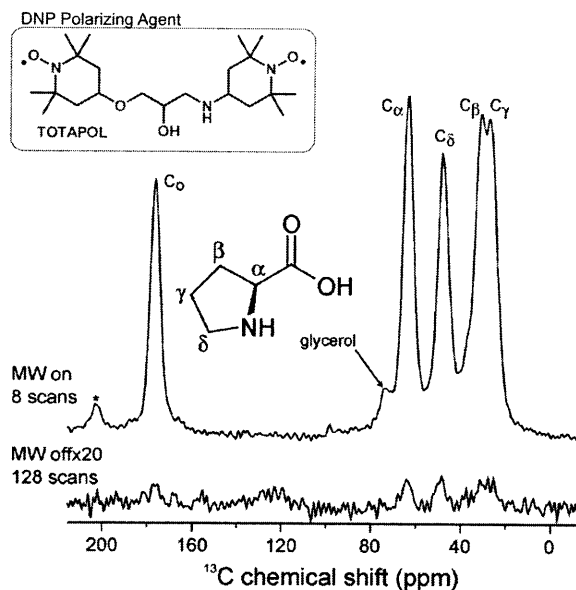


Figure 4. ¹³C-NMR spectrum of a 0.2 M proline solution containing 5 mM TOTAPOL (blue) with (top) and without (bottom) DNP enhancement. The sample was prepared in *d*₈-glycerol/D₂O/H₂O (60:25:15 w/w/w) and recorded with 7.4 kHz MAS (2.5 mm rotor) at 90 K and 5T. The asterisk indicates a rotational sideband. Adapted from reference 4.

In Figure 5a, where only trityl radical is used as the polarizing agent, minimal enhancements are observed via the solid-effect. In Figure 5b, where only TEMPO is used, a larger enhancement of 45-fold is observed via the thermal-mixing mechanism. In Figure 5c, where a 1:1 mixture of trityl and TEMPO is employed, a significantly greater enhancement of 160 is observed via the cross-effect mechanism. The improved polarization observed in (c) is a consequence of the difference between the maxima of the g_{yy} component of the TEMPO spectrum and trityl's EPR absorption maxima being 224 MHz, which is close to the ¹H resonance of 211 MHz. The fact that the separation between the two peaks is near the matching condition described earlier (compare Figure 1a and Figure 5b) allows for more efficient microwave excitation because the microwaves can be centered on the narrow trityl peak. In order to fully realize the benefits of this strategy, the two dif-

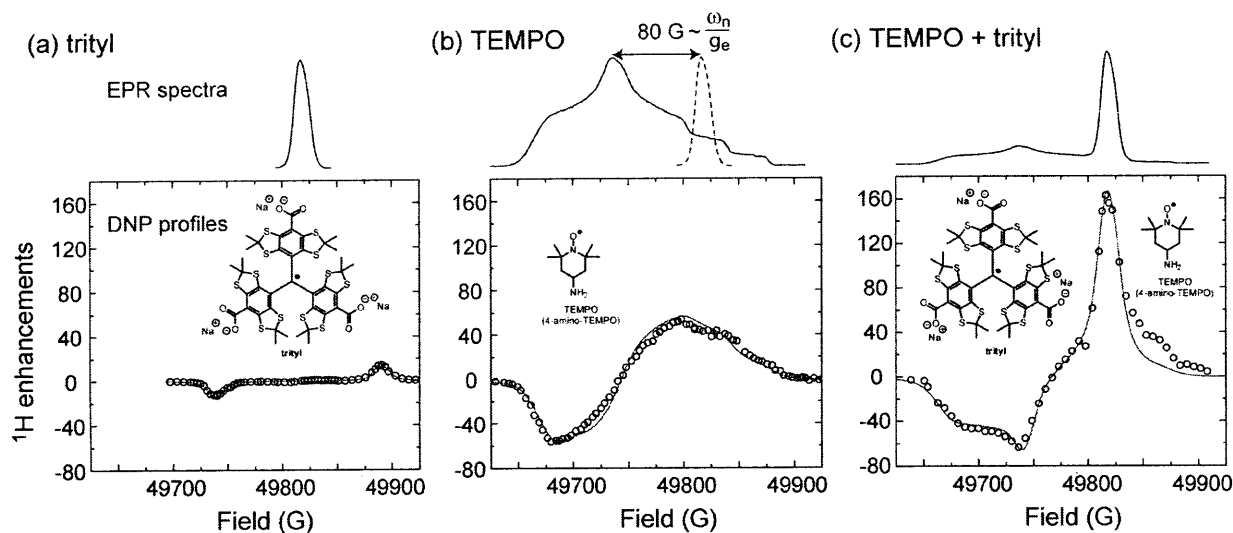


Figure 5.

Solid state EPR spectra and DNP enhancement profiles of trityl (a), TEMPO (b), and a 1:1 trityl/TEMPO mixture (c). Note that the separation of the trityl maxima and the g_{yy} component of the TEMPO spectrum satisfies the matching condition $\omega_{0s1} - \omega_{0s2} = \omega_{0l}$. Adapted from reference 15.

ferent radicals must be incorporated into a biradical, therefore making the process more efficient and allowing for the overall radical concentration to be significantly lowered. Progress towards this goal is described in Chapters 2 and 3.

The second strategy involves designing di-nitroxide biradicals that rigidly hold the radicals in an orthogonal geometry. The EPR spectrum of TEMPO (and derivatives thereof) is broadened by g -anisotropy, which means that the g -value of the radical changes depending on its orientation relative to the magnetic field. Figure 6 illustrates how the observed EPR signal is the sum of the signals from all the possible orientations (i.e. g_{xx} , g_{yy} , g_{zz}) and corresponding resonance energies of TEMPO. Note that g_{zz} is a triplet, g_{yy} is a doublet, and g_{xx} has unresolved hyperfine couplings. If it were possible to make a glass of TEMPO where all of the radicals were aligned relative the magnetic field as is shown for g_{xx} , then the signal would be dominated by the area highlighted in blue, with the same being true for g_{yy} and g_{zz} .

Controlling the relative orientation of TEMPO radicals has the potential to provide better energy matching to the nuclear Larmor frequency of neighboring protons. A biradical in which

both TEMPO radicals are held in the same orientation with respect to the magnetic field would not be an effective polarization agent because it would not allow for the energy separation required for polarization. In Figure 6c, three possible biradical orientations are displayed. A biradical possessing geometry **i** would not be optimal because the energy separation is too small, and the energy separation in orientation **ii** would be too large. The biradical that best matches the requirements for polarization has orientation **iii**.

A biradical having geometry **iii** has been previously synthesized and has shown enhanced DNP as compared to TOTAPOL.¹⁶ Unfortunately this compound is not very soluble in aqueous solutions and thus has decreased utility for DNP-NMR. As I will discuss in Chapter 4, I synthesized dinitroxide biradicals with a similar geometry and studied how to optimize their solubility for DNP applications.

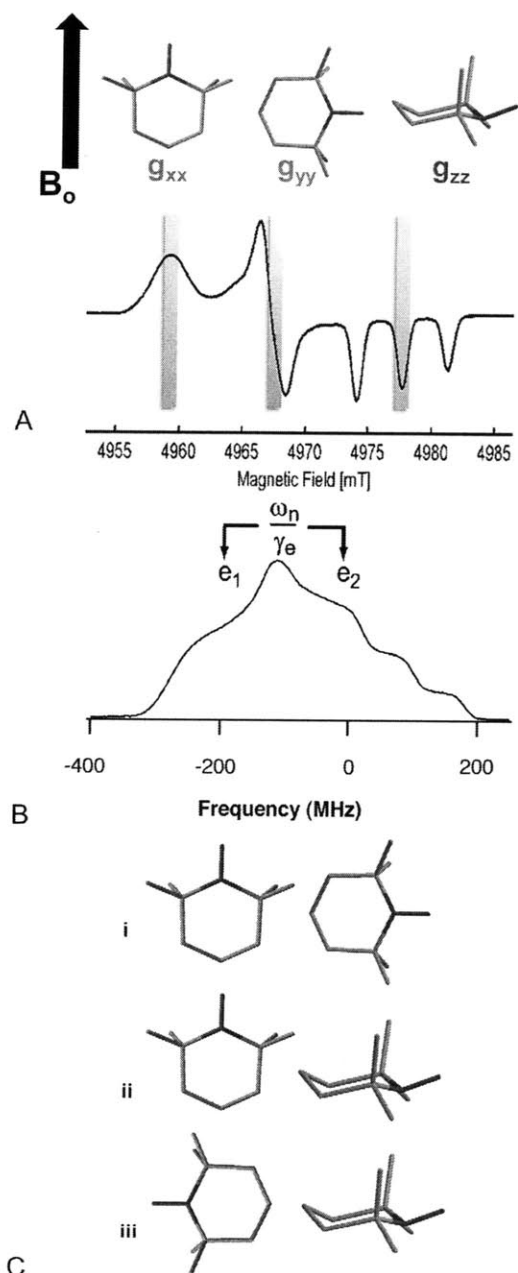


Figure 6. (a) Typical 140 GHz EPR spectrum of TEMPO. The structures above the spectrum represent the orientations of TEMPO associated with each of the g -tensors, which are highlighted below in the parts of the spectrum where each dominates. (b) The integrated form of the TEMPO spectrum is shown with the DNP matching condition. (c) Three possible biradical orientations for rigid dinitroxide DNP polarization agents.

1.4 References

- (1) Weishaupt, D.; Kockli, V. D.; Marincek, B. "How Does MRI Work?" 2nd Ed. Springer, Heidelberg, 2006.
- (2) Haacke, E. M.; Brown, R. W., Thompson, M. R.; Venkateson, R. *Magnetic Resonance Imaging – Physical Principles and Sequence Design*; Wiley-Liss, New York, **1999**, 331-380.
- (3) Hu, K.-N.; Yu, H.-h. Swager, T. M.; Griffin, R. G. *J. Am. Chem. Soc.* **2004**, 126, 10844-10845.
- (4) Song, C.; Hu, K-N.; Swager, T. M.; Griffin, R. G. *J. Am. Chem. Soc.* **2006**, 128, 11385-11390.
- (5) Hu, K-N.; Song, C.; Yu, H.-h.; Swager, T. M.; Griffin, R. G. *J. Chem. Phys.* **2008**, 128, article # 052302.
- (6) Joo, C-G.; Hu, K-N.; Bryant, J. A.; Griffin, R. G. *J. Am. Chem. Soc.* **2006**, 128, 9428-9432.
- (7) Wind, R. A.; Duijvestijn, M. J.; van der Luat, C.; Manenschijn, A.; Vriend, J. *Prog. Nucl. Magn. Reson. Spectrosc.* **1985**, 17, 33.
- (8) (a) Becerra, L. R.; Gerfen, G. J.; Temkin, R. J.; Singel, D. J.; Griffin, R. G. *Phys. Rev. Lett.* **1993**, 71, 3561-3564. (b) Gerfen, G. J.; Becerra, L. R.; Hall, D. A.; Griffin, R. G.; Temkin, R. J.; Singel, D. J. *Journal of Chemical Physics* **1995**, 102, 9494-9497. (c) Weis, V.; Bennati, M.; Rosay, M.; Bryant, J. A.; Griffin, R. G. *J. of Mag. Res.* **1999**, 140, 293-299. (d) Rosay, M.; Zeri, A. C.; Astrof, N. S.; Opella, S. J.; Herzfeld, J.; Griffin, R. G. *J. Am. Chem. Soc.* **2001**, 123, 1010-1011. (e) Rosay, M.; Weis, V.; Kreisler, K. E.; Temkin, R. J.; Griffin, R. G. *J. Am. Chem. Soc.* **2002**, 124, 3214-3215. (f) Bajaj, V. S.; Farrar, C. T.; Hornstein, M. K.; Mastovsky, I.; Viereg, J.; Bryant, J.; Elena, B.; Kreisler, K. E.; Temkin, R. J.; Griffin, R. G. *J. Mag. Res.* **2003**, 160, 85-90.
- (9) (a) Hwang, C. F.; Hill, D. A. *Phys. Rev. Letters* **1967**, 18, 110-112. (b) Hwang, C. F.; Hill, D. A. *Phys. Rev. Letters* **1967**, 19, 1011-1013. (c) Wollan, D. S. *Phys. Rev. B* **1976**, 13, 3671-3685. (d) Wollan, D. S. *Phys. Rev. B* **1976**, 13, 3686-3696.
- (10)(a) Atsarkin, V. A. *Soviet Physics Solid State* **1978**, 21, 725-744. (b) Farrar, C. T., D. A. Hall, G. J. Gerfen, S. J. Inati and R. G. Griffin *J. of Chem. Phys.* **2001**, 114(11), 4922-4933.
- (11) Gagnaire, G.; Jeunet, A.; Pierre, J. L. *Tetrahedron Lett.* **1991**, 32, 2021-2024.

- (12) Luckhurst, G. in "Spin Labeling: Theory and Applications" Berliner, L. J., Ed.; Academic Press: New York, 1976, pp 133-181.
- (13) Rosay, M.; Lansing, J. C.; Haddad, K. C.; Bachovchin, W. W.; Herzfeld, J.; Temkin, R. J.; Griffin, R. G. *J. Am. Chem. Soc.* **2003**, 125, 13626-13627.
- (14) (a) van der Wel, P. C. A.; Lewandowski, J. R.; Griffin, R. G. *J. Amer. Chem. Soc.* **2007** 129 (16), 5117-5130. (b) Dobson, C. M. *Trends in Biochemical Sciences* **1999**, 24, 329-332.
- (15) Hu, K.-N., V. S. Bajaj, M. M. Rosay and R. G. Griffin *J. Chem. Phys.* **2007**, 126, 044512.
- (16) Matsuki, Y.; Maly, T.; Ouari, O.; Karoui, H.; Le Moigne, F.; Rizzato, E.; Lyubenova, S.; Herzfeld, J.; Prisner, T.; Tordo, P.; Griffin, R. G. *Angew. Chem., Int. Ed.* **2009**, 121, 5096.

CHAPTER 2

Synthesis of a BDPA-TEMPO Biradical

Adapted from:

Dane, E. L.; Maly, T.; Debelouchina, G. T.; Griffin, R. G.; Swager, T. M. "Synthesis of a BDPA-TEMPO Biradical" *Org. Lett.* **2009**, *11* (9), 1871–1874.

2.1 Introduction

Biradicals are of considerable interest as polarizing agents for microwave driven dynamic nuclear polarization (DNP) NMR experiments.^{1,2} Irradiation of the biradical's electron paramagnetic resonance (EPR) drives electron-nuclear transitions that transfer the large polarization of the electrons to the nuclear spins and thereby enhances the signal-to-noise ratio in NMR experiments. The enhancement factors can reach a theoretical maximum of ~660 for electron-¹H polarization transfer and ~2600 when ¹³C is the nuclear spin of interest.³ Thus, optimized biradical polarizing agents can dramatically decrease acquisition times. These signal enhancements are important for a variety of applications involving solid-state NMR, particularly for systems that are not amenable to crystallographic studies, such as amyloid⁴ and membrane⁵ proteins.

In previous work, it was demonstrated that bis-nitroxide biradicals, which contain two tethered 2,2,6,6-tetramethylpiperidine-1-oxyl (TEMPO) free radicals, provide ¹H/¹³C-signal enhancements of ~200 fold in solid-state magic-angle-spinning (MAS) NMR spectra.² These biradicals produce DNP by a cross effect (CE) mechanism³ that involves three spins, two dipolar coupled electrons and a nuclear spin (usually ¹H), denoted by S_1 and S_2 and I , with electron and nuclear Larmor frequencies, ω_{oS1} , ω_{oS2} , and ω_{oI} , respectively. During DNP, microwave irradiation of the biradical's EPR spectrum induces the two electrons to undergo a spin flip-flop process, during which a nuclear spin is polarized if the electron Larmor frequencies are separated by the nuclear Larmor frequency and therefore satisfy the matching condition, $\omega_{oS1} - \omega_{oS2} = \omega_{oI}$. The resulting increase in ¹H polarization is then transferred via cross-polarization to ¹³C or ¹⁵N, resulting in an enhanced MAS NMR spectrum.⁶

The efficiency of the CE mechanism depends on how many pairs of electrons satisfy the matching condition. Thus, the ideal CE polarizing agent would be a biradical with an EPR spectrum consisting of two sharp lines separated by ω_{oI} . However, at the high magnetic fields (> 5T) where contemporary NMR experiments are performed, only a few known radicals exhibit narrow spectra. Among them are two stable species – trityl radical derivatives⁷ and the BDPA radical⁸

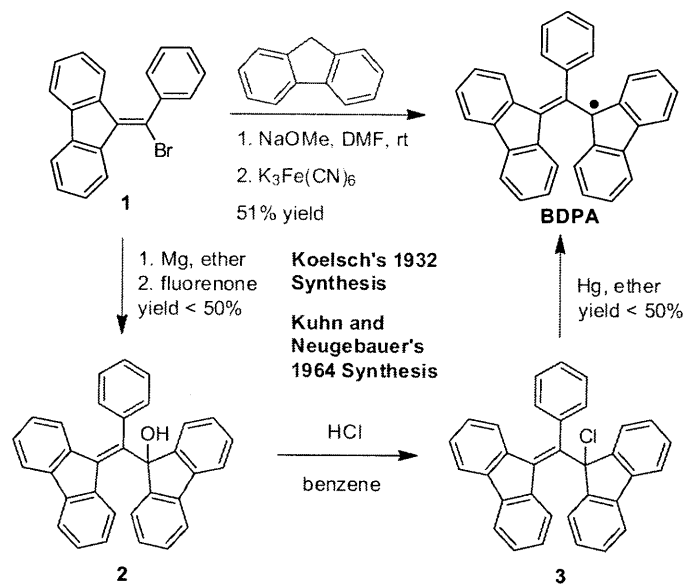
(Scheme 1), which have similar isotropic g-values ($g_{\text{iso}}(\text{trityl})= 2.00307$,¹ $g_{\text{iso}}(\text{BDPA})= 2.00264$). If trityl or BDPA serves as one of the lines in the EPR spectrum of a polarizing agent, then to satisfy the CE matching condition it is necessary to introduce another radical with a line separated from the first by ω_{or} . There are no known stable radicals that provide a narrow line and meet this condition, however TEMPO derivatives have a broad line with significant spectral density at a frequency separation matching ω_{or} .

Griffin and co-workers have shown that the enhancements observed with a trityl-TEMPO mixture are a factor of ~ 4 larger than those obtained with TEMPO alone (see Chapter 1, Figure 5).¹ The success of this experiment provides the rationale for the synthesis of a biradical that covalently combines a narrow- and broad-line radical, therefore increasing the dipolar coupling. BDPA was chosen as the narrow-line species, because it has greater stability and a narrower line width than trityl at high magnetic fields. Currently, DNP is performed in aqueous solutions that form a rigid glass at $T < 90\text{K}$. Due to the challenges of making the nonpolar BDPA and TEMPO radicals water-soluble, I chose to first synthesize a hydrophobic BDPA-TEMPO biradical as a model compound. As described in this chapter, I have developed synthetic methods to join the two sensitive functionalities and studied the biradical's EPR properties.

2.2 Synthesis of a BDPA-TEMPO biradical

In attempting to synthesize a BDPA-TEMPO biradical, work began by investigating how BDPA was previously made. Koelsch's original method⁹ (Scheme 1, blue) involves the formation of alcohol **2**, the displacement of the hydroxyl-group with a chloride to form **3**, and the removal of a chlorine radical with mercury. The method developed by Kuhn and Neugebauer¹⁰ (Scheme 1, red) involves a conjugate addition of the fluorene anion to **1**, followed by a one-electron oxidation of the stable carbanion intermediate. The latter method was pursued to synthesize a functionalized BDPA derivative because it requires fewer steps and provides higher yields.

Efforts to synthesize BDPA derivatives have been limited.¹¹ Kuhn¹⁰ reported halogenated

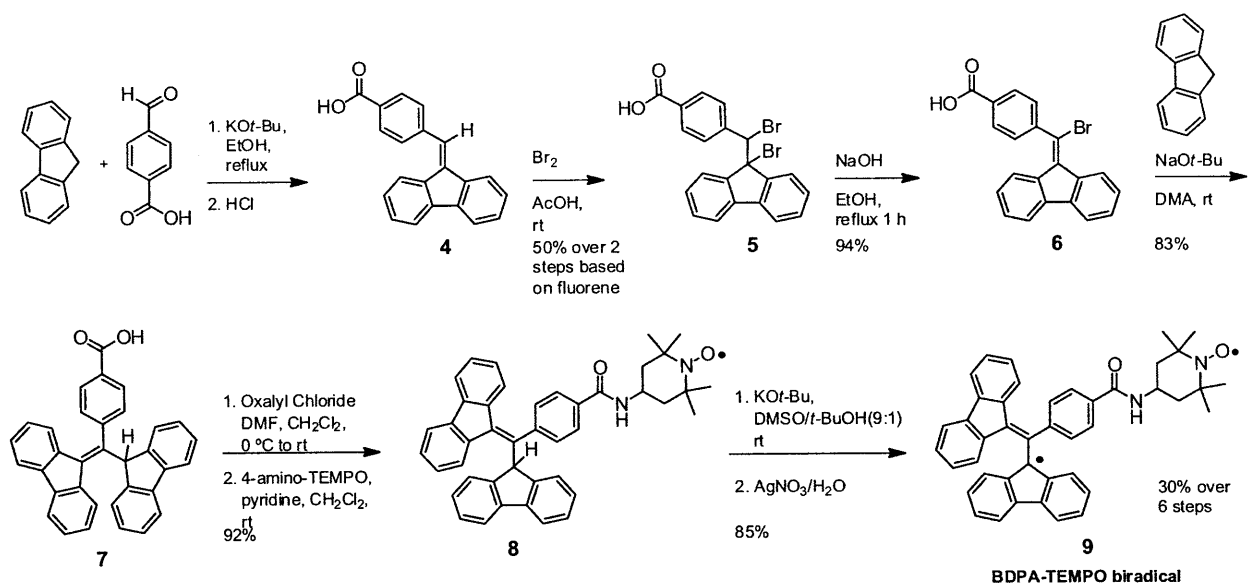


Scheme 1. Previous Syntheses

BDPA derivatives, and Fox¹² reported the synthesis of BDPA derivatives with methoxy-, cyano-, and nitro-groups at the 4-position of the phenyl ring. Previously synthesized biradicals containing BDPA have been limited to molecules containing two BDPA radicals linked through the phenyl ring.¹⁰

The reactivity of the BDPA radical complicates its incorporation in biradicals. Although the radical is remarkably stable to oxygen in the solid state,⁹ and has been reported to be indefinitely stable to oxygen in solution with the exclusion of light, its photoreactivity produces a variety of oxidation products in solution.¹² Additionally, solutions of the radical are reduced to give the corresponding carbanion when exposed to strong bases, such as hydroxide or alkoxide, and BDPA also reacts with strong acids.⁹ The unpaired electron of BDPA is delocalized throughout the fluorenyl rings, but it is not appreciably delocalized into the phenyl ring.¹³ Based on this fact, TEMPO was connected through an amide linkage¹⁴ at the *para*-position of the phenyl ring to minimize disruption of the radical's stability and its propeller-like geometry.

The synthesis of the BDPA-TEMPO biradical is shown in Scheme 2. Compound **4** was prepared by a condensation of fluorene and 4-carboxybenzaldehyde. Purification of **4** was inefficient



Scheme 2. Synthesis of a BDPA-TEMPO Biradical

as a result of the presence of 4-methylbenzoic acid, which is difficult to remove from commercial 4-carboxybenzaldehyde.¹⁵ Nevertheless, pure acid **4** was obtained by recrystallization (tetrahydrofuran/acetic acid), but with a significant loss of material. Carrying forward the impure material proved a better option, because bromination of acid **4** gives compound **5**, which has lower solubility and allows isolation of the pure solid by simple filtration. Dibromide **5** was refluxed in ethanol with sodium hydroxide to eliminate hydrogen bromide and produce bromide **6**. We found this reaction to be concentration sensitive. At higher concentrations, bromine (Br₂) instead of hydrogen bromide was eliminated. Subsequent reaction of **6** with the fluorene anion, which is generated by deprotonation with sodium *tert*-butoxide in dimethylacetamide (DMA), yields a deep blue solution of the stabilized carbanion. This intermediate is quenched with 2M HCl and purified to give the functionalized BDPA precursor **7**, which is isolated as a white, air-stable powder.

The X-ray crystal structure of **7** (Figure 1) suggests the molecule's preferred geometry in solution, and therefore sheds light on its unique ¹H-NMR spectrum. For example, one ¹H-nucleus resonates at 5.90 ppm. The upfield shift is caused by the nearby phenyl group's local magnetic field. In contrast, the ¹H-nucleus on the opposite side of the fluorene moiety resonates at 8.52 ppm,

and appears to interact with the proximate proton on the sp^3 -hybridized carbon. This interaction has been confirmed by the observation of a 20% NOE enhancement in solution. In the process of characterizing **7** by NMR, we observed a second rotamer, **7b**, that appears stable in the solid state, but which slowly converts to the more stable form, **7a**, in solution (Figure 1). Rotamer **7b** is observed in the proton NMR of non-recrystallized **7**. The conversion of **7b** to **7a** was monitored by NMR and was complete within a week in d_8 -tetrahydrofuran at room temperature. Additionally, **7b** can be regenerated from samples of pure **7a** by deprotonation followed by an acid quench.

To synthesize **9**, carboxylic acid **7** was converted to the acid chloride with oxalyl chloride and catalytic DMF, and then reacted with 4-amino TEMPO. The proton on the sp^3 -hybridized carbon of **8** was presumed to be slightly more acidic than that of the protonated BDPA precursor due to the addition of the electron withdrawing amide group ($pK_a = 14$, DMSO).¹⁶ To avoid side reactions, the weak base pyridine was used to accelerate amide formation and scavenge protons. A portion of **8** was reduced with ascorbic acid, converting the TEMPO radical to the hydroxylamine, for characterization using 1H and ^{13}C NMR. The biradical **9** was generated by deprotonating **8**, followed by one-electron oxidation.

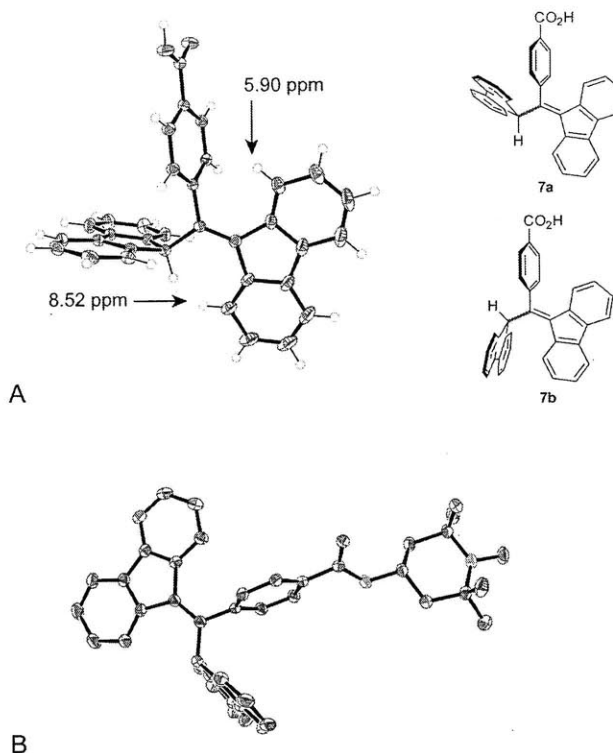


Figure 1. (a) X-ray ORTEP diagram of **7** (50% probability level) and rotamers of **7** (left). (b) X-ray ORTEP diagram of **8** (50% probability level).

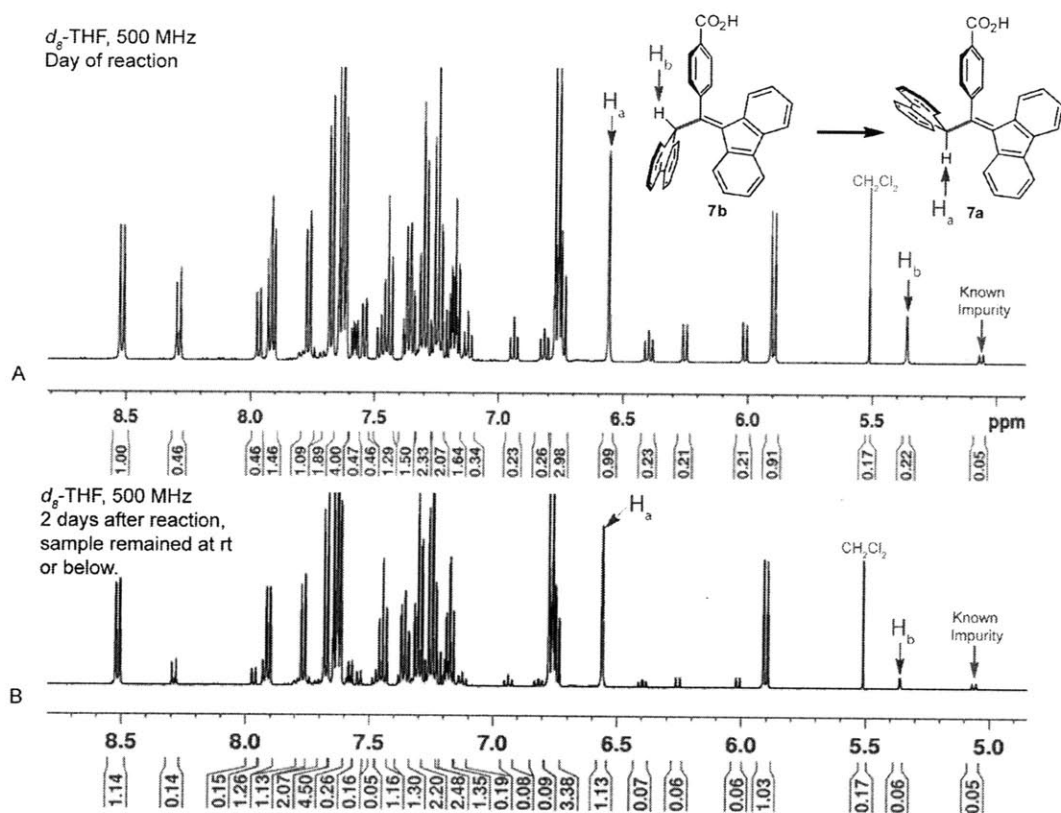


Figure 2.

Spectrum (a) shows the aromatic portion of the ^1H NMR of compound **7** after chromatography but before recrystallization. Both rotamers are present in a ratio of 4:1 (**7a**:**7b**) based on integration of the signals. Spectrum (b) shows the same sample after 2 days. The ratio of **7a** to **7b** increases to 95:5, using the integration of both the DCM signal and an impurity of known structure present at slightly above 5.00 ppm as standards. After a week under the same conditions, **7b** can no longer be detected. The known impurity is a reduced form of **7** in which the double bond has been hydrogenated. This compound is formed by the addition of fluorene to residual compound **4** during the conjugate addition reaction.

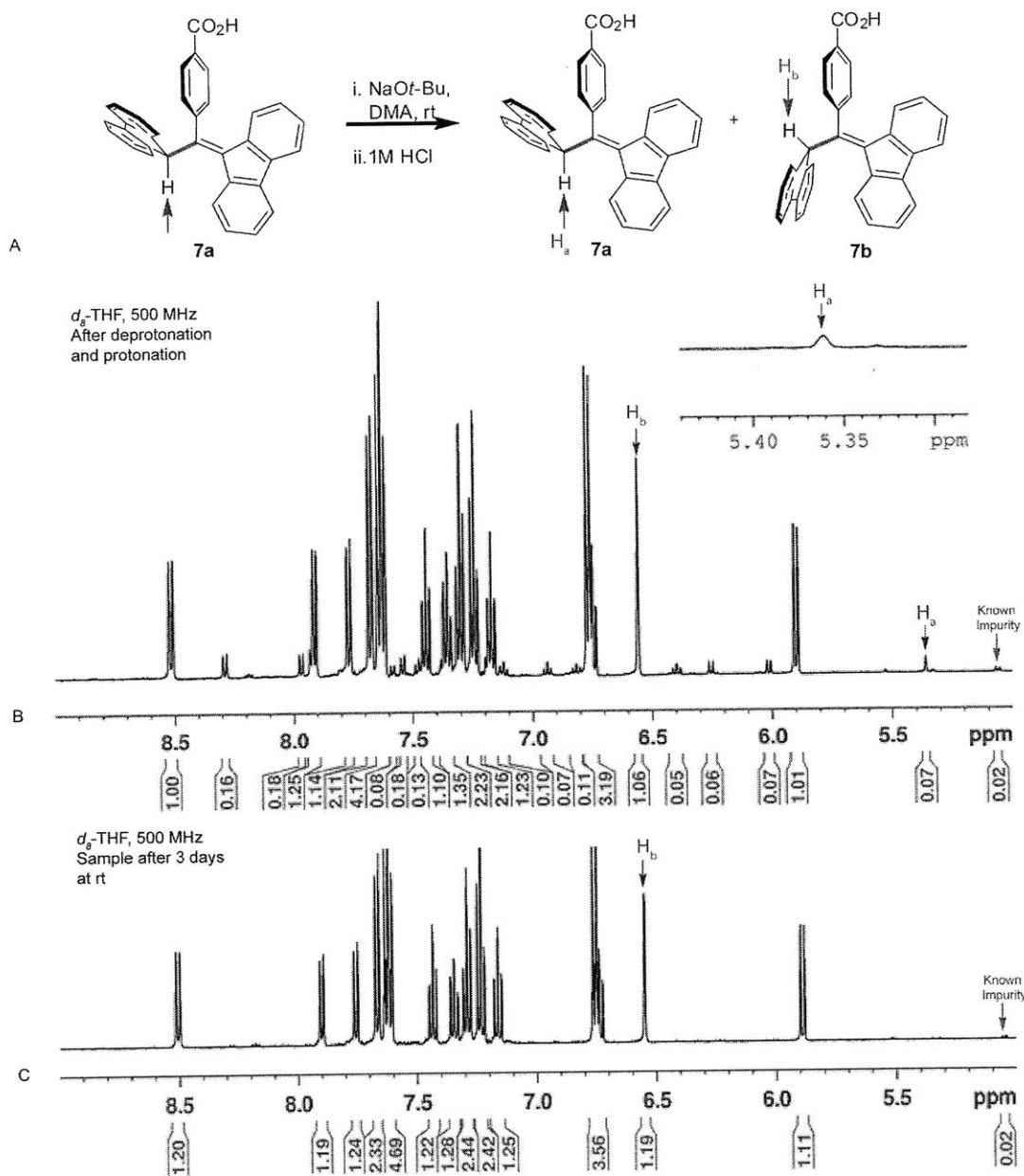


Figure 3.

(a) Deprotonation and protonation of **7**. (b) The aromatic portion of the ^1H NMR of compound **7** after the pure compound, displaying only the major rotamer in ^1H NMR, was deprotonated in DMA with sodium *tert*-butoxide and quenched with acid. As can be seen, the minor rotamer reappears (see Figure 2). (c) After three days the minor rotamer (**7b**) is no longer visible in the sample.

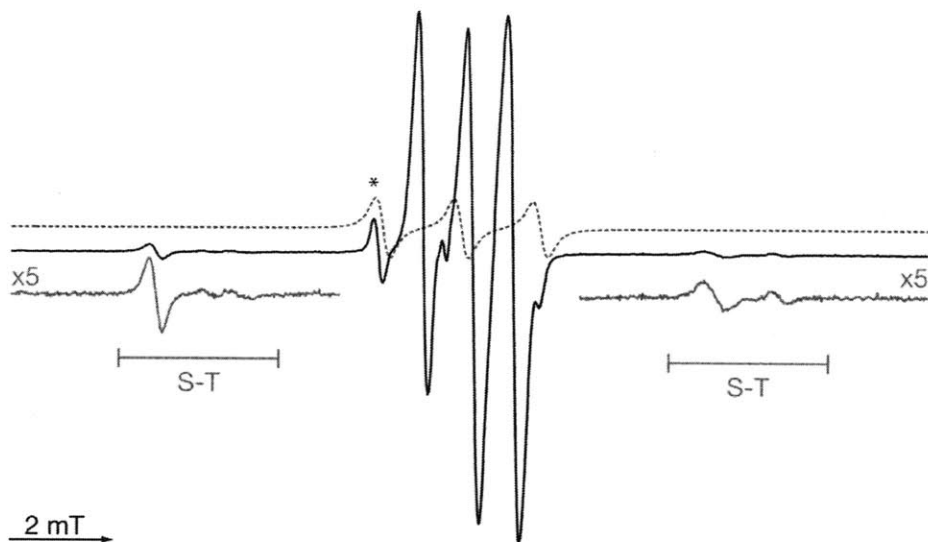


Figure 4.

Liquid-state 9 GHz EPR of **9** (black) and **8** (red) in toluene. The regions with enlarged vertical scales (gray) show the forbidden singlet-triplet transitions. Experimental parameters: rt, microwave power 2 mW, sweep width 20 mT, modulation amplitude 10 mT.

2.3 EPR Characterization of Biradical

The 9 GHz liquid-state EPR spectrum of **9** and of precursor **8** are shown in Figure 2. A typical spectrum of a nitroxide radical consists of three sharp lines. The spectrum of the biradical differs due to the presence of the BDPA radical and the interaction between the two paramagnetic centers. Additionally, several new resonances are observed well separated from the central region of the spectrum. These features arise from forbidden singlet-triplet transitions (S-T) and are common in spectra of biradicals that feature an intermediate J-coupling. A J-coupling of 140 MHz was measured based on the separation of the peaks from the central region.¹⁷

Present in the spectrum is an impurity with an EPR signal characteristic of a TEMPO radical attached to a diamagnetic fragment (Figure 2, indicated by asterisk), which we attribute to unreacted **8**. We have evaluated the efficiency of the conversion of **8** to **9** using several pieces of evidence. First, we obtain nearly quantitative mass recovery (95%), and see no indication of amide-bond cleavage under the reaction conditions in TLC. Additionally, the TEMPO moiety is

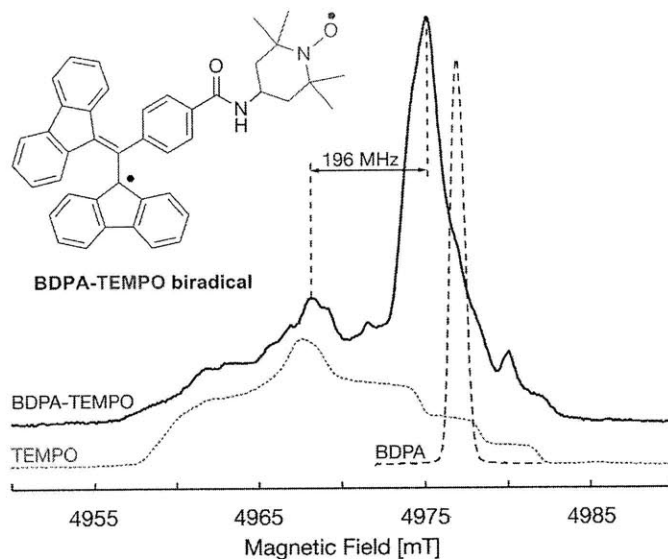


Figure 5.

Echo-detected 140 GHz solid-state EPR spectra of **9** (black), TEMPO (red), and BDPA (blue) in toluene. Experiments are performed at 20 K, with $t_p(\pi/2)$ 44 ns, and typically 100 scans are averaged for each point. Spectra were collected by T. Maly and G. Debelouchina of the Griffin group.

unaffected by the reaction conditions. Integration of the EPR signal indicates that on a per molecule basis there is less than 10% of the monoradical impurity present (see Section 2.7). Based on this evidence, we estimate the efficiency of the reaction to be 85%.

For high-field (HF) DNP experiments, the HF-EPR spectrum in the solid-state is of particular interest (Figure 3). The spectrum of the biradical shows features characteristic of both BDPA and TEMPO, as well as new features that indicate the presence of an electron-electron interaction. Most notable is the shift of the BDPA line to lower field.

2.4 Conclusions

In summary, we have developed a general method to functionalize BDPA by synthesizing a BDPA precursor (**7**) with a carboxylic acid functional group. We have used this precursor to synthesize a BDPA-TEMPO biradical (**9**) in good yield and studied the resulting EPR spectrum. The HF-EPR spectrum, with two peaks, one narrow and one broad, separated by a value close to the ^1H Larmor frequency, has the desired characteristics for DNP. Future work will focus on add-

ing water-solubilizing groups so that the biradical can be tested for DNP-enhancements in aqueous solutions.

2.5 Experimental Section

Materials. All chemicals, reagents, and solvents were used as received from commercial sources without further purification except dimethylacetamide, dimethylformamide, and dimethylsulfoxide, which were dried over oven-activated 4-Å molecular sieves.

Instrumentation. Proton nuclear magnetic resonance (^1H NMR) spectra and carbon nuclear magnetic resonance (^{13}C NMR) spectra were recorded on an Inova-500 (500 MHz) NMR spectrometer. The mass spectrometry data were obtained at the MIT mass spectrometry facility, using a Bruker Daltonics APEX II 3T FT-ICR-MS. Elemental analysis was obtained by Columbia Analytical Services, Tucson, AZ.

4-((9H-fluoren-9-ylidene)methyl)benzoic acid (4). To an oven-dried 500 mL flask were added 5.00 g (30.1 mmol, 1.00 equiv) of fluorene and 9.27 g (82.8 mmol, 2.75 equiv) of *t*-BuOK, followed by 300 mL of absolute ethanol. The reaction mixture was heated to reflux, at which time 5.50 g (36.7 mmol, 1.20 equiv) of 4-carboxybenzaldehyde was added and the reaction was allowed to reflux overnight. After being allowed to cool to room temperature, the reaction mixture was poured into a large flask containing excess 1M HCl and ice. This mixture was extracted with 2 portions of ethyl acetate (approximately 500 mL total), and the combined organic layers were washed with dilute sodium bicarbonate solution (pH 9) (3 x 100 mL) to remove terephthalic acid, which is an impurity in the 4-carboxybenzaldehyde starting material. The organic layer was washed with brine and dried over sodium sulfate. After removal of the ethyl acetate, the dark yellow material was twice refluxed in 30 mL of toluene, allowed to cool, and then filtered, to obtain 6.25 g of a bright yellow powder that contains a small amount of 4-methylbenzoic acid. This material can be purified by recrystallization from a refluxing mixture of tetrahydrofuran and acetic acid

with a significant loss of material (3.38 g of material yielded 1.87 g of pure material). Therefore, the impure material was carried through to the next step. ¹H NMR (500 MHz, *d*₆-DMSO, δ) (all coupling constants (*J*) in Hz): 13.11 (s br, 1H), 8.07 (d, *J* = 7.5, 2H), 7.99 (d, *J* = 7.5, 1H), 7.96 (s, 1H), 7.89 (d, *J* = 7.5, 1H), 7.87 (d, *J* = 7.5, 1H), 7.73 (d, *J* = 8.0, 2H), 7.44 (m, 2H), 7.37 (t, *J* = 7.0, 2H), 7.13 (td, *J* = 7.0, 1.0, 1H); ¹³C NMR (126 MHz, *d*₆-DMSO, δ): 167.0, 140.9, 140.8, 138.7, 138.5, 136.5, 135.4, 130.2, 129.6, 129.3, 129.1, 128.7, 127.3, 127.2, 127.0, 123.8, 121.0, 120.3, 119.9; HRMS (ESI): 297.0924 [calc'd for M-H: 297.0921]; IR: ν_{\max} (KBr)/cm⁻¹ 1674, 1601, 1419, 1290, 722; mp 250-255 °C (tetrahydrofuran/acetic acid).

4-(bromo(9-bromo-9H-fluoren-9-yl)methyl)benzoic acid (5). To an oven-dried 250 mL flask were added 2.57 g of acid **4** (8.61 mmol, 1.00 equiv) and 65 mL of glacial acetic acid. The resulting suspension was heated to reflux and additional acetic acid was added drop-wise until a homogeneous solution was formed. The mixture was cooled to room temperature and a slight excess of bromine (0.470 mL, 1.45 g, 9.06 mmol, 1.10 equiv) was added slowly over 5 minutes. The suspension became a homogeneous red solution and was allowed to stir overnight at room temperature until a white precipitate formed. The resulting suspension was filtered and the filter cake was washed with hexanes to afford 2.85 g (6.22 mmol) of a white powder and a yield of 50% over two steps based on fluorene as the limiting reagent. ¹H NMR (500 MHz, *d*₈-tetrahydrofuran, δ) (all coupling constants (*J*) in Hz): 10.86 (s br, 1H), 8.21 (d, *J* = 7.5, 1H), 7.69 (d, *J* = 7.5, 1H), 7.60 (d, *J* = 7.5, 1H), 7.56 (d, *J* = 8.0, 2H), 7.44 (m, 3H), 7.25 (m, 2H), 6.97 (d, *J* = 8.0, 2H), 6.19 (s, 1H); ¹³C NMR (125 MHz, *d*₆-dimethylsulfoxide): 166.2, 144.0, 140.8, 138.6, 137.7, 130.1, 129.8, 129.4, 128.7, 127.8 (2), 127.7 (2), 126.0, 125.6, 120.2, 120.0, 65.8, 59.9; HRMS (ESI): 454.9291 [calc'd for M-H: 454.9288]; FT-IR: ν_{\max} (KBr)/cm⁻¹ 1690, 1420, 1286, 743; mp 185-187 °C with decomposition (acetic acid).

4-(bromo(9H-fluoren-9-ylidene)methyl)benzoic acid (6). To an oven-dried 250 mL round-bottom flask were added 1.01 g of dibromide **5** (2.21 mmol, 1.00 equiv) and 125 mL of absolute etha-

nol. To the flask was added 5.00 g (50 pellets) of NaOH (125 mmol, 56.6 equiv) dissolved in the minimum amount of water needed and a water-cooled reflux condenser was attached. The reaction was refluxed for 1 h and then allowed to cool to room temperature. The solution was acidified with dilute hydrochloric acid and extracted with 100 mL of ethyl acetate, washed with brine, and dried over sodium sulfate. Removal of the solvent yielded 0.786 g (2.08 mmol, 94%) of a yellow powder. ¹H NMR (500 MHz, *d*₆-DMSO, δ): 8.76 (d, *J* = 7.5, 1H), 8.12 (dd, *J* = 7.5, 1.5, 1H), 7.94 (d, *J* = 7.5, 1H), 7.85 (d, *J* = 7.5, 1H), 7.62 (d, *J* = 7.5, 2H), 7.52 (t, *J* = 7.0 Hz, 1H), 7.45 (t, *J* = 7.0, 1H), 7.28 (*J* = 7.0 Hz, 1H), 6.92 (t, *J* = 7.0, 1H), 6.08 (t, *J* = 7.5, 1H). ¹³C NMR (126 MHz, *d*₆-DMSO, δ): 166.6, 146.0, 140.6, 139.3, 136.9, 136.8, 135.4, 131.5, 130.4, 129.8, 128.8, 128.5, 127.4, 127.2, 125.5(2), 123.0, 120.2, 120.0. HRMS (EI): 376.0106 [calc'd for M: 376.0093]. IR: ν_{\max} (KBr)/cm⁻¹ 1691, 1604, 1445, 728.

4-((9H-fluoren-9-yl)(9H-fluoren-9-ylidene)methyl)benzoic acid (7). To an oven-dried 100 mL flask were added 0.182 g (1.10 mmol, 1.50 equiv) of fluorene and 0.350 g (3.65 mmol, 5.00 equiv) of sodium *tert*-butoxide. The flask was evacuated under high vacuum and refilled with argon three times and 25 mL of dry dimethylacetamide (DMA) was added. The solution appeared dark red and was allowed to stir for 5 minutes. In a separate oven-dried 25 mL flask, 0.272 g (0.730 mmol, 1.00 equiv) of bromide **6** was added. The flask was evacuated under high vacuum and refilled with argon three times and 10 mL of dry DMA was added. After complete dissolution of bromide **6** in the DMA, the solution was slowly added over a period of 10 minutes to the 100 mL flask by cannulation. The reaction immediately turned deep blue and was stirred for 1 h at room temperature. The flask was cooled in an ice bath and aqueous 2M HCl was added until the blue color disappeared. The solution was then further diluted with water and extracted into ethyl acetate (2 x 20 mL), which was washed with water (2 x 50 mL) and once with brine. The organic layer was dried over sodium sulfate and then removed to yield an orange solid. This orange solid was purified by silica gel flash chromatography eluting with a gradient from pure DCM to 95 DCM : 5

MeOH. The solvent was removed and the solid was dissolved in approximately 1 mL of THF and 2 mL of acetic acid with heating. This solution was allowed to cool to room temperature and the THF was allowed to evaporate, yielding, after filtration and washing with hexanes, 0.280 g (0.605 mmol, 83%) of acid **7** as an off-white powder. ¹H NMR (500 MHz, *d*₈-tetrahydrofuran, δ): 8.52 (dd, *J* = 7.5, 1.0 Hz, 1H), 7.92 (d, *J* = 7.5, 1H), 7.77 (d, *J* = 7.5, 1H), 7.68 (d, *J* = 7.5, 2H), 7.63 (m, 4H), 7.45 (td, *J* = 7.5, 1.0, 1H), 7.36 (td, *J* = 7.5, 1.0, 1H), 7.31 (td, *J* = 7.5, 1.0, 2H), 7.25 (td, *J* = 7.5, 1.0 Hz, 2H), 7.18 (td, *J* = 7.5, 1.0, 1H), 6.77 (d, *J* = 7.5, 2H), 6.75 (m, 1H), 6.56 (s, 1H), 5.90 (d, *J* = 7.5, 1H). ¹³C NMR (126 MHz, *d*₈-tetrahydrofuran, δ): 167.3, 145.1, 145.0, 144.3, 143.2, 142.5, 141.1, 140.2, 139.6, 137.2, 130.8, 130.1, 129.6, 129.3, 128.6, 128.5, 128.4, 127.9, 127.4, 127.0, 126.3, 125.2, 121.0, 120.8, 120.6, 120.1, 53.6. HRMS (ESI): 461.1552 [calc'd for M-H: 461.1547]; IR: ν_{max} (KBr)/cm⁻¹ 1692, 1606, 1445, 1290, 730. mp 280 °C with decomposition (tetrahydrofuran/acetic acid).

4-((9H-fluoren-9-yl)(9H-fluoren-9-ylidene)methyl)-N-(4-amino-2,2,6,6-tetramethylpiperidine-1-oxyl)benzamide (8). To an oven-dried 100 mL flask was added 0.200 g (0.432 mmol, 1.00 equiv) of acid **7**. The flask was evacuated under high vacuum and refilled with argon three times and 10 mL of dry DCM was added along with three drops of dry DMF. The reaction flask was cooled to 0 °C in an ice-bath and 0.080 mL (0.86 mmol, 2.0 equiv) of oxalyl chloride was added. The flask was slowly warmed to room temperature. After 1 h at room temperature, the solvent was removed under high vacuum to obtain a yellow solid, which was then dissolved in 20 mL of dry DCM. In a separate flask, 0.149 g (0.864 mmol, 2.00 equiv) of 4-amino-TEMPO was added and the flask was evacuated and refilled with argon three times. To the flask was added 10 mL of dry DCM and 0.14 mL of dry pyridine (4.0 equiv) and the resulting solution was stirred in an ice-bath. The solution containing the acid chloride of **7** was slowly added to the amine-containing flask, after which the flask was allowed to warm to room temperature overnight with stirring. The solution was washed three times with dilute acid and once with brine. It was dried over sodium

sulfate and the solvent was removed. The material was purified by silica gel flash chromatography eluting with a gradient from pure DCM to 90 DCM : 10 ethyl acetate. After removing the solvent, 0.246 g (0.399 mmol, 92 % yield) of amide **8** was obtained as a pink powder. HRMS (ESI): 616.3067 [calc'd for M+H: 616.3084]; Elemental Analysis: Theoretical: C: 83.87, H: 6.38, N: 4.55 Found: C: 82.99 H: 6.31 N: 4.34, the failure of the elemental analysis maybe a result of the instability of the material to oxygen over time; IR: ν_{\max} (KBr)/cm⁻¹ 1652, 1607, 1539, 1498, 1446, 1322, 1242, 732. To characterize by NMR, 20 mgs of material was dissolved in 2 mL methanol and excess ascorbic acid was added to reduce the TEMPO radical to a hydroxylamine (compound **8H**). After 10 minutes, the solvent was removed and the reduced compound was taken up in 2 mL of chloroform. After removal of the chloroform, the resulting white solid was dissolved in 0.7 mL of *d*₆-acetone. The material still contained ascorbic acid and its oxidation products. ¹H NMR (500 MHz, *d*₆-acetone, δ): 8.57 (dd, *J* = 7.5, 1.0, 1H), 8.01 (dd, *J* = 7.5, 1.0, 1H), 7.87 (d, *J* = 7.5, 1H), 7.76 (d, *J* = 7.5, 2H), 7.69 (d, *J* = 7.5, 2H), 7.56 (d, *J* = 7.5, 2H), 7.52 (t, *J* = 7.0, 1H), 7.45 (t, *J* = 7.0, 1H), 7.35 (m, 5H), 7.25 (t, *J* = 7.0 Hz, 1H), 6.79 (m, 1), 6.78 (d, *J* = 7.5, 2H), 6.54 (s, 1H), 5.85 (d, *J* = 7.5, 1H), 4.28 (m, 1H), 1.82 (dd, *J* = 12.0, 3.0, 2H), 1.50 (t, *J* = 12.0, 2H), 1.18 (s, 6H), 1.12 (s, 6H). ¹³C NMR (126 MHz, *d*₆-acetone): 166.1, 146.0, 145.8, 143.8, 143.5 (2), 143.0, 141.8, 140.4, 140.2, 137.8, 135.4, 130.3, 130.3, 129.6, 129.5 (2), 128.9, 128.5, 128.3, 127.8, 127.2, 127.0, 121.9, 121.8, 121.1, 53.3, 45.4, 41.9, 32.3, 20.3. HRMS (ESI): 617.3142 [calc'd for M+H: 617.3163].

BDPA-TEMPO Biradical (9): To an oven-dried flask, 0.0800 g (0.130 mmol, 1.00 equiv) of **8** and 0.0440 g (0.390 mmol, 3.00 equiv) of potassium *tert*-butoxide were added and the flask was evacuated and refilled with argon three times. To the flask was added 80 mL of a dry 9:1 mixture of DMSO and *tert*-butyl alcohol. The flask was vigorously stirred for 20 minutes and then 0.0660 g (0.390 mmol, 3.00 equiv) of silver nitrate dissolved in 1.5 mL of water was added. After stirring for 1 minute, additional water was added and the solution was extracted with diethyl ether (4

x 50 mL). The ether was washed once with water and brine, and then dried over sodium sulfate. The ether solution was filtered through a plug of silica to ensure that any remaining silver particles were removed. Removal of the ether yielded 0.0760 g (0.124 mmol, 95% mass recovery) of a dark brown material with a metallic luster. Based on EPR measurements, the purity of material was estimated to be at least 90%, with the major impurity being the starting material, **8**. Therefore, taking into account mass recovery and purity, we estimate the yield of the reaction to be at least 85%. FT-IR: ν_{\max} (KBr)/cm⁻¹ 1646, 1607, 1539, 1497, 1444, 1324, 1242, 731. HRMS (ESI): 614.2938 [calc'd for M⁻: 614.2939].

2.6 References

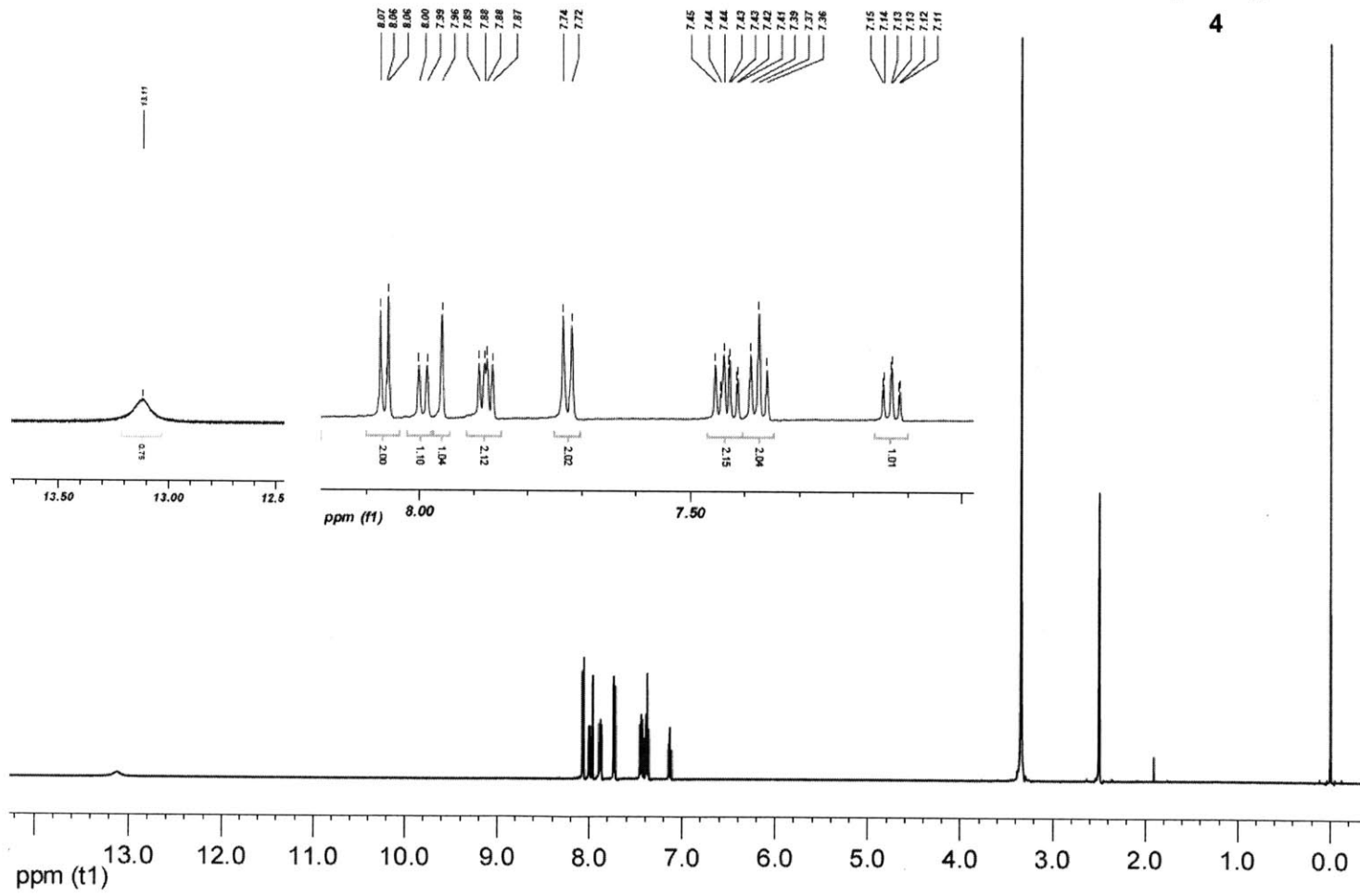
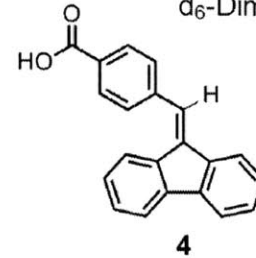
- (1) Hu, K.-N.; Bajaj, V. S.; Rosay, M. M.; Griffin, R. G. *J. Chem. Phys.* **2007**, *126*, 044512.
- (2) (a) Hu, K.-N.; Yu, H.-h.; Swager, T. M.; Griffin, R. G. *J. Am. Chem. Soc.* **2004**, *126*, 10844. (b) Song, C.; Hu, K.-N.; Swager, T.M.; Griffin, R.G. *J. Am. Chem. Soc.* **2006**, *128*, 11385.
- (3) (a) Maly, T.; Debelouchina, G. T.; Bajaj, V. S.; Hu, K.-N.; Joo, C.-G.; Mak-Jurkauskas, M. L.; Sigirhi, J. R.; van der Wel, P. C. A.; Herzfeld, J.; Temkin, R. J.; Griffin, R. G. *J. Chem. Phys.* **2008**, *128*, 052211. (b) Barnes, A. B.; Paëpe, G. D.; Wel, P. C. A. v. d.; Hu, K.-N.; Joo, C.-G.; Bajaj, V. S.; Mak-Jurkauskas, M. L.; Sirigiri, J. R.; Herzfeld, J.; Temkin, R. J.; Griffin, R. G. *Appl. Magn. Reson.* **2008**, *34*, 237.
- (4) (a) Jaroniec, C. P.; MacPhee, C. E.; Bajaj, V. S.; McMahon, M. T.; Dobson, C. M.; Griffin, R. G. *Proc. Natl. Acad. Sci. U.S.A.* **2004**, *101*, 711. (b) van der Wel, P. C. A.; Hu, K.-N.; Lewandowski, J. R.; Griffin, R. G. *J. Am. Chem. Soc.* **2006**, *128*, 10840. (c) van der Wel, P. C. A.; Lewandowski, J. R.; Griffin, R. G. *J. Am. Chem. Soc.* **2007**, *129*, 5117.
- (5) (a) Bajaj, V. S.; Hornstein, M. K.; Kreischer, K. E.; Sirigiri, J. R.; Woskov, P. P.; Mak-Jurkauskas, M. L.; Herzfeld, J.; Temkin, R. J.; Griffin, R. G. *J. Magn. Reson.* **2007**, *189*, 251. (b) Mak-Jurkauskas, M. L.; Bajaj, V. S.; Hornstein, M. K.; Belenky, M.; Griffin, R. G. *Proc. Natl. Acad. Sci. U.S.A.* **2008**, *105*, 883.
- (6) (a) Pine, A.; Gibby, M. G.; Waugh, J. S. *J. Chem. Physics* **1972**, *56*, 1776. (b) Bennett, A. E.; Rienstra, C. M.; Auger, M.; Lakshmi, K. V.; Griffin, R. G. *J. Chem. Physics* **1995**,

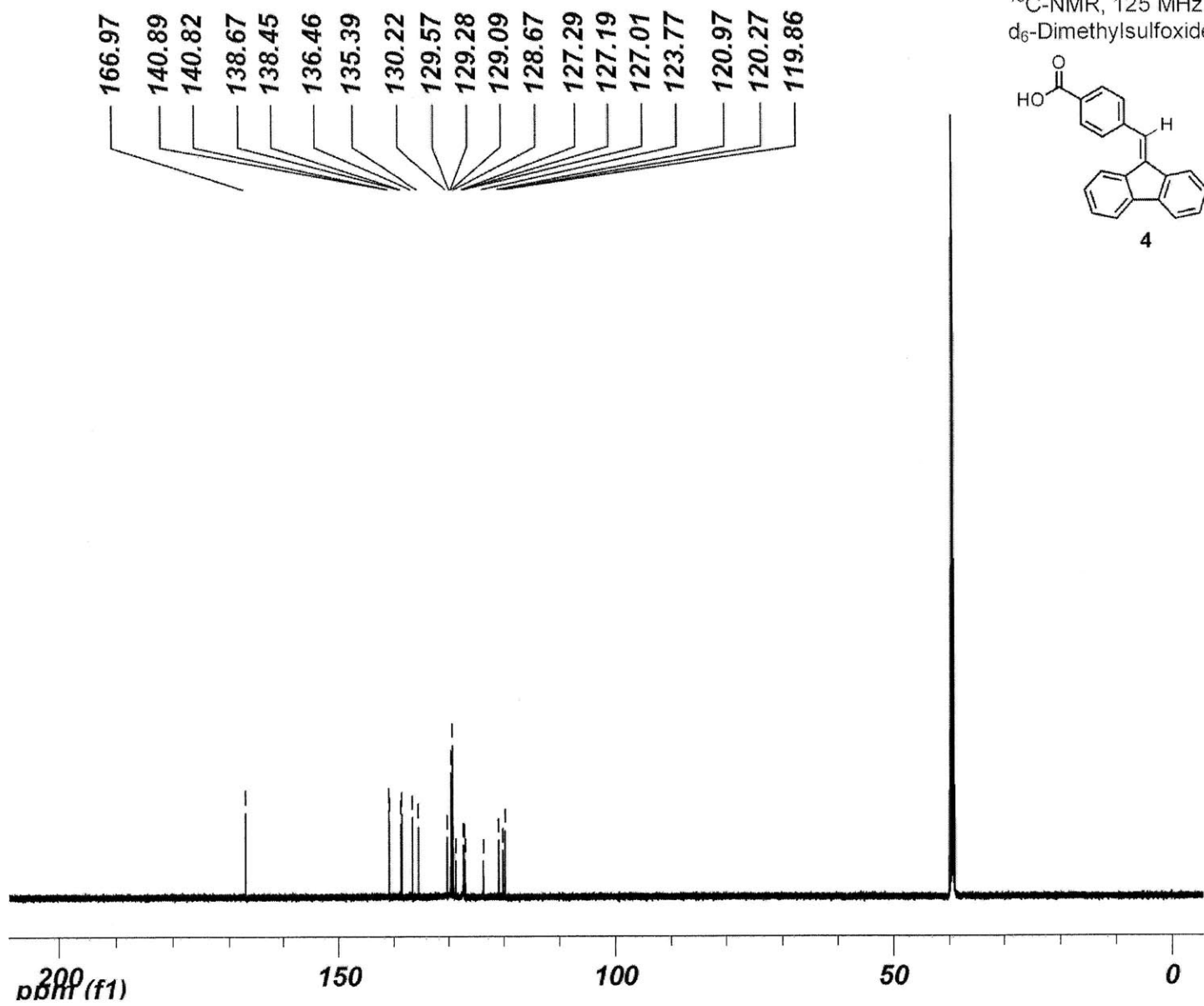
103, 6951.

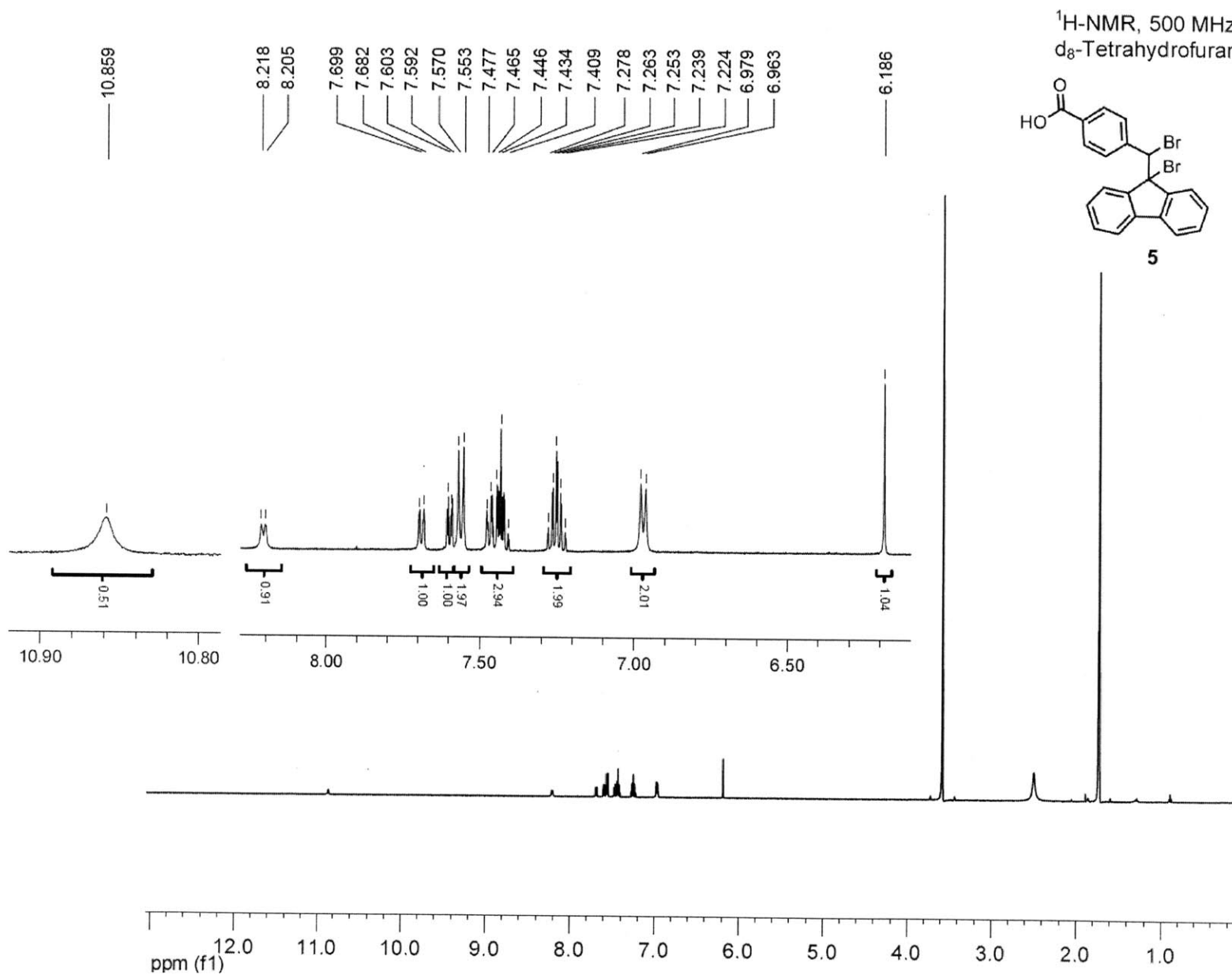
- (7) (a) Reddy, T. J.; Iwama, T.; Halpern, H. J.; Rawal, V. H. *J. Org. Chem.* **2002**, *67*, 4635. (b) Bowman, M. K.; Mailer, C.; Halpern, H. J. *J. Magn. Reson.* **2005**, *172*, 254. (c) Liu, Y.; Villamena, F. A.; Sun J.; Xu Y.; Dhimitruka, I.; Zweier, J. L. *J. Org. Chem.* **2008**, *73*, 1490.
- (8) 1,3-bisdiphenylene-2-phenylallyl (BDPA) free radical and 2,2,6,6-tetramethylpiperidine-1-oxyl (TEMPO) free radical will be referred to as simply BDPA and TEMPO throughout the text.
- (9) Koelsch, C. F. *J. Am. Chem. Soc.* **1957**, *79*, 4439.
- (10) Kuhn, R.; Neugebauer, F. A. *Monatsh. Chem.* **1964**, *95*, 3.
- (11) (a) Plater, M. J.; Kemp, S.; Lattmann, E. *J. Chem. Soc., Perkin Trans. 1*, **2000**, 971. (b) Nishide, H.; Yoshioka, N.; Saitoh, Y.; Gotoh, R.; Miyakawa, T.; Tsuchida, E. *J. Macromol. Sci. Pure Appl. Chem.* **1992**, *A29*, 775.
- (12) Breslin, D. T.; Fox, M. A. *J. Phys. Chem.* **1993**, *97*, 13341.
- (13) Azuma, N.; Ozawa, T.; Yamauchi, J. *Bull. Chem. Soc. Jpn.* **1994**, *67*, 31.
- (14) Sosnovsky, G.; Lukszo, J.; Brasch, R. C.; Eriksson, U. G.; Tozer, T. N. *Eur. J. Med. Chem.* **1989**, *24*, 241.
- (15) The impurity was identified by ¹H-NMR and in our hands could not be removed from the commercial material through recrystallization, extraction, or vacuum sublimation.
- (16) Kuhn, R.; Rewicki, D. *Liebigs Ann. Chem.* **1967**, *706*, 250.
- (17) (a) Eaton, S., S.; DuBois, D. L.; Eaton, G. R. *J. Magn. Reson.* **1978**, *32*, 251. (b) Eaton, G. R.; Eaton, S. S. *Spin Labelling, Theory and Applications*; Berliner, L. J., Reuben, J., Eds.; Plenum Press: New York, NY, 1989; pp 339-397.

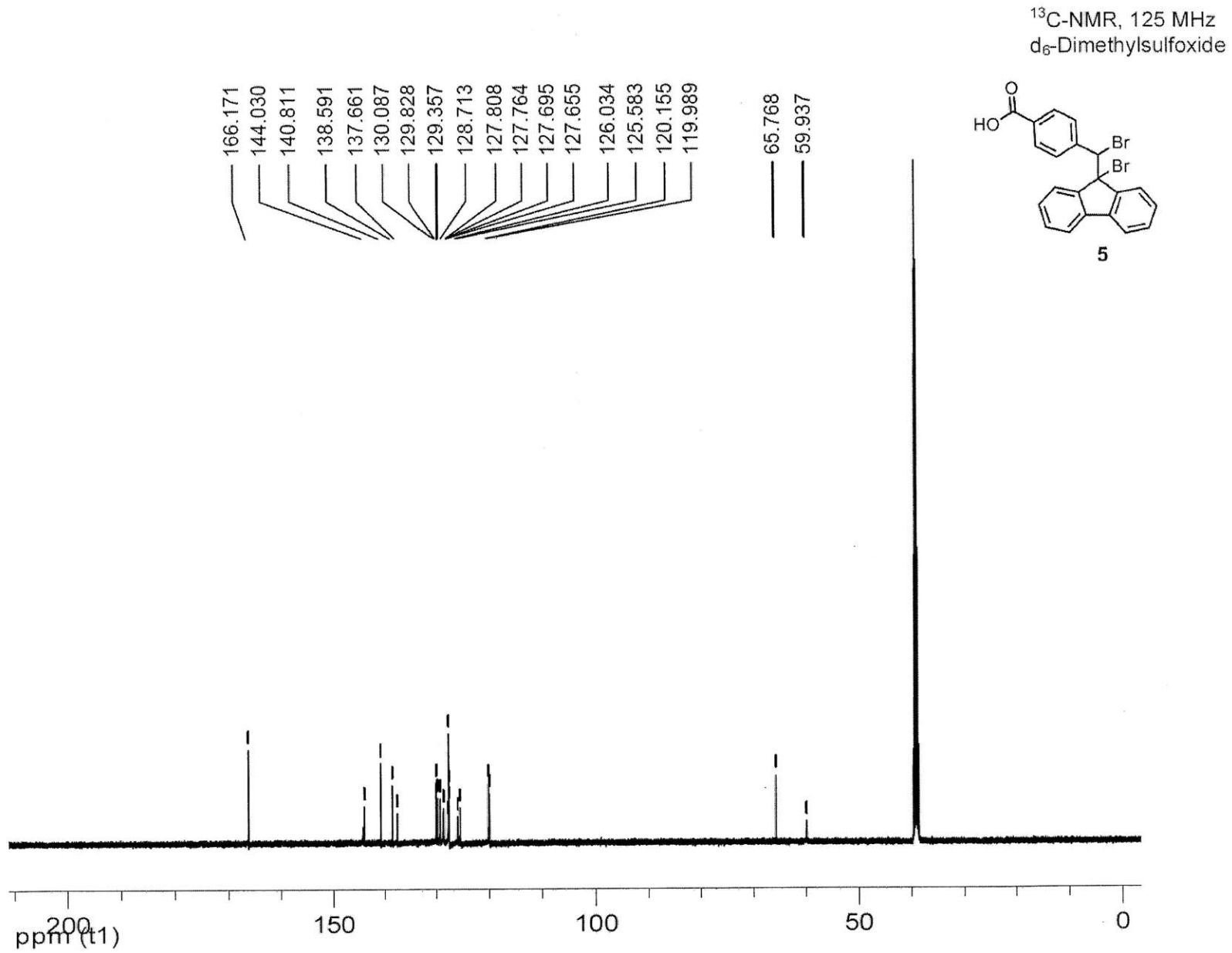
2.7 *NMR and EPR Spectra*

¹H-NMR, 500 MHz
d₆-Dimethylsulfoxide

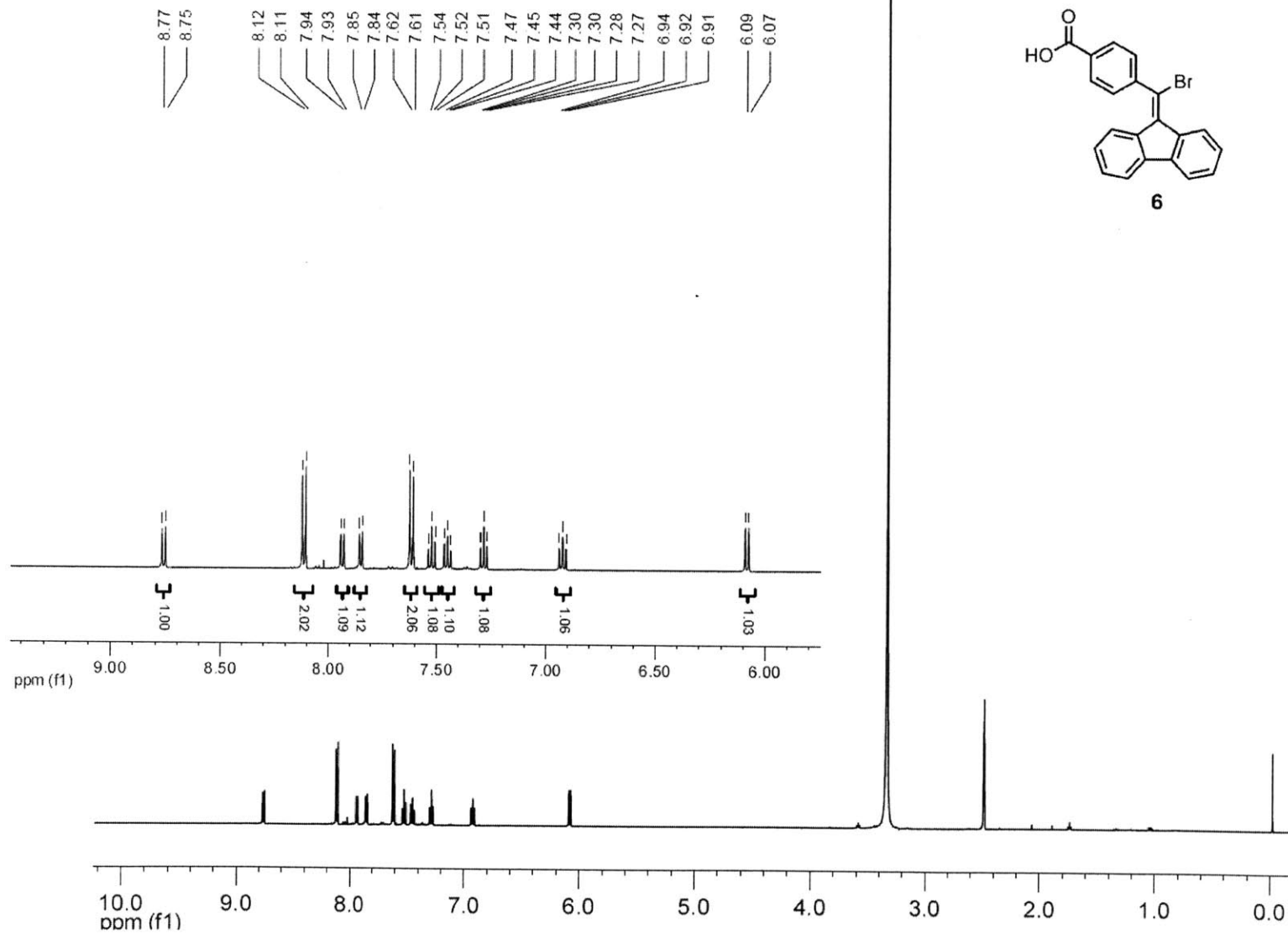
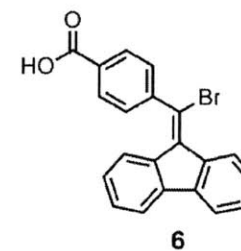


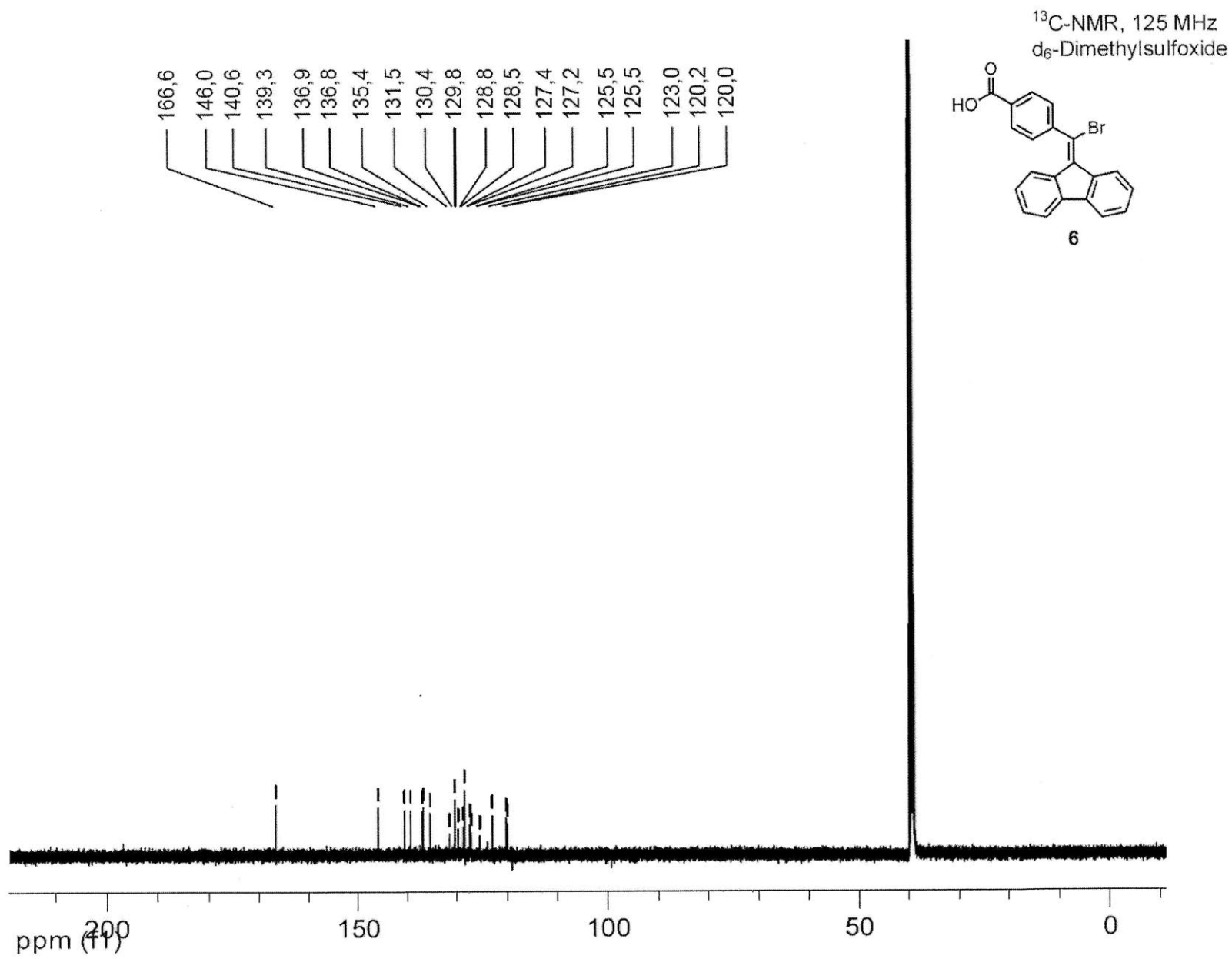


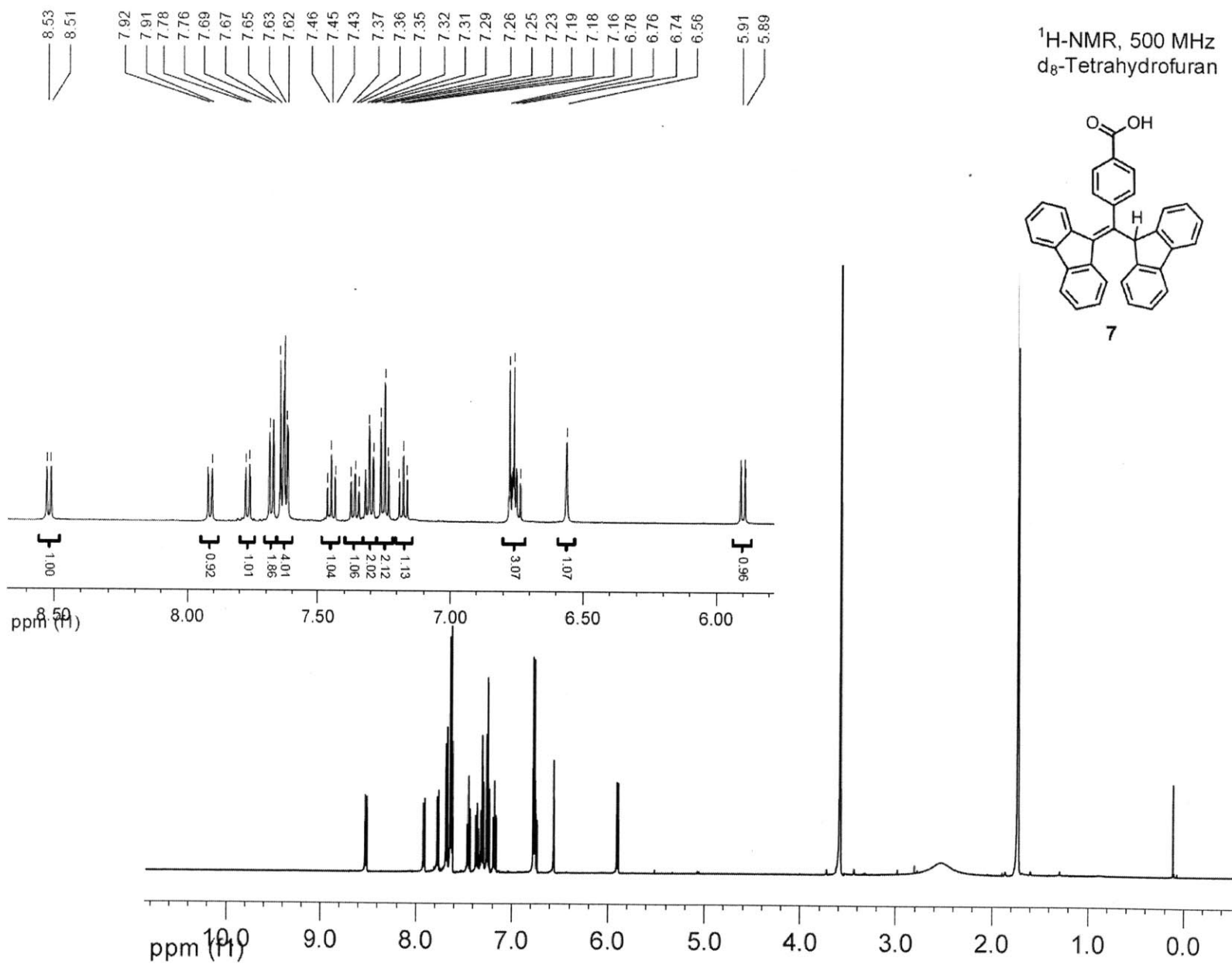


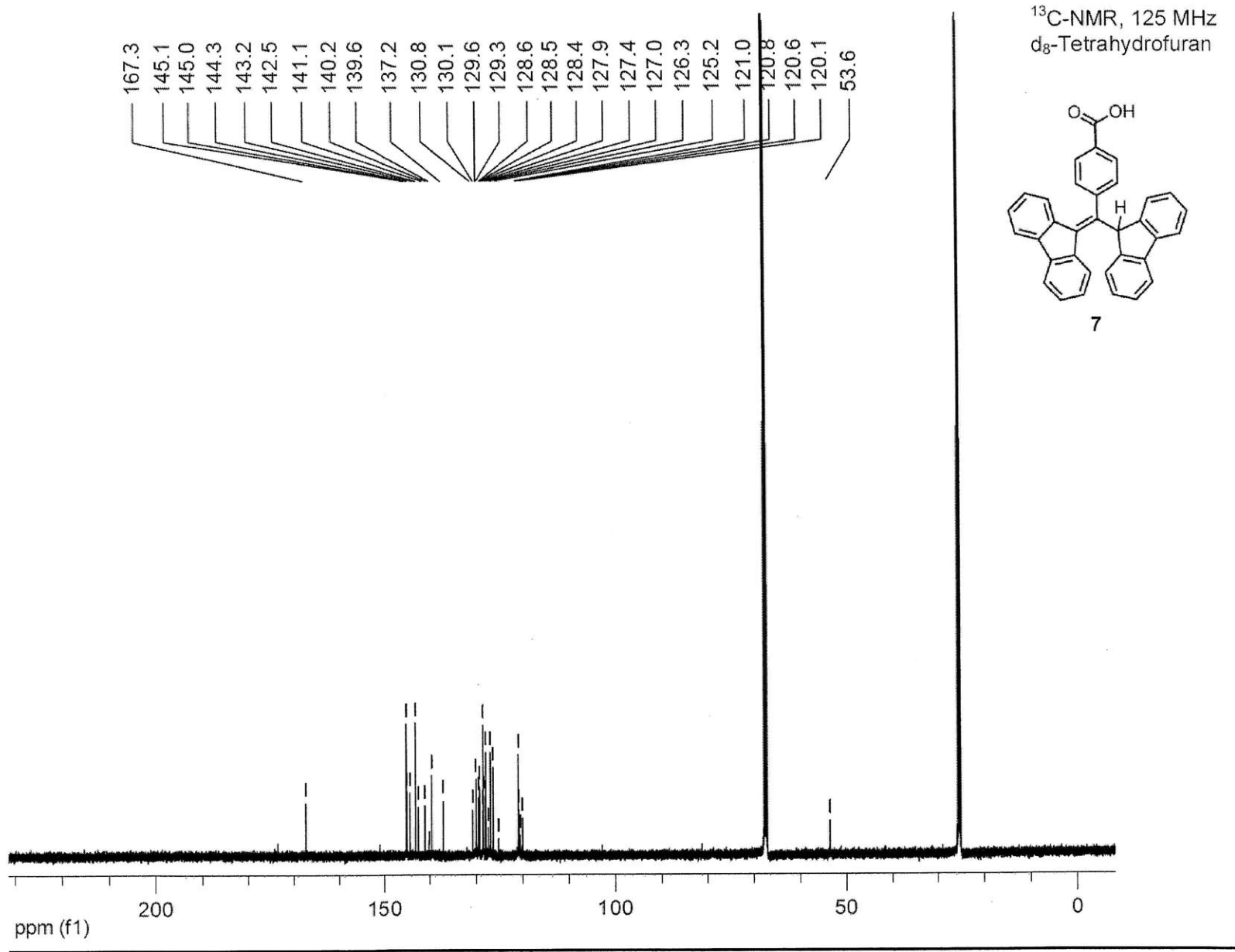


¹H-NMR, 500 MHz
d₆-Dimethylsulfoxide

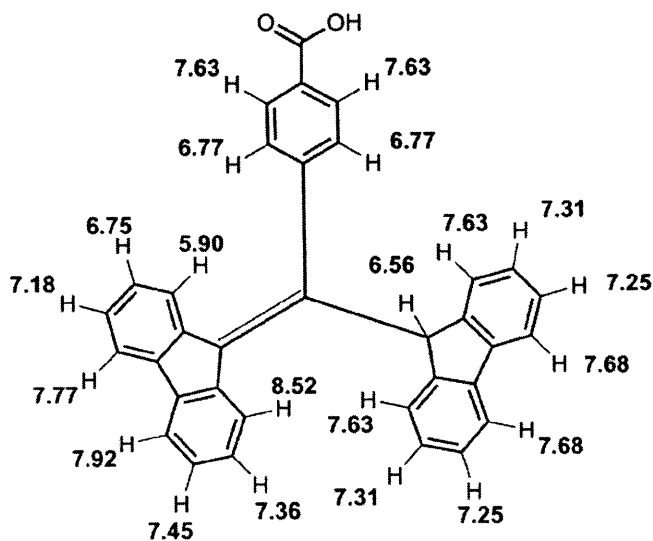
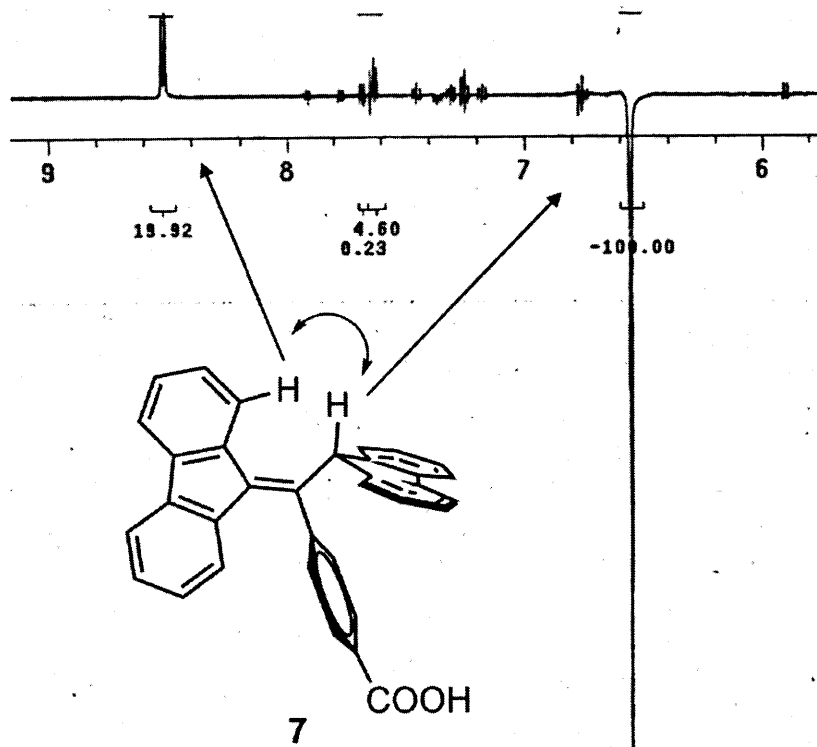






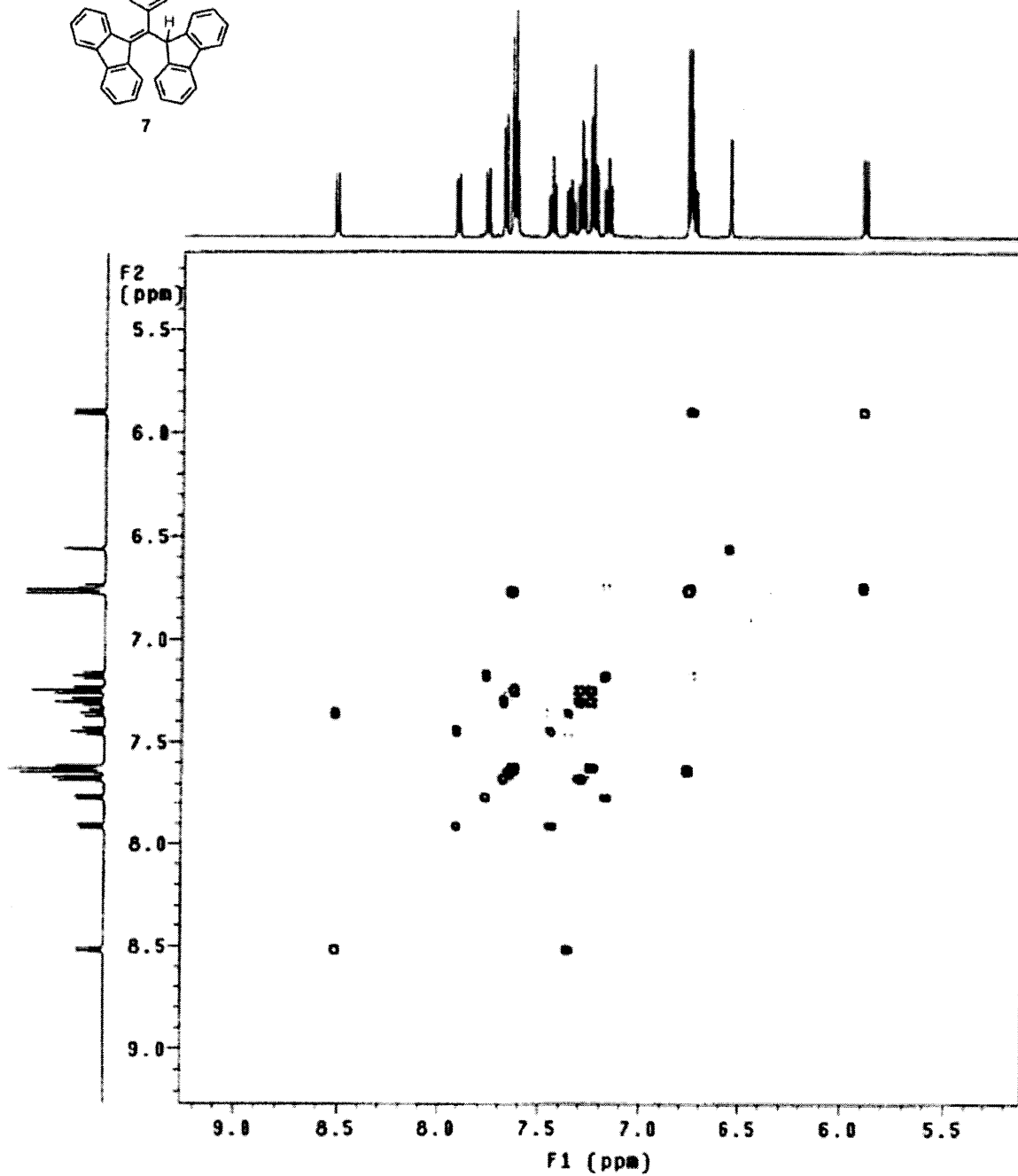
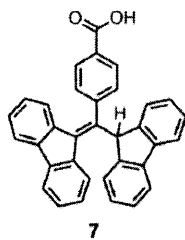


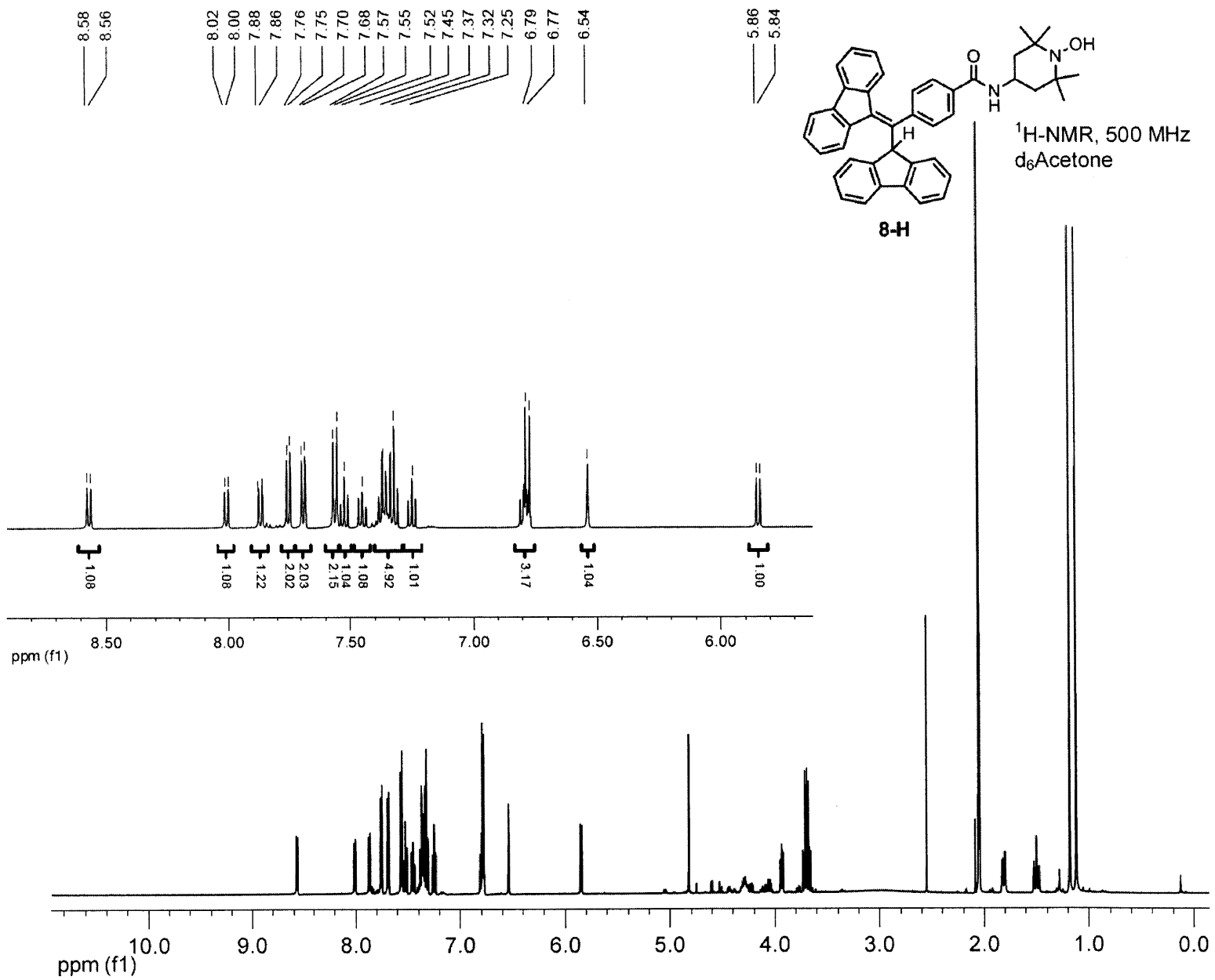
Measurement of NOE enhancement between the proton at 6.56 ppm and the proton at 8.52 ppm (in d_8 -tetrahydrofuran, room temperature, 500 MHz).

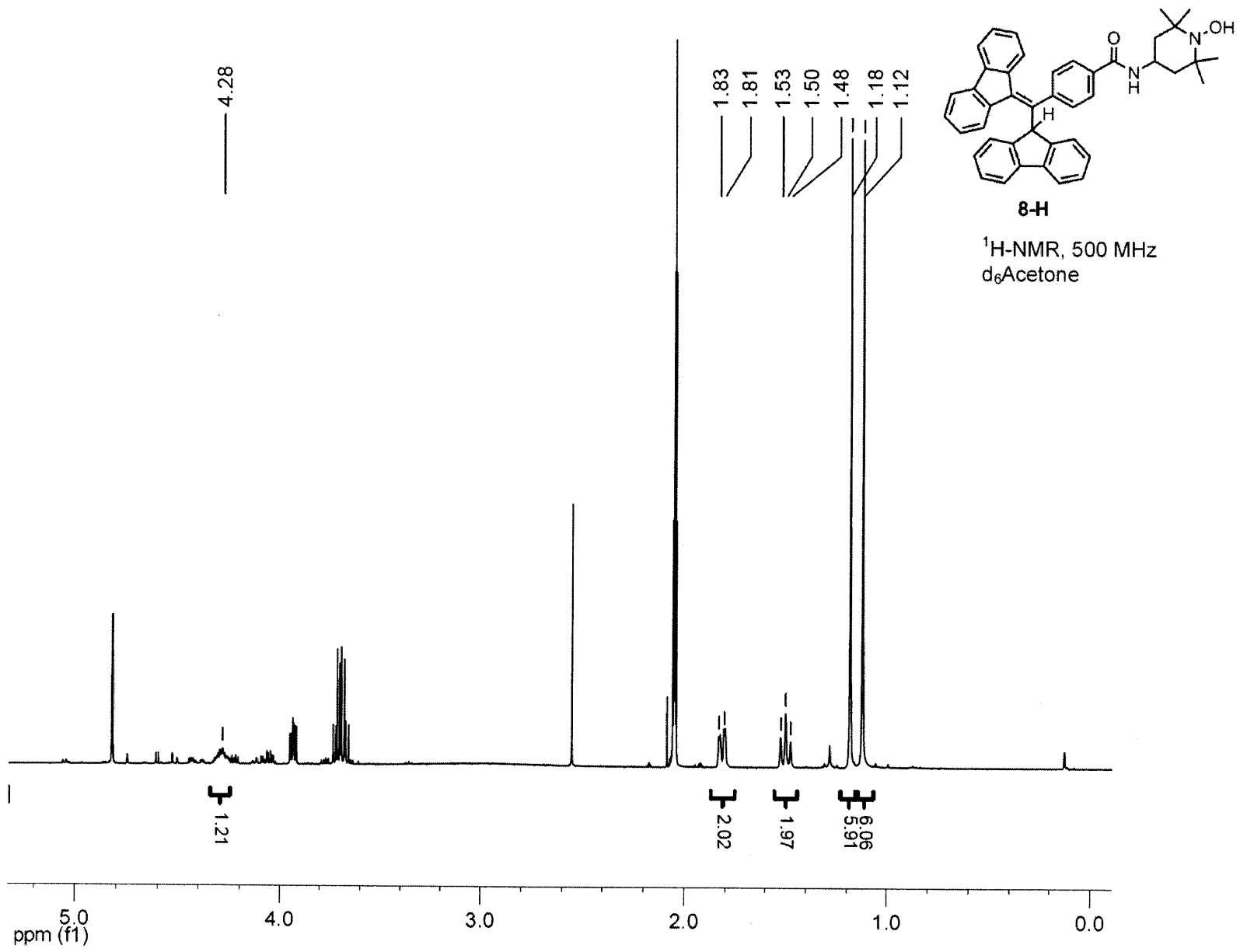


Peak assignment for compound 7 in ppm based on NOE-measurement and gCOSY (next page).

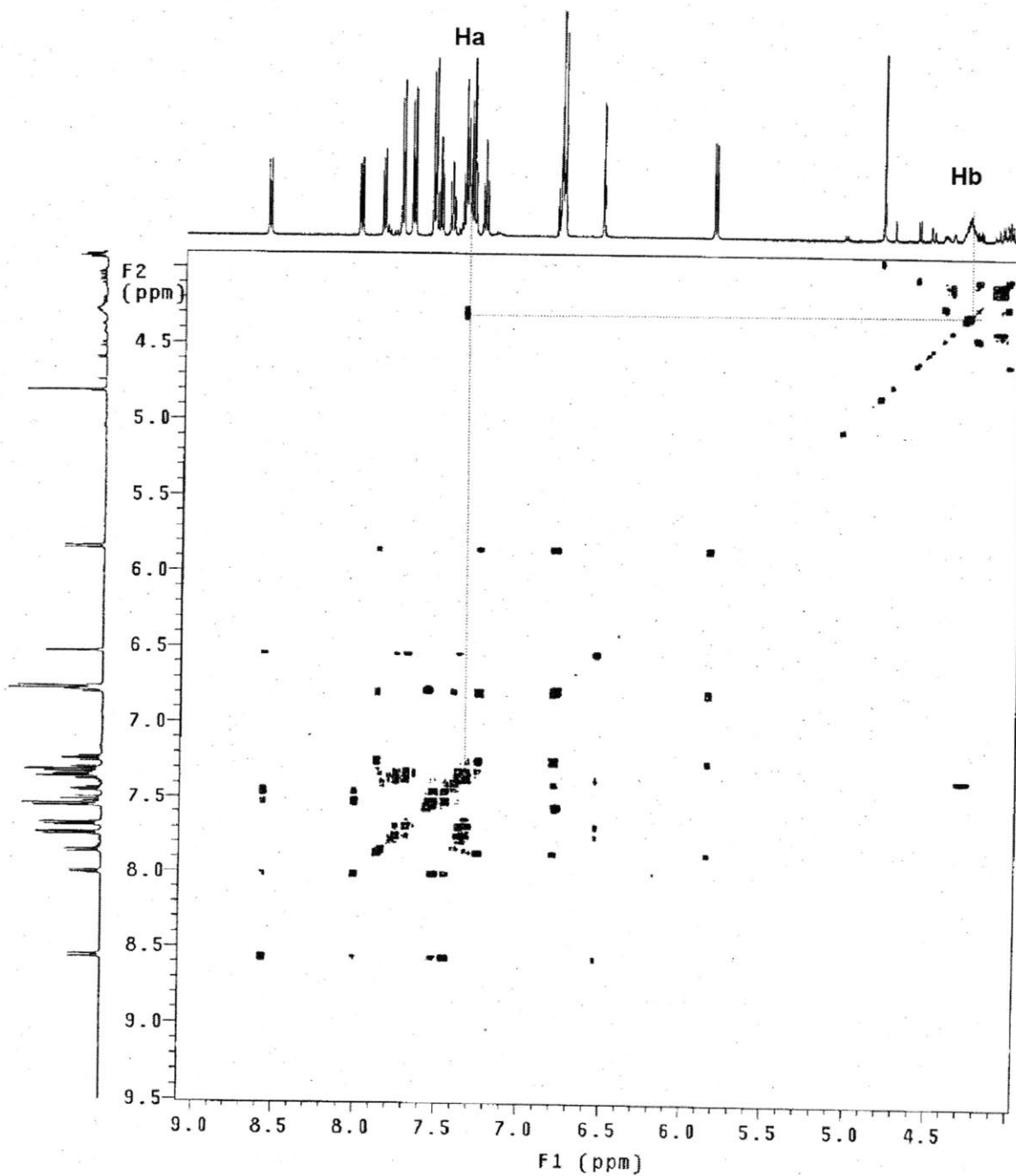
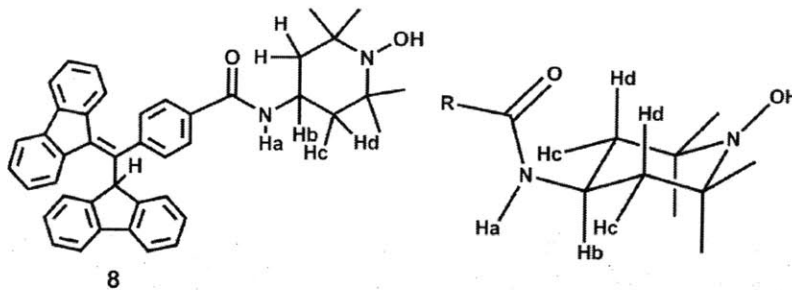
¹H-gCOSY-NMR, 500 MHz (see previous page for assignment of peaks).
d₈-Tetrahydrofuran



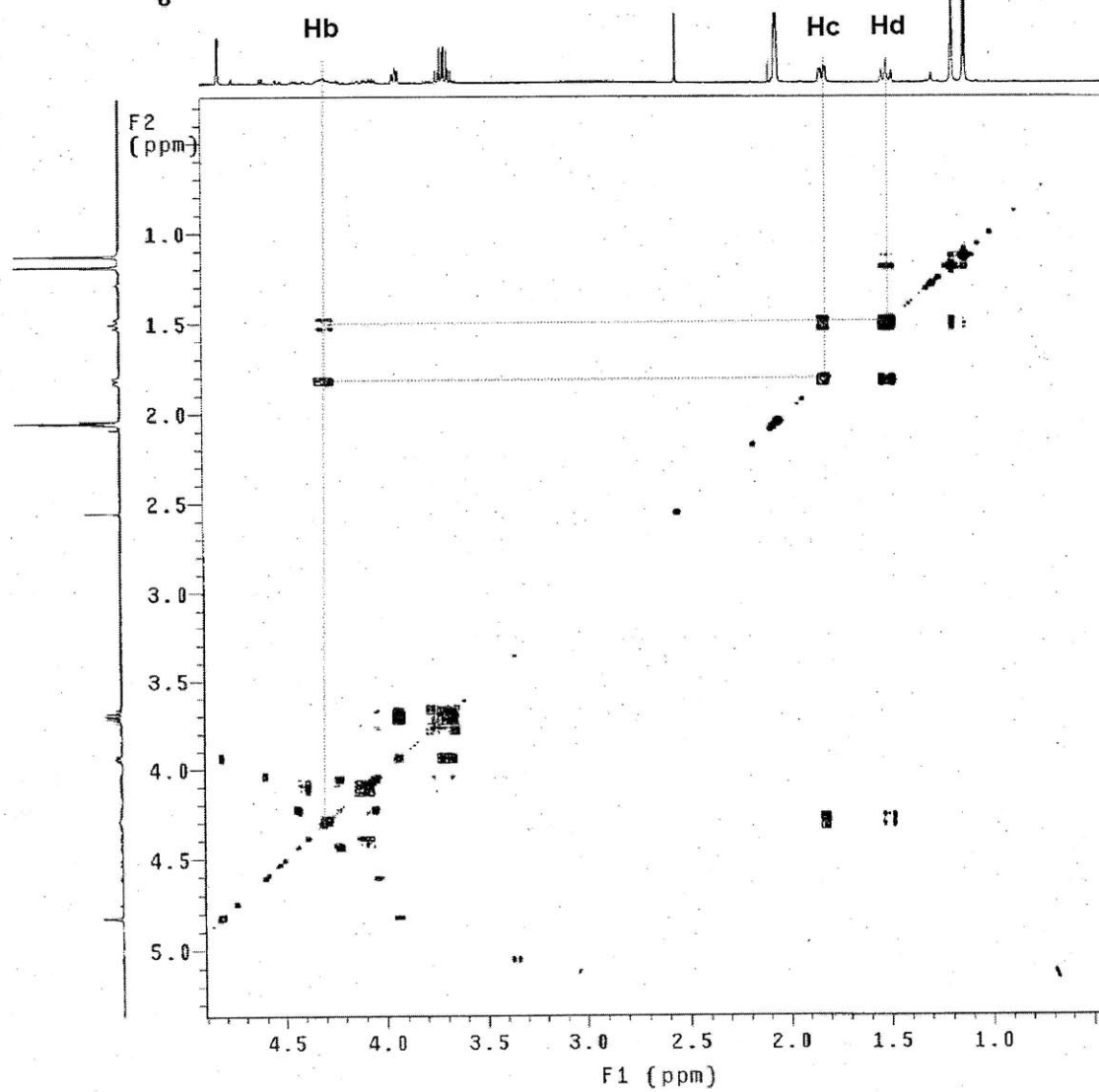
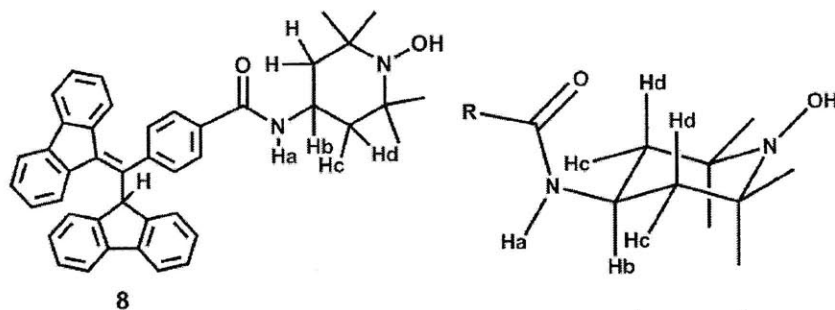


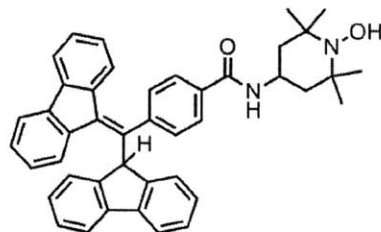
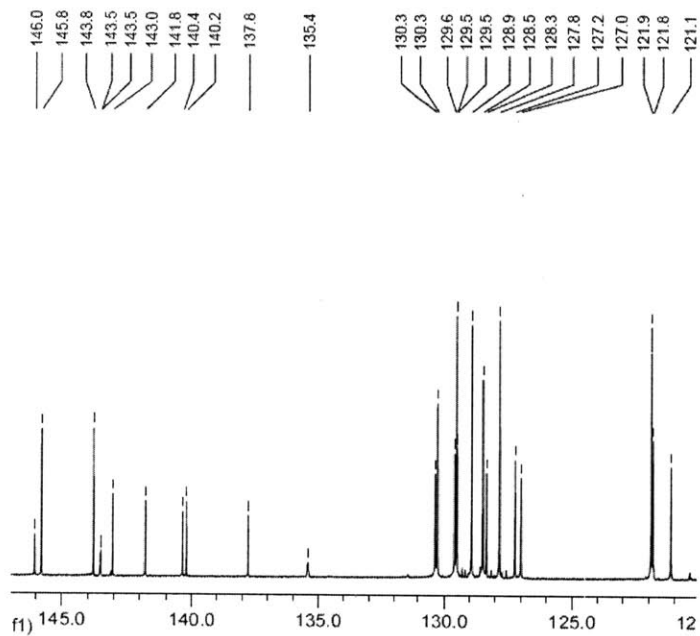


gCOSY NMR, 500 MHz
d₆-Acetone



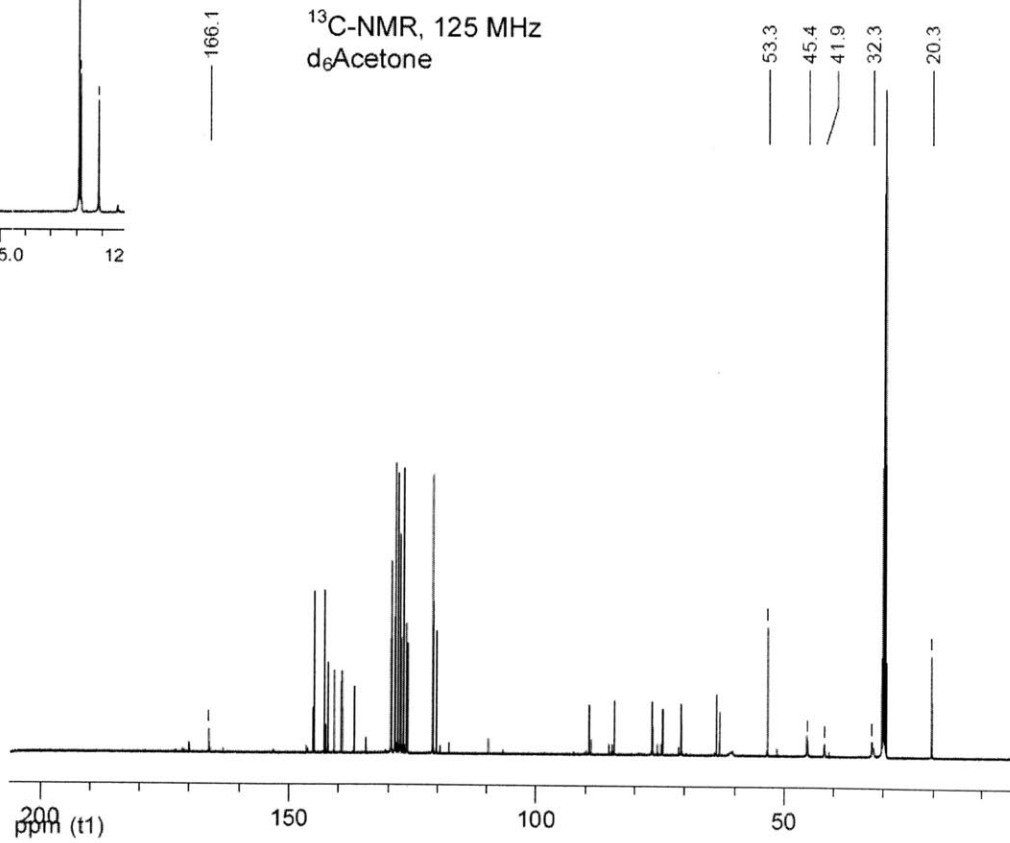
gCOSY NMR, 500 MHz
d₆Acetone

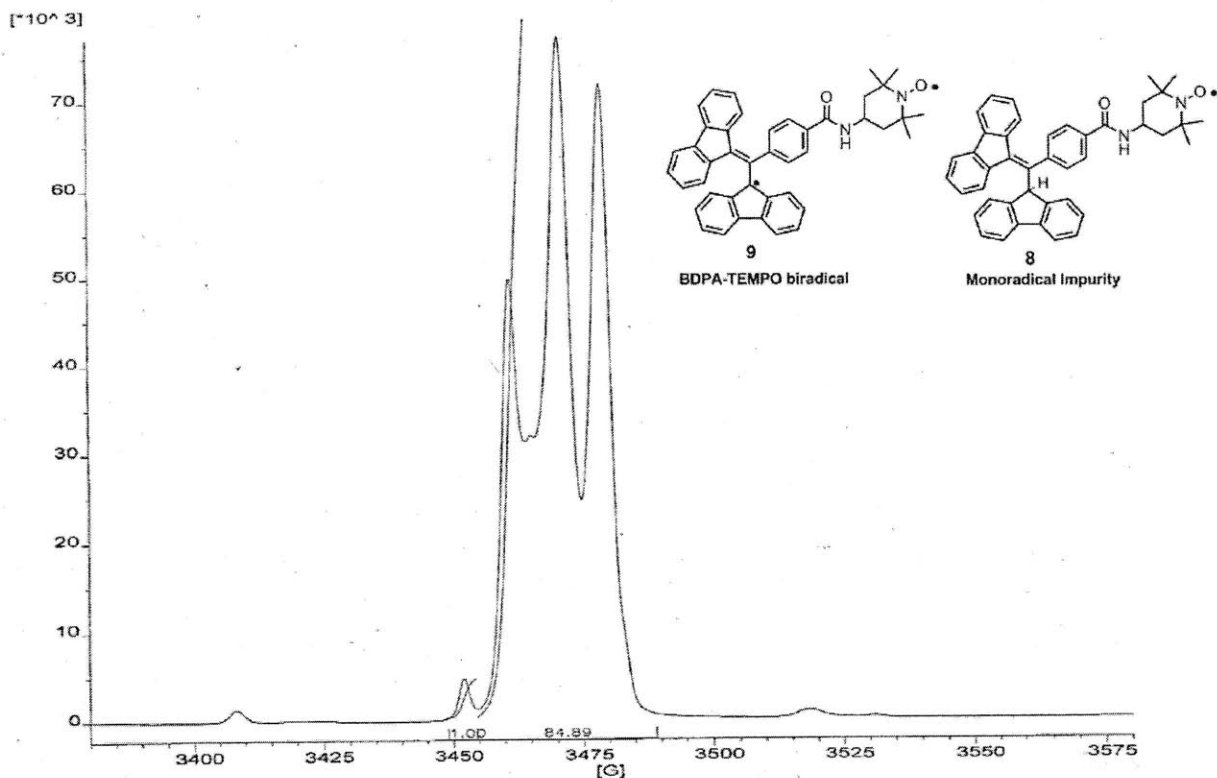




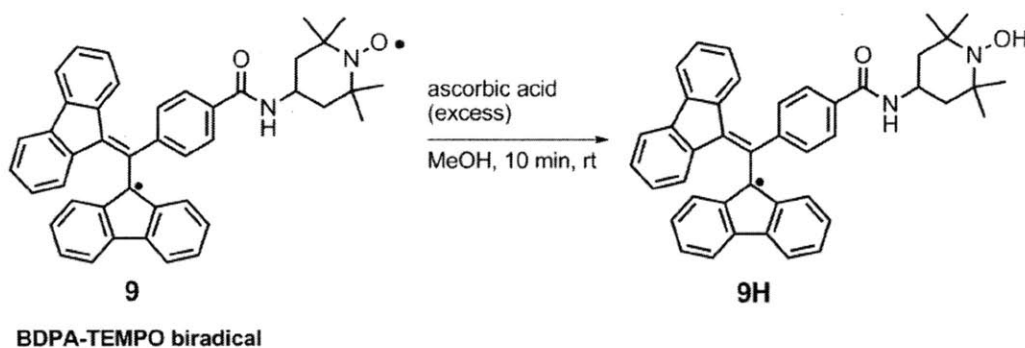
8-H

¹³C-NMR, 125 MHz
d₆Acetone

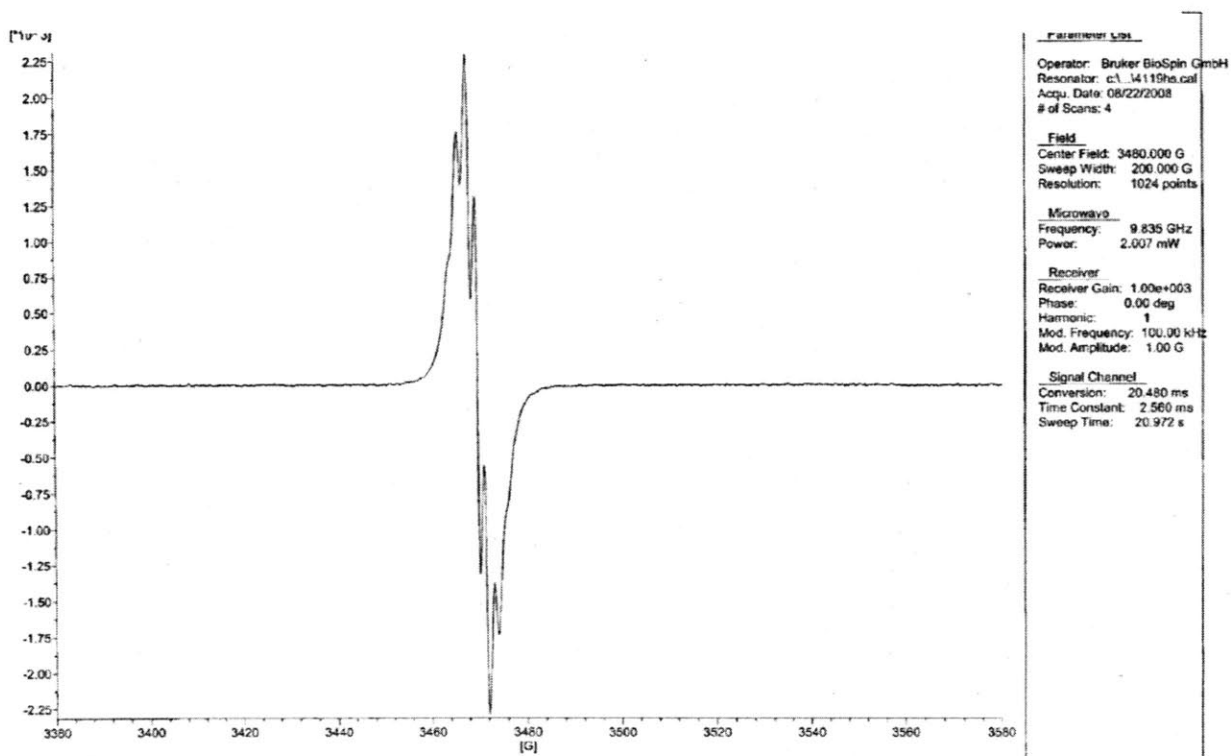




9 GHz EPR of **9** is shown above. The peak between 3450-3455 G, which is attributed to the monoradical impurity, is integrated and given the arbitrary value 1.00. The rest of the middle portion, which contains most of the biradical signal and two-thirds of the impurity signal, integrates to 84.89. The smaller integral represents one-third of the impurity's signal because it represents one of the three peaks of the triplet. Therefore, the portion of the larger intergral that is due to the biradical is 82.89 (84.89 – 2.00). Each biradical has two spins and therefore gives twice the signal compared to the monoradical impurity. Therefore, to compare on a molar basis the biradical's signal must be divided by 2, giving 41.45. The percentage of monoradical impurity is therefore $(3.00/(3.00 + 41.45)) \times 100 = 6.7 \%$ and percentage of the biradical is $(41.45/(3.00 + 41.45)) \times 100 = 93.3 \%$ based on integration of the EPR signal. Experimental parameters: rt, microwave power 2 mW, sweep width 20 mT, modulation amplitude 10 mT.



Below is the 9 GHz solution EPR spectrum of **9H**, which is formed when the BDPA-TEMPO biradical is treated with excess ascorbic acid. Ascorbic acid reduces TEMPO, but does not reduce BDPA. The spectrum shown matches that of BDPA, a narrow linewidth with hyperfine coupling to protons on the fluorene rings.



CHAPTER 3

Synthesis of a Water-Soluble BDPA Radical

Adapted from: Dane, E. L.; Swager, T. M. *J. Org. Chem.* **2010**, *75*, 3533.

3.1 Introduction

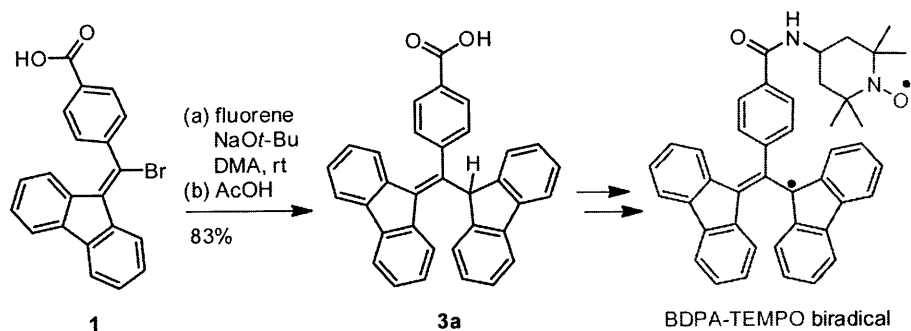
The 1,3-*bis*(diphenylene)-2-phenylallyl (BDPA) radical¹ (Scheme 1, green) is an air-stable, carbon-centered radical that is unique among organic radicals in the extent of delocalization of its unpaired electron. The unpaired electron is predominantly located at the 1- and 3-positions of the compound's allyl core, but is further stabilized by delocalization into the two biphenyl ring systems attached at those positions.² In addition, the propeller-like geometry of the compound has been suggested to sterically shield and further protect the radical from potential reaction partners.³

The BDPA radical's resonance has a narrow line width in high-field EPR, presumably because it is highly delocalized, which makes it attractive for use in certain NMR experiments utilizing dynamic nuclear polarization (DNP).⁴ DNP can be used to increase the signal-to-noise ratio in NMR spectra by transferring the polarization of electrons to nuclei.⁵ Electrons are inherently easier to polarize because of their larger magnetic moment. Unfortunately, BDPA cannot be used in experiments that require an aqueous cosolvent, such as studies using DNP to improve NMR protein structure determination, because of its hydrophobicity.^{5b}

The synthesis of a water-soluble BDPA (WS-BDPA) radical is reported. Previous syntheses of BDPA derivatives have not focused on imparting water solubility.^{1b,3a,6} However, there are several reports of water-soluble derivatives of the triarylmethyl (trityl) radical.⁷ In addition to their use in DNP-NMR, some water-soluble trityl derivatives have been used as EPR probes for oxygen concentration and pH, which is a possible application of water-soluble BDPA derivatives.⁸

3.2 Synthesis

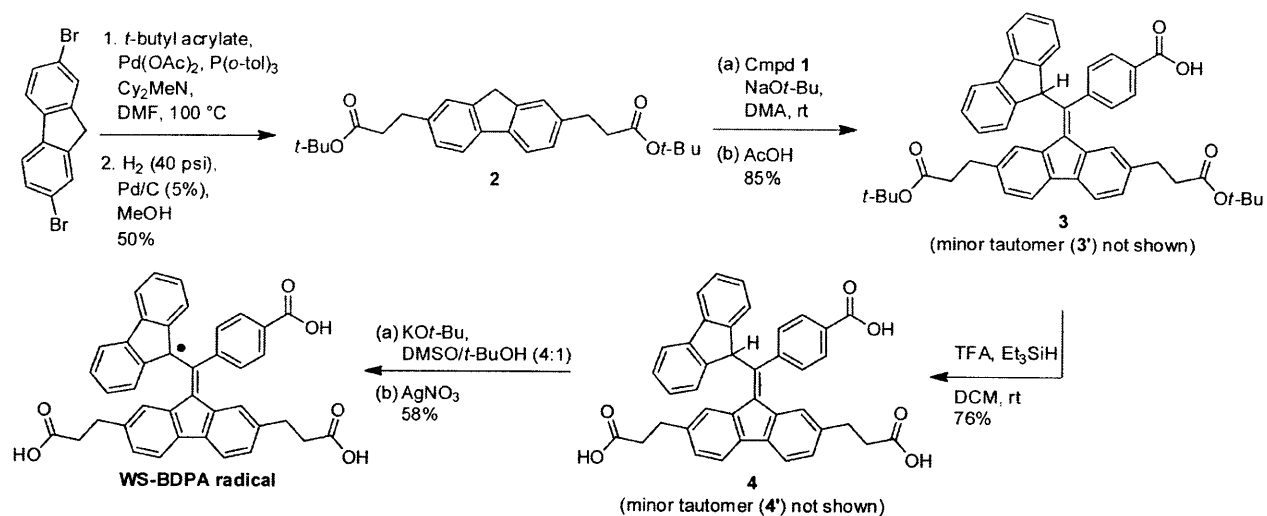
Building on the previously reported synthesis of a BDPA-TEMPO biradical⁹ (Scheme 1, also Chapter 2), the conjugate addition of a fluorene anion to compound **1** became the crucial transformation in our route to WS-BDPA. Compound **1** contains a carboxylic acid at the *para*-position of its phenyl ring that can aid in aqueous solubility. It was reasoned that the addition of two additional carboxylic acids, masked as esters, at the 2- and 7-positions of the fluorene nucleophile



Scheme 1. Synthesis of a BDPA-TEMPO Biradical

would greatly improve the solubility of the resultant BDPA radical in polar solvents. However, it was observed that adding electron-withdrawing groups to fluorene slows the conjugate addition. For example, when 2,7-dibromofluorene ($pK_a = 17.9$ in DMSO) is used as the nucleophile instead of fluorene ($pK_a = 22.6$ in DMSO)¹⁰ the required reaction time increases from 1 hour to 24 hours. The stabilization of the fluorene carbanion results in decreased nucleophilicity and less driving force to form the more stabilized BDPA carbanion ($pK_a = 14$)¹¹. As a result, a fluorene with esters directly attached would likely not be a good reaction partner with **1**. A fluorene derivative with a saturated carbon between the aromatic ring system and the ester would likely have the desired nucleophilicity at the 9-position, but its benzylic protons located alpha to an ester could be deprotonated under the reaction conditions. The simplest route to separate the esters from the conjugated system and still maintain selectivity for deprotonation at the 9-position of the fluorene ring system was to introduce an ethylene linker, as in **2** (protons alpha to the ester in **2** have a $pK_a \approx 30$ in DMSO¹²).

Diester **2** was synthesized in moderate yield from 2,7-dibromofluorene and *tert*-butyl acrylate via a Heck reaction¹³ followed by hydrogenation (Scheme 2). The reaction conditions for the addition of **2** to **1** required adjustment from those of the previous procedure (see Chapter 2).⁹ The slow addition of **2** to a stirring solution of **1** and excess sodium *tert*-butoxide in dimethylacetamide (DMA) improved yields, as compared to the previous procedure in which **1** was added to a solution of the fluorene anion. Maintaining a low concentration of fluorene anion inhibits side reactions. In



Scheme 2. Synthesis of a water-soluble BDPA radical.

addition, freshly prepared sodium *tert*-butoxide¹⁴ was superior to the commercially available material, likely because it contained less sodium hydroxide and therefore caused less unwanted ester cleavage. In this regard, the use of dry DMA was also important. After protonation and purification, the product was isolated as a 2:1 mixture of tautomers.

The tautomers have distinct ¹H-NMR spectra, as shown in Figure 1. Previously reported NMR experiments and an X-ray crystal structure of **3a** suggest the origin of the signals outside the normal range of aromatic protons, specifically those above 8.0 ppm and below 6.0 ppm.⁹ The upfield shift in signals H_c and H_{c'} is caused by an interaction with the magnetic field of the nearby phenyl ring. The downfield signals (H_B, H_{B'}) result from a steric interaction with H_A and H_{A'}.¹⁵ An NOE of 20% was measured between the analogous protons in **3a**.⁹ To prepare triacid **4**, removal of the *tert*-butyl groups is achieved with trifluoroacetic acid in dichloromethane with the addition of triethylsilane as a carbocation trap.¹⁶ The acidic conditions do not cause a change in the ratio of tautomers in **4** as compared to **3**.

In order to generate the radical by one-electron oxidation, compound **4** was deprotonated to form the tetra-anion (see Figure 2, blue solution). A large excess (20 equiv) of potassium *tert*-butoxide in a 4:1 solution of DMSO/*tert*-butyl alcohol provided the best results. Because excess base can cause reduction of the radical back to the carbanion, the amount of oxidant had to be increased

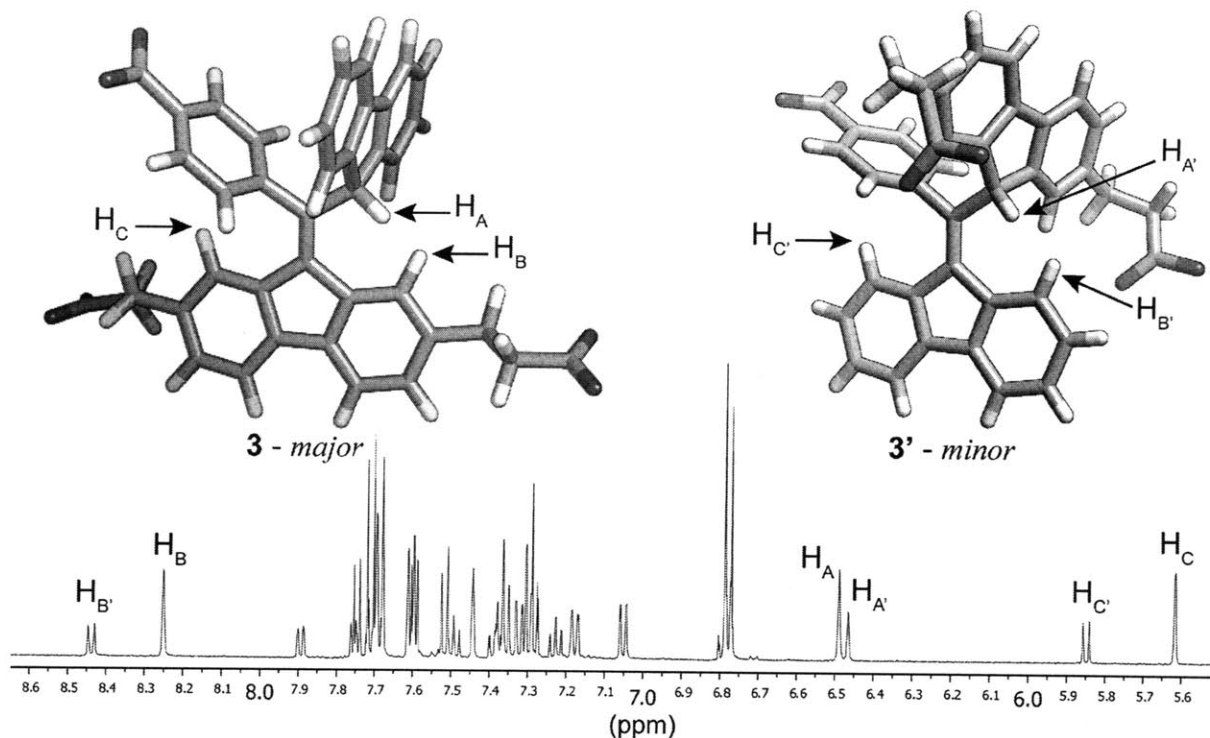


Figure 1.

Molecular models of **3/3'** (*tert*-butyl groups have been omitted for clarity) and aromatic region of $^1\text{H-NMR}$ spectrum.

to ensure complete oxidation. Addition of the oxidant was quickly followed by a dilution of the reaction mixture with acidic water ($\text{pH} = 2$), and subsequent extraction of the triacid into diethyl ether. The isolated red-brown powder showed no $^1\text{H-NMR}$ signals at a concentration of 20 mM in d_4 -methanol beyond those of the solvent and water, as would be expected for a paramagnetic compound. HRMS and IR agreed with the proposed structure. As shown in Figure 2, in a glycerol and water solution (3:2) the radical has a strong absorption in the visible region ($\lambda_{\text{max}} = 496 \text{ nm}$) and a weak absorption in the near-infrared region ($\lambda_{\text{max}} = 867 \text{ nm}$). BDPA in dichloromethane has similar absorbance maxima, which are 485 nm and 859 nm, respectively.^{1b,3a}

3.3 EPR studies

The solubility of the radical in aqueous solution (PBS buffer, $\text{pH} = 8.0$) was approximately 1.0 mM. Because the material was designed for use in DNP-NMR experiments dealing

with biomolecules, the solubility of the radical was tested in a 3:2 solution of glycerol and water, a solvent mixture favored for those experiments.^{5b} The radical was soluble at 1 mM at pH =7, but required the addition of sodium bicarbonate to be soluble at 10 mM (pH = 8). Figure 3 shows the 9 GHz EPR spectrum of WS-BDPA in glycerol/water beneath the spectrum of BDPA in toluene. The radicals have the same g-value ($g = 2.003$) and a similar coupling pattern (see Section 3.6 for simulated spectrum).^{1b,2,17} In addition, the radical was persistent at room temperature both in the solid-state and in solution, but detailed studies of its stability as compared to BDPA have not yet been performed.

In conclusion, the design and synthesis of a water-soluble derivative of the BDPA radical is reported. The pair of tautomers that are a consequence of constructing the BDPA skeleton with non-identical fluorene rings are characterized. Finally, the generation of the stable radical and its characterization by EPR spectroscopy in a water/glycerol solution are reported.

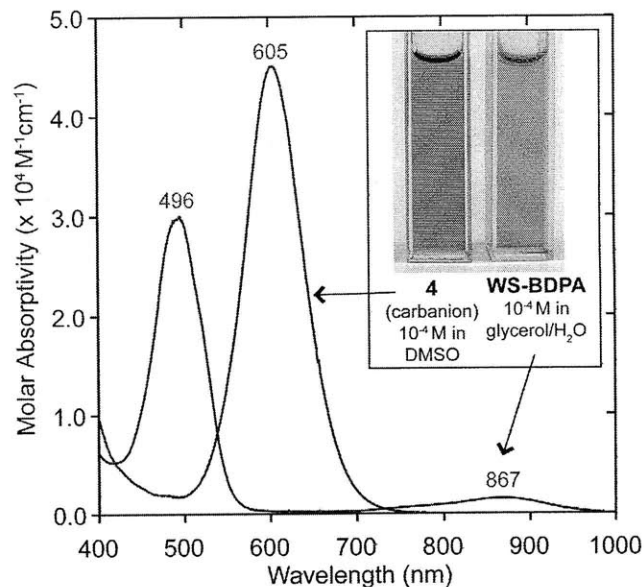


Figure 2. Absorption spectra of carbanion **4** in DMSO and WS-BDPA in 3:2 glycerol/water.

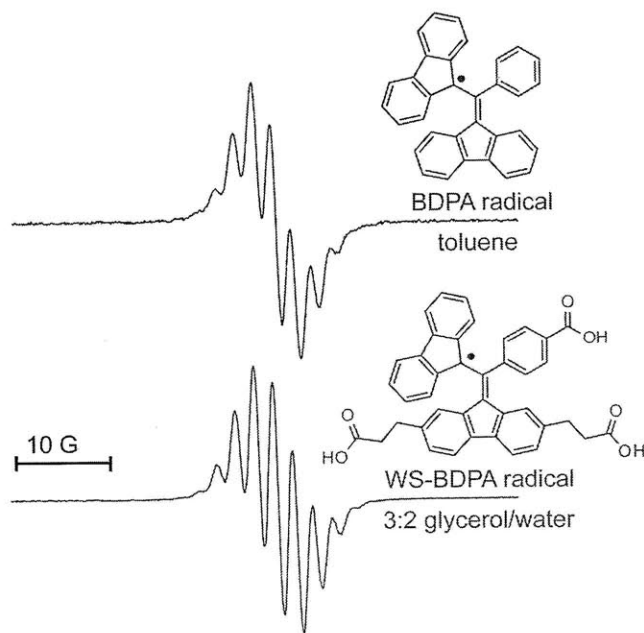


Figure 3. 9 GHz EPR of BDPA (0.1 mM, 4 mm diameter tube) in toluene and WS-BDPA (10 mM, 150 μ L flat cell) in glycerol water. Experimental parameters: rt, 2 mW, modulation amplitude 10 mT.

3.4 Experimental Section

Materials. All chemicals, reagents, and solvents were used as received from commercial sources without further purification except *tert*-butyl alcohol, which was distilled over calcium hydride onto oven-activated 4-Å molecular sieves, dimethylacetamide, which was dried by distilling over barium oxide onto oven-activated 4-Å molecular sieves and dimethylsulfoxide, which was dried over oven-activated 4-Å molecular sieves.

Instrumentation. Proton nuclear magnetic resonance (^1H NMR) spectra and carbon nuclear magnetic resonance (^{13}C NMR) spectra were recorded on an Inova-500 (500 MHz) NMR spectrometer. The mass spectrometry data were obtained at the MIT mass spectrometry facility, using a Bruker Daltonics APEX II 3T FT-ICR-MS.

di-*t*-butyl 3,3'-(9H-fluorene-2,7-diyl)dipropionate (2). To a 250 mL flask were added 5.00 g (15.4 mmol, 1.0 equiv) of 2,7-dibromofluorene, 0.087 g (0.390 mmol, 2.5 mol %) palladium acetate, 0.470 g (0.780 mmol, 5 mol %) tri(*o*-tol)phosphine, 5 mL of dicyclohexylmethylamine, and 100 mL of anhydrous dimethylformamide. The solution was degassed with bubbling argon and 7.00 mL (6.13 g, 47.8 mmol, 3.1 equiv) of *t*-butyl acrylate was added. After heating to 80 °C for 4 hours and cooling overnight, excess water was added and the resulting solid was filtered, washed with water, and dried on the filter pad. The material was suspended in 150 mL of methanol and 1.00 g of 5% Pd/C was added. Hydrogenation was performed overnight in a Parr Hydrogenator at 40 PSI with shaking. After removal of the methanol, the crude material was chromatographed using silica gel and eluted with increasingly polar mixtures of hexane and ethyl acetate to yield 3.25 g (50%) of a white powder. ^1H NMR (500 MHz, CD_2Cl_2 , δ) (all coupling constants (*J*) in Hz): 7.64 (d, *J* = 7.5, 2H), 7.36 (s, 2H), 7.18 (d, *J* = 8.0, 2H), 3.82 (s, 2H), 2.94 (t, *J* = 7.5, 4H), 2.54 (t, *J* = 7.5, 4H), 1.39 (s, 18 H); ^{13}C NMR (126 MHz, CD_2Cl_2 , δ) 172.6, 144.1, 140.2, 140.0, 127.4, 125.6, 119.9, 80.6, 37.8, 37.2, 31.8, 28.4; HRMS (ESI): calcd for $\text{C}_{27}\text{H}_{34}\text{O}_4\text{Na}$ [$\text{M} + \text{Na}$] $^+$:

445.2349; found, 445.2329. FT-IR (KBr, thin film) ν_{\max} (cm⁻¹): 2978, 1729(s), 1454, 1365, 1257, 1133, 1009, 956, 817, 741; mp 99–101 °C (methanol).

4-((2,7-bis(3-(*t*-butoxy)-3-oxopropyl)-9H-fluoren-9-ylidene)(9H-fluoren-9-yl)methyl)benzoic acid (3) and 4-((2,7-bis(3-(tert-butoxy)-3-oxopropyl)-9H-fluoren-9-yl)(9H-fluoren-9-ylidene)methyl)benzoic acid (3'). To a 100 mL flask were added 0.100 g (0.265 mmol, 1.0 equiv) of bromide **2**, 0.255 g (2.65 mmol, 10 equiv) of sodium *t*-butoxide, and 6.0 mL of degassed, anhydrous dimethylacetamide (DMA). The solution was cooled to 0 °C. In a separate flask, 0.168 g (0.398 mmol, 1.5 equiv) of ester **1** was dissolved in 10 mL of DMA and this solution was slowly added to the first flask over a period of 20 minutes. The reaction became deep blue. After stirring at room temperature for 2 hours, excess (3 mL) of acetic acid was added, turning the reaction from deep blue to light yellow. Additional water was added and the solution was extracted with diethyl ether (3 x 30 mL). The ether was washed twice with water and once with brine and dried over sodium sulfate. After removal of the solvent, the crude material was purified by silica gel column chromatography using increasingly polar mixtures of ethyl acetate in dichloromethane, after which 0.163 g (85%) of a light yellow powder was isolated. ¹H NMR (500 MHz, CD₂Cl₂, δ) (all coupling constants (*J*) in Hz): Compound **3**: 8.25 (s, 1H), 7.75 (d, *J* = 8.0, 1H), 7.71 (d, *J* = 8.0, 2H), 7.69 (d, *J* = 8.0, 2H), 7.60 (ddd, *J* = 8.0, 1.0, 0.5, 2H), 7.59 (d, *J* = 8.0, 1H), 7.36 (td, *J* = 8.0, 1.0, 2H), 7.32 (dd, *J* = 8.0, 1.0, 1H), 7.29 (td, *J* = 8.0, 1.0, 2H), 7.05 (dd, *J* = 8.0, 1.0, 1H), 6.78 (d, *J* = 8.0, 2H), 6.49 (s, 1H), 5.62 (s, 1H), 2.95 (t, *J* = 7.5, 2H), 2.54 (t, *J* = 7.5, 2H), 2.45 (t, *J* = 7.5, 2H), 2.07 (t, *J* = 7.5, 2H), 1.35 (s, 9H), 1.30 (s, 9H); Compound **3'**: 8.44 (ddd, *J* = 8.0, 1.0, 0.5, 1H), 7.89 (ddd, *J* = 8.0, 1.0, 0.5, 1H), 7.75 (ddd, *J* = 8.0, 1.0, 0.5, 1H), 7.69 (d, *J* = 8.0, 2H), 7.52 (d, *J* = 8.0, 2H), 7.49 (td, *J* = 8.0, 1.0, 1H), 7.44 (s, 2H), 7.38 (td, *J* = 8.0, 1.0, 1H), 7.23 (td, *J* = 8.0, 1.0, 1H), 7.18 (d, *J* = 8.0, 2H), 6.79 (td, *J* = 8.0, 1.0, 1H), 6.78 (d, *J* = 8.0, 2H), 6.47 (s, 1H), 5.85 (d, *J* = 8.0, 1H), 2.90 (t, *J* = 7.5, 4H), 2.49 (t, *J* = 7.5, 4H), 1.35 (s, 18H); ¹³C NMR (126 MHz, CD₂Cl₂, δ): 172.5, 172.4, 172.3, 171.6, 171.5, 145.2, 144.9, 144.6, 144.4, 144.0, 143.5, 142.5, 141.8, 140.7, 140.6, 140.5, 140.4, 139.4 (2), 139.3, 139.0, 138.5, 136.7, 136.6, 130.0, 129.5, 129.2, 129.0, 128.6, 128.5

(3), 128.3, 128.2, 128.0, 127.7, 127.1, 126.5, 126.3, 125.9, 125.8 (2), 125.7, 120.6, 120.5, 120.2, 119.7, 119.3, 80.7 (2), 80.4, 52.8, 52.7, 37.8 (2), 36.7, 32.1, 31.7, 31.6, 28.3, 28.2; HRMS (ESI): calcd for $C_{48}H_{45}O_6$ [M-H]: 717.3222; found, 717.3206. FT-IR (KBr, thin film) ν_{\max} (cm⁻¹): 2977, 2930, 1727(s), 1694(s), 1607, 1447, 1419, 1367, 1260, 1148, 1018, 846, 822, 736.

3,3'-(9-((4-carboxyphenyl)(9H-fluoren-9-yl)methylene)-9H-fluorene-2,7-diyl)dipropionic acid (4) and 3,3'-(9-((4-carboxyphenyl)(9H-fluoren-9-ylidene)methyl)-9H-fluorene-2,7-diyl)dipropionic acid (4'). To a 50 mL flask were added 0.150 g (0.209 mmol, 1.0 equiv) of 3, 9.0 mL of anhyd CH₂Cl₂, 1 drop triethylsilane, and 4.5 mL of TFA. The reaction mixture was stirred under an argon atmosphere for 30 minutes, after which excess sodium bicarbonate solution was added. The aqueous layer was washed with diethyl ether (2 x 10 mL), and acidified with 2M HCl to a pH of 1. The aqueous layer was extracted with diethyl ether (3 x 10 mL). The combined ether layers were washed with brine and dried over sodium sulfate. Removal of the solvent followed by drying under high vacuum yielded 0.0960 g (0.158 mmol, 76 %) of an off-white powder. ¹H NMR (500 MHz, *d*₄-methanol, δ) (all coupling constants(*J*) in Hz): Compound 4: 8.25 (s, 2H), 7.73 (d, *J* = 8.0, 1H), 7.64 (d, *J* = 8.0, 2H), 7.63 (d, *J* = 8.0 Hz, 2H), 7.58 (d, *J* = 8.0, 4H), 7.32 (m, 3H), 7.25 (t, *J* = 8.0, 2H), 7.04 (d, *J* = 16.0, 1H), 6.71 (d, *J* = 8.5, 2H), 6.45 (s, 1H), 5.64 (s, 1H), 2.98 (t, *J* = 8.0, 2H), 2.62 (t, *J* = 8.0, 2H), 2.48 (t, *J* = 8.0, 2H), 2.17 (t, *J* = 8.0, 2H). Compound 4': 8.41 (d, *J* = 8.0 Hz, 1H), 7.87 (d, *J* = 7.5, 1H), 7.72 (d, *J* = 7.5, 1H), 7.64 (d, *J* = 8.0, 2H), 7.48 (d, *J* = 8.0, 2H), 7.46 (t, *J* = 8.0, 1H), 7.43 (s, 2H), 7.36 (t, *J* = 8.0, 1H), 7.19 (t, *J* = 8.0, 1H), 7.16 (d, *J* = 8.0, 2H), 6.74 (t, *J* = 8.0, 1H), 6.71 (d, *J* = 8.0, 2H), 6.42 (s, 1H), 5.85 (d, *J* = 8.0, 1H), 2.92 (t, *J* = 8.0, 4H), 2.57 (t, *J* = 8.0, 4H). ¹³C NMR (126 MHz, *d*₄-methanol and CDCl₃, δ): 176.3, 176.1, 175.8, 169.7, 144.9, 144.6, 144.3, 144.2, 144.0, 142.8, 142.1, 140.9, 140.4 (2), 139.7, 139.4, 139.2, 138.9, 136.8, 136.7, 129.8 (2), 129.6, 129.5, 129.3, 129.2, 128.4, 127.8, 127.2, 126.5, 126.0, 125.9, 125.7, 120.7 (2), 120.5, 119.9, 119.6, 53.1, 53.0, 36.9, 36.8, 35.8, 32.2, 31.8, 31.6. HRMS (ESI): calcd for $C_{40}H_{29}O_6$ [M-H]: 605.1970; found, 605.1968. FT-IR (KBr, thin film) ν_{\max} (cm⁻¹): 3600-2800

(br), 1700 (s), 1606, 1446, 1417, 1274, 1178, 1017, 824, 734.

WS-BDPA radical. To a 200 mL flask were added 0.040 g (0.066 mmol, 1.0 equiv) of compound **4**, 0.150 g (1.34 mmol, 20 equiv) of sublimed potassium *t*-butoxide, and 50 mL of a 4:1 mixture of DMSO/*t*-BuOH. After 30 minutes, 0.180 g (1.06 mmol, 16.0 equiv) of silver nitrate was added. The solution immediately became brown and was diluted after 1 minute with 400 mL of 0.01 M HCl, and extracted with diethyl ether (3 x 10 mL). The combined organic layers were washed with water (3 x 25 mL) and brine. After drying with sodium sulfate, the solvent was removed. The resulting solid was washed with hexane, and 0.023 g (58%) of a dark red-brown powder was isolated. HRMS (ESI): calcd for C₄₀H₂₉O₆ M⁻: 605.1970; found, 605.1968. FT-IR (KBr, thin film) ν_{\max} (cm⁻¹): 3600-2800 (br), 1708 (s), 1604, 1446, 1417, 1282, 1177, 1018, 824, 730. EPR (9 GHz) [WS-BDPA] = 10 mM in 3:2 glycerol/H₂O, quartz flat cell, g-value = 2.003.

3.5 References

- (1) (a) Koelsch, C. F. *J. Amer. Chem. Soc.* **1957**, *79*, 4439. (b) Kuhn, R.; Neugebauer, F. *A. Monatsh. Chem.* **1964**, *95*, 3.
- (2) Azuma, N.; Ozawa, T.; Yamauchi, J. *Bull. Chem. Soc. Jpn.* **1994**, *67*, 31.
- (3) (a) Breslin, D. T.; Fox, M. A. *J. Phys. Chem.* **1993**, *97*, 13341. (b) Griller, D.; Ingold, K. U. *Acc. Chem. Res.* **1976**, *9*, 13.
- (4) (a) Wind, R. A.; Duijvestijn, M. J.; van der Luat, C.; Manenschijn, A.; Vriend, J. *Prog. Nucl. Magn. Reson. Spectrosc.* **1985**, *17*, 33. (b) Afeworki, M.; Schaefer, J. *Macromolecules* **1992**, *25*, 4092. (c) Becerra, L. R.; Gerfen, G. J.; Temkin, R. J.; Singel, D. J.; Griffin, R. G. *Phys. Rev. Lett.* **1993**, *71*, 3561. (d) Weis, V.; Bennati, M.; Rosay, M.; Griffin, R. G. *J. Chem. Phys.* **2000**, *113*, 6795.

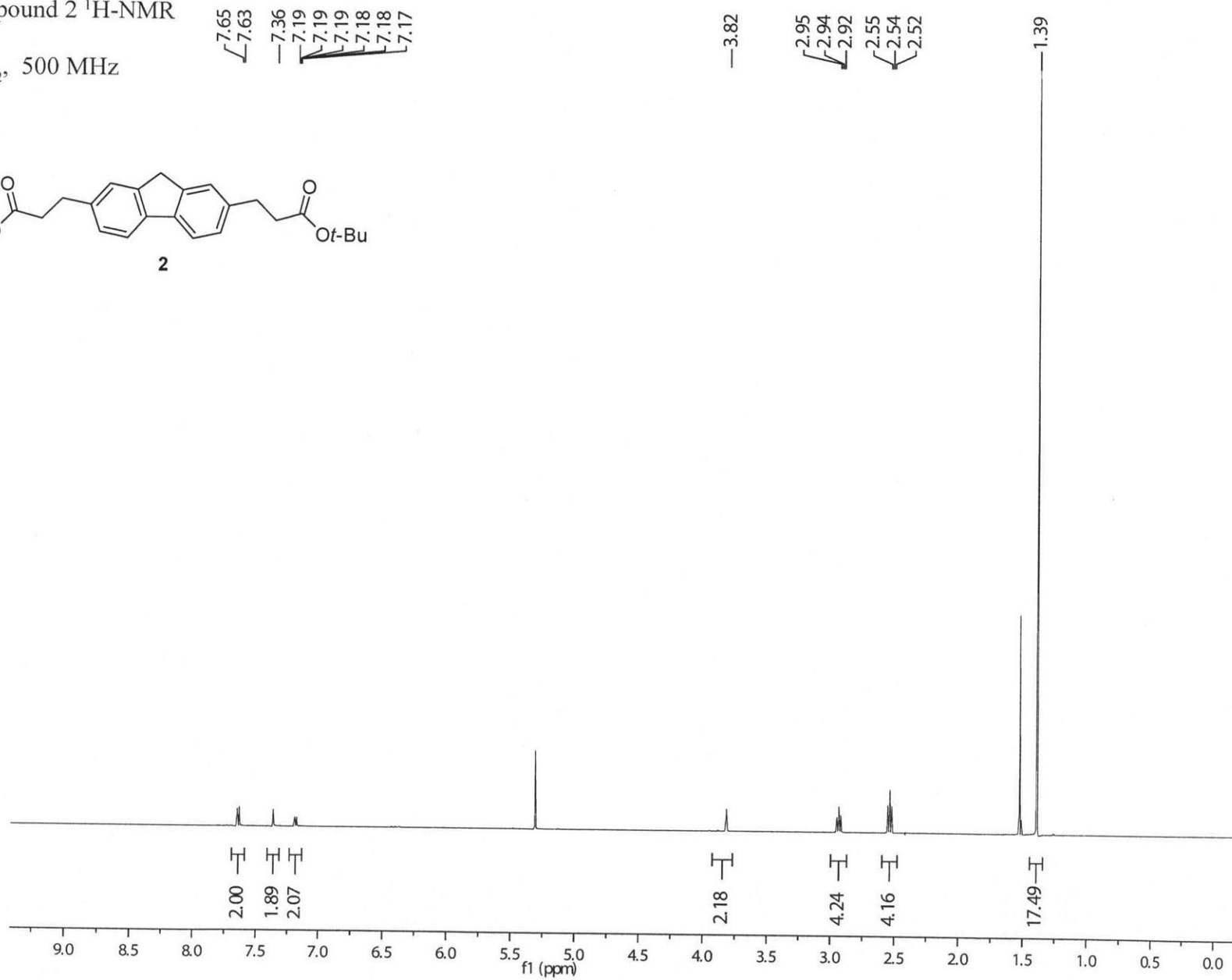
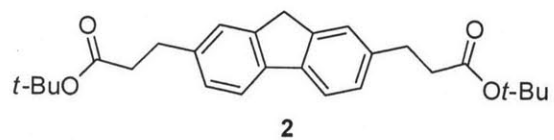
- (5) (a) Barnes, A. B.; Paëpe, G. D.; Wel, P. C. A. v. d.; Hu, K.-N.; Joo, C.-G.; Bajaj, V. S.; Mak-Jurkauskas, M. L.; Sirigiri, J. R.; Herzfeld, J.; Temkin, R. J.; Griffin, R. G. *Appl. Magn. Reson.* **2008**, *34*, 237. (b) Maly, T.; Debelouchina, G. T.; Bajaj, V. S.; Hu, K.-N.; Joo, C.-G.; Mak-Jurkauskas, M. L.; Sigirhi, J. R.; van der Wel, P. C. A.; Herzfeld, J.; Temkin, R. J.; Griffin, R. G. *J. Chem. Phys.* **2008**, *128*, 052211.
- (6) (a) Plater, M. J.; Kemp, S.; Lattmann, E. *J. Chem. Soc., Perkin Trans. 1*, **2000**, 971. (b) Nishide, H.; Yoshioka, N.; Saitoh, Y.; Gotoh, R.; Miyakawa, T.; Tsuchida, E. *J. Macromol. Sci. Pure Appl. Chem.* **1992**, *A29*, 775. (c) Solar, S. L. *J. Org. Chem.* **1963**, *28*, 2911.
- (7) (a) Reddy, T. J.; Iwama, T.; Halpern, H. J.; Rawal, V. H. *J. Org. Chem.* **2002**, *67*, 4635. (b) Bowman, M. K.; Mailer, C.; Halpern, H. J. *J. Magn. Reson.* **2005**, *172*, 254. (c) Roques, N.; Maspoch, D.; Wurst, K.; Ruiz-Molina, D.; Rovira, C.; Veciana, J. *Chem. Eur. J.* **2007**, *12*, 9238. (d) Liu, Y.; Villamena, F. A.; Sun J.; Xu Y.; Dhimitruka, I.; Zweier, J. L. *J. Org. Chem.* **2008**, *73*, 1490. (e) S. Anderson, K. Golman, F. Rise, H. Wikstrom, and L.-G. Wistrand, U.S. Patent No.: 5,530,140, 1996.
- (8) Bobko, A. A.; Dhimitruka, I.; Zweier, J. L.; Khramtsov, V. V. *J. Amer. Chem. Soc.* **2007**, *129*, 7240.
- (9) Dane, E. L.; Maly, T.; Debelouchina, G. T.; Griffin, R. G.; Swager, T. M. *Org. Lett.* **2009**, *11*, 1871.
- (10) Bordwell, F. G.; McCollum, G. J. *J. Org. Chem.* **1976**, *41*, 2391.
- (11) Kuhn, R.; Rewicki, D. *Liebigs Ann. Chem.* **1967**, *706*, 250.
- (12) Zhang, X.-M.; Bordwell, F. G.; Van Der Puy, M.; Fried, H. E. *J. Org. Chem.* **1993**, *58*, 3060.
- (13) Patel, B. A.; Ziegler, C. B.; Cortese, N. A.; Plevyak, J. E.; Zebovitz, T. C.; Terpko, M.; Heck, R. F. *J. Org. Chem.* **1977**, *42*, 3903.
- (14) Sodium *tert*-butoxide was prepared by refluxing sodium with excess freshly distilled *tert*-butyl alcohol followed by evaporation of excess solvent under high vacuum. The material was stored and weighed in a nitrogen glove box.
- (15) Cheney, B. V. *J. Am. Chem. Soc.* **1968**, *90*, 5386.
- (16) Mehta, A.; Jaouhari, R.; Benson, T. J.; Douglas, K. T. *Tett. Lett.* **1992**, *33*, 5441.

- (17) Watanabe, K.; Yamauchi, J.; Ohya-Nishiguchi, H.; Deguchi, Y.; Ishizu, K. *Bull. Inst. Chem. Res., Kyoto Univ.* **1975**, *53*, 161.

3.6 NMR and EPR Spectra

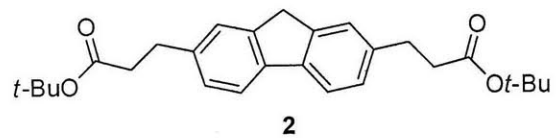
Compound 2 ¹H-NMR

D₂Cl₂, 500 MHz



Compound 2 ¹³C-NMR

D₂Cl₂, 125 MHz



— 172.6

— 144.1

— 140.2

— 140.0

— 127.4

— 125.6

— 119.9

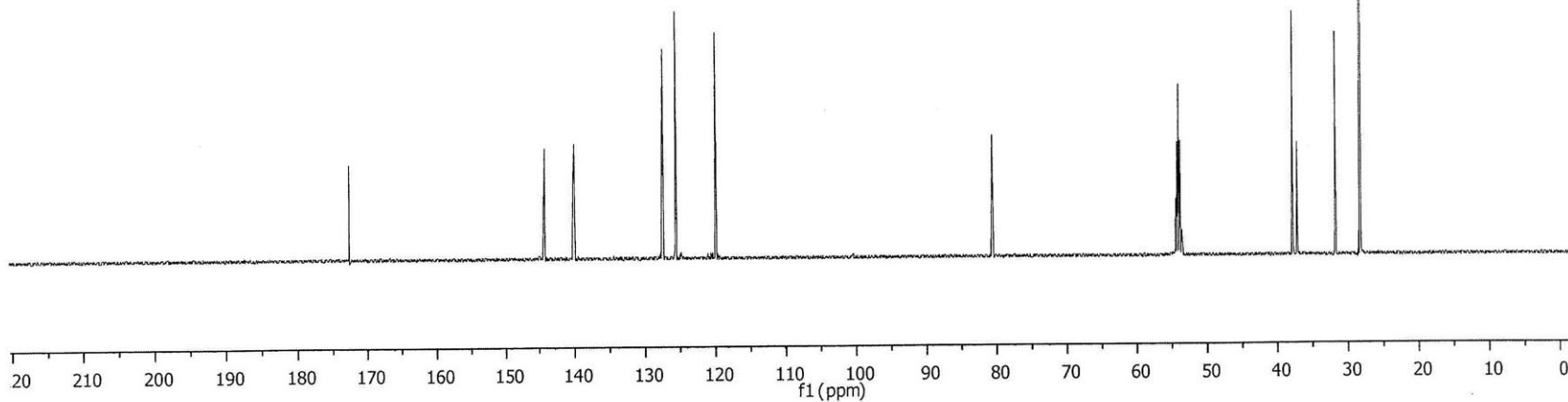
— 80.6

— 37.8

— 37.2

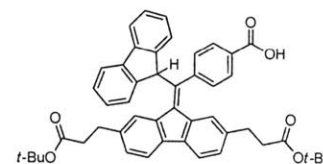
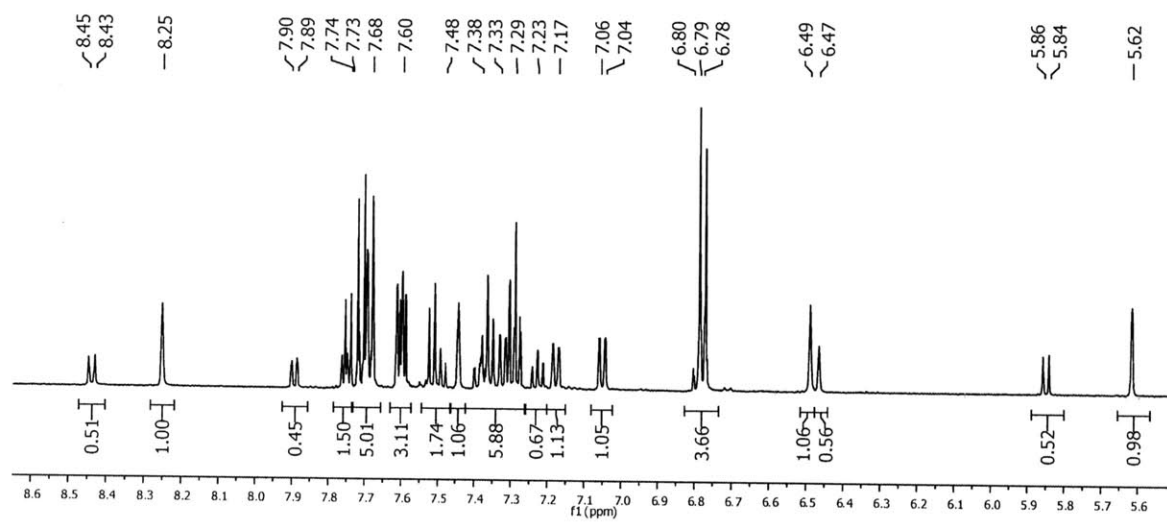
— 31.8

— 28.4

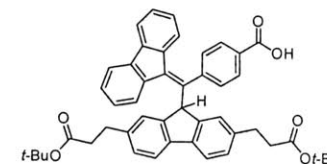
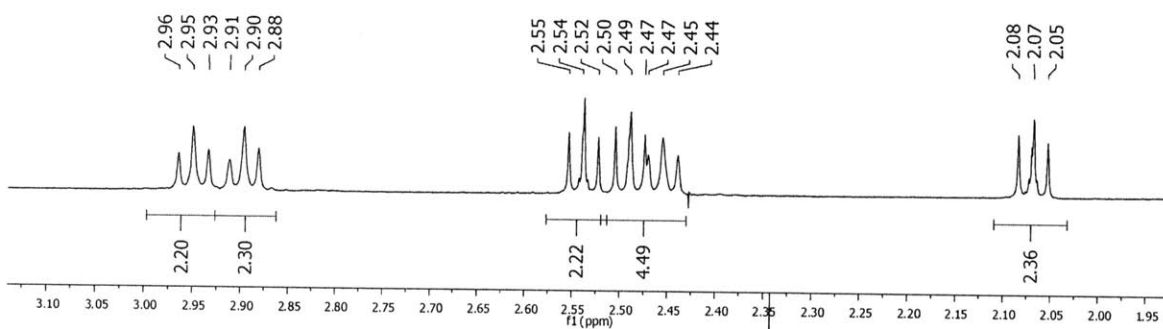


Compound 3 ¹H-NMR

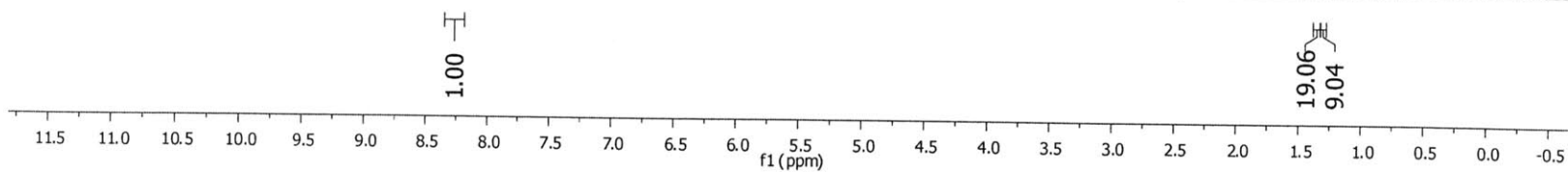
D₂Cl₂, 500 MHz



Integration of 1H = 1.00



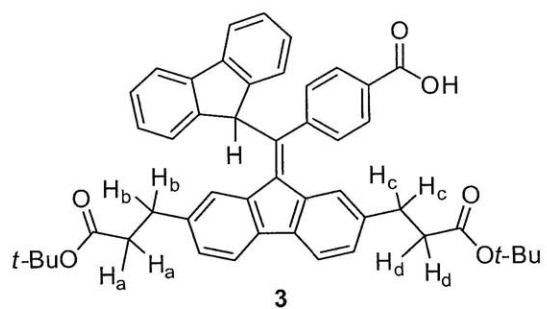
Integration of 1H = 0.50



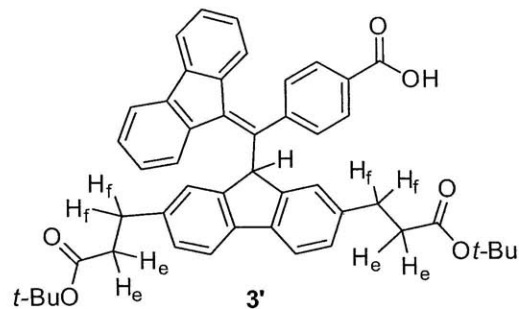
- LL -

Compound 3 g-COSY 2D-NMR

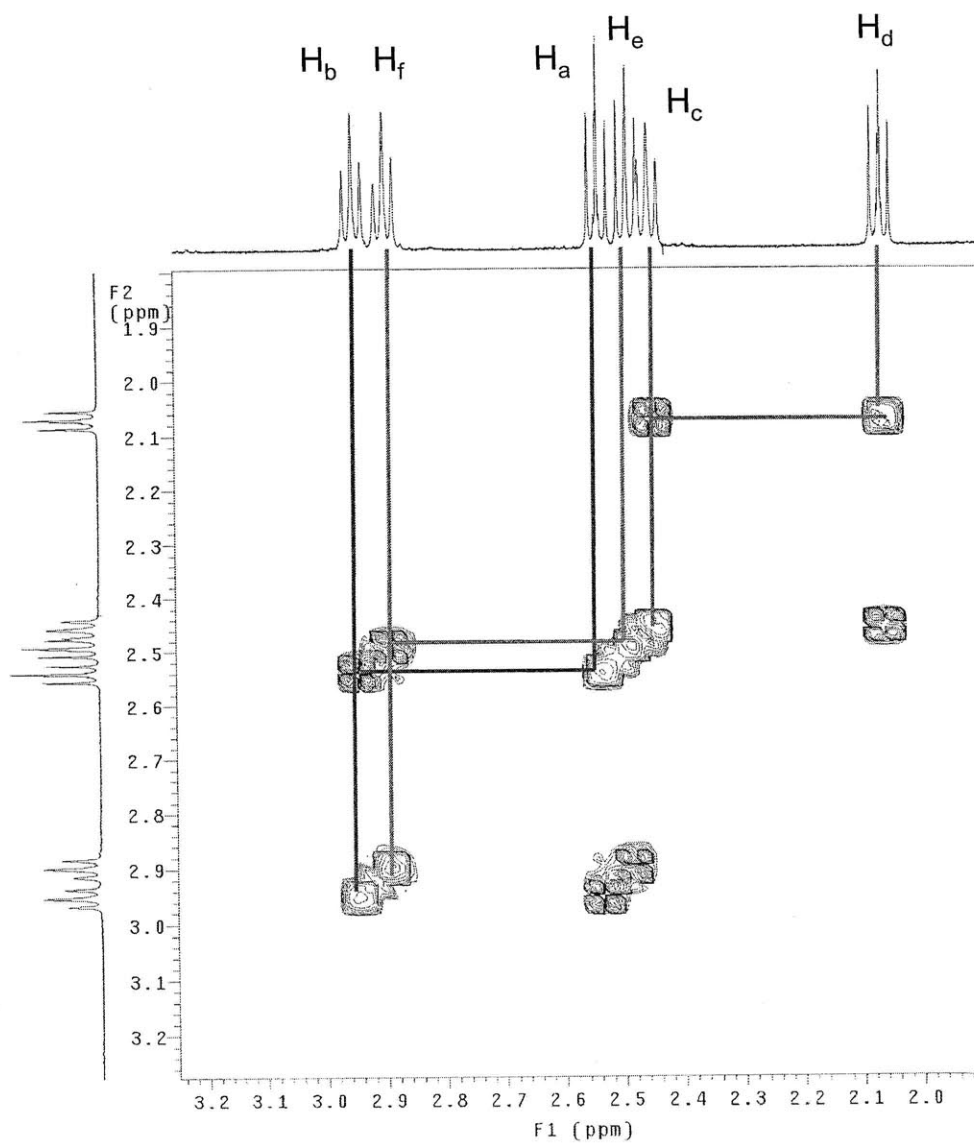
D₂Cl₂, 500 MHz



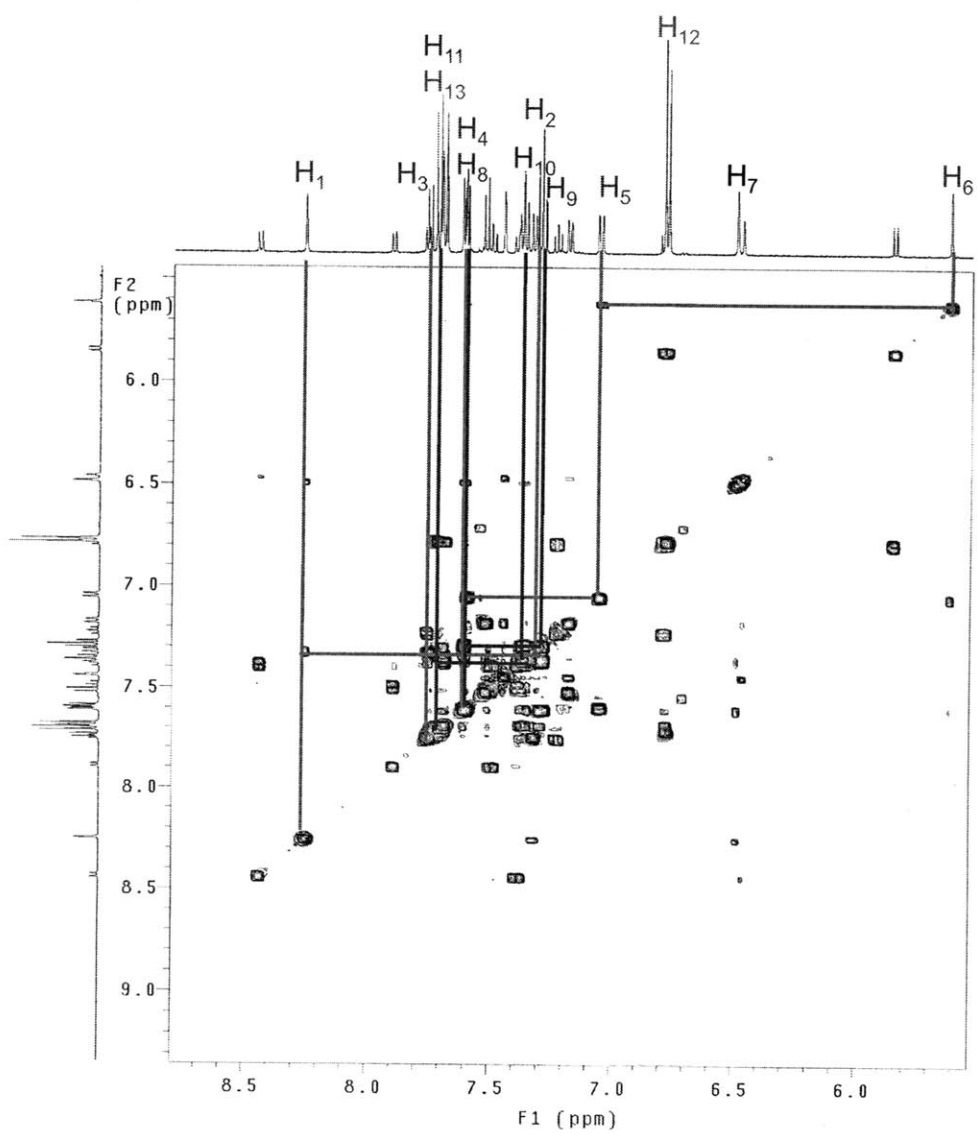
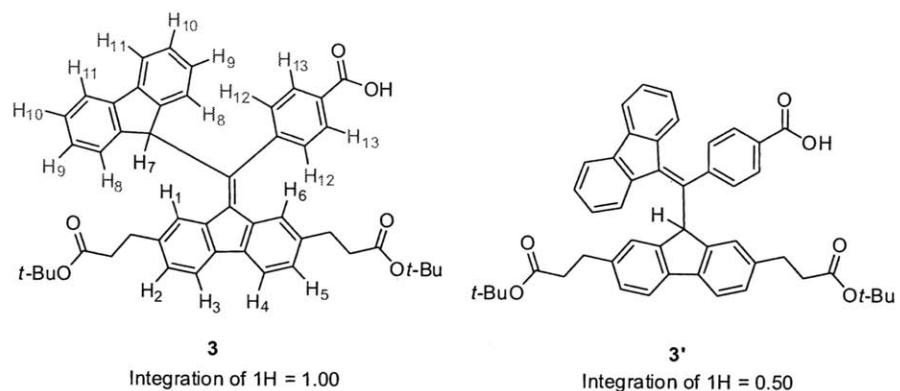
Integration of 1H = 1.00



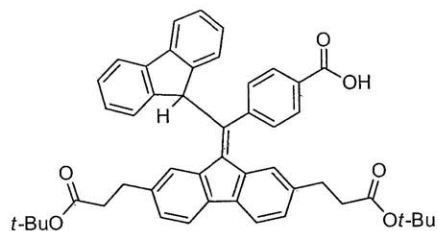
Integration of 1H = 0.50



Compound 3 g-COSY 2D-NMR
D₂Cl₂, 500 MHz

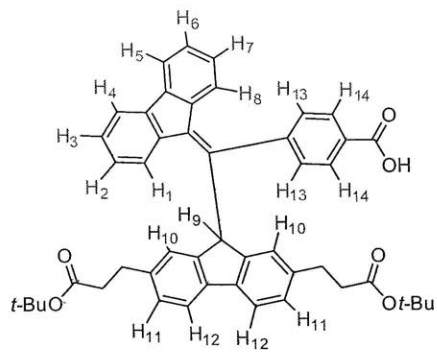


Compound 3 g-COSY 2D-NMR
D₂Cl₂, 500 MHz



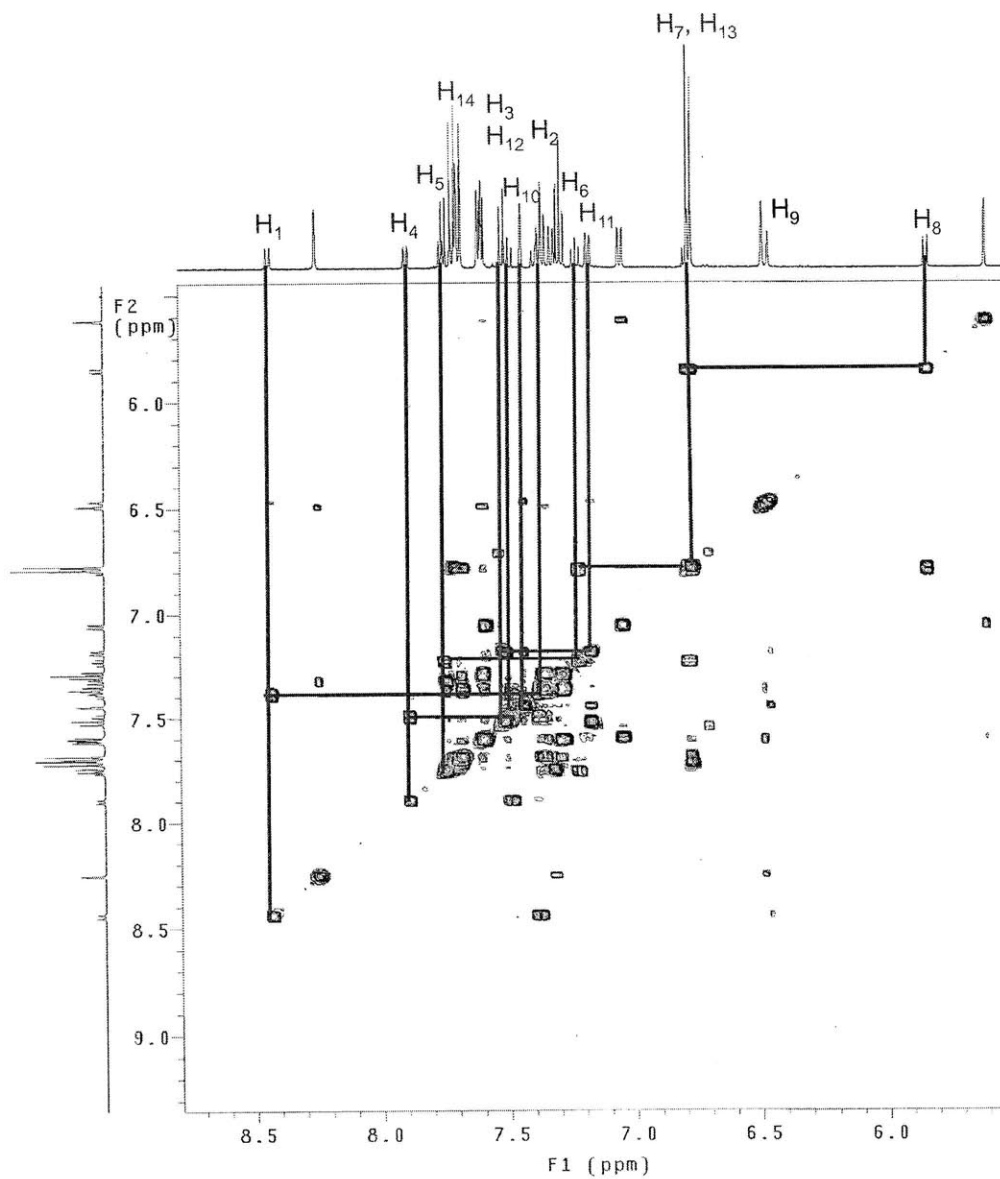
3

Integration of 1H = 1.00



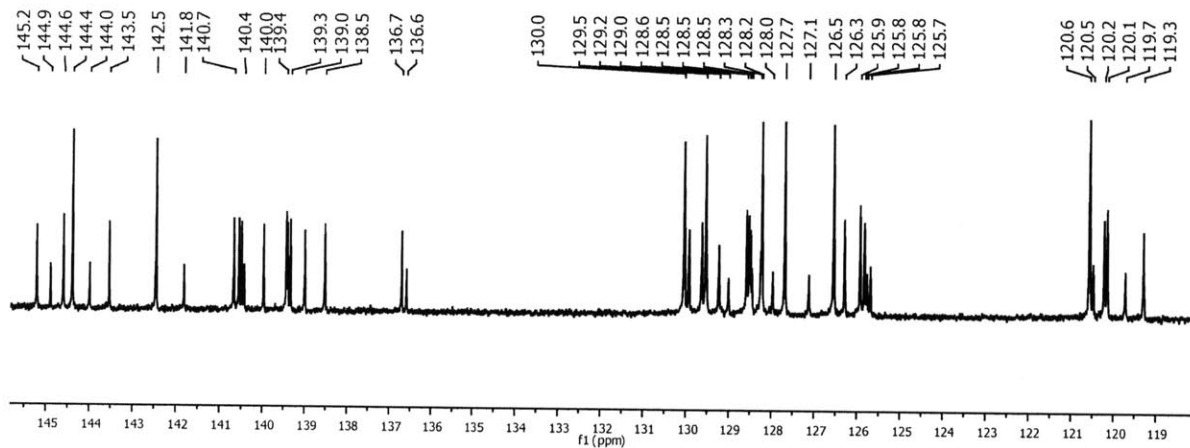
3'

Integration of 1H = 0.50

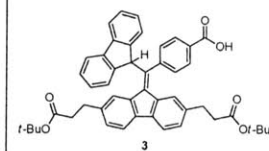
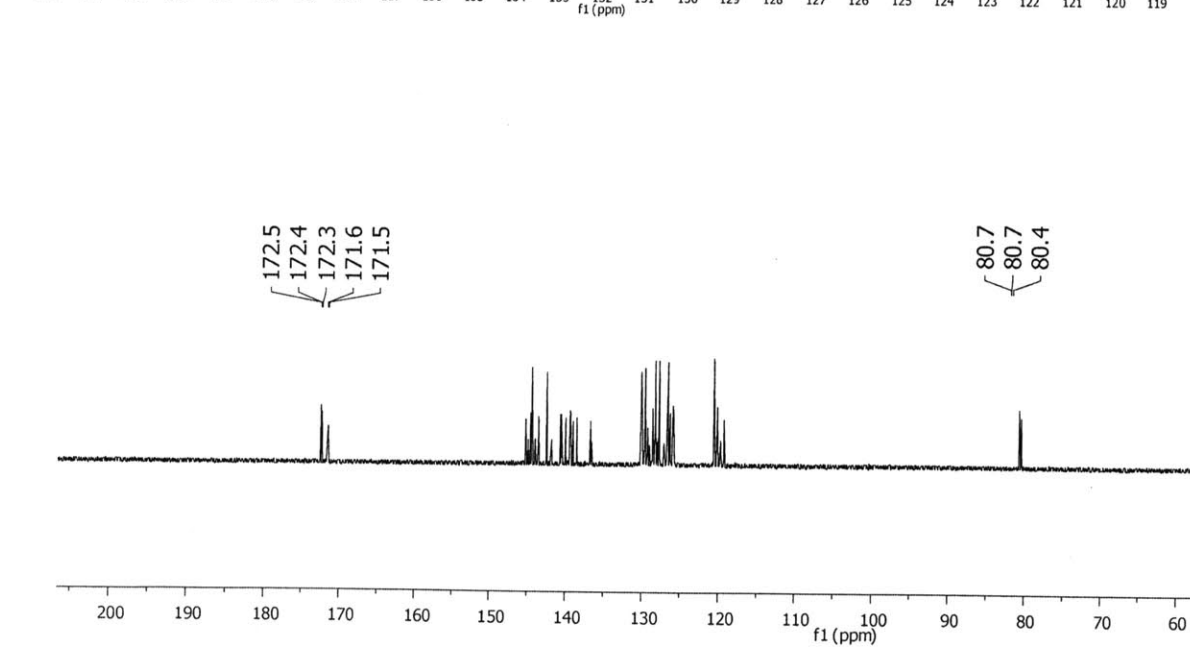


Compound 3

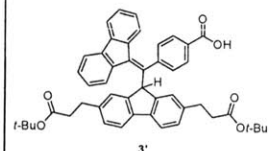
D₂Cl₂, 125 MHz



52.8, 52.7, 37.8, 37.8, 36.7, 32.1, 31.7, 31.6, 28.3, 28.2



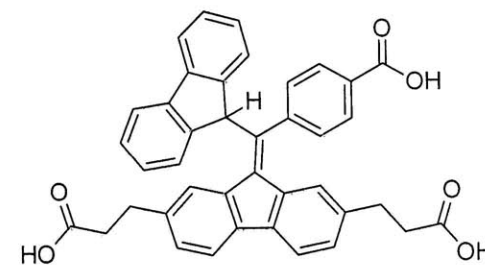
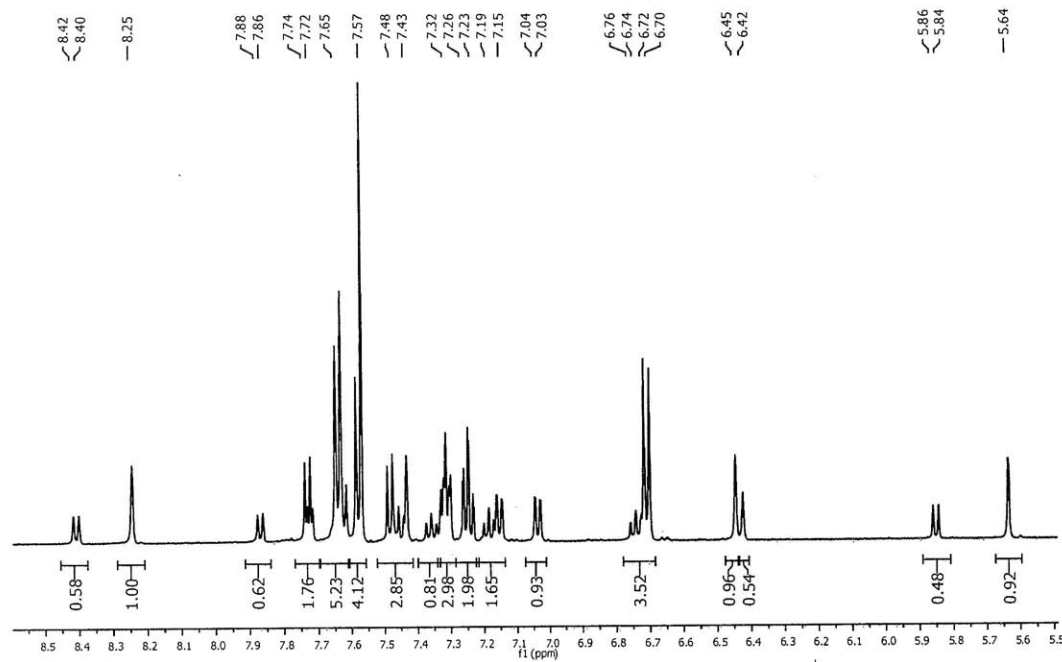
Integration of 1H = 1.00



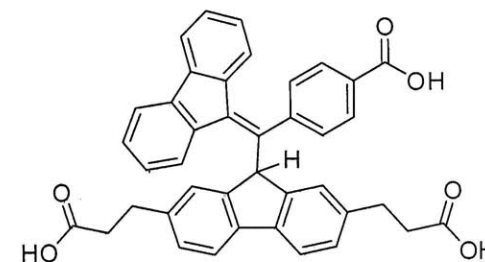
Integration of 1H = 0.50

Compound 4 ¹H-NMR

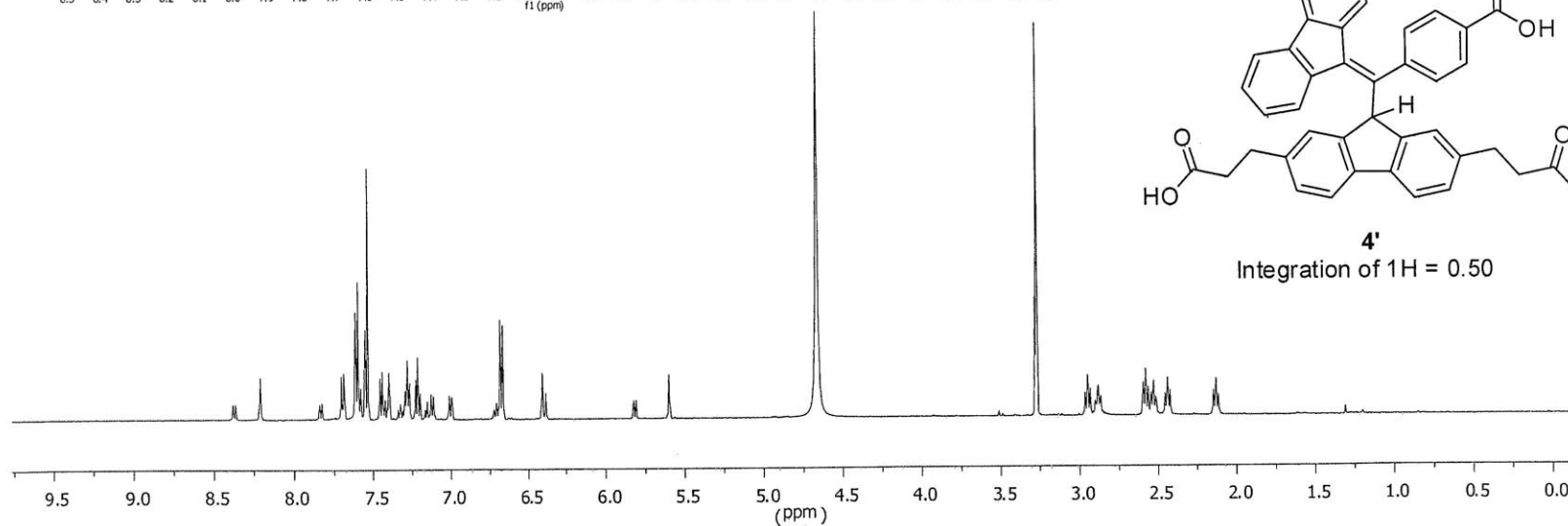
CD₃OD, 500 MHz



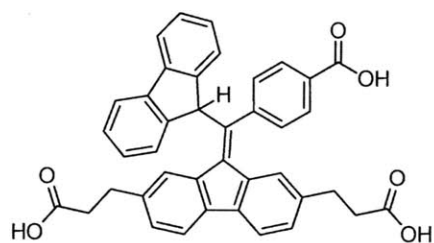
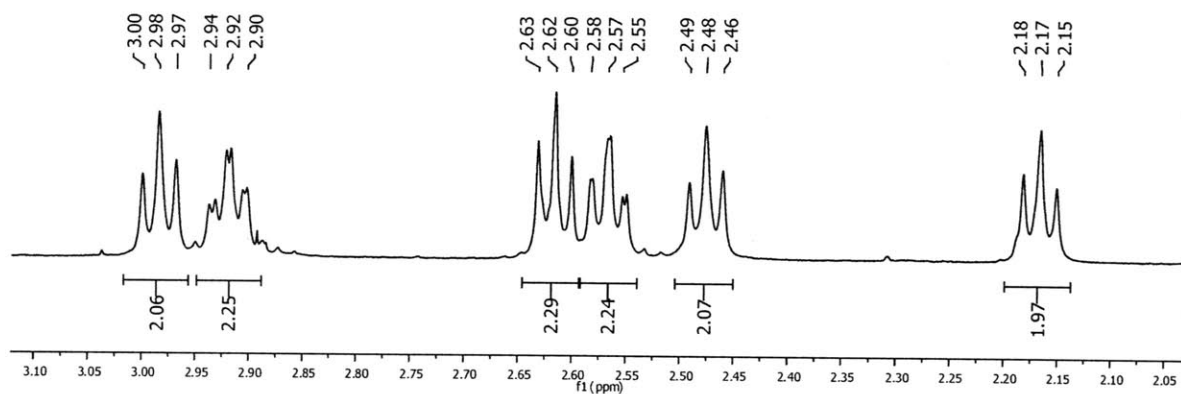
4
Integration of 1H = 1.00



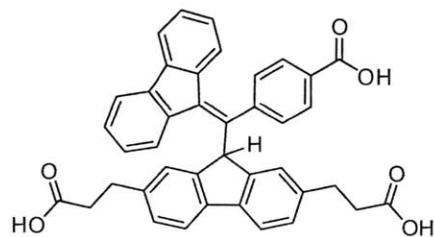
4'
Integration of 1H = 0.50



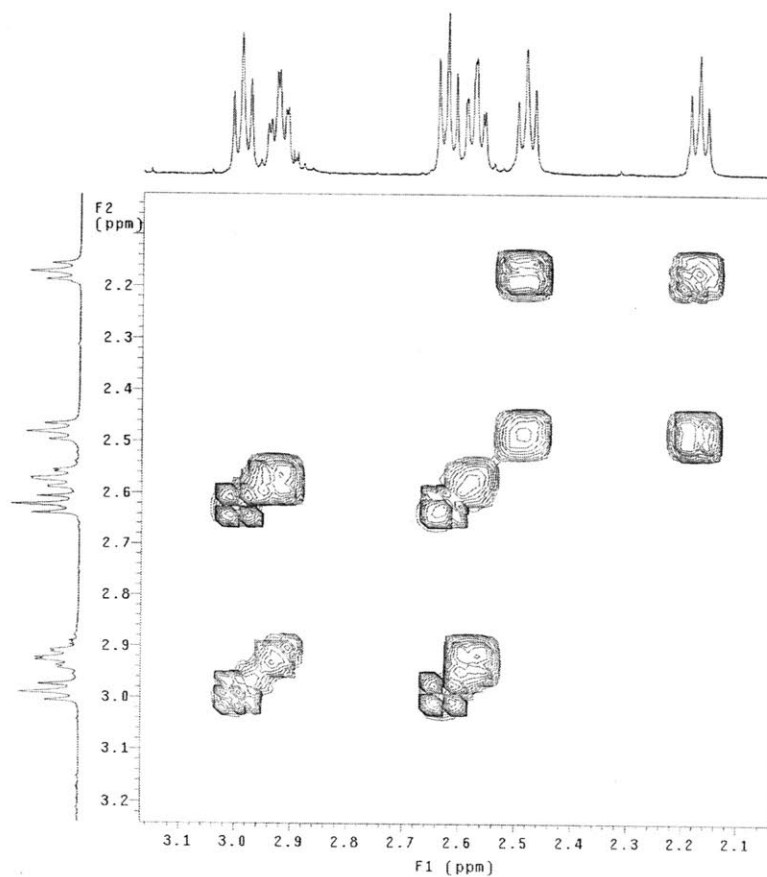
Compound 4 ¹H-NMR (con't.) and g-COSY 2D-NMR
 CD₃OD, 500 MHz



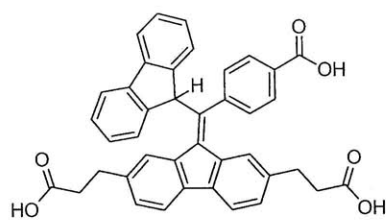
Integration of 1H = 1.00



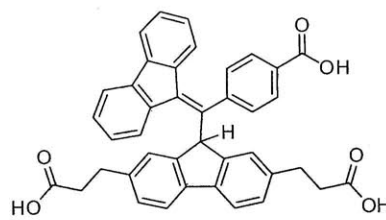
Integration of 1H = 0.50



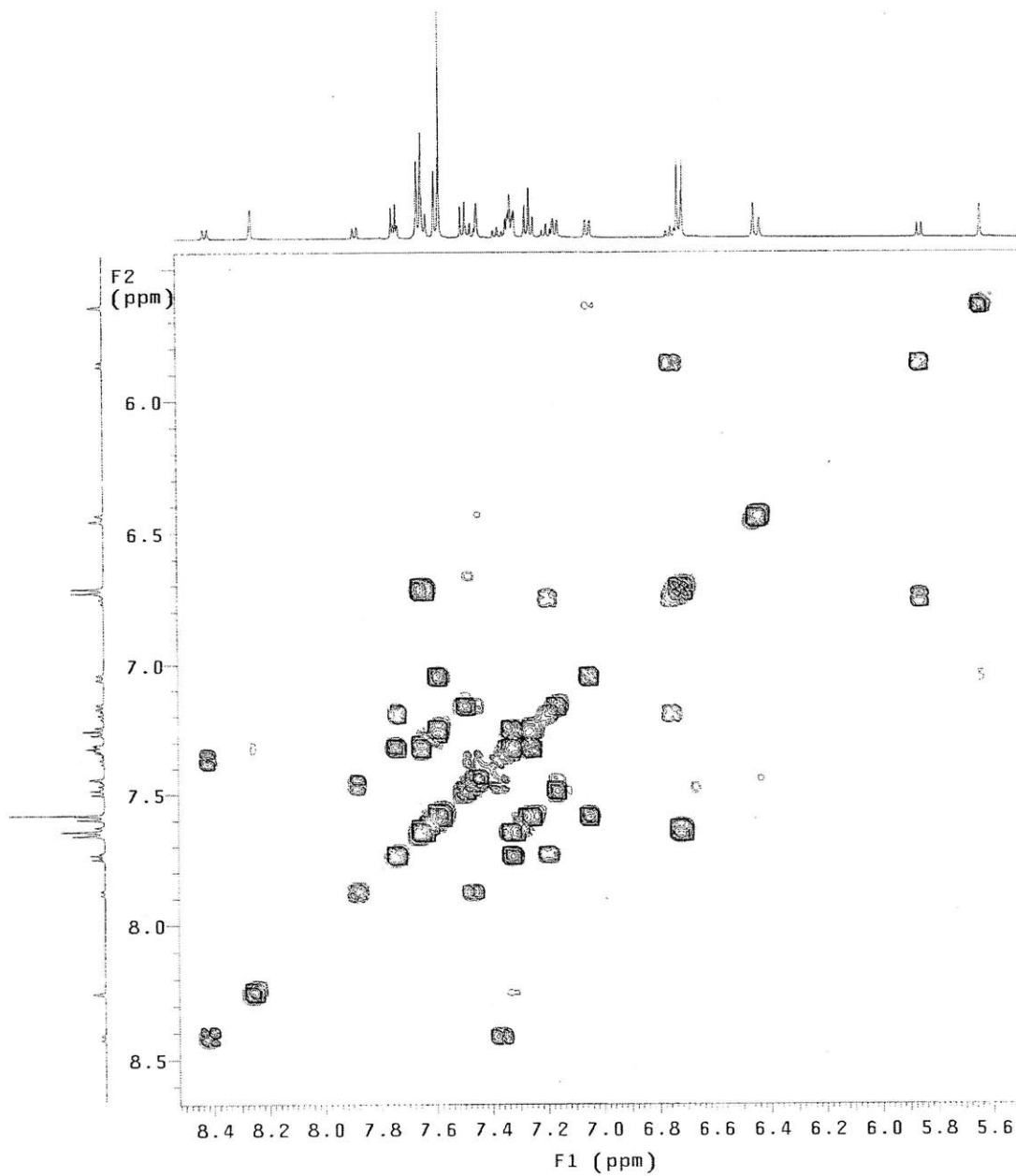
Compound 4 g-COSY 2D-NMR
CD₃OD, 500 MHz

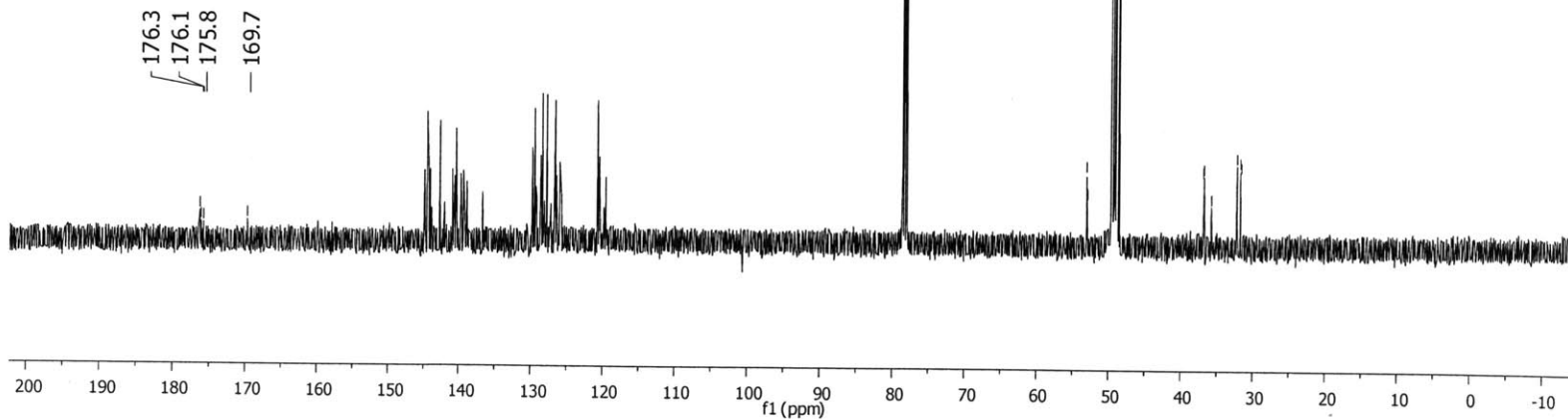
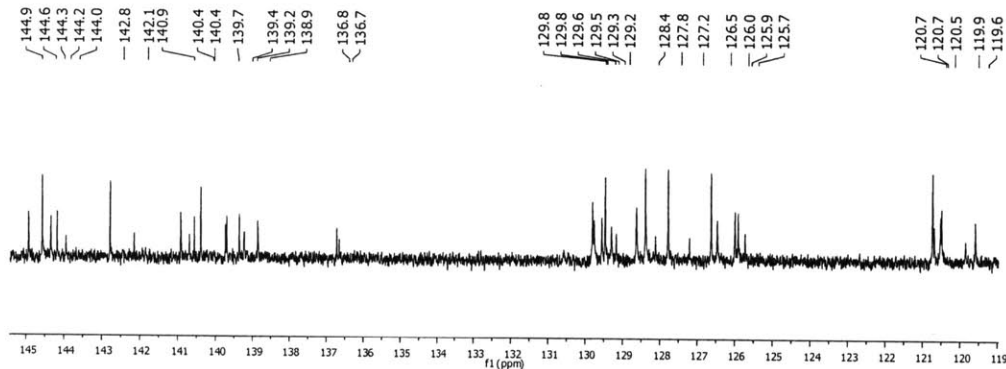


4
Integration of 1H = 1.00



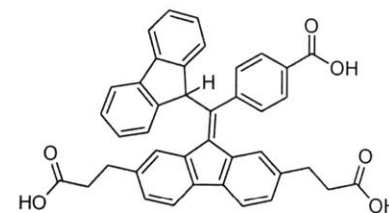
4'
Integration of 1H = 0.50





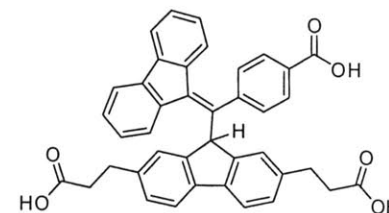
Compound 4 ¹³C-NMR

CD₃OD/CDCl₃, 125 MHz



4

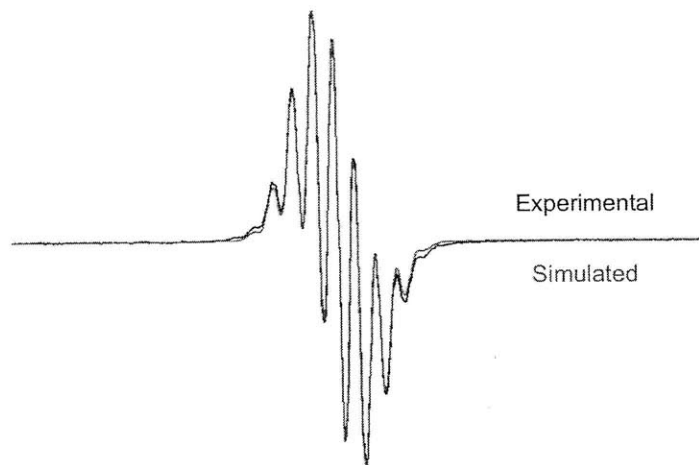
Integration of 1H = 1.00



4'

Integration of 1H = 0.50

WS-BDPA 9 GHz EPR Simulation



Experimental Parameters

[WS-BDPA] = 10 mM in 3:2 glycerol/water, rt, 2 mW, modulation amplitude 10 mT.

Simulation Parameters

Simulated using WinSim^a as a single radical with hyperfine couplings with 8 protons. ($A_1 = 1.986$, $A_2 = 1.725$, $A_3 = 1.894$, $A_4 = 2.24$, $A_5 = 1.717$, $A_6 = 1.633$, $A_7 = 2.164$, $A_8 = 2.019$).

^a Duling, D. R. *J. Magn. Reson., Series B* **1994**, *104*, 105.

CHAPTER 4

Rigid Orthogonal Dinitroxide Biradicals with Improved Solubility for DNP

4.1 Introduction

Nuclear magnetic resonance (NMR) is indispensable to the modern organic chemist¹ and is becoming increasingly more important to researchers interested in biological structure determination². In particular, NMR offers the opportunity to study polypeptides and proteins that are not amenable to X-ray crystallography, such as membrane proteins and amyloid fibers, in conditions more similar to their native environment than a well-ordered crystal.³ However, NMR is limited by sensitivity when nuclei of low natural abundance, such as ¹³C and ¹⁵N, are of interest. Dynamic nuclear polarization (DNP) offers a way to increase the sensitivity of NMR.^{4,5} In a given magnetic field, electrons are inherently more polarized than nuclei because of their larger magnetic moment, and thus electron paramagnetic resonance (EPR) is a more sensitive technique than NMR. DNP involves transferring the greater polarization of electrons to nuclei, thus increasing the polarization of the nuclei and the resultant NMR signal. Microwave-driven DNP using stable organic biradicals as the source of unpaired electrons is a technique that increases the signal-to-noise (S/N) ratio in solid-state (SS) NMR significantly, therefore enabling the use of less sample and shorter acquisition times.⁶

Stable organic biradicals, such as the dinitroxide biradical TOTAPOL (Chart 1), are more efficient polarizing agents in DNP than monomeric radicals, such as 4-amino-TEMPO, because covalently tethering the two radicals results in greater dipolar coupling at lower radical concentration.⁶ A high concentration of radicals causes undesirable line-broadening in NMR. Recently, Griffin and co-workers reported that a dinitroxide biradical (Chart 1, bTbk) with a defined geometry that rigidly holds the two nitroxide radicals in an orthogonal orientation shows greater enhancements than TOTAPOL under similar conditions.⁷ A detailed description of why this

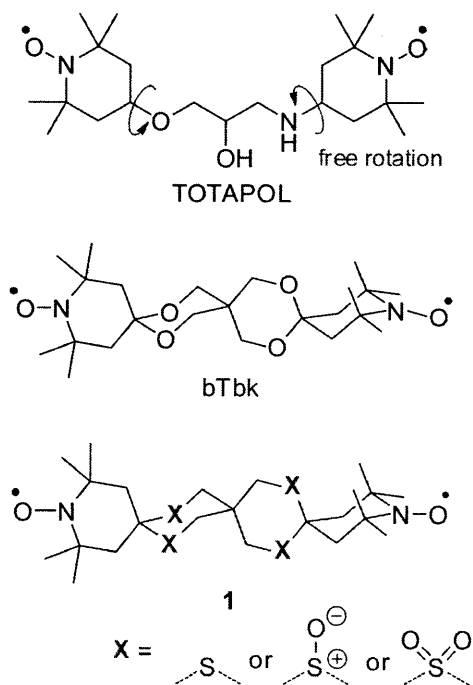


Chart 1.

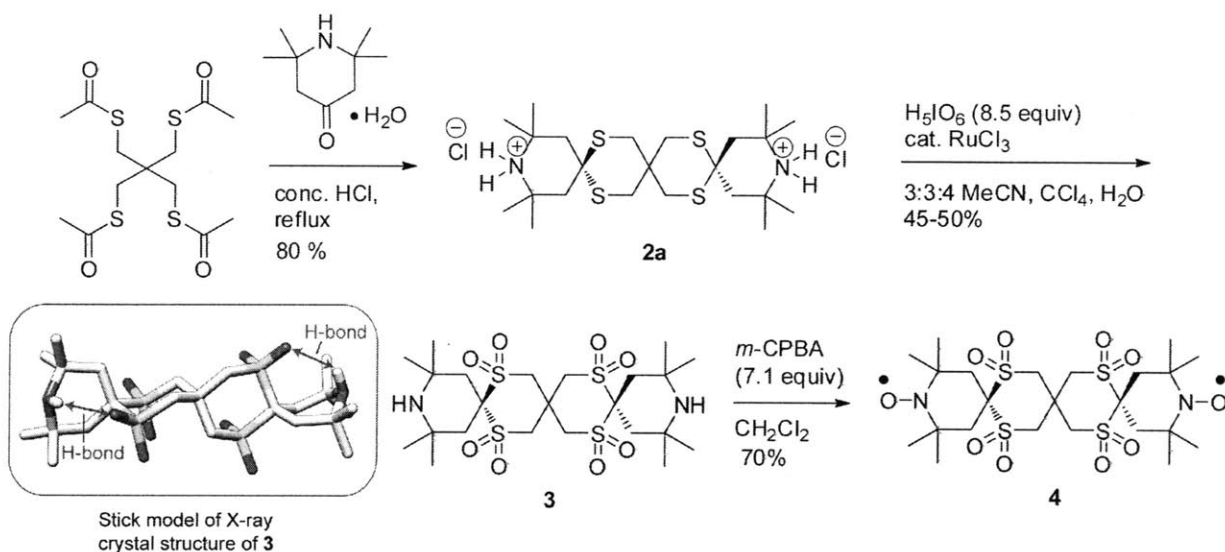
orthogonal geometry is advantageous is available in the literature.^{6,7} In brief, at high magnetic fields, a nitroxide radical's signal is dominated by its relative orientation to the magnetic field, a phenomenon known as *g*-anisotropy (see Chapter 1, Figure 6).⁸ Only certain orientations of the radicals provide the correct frequency difference between the two electrons to promote DNP via a three spin process (2 electrons, 1 nucleus) known as the cross effect.⁹ Therefore, constraining the relative orientation of the radicals to a geometry favorable to the cross effect makes for more efficient DNP.

The biradical bTbk is attractive in its ease of synthesis,¹⁰ but has very limited solubility in aqueous solutions. DNP using biradicals currently requires an aqueous cosolvent for optimal performance, with the solvent systems DMSO/H₂O (60:40) and glycerol/H₂O (60:40) being preferred.⁷ An aqueous cosolvent is needed to ensure the rigidity of the glasses formed by these solvents at 90 K. With lesser amounts of water, S/N-enhancements are attenuated.⁷

To synthesize a more soluble dinitroxide biradical retaining the desirable orientation of bTbk, we envisioned replacing the oxygen atoms with sulfur atoms (Chart 1, structure 1). Compounds containing the 2,4,8,10-tetrathia[5.5]undecane skeleton have been previously reported, but in general have been less studied than their oxygen counterparts.¹¹ It was reasoned that oxidation of the sulfur atoms to sulfoxides and sulfones would introduce polar groups to promote solubility in polar solvents. Reports of oxidized 1,3-dithianes in the literature suggested that the compounds might have the desired solubility.¹² We initially chose to synthesize the tetrasulfone version of **1** because we anticipated that it would be easier to characterize as compared to the intermediate oxidation products.

4.2 Synthesis

The synthesis began with the condensation of tetraacetyl pentaerythrithiol¹³ with 2.0 equivalents of 2,2,6,6-Tetramethyl-4-piperidone monohydrate in refluxing, concentrated hydrochloric acid (Scheme 1). The *bis*-ammonium chloride salt (**2a**) precipitated upon formation and was easily isolated by filtration as a pure compound. For the oxidation of the thioethers to sulfones, the



Scheme 1. Preparation of biradical **4** (measured H-bond length = 2.37 Å).

protonated form of compound **2** was used to protect against possible oxidation of the amine. After trying a variety of commonly used oxidants (such as KMnO_4 ,¹⁴ $\text{H}_2\text{O}_2/\text{AcOH}$,¹⁵ *m*-CPBA,¹⁶ Oxone,¹⁷ NaIO_4 ¹²), only ruthenium tetroxide,¹⁸ generated *in situ* from RuCl_3 and periodic acid, provided complete oxidation to the tetrasulfone, albeit in moderate yield. Tetrasulfone **3** was isolated as the free base by extraction from basic water. An X-ray crystal structure revealed intramolecular hydrogen bonds between the amine proton and a sulfone oxygen in each of the outer rings (Scheme 1). Tetrasulfone **3** was further oxidized with 3.0 equiv of *m*-chloroperbenzoic acid to

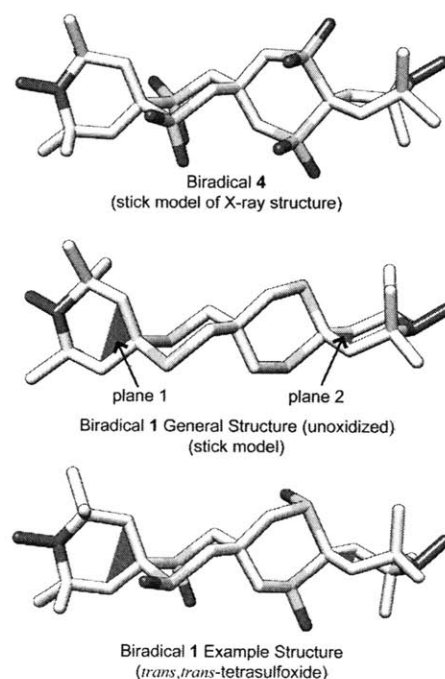


Figure 1. Effect of sulfur oxidation on geometry (top) Stick model of X-ray structure of biradical **4**. (middle) Model of general structure that was used in molecular mechanics calculations to assess the effect of sulfur oxidation on the biradical's geometry as measured by the dihedral angle between planes 1 and 2 (green). (bottom) Equilibrium geometry model of the *trans,trans*-tetrasulfoxide version of biradical **1**.

form biradical **4**.¹⁹

The X-ray crystal structure of **4** (Figure 1, top) shows that the nitroxide radicals are held in a near orthogonal geometry in the solid state. The 9 GHz liquid-state EPR spectrum of **4** in 1:1 DMSO/H₂O (1.0 mM) (Figure 2a) looks similar to the reported spectrum of bTbk, showing a generic nitroxide triplet due to hyperfine coupling to the ¹⁴N nuclei.²⁰ The rigid linker spatially separates the radicals, making the dipolar coupling unobservable in the liquid state. The g_{zz} band of the spectrum is broadened and attenuated, suggesting that the molecular tumbling of **4** is not sufficient to isotropically average the signal.

In solid-state EPR (Figure 2b), broadened doublets indicate the presence of through-space dipolar coupling between the radicals, which can be best seen in the g_{zz} band. The spectrum is similar to that of bTbk.²⁰

Biradical **4** showed excellent solubility in DMSO (>20 mM), but in a 60:40 mixture of DMSO/H₂O it was only sparingly soluble (< 2 mM). Sulfoxes are not known to be especially good at imparting water solubility although they do contain polar sulfur-oxygen bonds.²¹ However, biradical **4**'s lack of solubility in DMSO/H₂O could be a consequence of the structural rigidity that makes it promising as a DNP polarizing agent.

In order to improve the solubility both issues were addressed. Sulfoxides contain sulfur-oxygen bonds that are significantly more polarized than those in sulfones, and in addition they offer more opportunity for the solvent to interact with the electropositive sulfur atom as compared

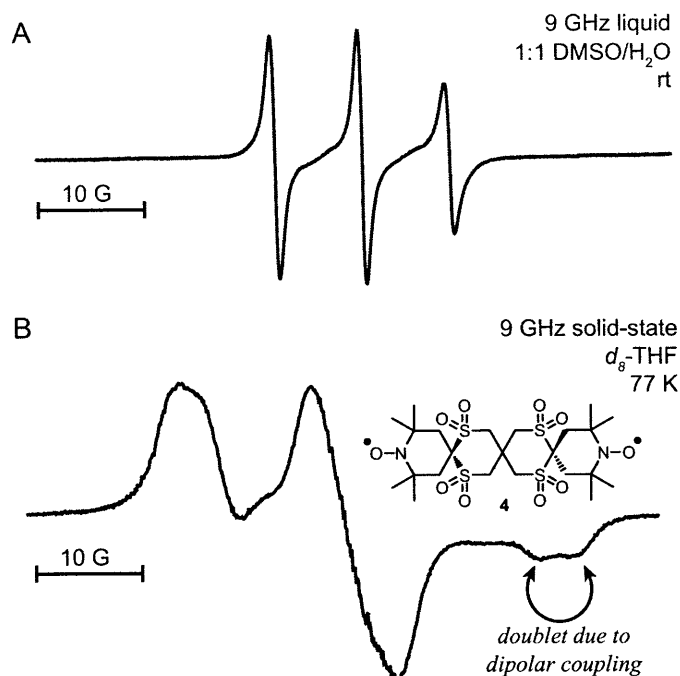


Figure 2. 9-GHz EPR spectra of biradical **4**.

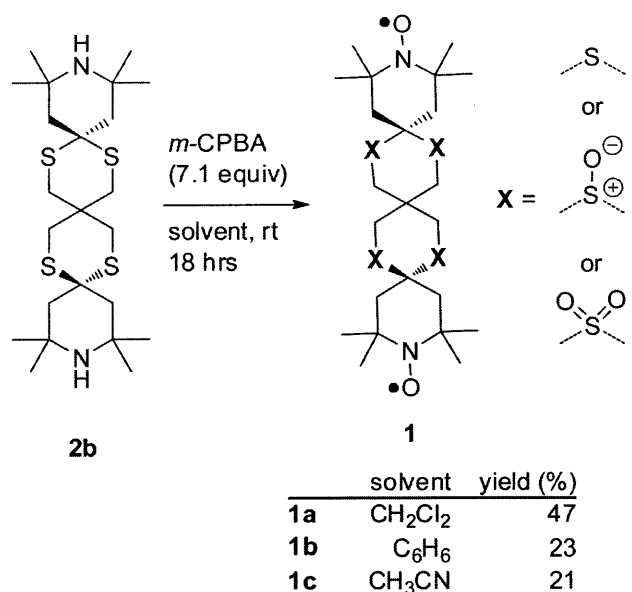
(a) The 9 GHz liquid-state spectrum of **4** shows the expected triplet from two nitroxide radicals which are only weakly interacting. (b) In the solid state, dipolar coupling is evident in the g_{zz} band (right) in the form of a broad doublet.

to more sterically shielded sulfones.²¹ In addition, sulfoxides can be chiral centers when the two carbon substituents are unsymmetrical because of their pyramidal geometry. It was reasoned that a complex mixture of diastereomers would be beneficial for improving solubility by keeping the concentration of any given species relatively low and therefore disfavoring crystallization.

I initially began by trying to selectively synthesize the tetrasulfoxide version of biradical **1**, but quickly found that this route entailed multiple difficulties. First, the conditions used to generate the nitroxyl radicals from amines are harsh enough to oxidize sulfoxides to sulfones.^{19,22} This suggested that I would need to generate and protect the nitroxide radicals before introducing the thioketal scaffold, adding at least one protection and one deprotection step. However, even if this were easily done, my initial studies suggested that selective oxidation to the tetrasulfoxide would be very difficult, and that any method would likely result in a range of oxidation products.¹⁶ In most examples in the literature, when 1,3-dithianes are oxidized to disulfoxides the reaction products are separated by chromatography, but in our case, even the pure tetrasulfoxide itself would be a mixture of 6 separable stereoisomers (5 pairs of enantiomers and one *meso*-compound).

In addition to being synthetically challenging, it was not clear that the oxidation state of the sulfur had a major impact on the relative geometry of the nitroxide radicals. The carbon-sulfur-carbon bond angles in thioethers, sulfoxides, and sulfones in dithianes are very similar. An examination of the Cambridge Structural Database found that in 1,3-dithiane structures of high quality the carbon-sulfur-carbon bond had an average angle of $101.7 \pm 1.4^\circ$ in thioethers, $100.5 \pm 1.7^\circ$ in sulfoxides, and $102.6 \pm 2.0^\circ$ in sulfones (thioether and sulfoxide angles were determined from structures that had bis-carbon substitution at the 2-position, whereas the sulfone angles came from structures without this constraint due to lack of examples). To better understand the effect of sulfur oxidation on the biradical's geometry, molecular mechanics (MM) calculations were performed on bTbk, biradical **4**, and a series of compounds representing a range of oxidation states of **1** (see Figure A1 in Section 4.7). The effect of sulfur oxidation on the orthogonal geometry was evaluated by measuring the dihedral angle between the two planes (plane 1, plane 2) formed by the three carbon atoms closest to the *spiro*-thioketal linkage in each nitroxide ring (Figure 1, green). It

should be noted that the MM program used was not capable of accurately modeling the 3-electron nature of the nitrogen-oxygen bond in nitroxides. However, when the results of using a single N-O bond and a double N=O were compared the differences were minimal. By measuring the angle between the planes rather than the Euler angle between the nitrogen-oxygen bonds the effect of the sulfur oxidation state on one aspect of the relative geometry can be



Scheme 2. Oxidation of **2b** to biradical **1**.

probed using simple calculations, without having to accurately describe the conformation of the nitroxide ring. The reported values were determined from structures with a single bond between the nitrogen and oxygen. In all cases, the angle was within a range of $90 \pm 6^\circ$, suggesting that the effect of the sulfur oxidation state on the orthogonal geometry between the nitroxide rings is minimal.

Based on the synthetic challenges and the unclear benefits of isolating pure samples of the intermediate oxidation states, we sought conditions that would allow us to simultaneously oxidize the amines to nitroxides and the sulfur atoms to sulfoxides, understanding that there would be some amount of overoxidation to sulfones. The common peracid oxidant *m*-CPBA has been reported in the literature to perform both oxidations at room temperature in common organic solvents, and thus seemed an excellent choice. As shown in Scheme 2, the oxidation was performed in three organic solvents (DCM, benzene, acetonitrile) with 7.1 equivalents of *m*-CPBA (3 equivalents to generate the two nitroxide radicals and 4 equivalents to oxidize the thioethers). The strength of *m*-CPBA as an oxidant is known to be attenuated in solvents that disrupt its intramolecular hydrogen bonding.²³ In order to generate a variety of mixtures, organic solvents of different polarity were chosen with the expectation that the sulfoxide/sulfone selectivity of the oxidant would be differ-

ent in each. The purification method was carefully designed to remove likely contaminants, because characterization of complex mixtures is difficult. Extraction with acidic and basic aqueous solutions removed unreacted amines and acidic groups (*i.e.* *m*-chlorobenzoic acid), respectively. Additionally, the reaction mixtures were stirred in CH₂Cl₂ under a basic aqueous solution of the oxidant potassium ferricyanide to ensure that any hydroxylamines were fully oxidized to nitroxyl radicals. Finally, the biradical mixture was precipitated from a 1:2 solution of CH₂Cl₂/hexane to remove organic soluble materials. The final products (**1a-c**) were isolated in moderate-to-low yield. The biradical mixtures were evaluated with proton NMR before and after reduction with zinc powder in *d*₄-methanol. Before reduction, at a concentration of 10 mg/mL, only solvent signals were visible. After reduction, a series of singlets became visible between 2.0 and 1.0 ppm, as expected. Molecules with a 2,4,8,10-tetrathia[5.5]undecane skeleton have complex NMR spectra due the conformational flexibility of the rings, which adds to the complexity already present due to the presence of a range of species.^{11a} IR was used to qualitatively evaluate relative sulfoxide and sulfone content (see Figure A2 in section 4.7). All three samples contained significant amounts of both sulfoxides and sulfones. A comparison of peak intensities indicates that **1a** has the largest ratio of sulfoxides to sulfones. IR also confirmed the presence of the nitroxyl radicals by observation of characteristic bands of the N-O bond at 1362 and 1235 cm⁻¹. The extent and range of oxidation was evaluated using electrospray ionization mass spectrometry (ESI-MS) (see Figures A3, A4, A5 in section 4.7). Based on a qualitative inspection of the ESI-MS spectra, **1a** and **1c** have an average of 4 sulfur-oxygen bonds per molecule, whereas **1b** appears to have an average of 5 sulfur-oxygen bonds. Elemental analysis performed on sample **1a** suggests an average of 4.5 sulfur oxygen bonds per molecule. All three samples (**1a-c**) were soluble at > 10 mM in 60:40 DMSO/H₂O, but they were not appreciably soluble in 60:40 glycerol/H₂O. DMSO is not a preferred solvent for protein applications because it can cause unfolding, but for other applications, such as obtaining spectra of small molecules, it is suitable.

4.3 DNP results

Samples of **1a-c** (10 mM) in d_6 -DMSO/D₂O/H₂O (60:34:6) with 1.0 M urea were used to test the DNP performance of the polarizing agents by monitoring the enhancement in urea's ¹³C-signal with and without microwave irradiation (Figure 3). All three samples gave the same enhancements within error, and the enhancements obtained were 30% greater than those for TOTAPOL under the same conditions. The consistency of the enhancements among **1a-c** is further confirmation that the oxidation state of the sulfur atoms has a minor affect on DNP performance beyond its important affect on solubility.

4.4 Conclusions

In summary, the synthesis of an oxidized *bis*-thioketal-*trisp*iro-dinitroxide biradical is reported. When fully oxidized to the tetrasulfone (**4**), the biradical has a rigid orthogonal geometry but lacks the desired solubility. We show that a biradical mixture (**1**) containing intermediate oxidations states improves solubility in aqueous cosolvents, likely as a result of the more polarized sulfur-oxygen bonds in sulfoxides and the presence of a range of regioisomers and diastereomers. The mixtures show DNP enhancements comparable to the previously reported biradical of similar geometry (bTbk) and improved performance over the geometrically unconstrained TOTAPOL biradical. Future work will focus on improving the solubility in glycerol/water solutions to broaden potential applications.

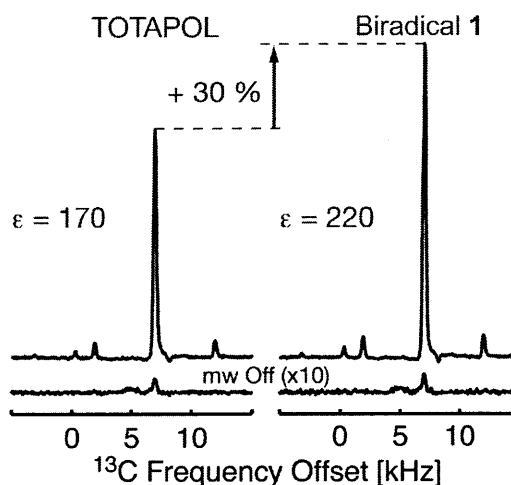


Figure 3. DNP enhancements of **1** vs TOTAPOL. The enhancement in the ¹³C-NMR signal of urea when Biradical **1** (blue) is used as the polarizing agent is 30% greater than when TOTAPOL (red) is used under the same conditions. The signal in the absence of DNP enhancement is shown at the bottom in grey (magnified 10X). Figure prepared by T. Maly.

4.5 Experimental section

Materials. All chemicals, reagents, and solvents were used as received from commercial sources without further purification except if otherwise noted.

Instrumentation. Proton nuclear magnetic resonance (^1H NMR) spectra and carbon nuclear magnetic resonance (^{13}C NMR) spectra were recorded on a Varian (500 MHz) NMR spectrometer. The mass spectrometry data were obtained at the MIT mass spectrometry facility, using a Bruker Daltonics APEX II 3T FT-ICR-MS. Elemental analysis was obtained by Columbia Analytical Services, Tucson, AZ.

Biradical mixture (1). In a flask, 0.300 g (0.620 mmol, 1.00 equiv) of **2b** was dissolved in 45 mL of dry solvent (CH_2Cl_2 , C_6H_6 , or CH_3CN). While stirring at room temperature, 1.03 g (4.37 mmol, 7.10 equiv) of *m*-chloroperbenzoic acid (73% pure by weight as determined by titration with iodine) was added in one portion, and the reaction was stirred for 18 h. For the reactions in benzene and acetonitrile, the organic solvent was removed under vacuum and the solid was dissolved in 45 mL of dichloromethane. The organic layer was washed with sat'd sodium bicarbonate (3 x 20 mL) and 0.1 M HCl (3 x 20 mL), after which it was transferred to a flask and stirred under an aqueous 0.5 M NaOH solution containing 0.200 g (0.620 mmol, 1.00 equiv) of potassium ferricyanide for 10 minutes. The organic layer was washed with brine and then dried over sodium sulfate. The solvent was removed, and the solid was dissolved with 5.0 mL of CH_2Cl_2 . To the solution was added 10.0 mL of hexane, which caused a precipitate to form. After 10 minutes, the solid was isolated by filtration. Mass recovery and yield based on addition of 6 oxygen atoms (MW = 596 g/mol): CH_2Cl_2 , 0.170 g (47%); C_6H_6 , 0.075 g (21%); CH_3CN , 0.083 g (23%). Elemental Analysis for sample **1a**: Found: C 47.89, H 7.08, N 4.67, S 21.21. Expected for $\text{C}_{23}\text{H}_{40}\text{N}_2\text{O}_{6.5}\text{S}_4$: C, 47.89; H, 6.99; N, 4.86; S, 22.24.

2,2,4,4,14,14,16,16-octamethyl-7,11,18,21-tetrathia-3,15-diazatrispiro[5.2.2.5¹².2⁹.2⁶] henicosan-3,15-dium dichloride (2a). To a 500-mL flask were added 0.895 g (5.20 mmol, 1.00 equiv) of 2,2,6,6-Tetramethyl-4-piperidone monohydrate, 0.990 g (2.70 mmol, 0.520 equiv) of tetraacetyl pentaerythritol, and 50 mL of concentrated hydrochloric acid. After attaching a water-cooled condenser, the reaction mixture was heated to reflux for 3 h. A white precipitate formed soon after heating began. After cooling, the solution was filtered and washed with THF to obtain 1.13 g (80% yield) of compound **2a** as a white powder. ¹H NMR (500 MHz, CD₃OD, δ): 3.18 (s, 8H), 2.40 (s, 8H), 1.62 (s, 24H); ¹³C NMR (126 MHz, δ) 57.8, 46.7, 45.2, 35.2, 28.8, 24.0; mp decomposes beginning at 330 °C (concentrated HCl); HRMS (ESI) of **2b** (free amine): 475.2198 [calc'd for C₂₃H₄₂N₂S₄ (M+H)⁺: 475.2304].

2,2,4,4,14,14,16,16-octamethyl-7λ⁶,11λ⁶,18λ⁶,21λ⁶-tetrathia-3,15-diazatrispiro [5.2.2.5¹².2⁹.2⁶] henicosan - 7,7,11,11,18,18,21,21-octone (3). To a flask were added 0.200 g (0.360 mmol, 1.00 equiv) of compound **2a**, 6.0 mL CCl₄, 6.0 mL of acetonitrile, 8.0 mL of water, 0.0060 g of RuCl₃ (0.028 mmol, 8.0 mol%), and 0.706 g periodic acid (3.10 mmol, 8.50 equiv). The reaction mixture was stirred for 30 minutes at room temperature and then filtered through celite on a fritted filter. The organic solvents were removed and sat'd sodium carbonate solution was added to reach pH = 12. The aqueous mixture was extracted with CH₂Cl₂ (2 x 15 mL), which was subsequently dried over sodium sulfate. After removal of the solvent and drying under vacuum, 0.090 g (46%) of **3** was obtained. ¹H NMR (500 MHz, CD₃OD/CDCl₃, δ): 3.84 (s, 8H), 2.36 (s, 8H), 1.29 (s, 24H); ¹³C NMR (126 MHz, d₆-DMSO/CDCl₃ with 2.0 equivalents of trifluoroacetic acid added to improve solubility, 50 °C, δ): 82.5, 53.1, 50.1, 29.5, 29.0(2); HRMS (ESI): 603.1890 [calc'd for M + H = 603.1897]; IR: ν_{max} (KBr)/cm⁻¹: 3350 (br), 2919, 1450, 1388, 1373, 1343, 1314, 1167, 1149, 1129, 1019, 815, 666, 620, 579, 520. Mp decomposes beginning at 325 °C (methanol).

2,2,4,4,14,14,16,16-octamethyl- 7λ⁶ ,11λ⁶ ,18λ⁶ ,21λ⁶-tetrathia-3,15-dinitroxyltrispiro [5.2.2.5¹².2⁹.2⁶] henicosan-7,7,11,11,18,18,21,21-octone (4). To a flask were added 0.078 g (0.13

mmol, 1.0 equiv) of compound **3**, 0.096 g (0.39 mmol, 3.0 equiv) of *m*-chloroperbenzoic acid (75% purity), 6.0 mL CH₂Cl₂, and 6.0 mL of isopropyl alcohol. The solution was stirred at room temperature overnight. In a separatory funnel, the organic layer was washed with excess sat'd sodium bicarbonate solution (10 mL), with 0.1 M HCl (2 x 10 mL), and brine, before being dried over sodium sulfate. After removal of the solvent and recrystallization from acetone, 0.058 g (70%) of biradical **4** was isolated as a light yellow crystal. HRMS (ESI): 631.1504 [calc'd for M - H = 631.1493]; IR: ν_{\max} (KBr)/cm⁻¹: 2935, 1456, 1388, 1373, 1362, 1345, 1314, 1234, 1150, 1131, 1018, 865, 666, 617, 589, 522; Mp decomposes beginning at 200 °C (acetone). For NMR characterization, 0.010 g of the biradical was reduced with 3.1 equivalents (~ 5.0 μ L) of phenylhydrazine in *d*₆-acetone. ¹H NMR (500 MHz, *d*₆-acetone, δ): 3.80 (s, 8H), 2.53 (s, 8H), 1.25 (s, 24H).

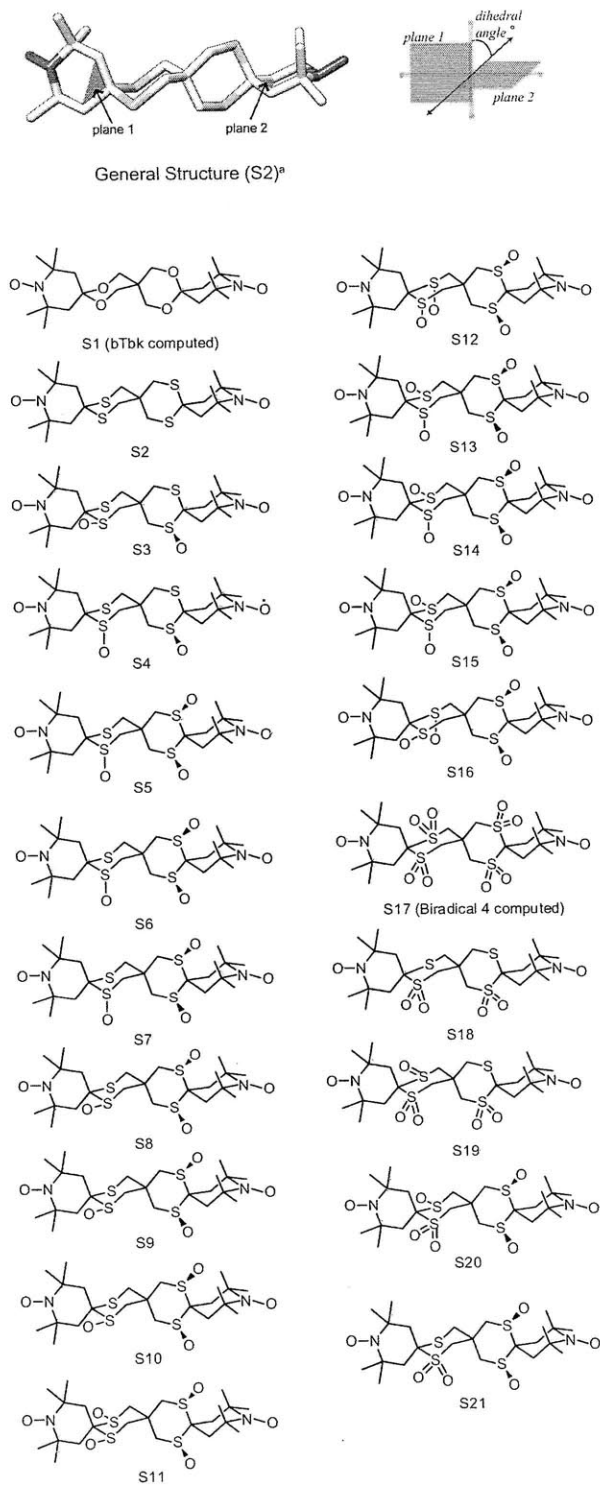
4.6 References

- (1) Clayden, J.; Greeves, N.; Warren, S.; Wothers, P. "Organic Chemistry" Oxford University Press, Oxford, 2001.
- (2) Dyson, H. J.; Wright, P. E. *Chem. Rev.* **2004**, *104*, 3517.
- (3) Opella, S. J.; Marassi, F. M. *Chem. Rev.* **2004**, *104*, 3587.
- (4) Wind, R. A.; Duijvestijn, M. J.; van der Lugt, C.; Manenschijn, A.; Vriend, J. *Prog. Nucl. Magn. Reson. Spectrosc.* **1985**, *17*, 33.
- (5) (a) Maly, T.; Debelouchina, G. T.; Bajaj, V. S.; Hu, K.-N.; Joo, C.-G.; Mak-Jurkauskas, M. L.; Sigirhi, J. R.; van der Wel, P. C. A.; Herzfeld, J.; Temkin, R. J.; Griffin, R. G. *J. Chem. Phys.* **2008**, *128*, 052211. (b) Barnes, A. B.; Paëpe, G. D.; Wel, P. C. A. v. d.; Hu, K.-N.; Joo, C.-G.; Bajaj, V. S.; Mak-Jurkauskas, M. L.; Sirigiri, J. R.; Herzfeld, J.; Temkin, R. J.; Griffin, R. G. *Appl. Magn. Reson.* **2008**, *34*, 237.
- (6) (a) Hu, K.-N.; Yu, H.-h. Swager, T. M.; Griffin, R. G. *J. Am. Chem. Soc.* **2004**, *126*, 10844. (b) Song, C.; Hu, K.-N.; Swager, T. M.; Griffin, R. G. *J. Am. Chem. Soc.* **2006**, *128*, 11385. (c) Hu, K.-N.; Song, C.; Yu, H.-h.; Swager, T. M.; Griffin, R. G. *J. Chem. Phys.* **2008**, *128*, article # 052302. (d) Joo, C.-G.; Hu, K.-N.; Bryant, J. A.; Griffin, R. G. *J. Am. Chem. Soc.* **2006**, *128*, 9428.
- (7) Matsuki, Y.; Maly, T.; Ouari, O.; Karoui, H.; Le Moigne, F.; Rizzato, E.; Lyubenova, S.; Herzfeld, J.; Prisner, T.; Tordo, P.; Griffin, R. G. "Angew. Chem., Int. Ed." **2009**,

121, 5096.

- (8) Grinberg, O. Y.; Berliner, L. J. "Very High Frequency (VHF) ESR/EPR" *Biological Magnetic Resonance Vol. 22*. Kluwer Academic/Plenum Publishers, New York 2004.
- (9) (a) Farrar, C. T.; Hall, D. A.; Gerfen, G. J.; Inati, S. J.; Griffin, R. G. *J. Chem. Phys.* **2001**, *114*, 4922. (b) Goldman, M. *Appl. Magn. Reson.* **2008**, *34*, 219. (c) Wollan, D. S. *Phys. Rev. B* **1976**, *13*, 3671. (d) Wollan, D. S. *Phys. Rev. B* **1976**, *13*, 3686.
- (10) Fujita, T.; Yoshioka, T.; Soma, N. *J. Polym. Sci. Polym. Lett. Ed.* **1978**, *16*, 515.
- (11) (a) Gaz, S. A.; Condamine, E.; Bogdan, N.; Terec, A.; Bogdan, E.; Ramondenc, Y.; Grosu, I. *Tetrahedron* **2008**, *64*, 7295. (b) Backer, H. J.; Evenhuis, N. *Recl. Trav. Chim. Pays-Bas* **1937**, *56*, 681. (c) Wan, Y.; Mitkin, O.; Barnhurst, L.; Kutateladze, A. *Org. Lett.* **2000**, *2*, 3817. (d) Mitkin, O. D.; Wan, Y.; Kurchan, A. N.; Kutateladze, A. G. *Synthesis* **2001**, 1133.
- (12) Aggarwal, V. K.; Davies, I. W.; Maddock, J.; Mahon, M. F.; Molloy, K. C. *Tet. Lett.* **1990**, *31*, 135.
- (13) Wade, E. O.; Valiulin, R. A.; Ruybal, L. A.; Kutateladze *Org. Lett.* **2006**, *8*, 5121.
- (14) Fatiadi, A. J. *Synthesis* **1987**, 85.
- (15) (a) Bryan, R. F.; Carey, F. A.; Miller, R. W. *J. Org. Chem.* **1979**, *44*, 1540. (b) Kuhn, R.; Neugebauer, F. A. *Chem. Ber.* **1961**, *94*, 2629.
- (16) (a) Carey, S. A.; Blambert, J.; Hernandez, O.; Carey, F. A. *J. Am. Chem. Soc.* **1975**, *97*, 1468. (b) Bien, S.; Celebi, S. K.; Kapon, M. *J. Chem. Soc. Perkin Trans. 2* **1990**, 1987. (c) Aggarwal, V. K.; Davies, I. W.; Franklin, R.; Maddock, J.; Mahon, M. F.; Molloy, K. C. *J. Chem. Soc. Perkin Trans.* **1994**, 2363. (d) Paquette, L. A.; Carr, R. V. C. *Org. Synth. Coll.* **1990**, *7*, 453.
- (17) (a) Kennedy, R. J.; Stock, A. M. *J. Org. Chem.* **1960**, *25*, 1901. (b) Trost, B. M.; Curran, D. P. *Tetrahedron Lett.* **1981**, *22*, 1287.
- (18) Rodriguez, C. M.; Ode, J. M.; Palazon, J. M.; Martin, V. S. *Tetrahedron*, **1992**, *48*, 3571.
- (19) Volodarsky, L. B.; Reznikov, V. A.; Ovcharenko, V. I. "Synthetic Chemistry of Stable Nitroxides" CRC Press, Boca Raton, 1994.
- (20) Gafurov, M.; Lyubenova, S.; Denysenkov, V.; Ouari, O.; Karoui, H.; Le Moigne, F.; Tordo, P.; Prisner, T. *Appl. Magn. Reson.* **2010**, *37*, 505.

4.7 Additional Figures



Structure	Dihedral Angle (°)	O to O distance (Å)	N to N Distance (Å)
1 (bTbk computed)	91.5	12.6	11.1
bTbk (X-ray CS)	<i>n.d.</i>	13.0	10.7
2	90.9	14.4	12.1
3	90.0	14.5	12.4
4	94.1	14.6	12.4
5	92.4	14.6	12.3
6	91.0	14.6	12.1
7	95.4	14.4	11.9
8	91.0	14.8	12.1
9	91.5	14.5	12.0
10	93.3	14.7	12.4
11	91.2	14.8	12.1
12	90.5	14.7	12.0
13	92.2	14.7	12.4
14	95.5	14.5	12.3
15	95.2	14.7	12.3
16	91.5	14.6	11.9
17	92.5	14.9	12.2
Biradical 4 (X-ray CS)	93.6	14.6	12.2
18	92.0	14.6	11.9
19	91.0	14.6	11.9
20	93.2	14.9	12.1
21	95.3	14.7	12.1

Figure A1.

Modeling of the effect of oxidation state on biradical geometry.

^a Molecular Mechanics calculations were performed with MacSPARTAN '06 MECHANICS PROGRAM using MMFF94 for optimization.

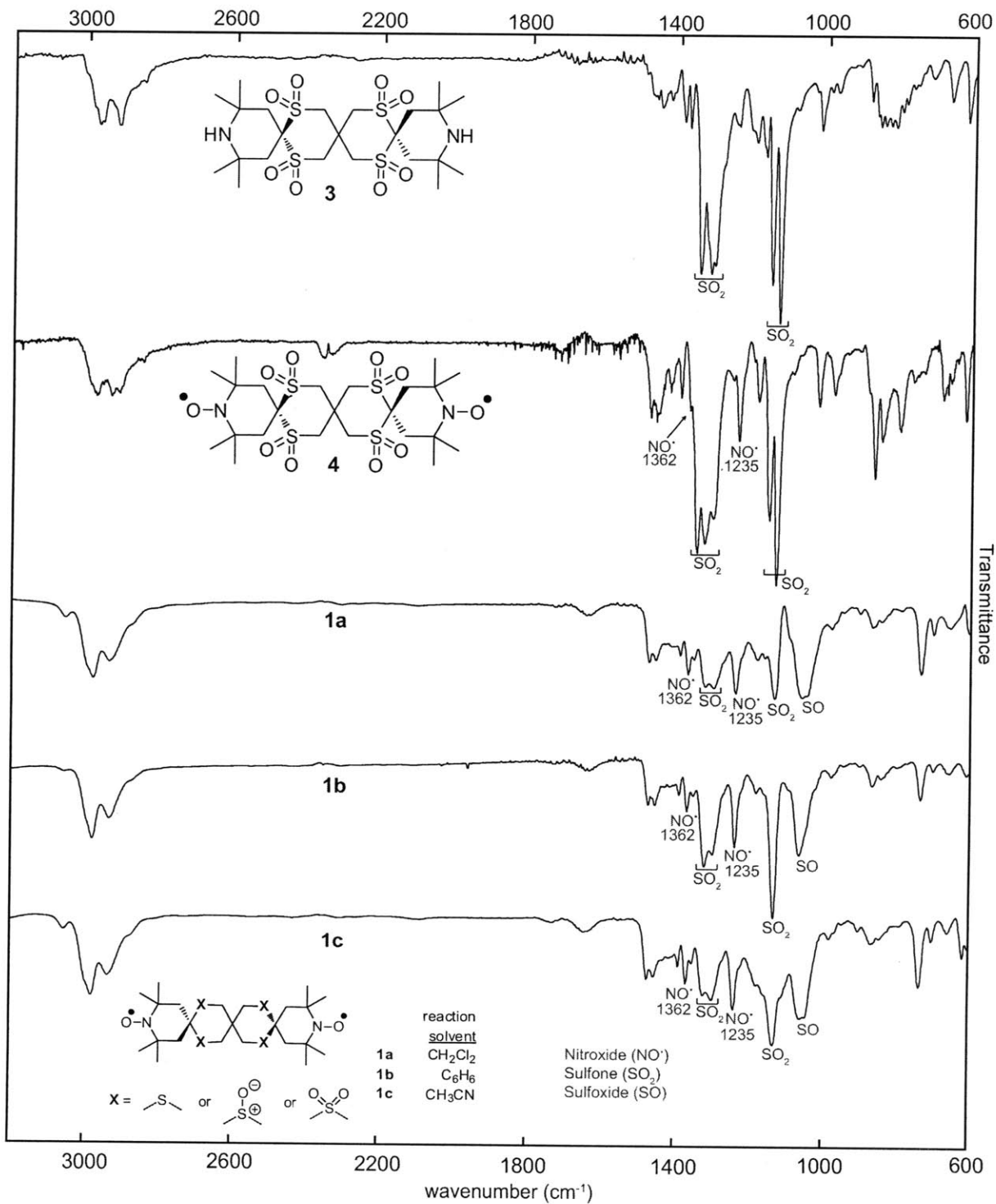


Figure A2.
FT-IR of compounds 3, 4, 1a, 1b, and 1c.

species (M_x): ($a + b + c + d$) = x	M_2	M_3	M_4	M_5	M_6
	example structure:				
molecular weight (amu): error = ± 1 amu	$[M_2 + 2H]^+ = 538$ $[M_2 + Na]^+ = 559$	$[M_3 + 2H]^+ = 554$ $[M_3 + Na]^+ = 575$	$[M_4 + 2H]^+ = 570$ $[M_4 + Na]^+ = 591$	$[M_5 + 2H]^+ = 586$ $[M_5 + Na]^+ = 607$	$[M_6 + 2H]^+ = 602$ $[M_6 + Na]^+ = 623$

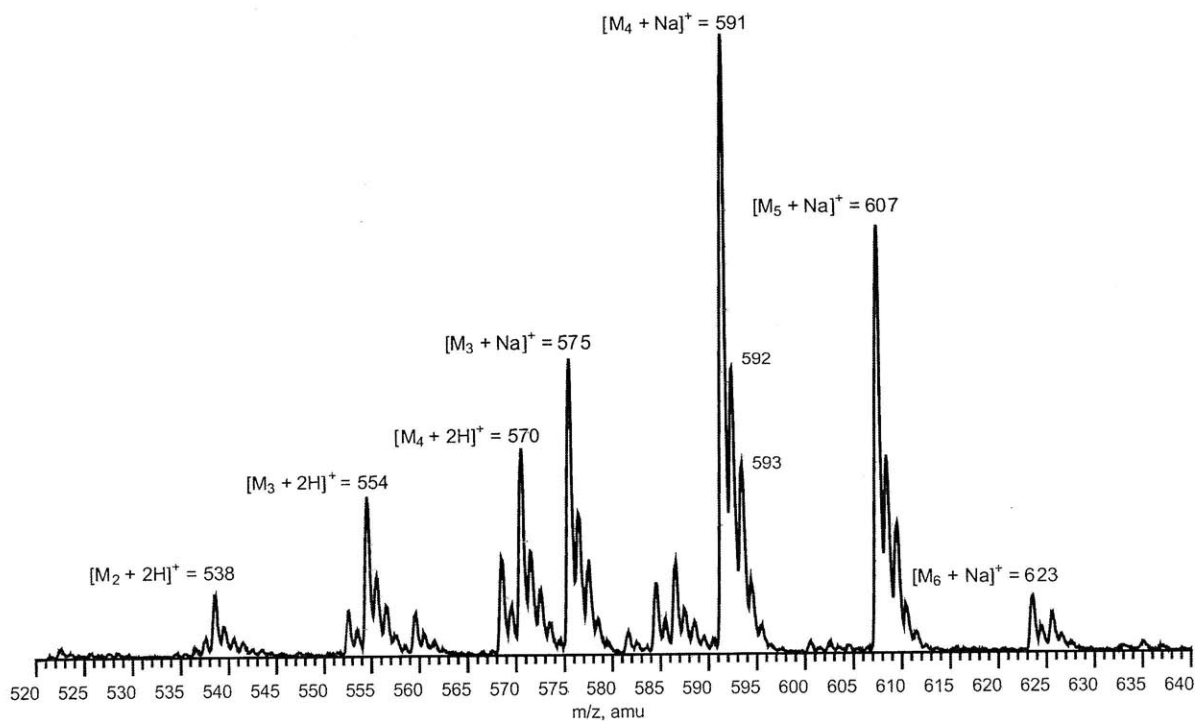


Figure A3.

Electrospray Ionization (ESI) MS of biradical mixture **1a**. Sample was loaded in a methanol solution with 0.1 mM sodium perchlorate and detected in positive ion mode.

species (M_x): ($a + b + c + d$) = x	M_2	M_3	M_4	M_5	M_6
	example structure:				
1b $a, b, c, d = 0, 1, \text{ or } 2$ $a + b + c + d = 3 - 6$					
molecular weight (amu): error = ± 1 amu	$[M_2 + 2H]^+ = 538$ $[M_2 + Na]^+ = 559$	$[M_3 + 2H]^+ = 554$ $[M_3 + Na]^+ = 575$	$[M_4 + 2H]^+ = 570$ $[M_4 + Na]^+ = 591$	$[M_5 + 2H]^+ = 586$ $[M_5 + Na]^+ = 607$	$[M_6 + 2H]^+ = 602$ $[M_6 + Na]^+ = 623$

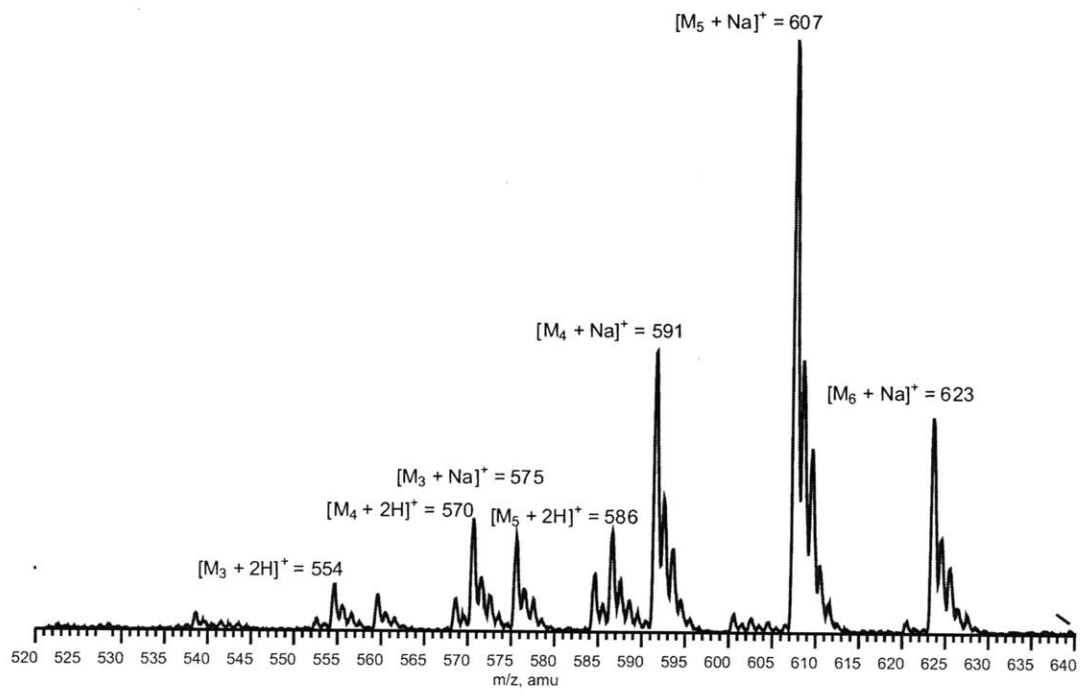


Figure A4. Electrospray Ionization (ESI) MS of biradical mixture **1b**. Sample was loaded in a methanol solution with 0.1 mM sodium perchlorate and detected in positive ion mode.

species (M_x): ($a + b + c + d$) = x	M_2	M_3	M_4	M_5	M_6
	example structure:				
molecular weight (amu):	$[M_2 + 2H]^+ = 538$	$[M_3 + 2H]^+ = 554$	$[M_4 + 2H]^+ = 570$	$[M_5 + 2H]^+ = 586$	$[M_6 + 2H]^+ = 602$
error = ± 1 amu	$[M_2 + Na]^+ = 559$	$[M_3 + Na]^+ = 575$	$[M_4 + Na]^+ = 591$	$[M_5 + Na]^+ = 607$	$[M_6 + Na]^+ = 623$

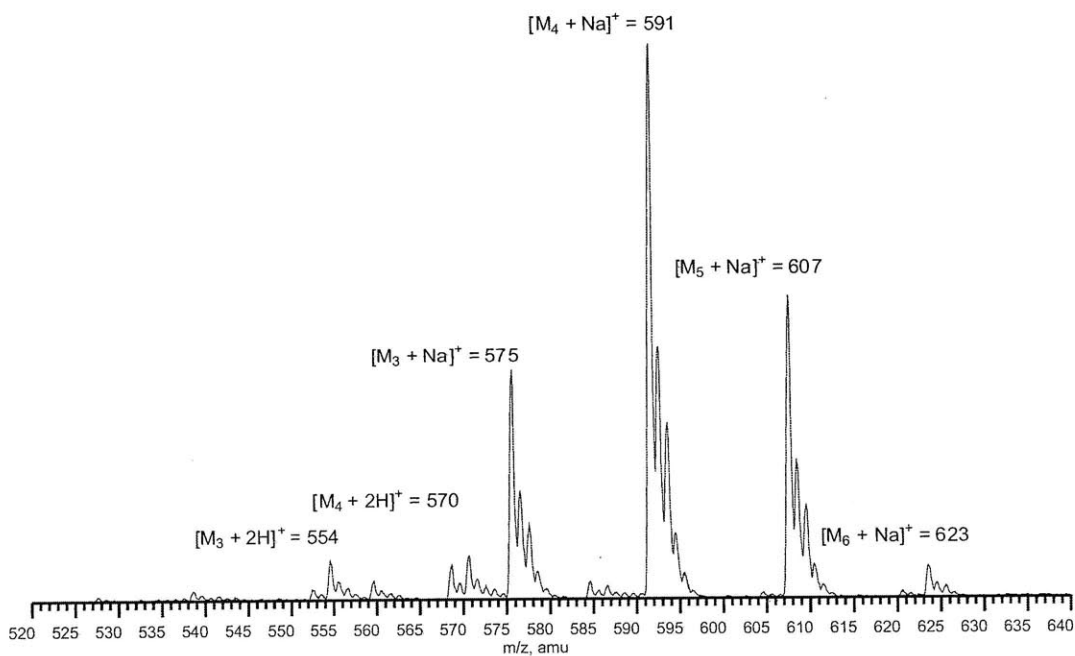
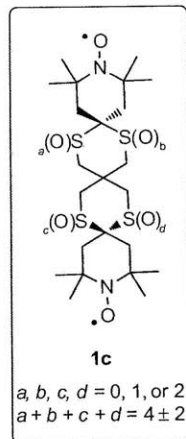


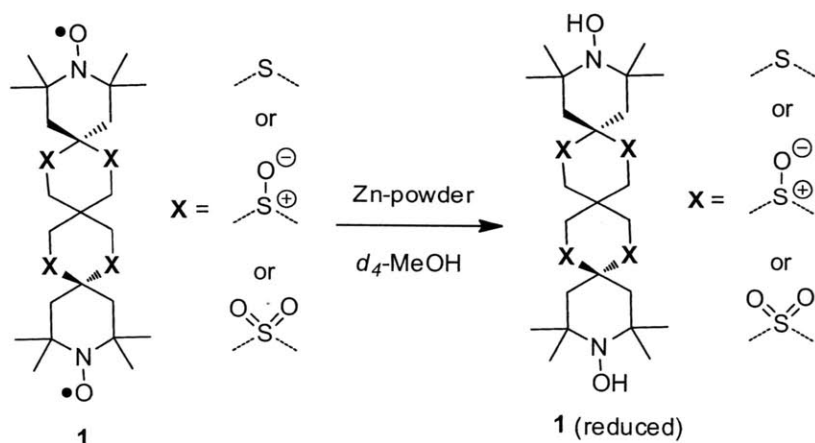
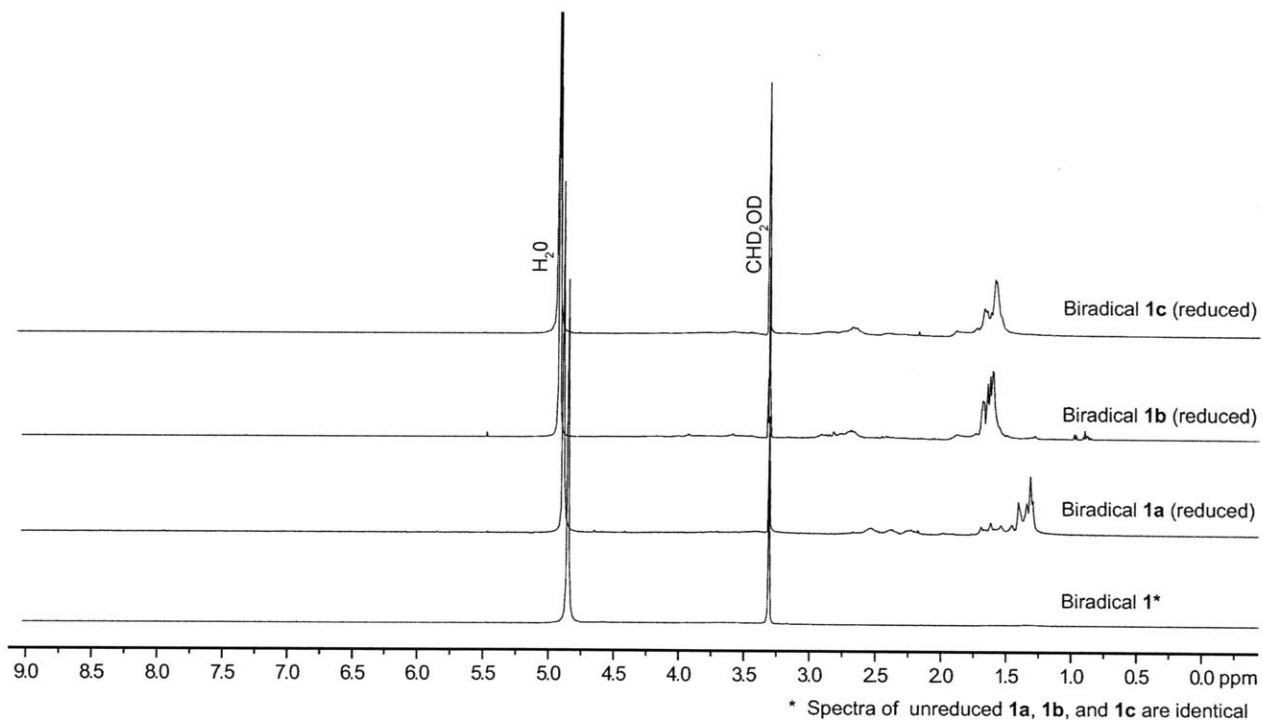
Figure A5.

Electrospray Ionization (ESI) MS of biradical mixture **1c**. Sample was loaded in a methanol solution with 0.1 mM sodium perchlorate and detected in positive ion mode.

4.8 NMR spectra

Biradical **1** ¹H-NMR

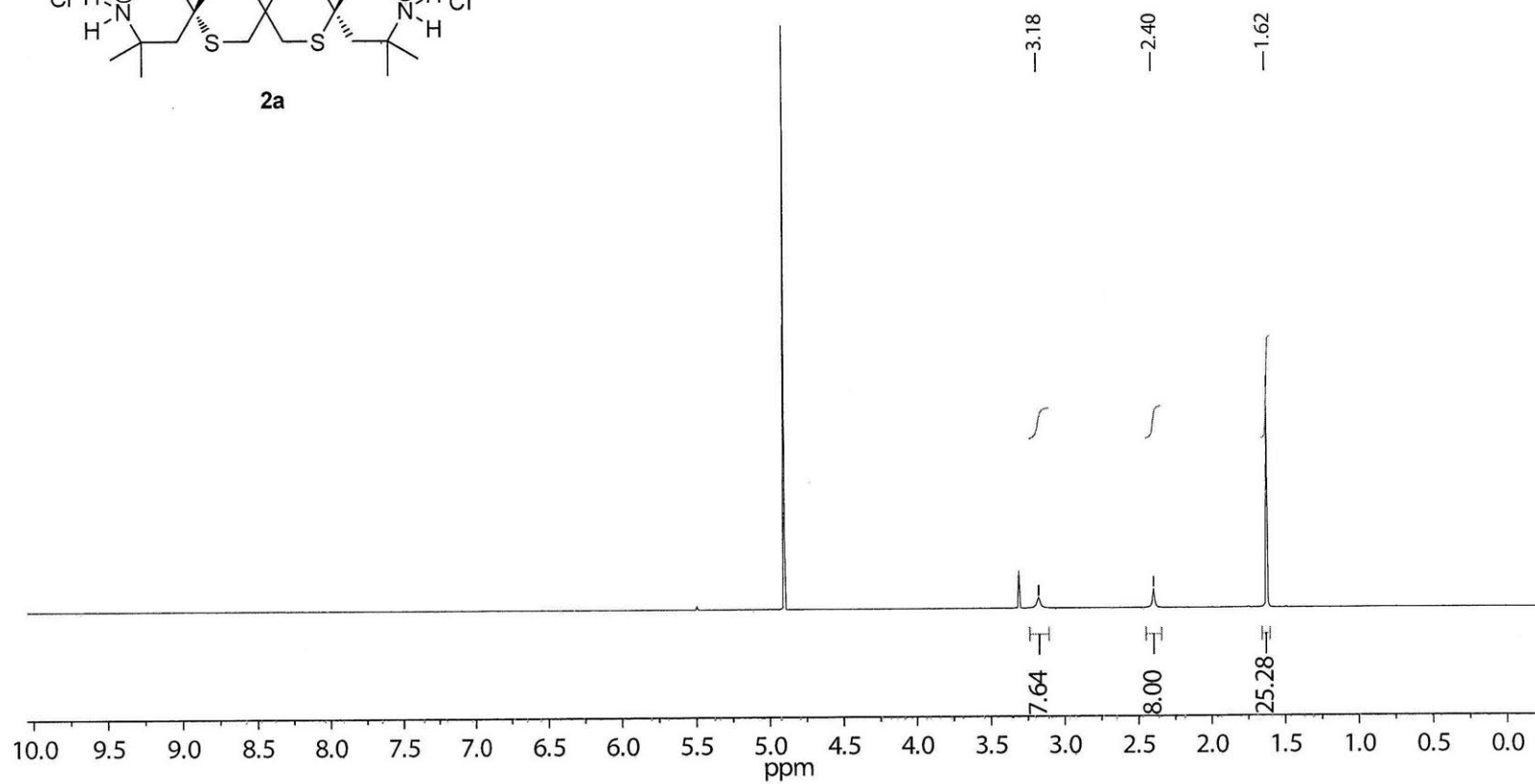
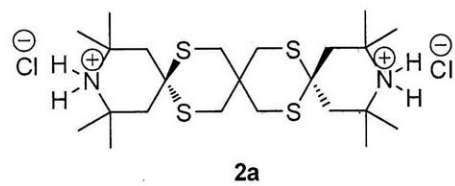
CD₃OD, 500 MHz



	reaction solvent
1a	CH ₂ Cl ₂
1b	C ₆ H ₆
1c	CH ₃ CN

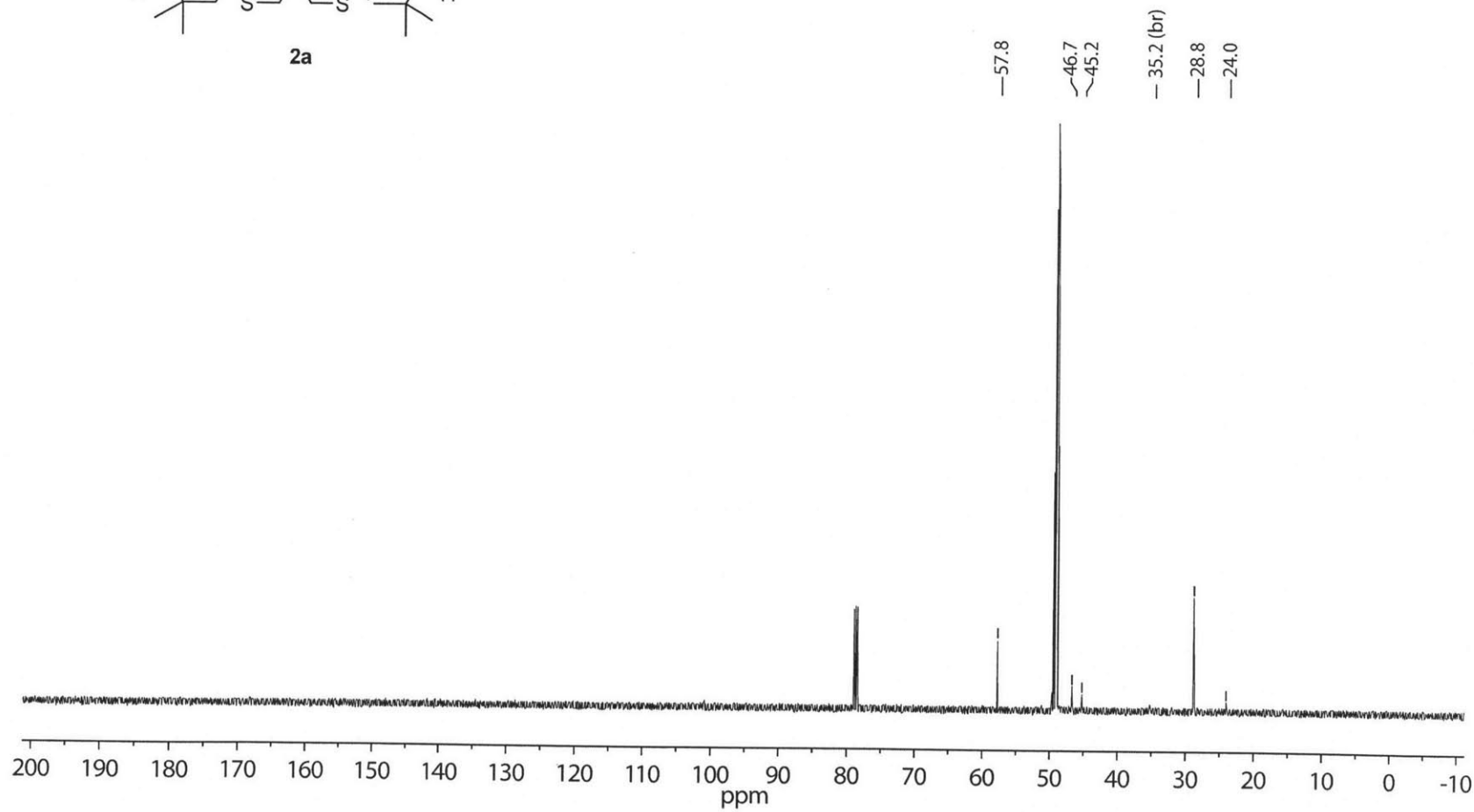
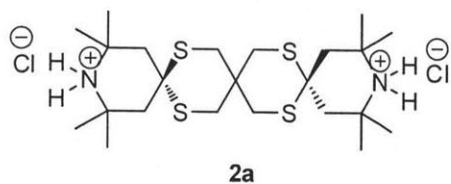
Compound **2a** ¹H-NMR

CD₃OD, 500 MHz



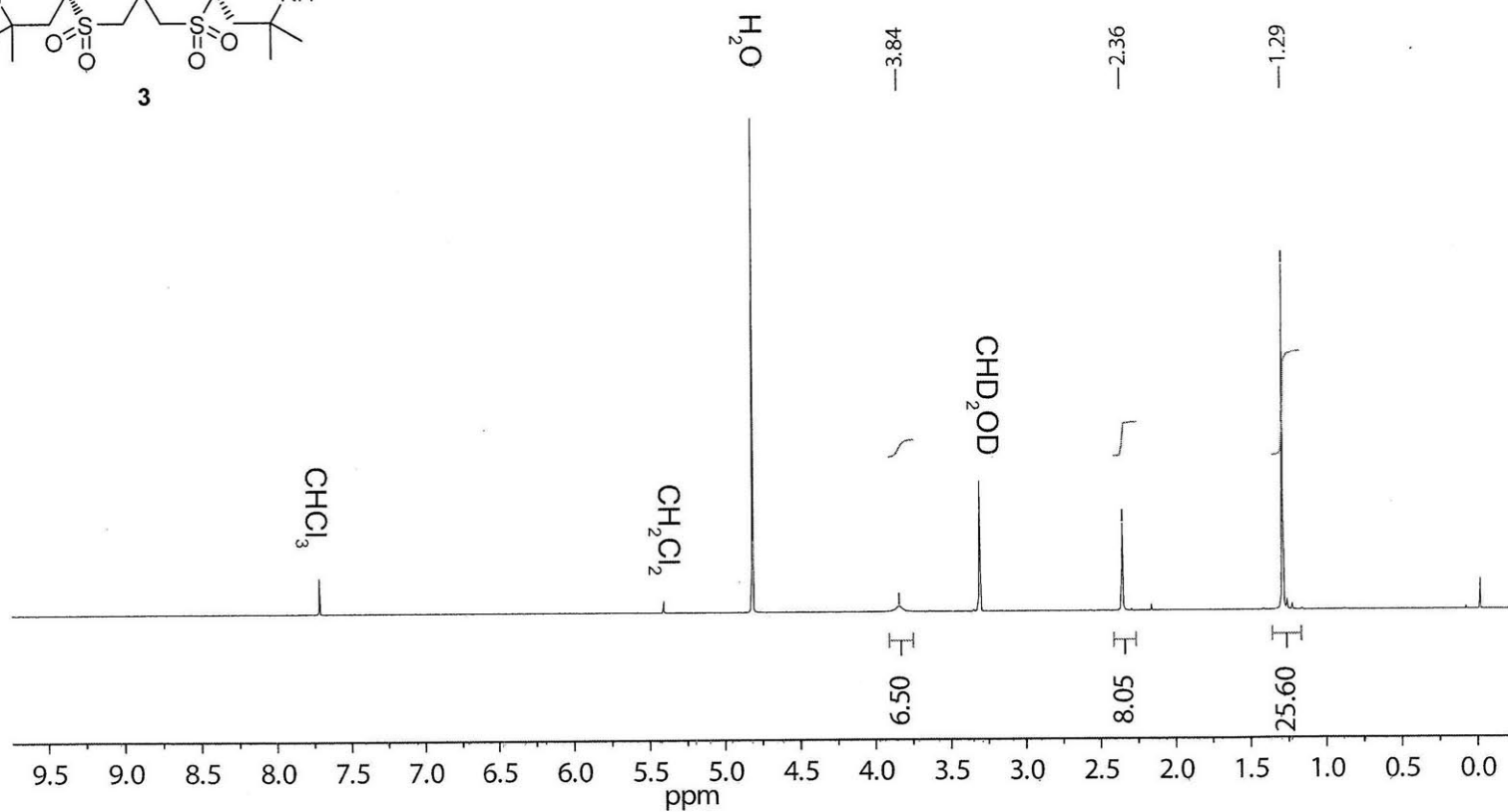
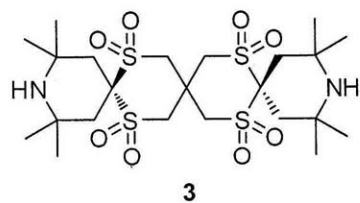
Compound **2a** ^{13}C -NMR

CD_3OD , 126 MHz



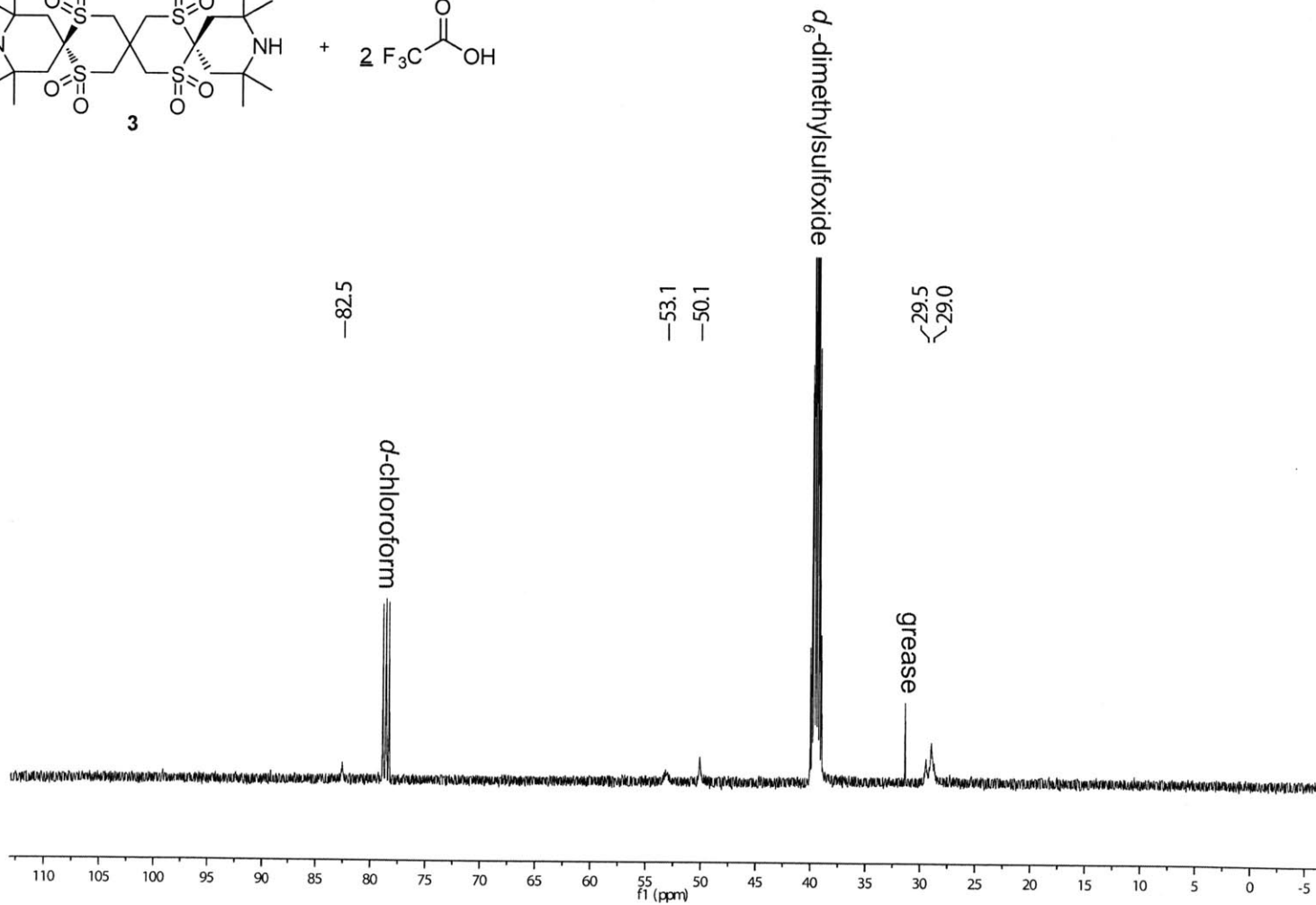
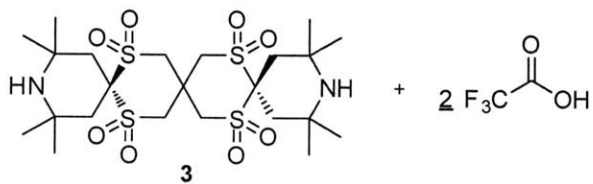
Compound **3** $^1\text{H-NMR}$

$\text{CD}_3\text{OD}/\text{CDCl}_3$, 500 MHz



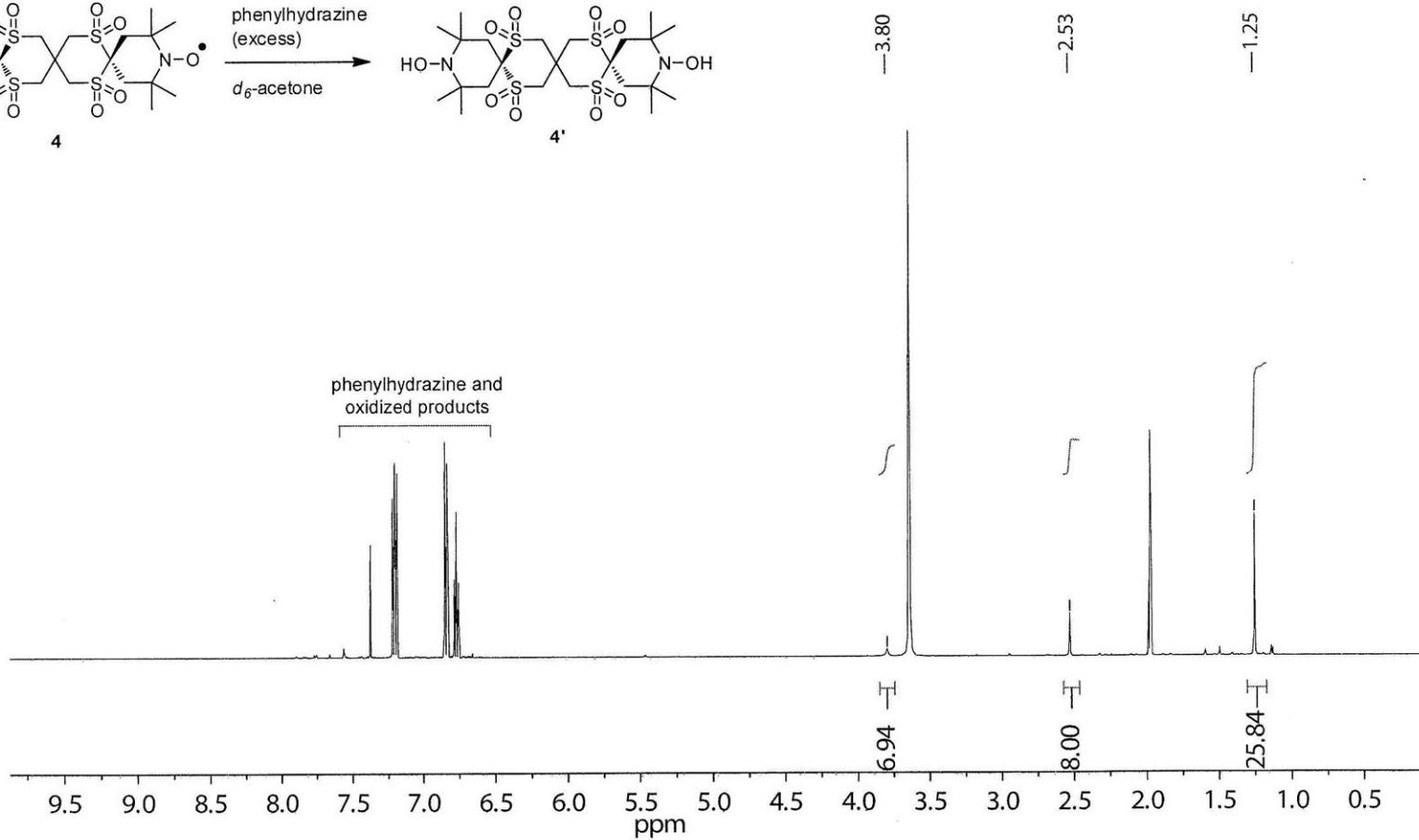
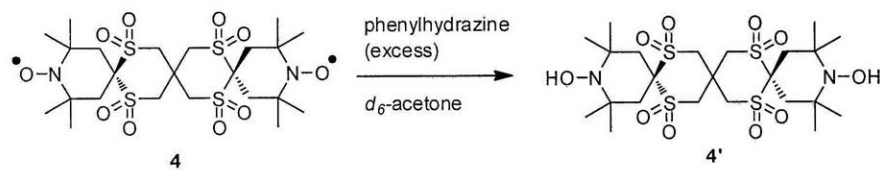
Compound **3** ^{13}C -NMR

d_6 -DMSO/ d -chloroform, 126 MHz, T = 50 °C



Compound **4'** (reduced) ¹H-NMR

C₂D₆O, 500 MHz



CHAPTER 5

Conjugated Polymers That Respond to Oxidation with Increased Emission

Adapted from:

Dane, E. L.; King, S. B.; Swager, T. M. *J. Am. Chem. Soc.* **2010**, *132*, 7758.

5.1 Introduction

Living in an oxidizing environment is essential for most life, but it has generally been an impediment to the use of fluorescent conjugated polymers (CPs) in practical applications. Fluorescent CPs are an important class of functional materials that have found use in applications ranging from organic light emitting diodes (OLEDs)¹ to the detection of TNT vapor at ppb-levels via amplified fluorescence quenching.² Because most conjugated polymers become less emissive when oxidized, photobleaching attributed to reactions involving oxygen has limited their use.³ In order to better understand how to synthesize materials that are robust in our oxygen-rich atmosphere, we became interested in CPs that upon oxidation showed productive changes in emission, such as a large increase in emission, a significant shift in emission wavelength, or greater photostability.

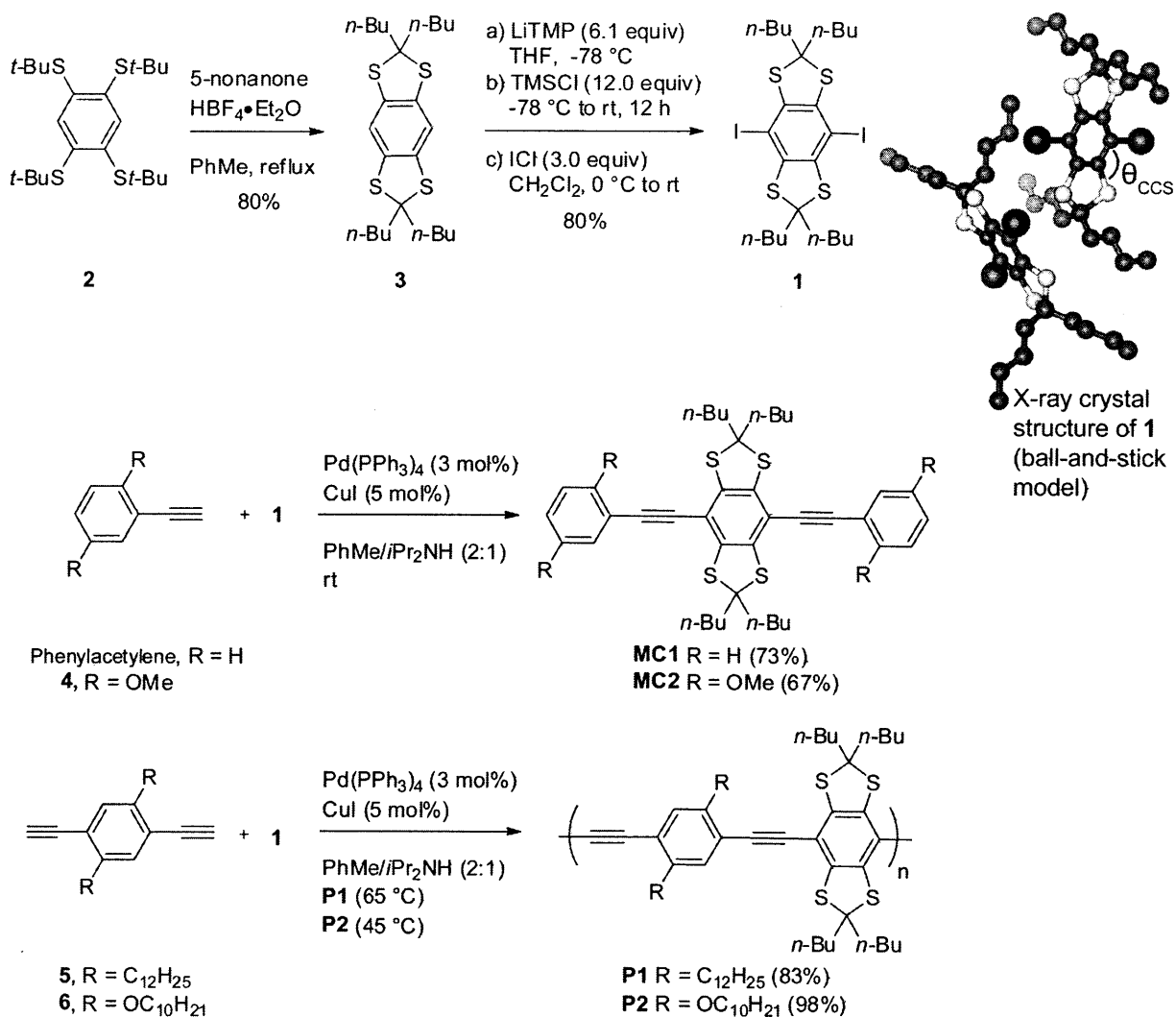
Materials that show an increase in emission when oxidized are also candidates for the turn-on fluorescence detection of peroxide oxidants. Being able to detect organic peroxides, such as triacetone triperoxide (TATP), is important because they can be used to make dangerous explosive devices.⁴ On the other hand, hydrogen peroxide plays important biological roles, including being a disease marker and acting as a signaling molecule.⁵ Therefore, compounds that show an increase in fluorescence when oxidized by peroxides are important to the development of new sensing materials.

Previous studies on the photobleaching of fluorescent CPs have focused on understanding the mechanism. For example, fluorenone defects in polyfluorene act as low-energy trap sites that cause decreased emission intensity.⁶ In poly(*paraphenylene-vinylene*) (PPV) polymers, it has been suggested that the main degradation pathway involves the reaction of singlet oxygen with the alkenyl-group, resulting in the formation of carbonyl defects that eventually result in chain scission.³ In poly(*paraphenylene-ethynylene*) (PPE)⁷ polymers, the mechanism of photobleaching has not been elucidated, but studies suggest that in model systems alkynes are less prone to reaction with singlet oxygen than alkenes.⁸ However, it is not clear that the observed photobleaching results solely from covalent bond formation between the CPs and oxygen species, because in some

cases it has been shown to be reversible.⁹ Although the specific mechanism is not known, CPs show greater photostability when irradiated under anaerobic conditions indicating that the presence of oxygen is important to photobleaching.¹⁰ Previous work from our group has found that antioxidants and triplet-quenchers, such as cyclooctatetraene derivatives, can be added to thin-films of CPs to attenuate photobleaching under irradiation.¹¹ Additionally, we have shown that polymers with high ionization potentials, due to the presence of electron-withdrawing perfluoroalkyl substituents, showed resistance to photobleaching.¹² Building on these previous investigations, this report focuses on designing CPs that respond positively to oxidation.

Previous examples of conjugated polymers where it was shown that oxidation did not cause a decrease in emission include polyfluorenes that contain small amounts of either a phosphafluorene or phosphafluorene-oxide comonomer.¹³ Compared to the phosphine polymer's emission, the phosphine oxide polymer's emission was red-shifted in the solid state, but not in solution. However, the oxidized polymers had roughly the same emission efficiency as the unoxidized polymers, and in this example, the oxidation was carried out on the monomer before polymerization. We chose to append sulfur atoms, in the form of thioethers, directly to the polymer backbone because thioethers can be selectively oxidized in the presence of alkynes. We were interested in what effect oxidation of a thioether to a sulfoxide or a sulfone would have on the photophysical properties of a PPE. Additionally, we hypothesized that the electron-withdrawing nature of the sulfoxides and sulfones would lead to changes in absorption and emission wavelengths due to donor-accepter interactions.

Conjugated polymers that contain sulfur atoms are ubiquitous in materials chemistry, but almost exclusively the sulfur atom is contained in a thiophene ring.¹⁴ Surprisingly, we can find relatively few examples of the incorporation of thioethers into CPs, though a review by Gingras¹⁵ summarizes how chemists have exploited the properties of persulfurated aromatic compounds. Lehn¹⁶ synthesized a series of diacetylene-linked poly(phenylthio)-substituted benzenes that showed the ability to be multiply reduced, taking advantage of sulfur's ability to stabilize negative charge. Additionally, several examples of thioether-containing PPV CPs have been reported.¹⁷ In



Scheme 1. Synthesis of **1**, **MC1**, **MC2**, **P1**, and **P2**.

general, aromatic sulfones, and especially aromatic sulfoxides, have not been extensively utilized in materials chemistry.

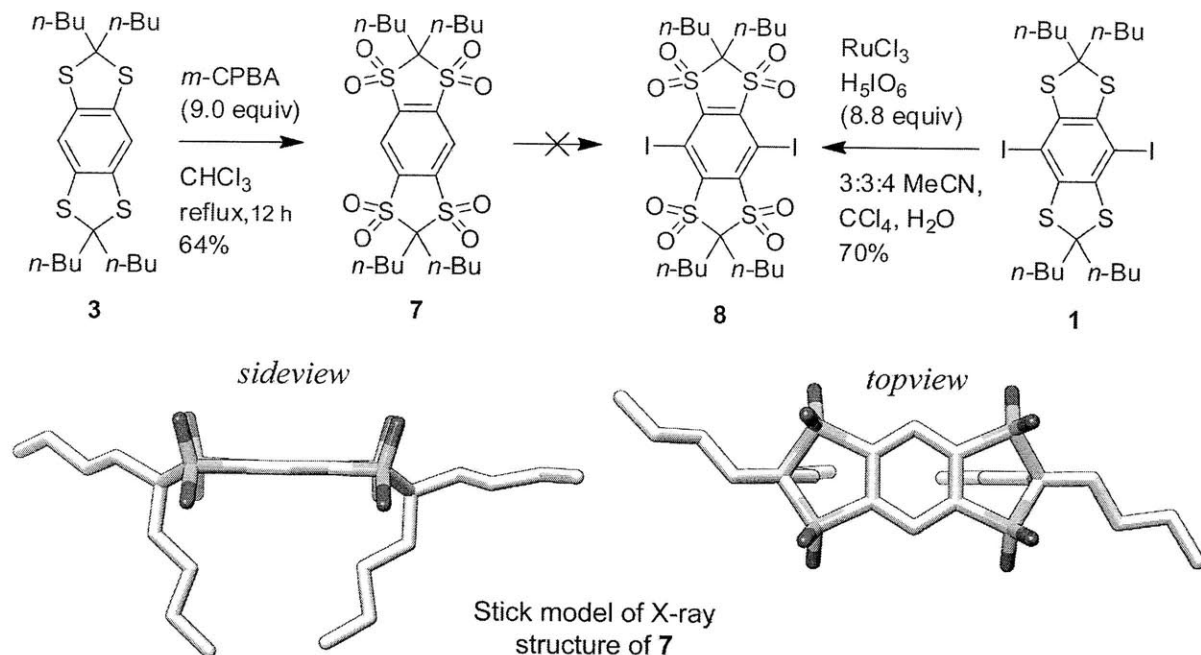
We designed a monomer that contains four thioethers divided between two dithiolane rings. Because the sulfur atoms of **1** (Scheme 1) are not members of an aromatic ring system, it was anticipated that they would behave differently than a sulfur atom in a thiophene ring system. The five-member rings have the advantage of tying back the sulfur atoms ($\theta_{\text{CCS}} = 123\text{-}124^\circ$, see Scheme 1, X-ray structure of **1**) and minimizing their steric interference with the reactive positions used in polymerization. Additionally, they allow for the facile introduction of solubilizing groups from

readily available symmetrical and asymmetrical ketones via acid-catalyzed condensation. It was anticipated that the branching of the aliphatic solubilizing groups would aid in solubility and prevent aggregation in the solid-state. Monomers and polymers with a similar geometry with oxygen in place of sulfur have been recently described.¹⁸

5.2 Synthesis

Monomer **1** is available in three steps from inexpensive starting materials without the need for chromatography. Compound **2** was synthesized via complete nucleophilic aromatic substitution of 1,2,4,5-tetrachlorobenzene with sodium 2-methylpropane thiolate in refluxing dimethylformamide, followed by recrystallization from refluxing methanol (59% yield).¹⁹ The *tert*-butyl groups were deprotected *in situ* and the resulting thiols were condensed with 5-nonanone in the presence of $\text{HBF}_4 \cdot \text{Et}_2\text{O}$ in refluxing toluene. Compound **3** could not be successfully brominated or iodinated via electrophilic aromatic substitution, presumably due to nucleophilic attack by the thioethers on the electrophilic reagents and subsequent side-reactions. Rather than pursue a method of sequential lithiations, we used an excess of lithium tetramethylpiperidine and chlorotrimethylsilane to drive the double deprotonation of **3** to completion.²⁰ The resulting di-trimethylsilyl product was carried through to be iodinated with ICl in CH_2Cl_2 . Monomer **3** was purified by recrystallization from hexane and obtained in an overall yield of 38% as an air-stable yellow solid.

Model compounds (**MC1** and **MC2**) and polymers (**P1** and **P2**) were synthesized via Sonogashira cross-coupling in good yield. **P1** was isolated as a high molecular weight polymer ($M_n = 236,000$ g/mol) according to gel permeation chromatography (GPC) and was soluble in common organic solvents such as CH_2Cl_2 and THF. Under the same conditions, **P2** formed high molecular weight polymers that became insoluble, either because with increased chain length the polymers become insoluble or because of the presence of cross-linking. In order to isolate soluble polymers, the temperature of the polymerization was lowered from 65 °C to 45 °C. At the lower reaction temperature, the molecular weight of **P2** ($M_n = 18,900$ g/mol) decreased and the isolated polymer was soluble. In addition to GPC, the polymers were characterized by ^1H and ^{13}C NMR and IR.

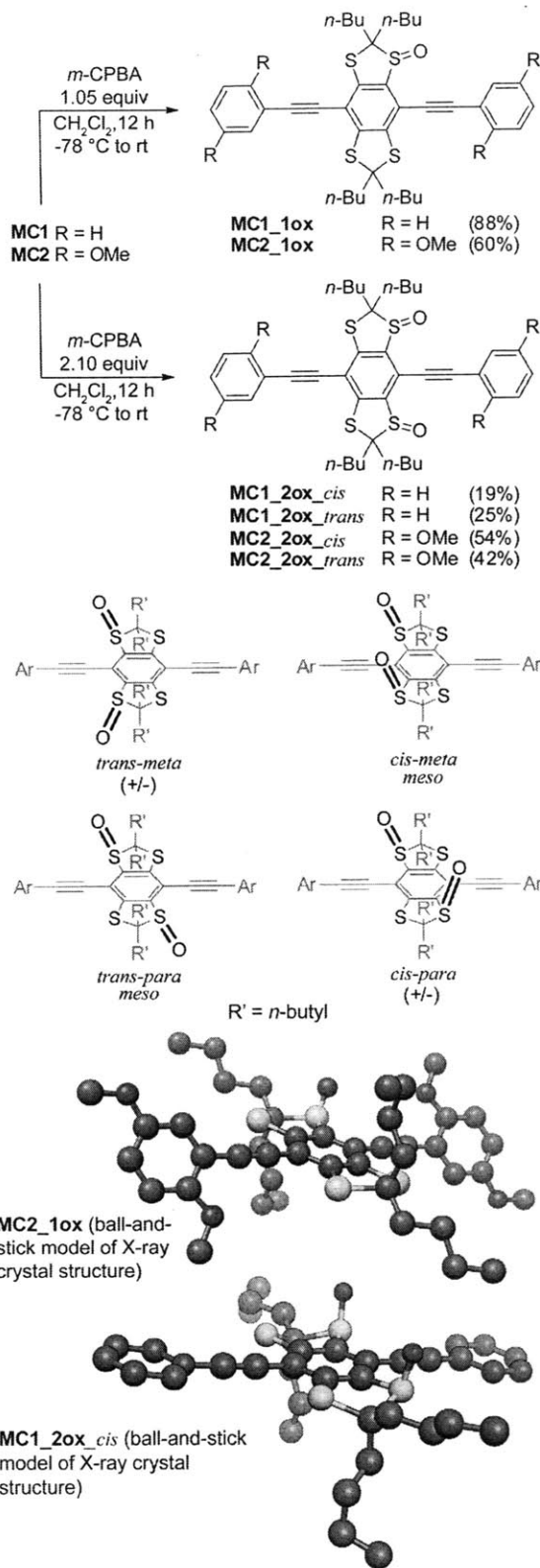


Scheme 2. Synthesis of 7 and 8.

The fully oxidized form of monomer **1** was desired so that the fully oxidized model compounds and polymers could be synthesized. Compound **3** could be oxidized to tetrasulfone **7** in refluxing chloroform with a slight excess of *m*-CPBA (Scheme 2). Attempts to halogenate **7** via electrophilic aromatic bromination or iodination were unsuccessful, likely as a result of the electron-poor nature of the aromatic ring. Attempts to employ the same lithiation strategy as was used to convert **3** to **1** were also unsuccessful, as were strategies of sequential lithiation and halogenation. The lack of success using lithiation strategies may be the result of a charge-transfer interactions between the lithium reagents and the substrate. This speculation is based on the observation of deeply colored reaction mixtures and the recovery of the starting material. Monomer **1** could be oxidized with ruthenium tetroxide, generated *in situ* from ruthenium (III) chloride, to obtain the desired tetrasulfone **8**.²¹ Unfortunately, attempts to use **8** in cross-coupling reactions with both mono- and dialkynes were unsuccessful. Proton NMR of the crude reaction mixtures suggested that **8** underwent de-iodination to form **7** in the reaction mixtures.

5.3 Oxidation of Model Compounds

Model compounds **MC1** and **MC2** were oxidized with one and two equivalents of *m*-chloroperbenzoic acid and the mono- and disulfoxides of each (**MC1_1ox**, **MC1_2ox**, **MC2_1ox**, and **MC2_2ox**) were isolated (Scheme 3). The mono- and disulfoxides were characterized with ¹H and ¹³C NMR, IR, and HRMS. For **MC2_1ox** and **MC1_2ox_cis**, X-ray crystallography was used to ensure the identity of the compound (Scheme 3). For each of the disulfoxides, four diastereomers were obtained (Scheme 3). The *cis*-isomers, in which the polar sulfoxide bonds point in the same direction and increase the overall dipole of the molecule, had a significantly longer retention time on silica gel as compared to the *trans*-isomers, in which the dipoles point in opposite directions. The two isomers were easily separated via chromatography. As expected, the directing influence of the thioethers favored a *meta*-orientation for the sulfoxides over a *para*- or an *ortho*-relationship, although a small amount of *para*-compound was observed in each case. The *meta*- and *para*-isomers show diagnostic ¹H and ¹³C NMR, with the *para*-isomer having fewer unique ¹H and ¹³C signals because of its higher symmetry. For



Scheme 3. Oxidation of **MC1** and **MC2** to mono- and disulfoxides.

MC1_2ox, the *cis*- and *trans*-products contained less than 10% of the *para*-isomer according to integration of the proton NMR. For **MC2_2ox**, the isolated *cis*- and *trans*-products contained the *meta*- and *para*-isomer in a ratio of roughly 3:1. The selectivity for the second oxidation to occur at the *meta*-position as opposed to the *para*-position results from the first sulfoxide withdrawing electron-density from the sulfur atoms in an *ortho*- and *para*-orientation more effectively than from the sulfur in a *meta*-orientation. The *ortho*-compound was not observed. The oxidation of the second sulfur in dithioacetals is often much slower as compared to the oxidation of the first, with the oxidation of the sulfoxide to sulfone as a competing process.²²

5.4 Optical and Photophysical Properties of the Model Compounds in Solution.

Both **MC1** and **MC2** have similar absorbance and emission properties (see Table 1, Figure 1) in solution (CH_2Cl_2). **MC1** and **MC2** have strong absorbance peaks between 300 and 400 nm, with a weaker absorbance between 400 and 500 nm. The absorbance maxima for **MC2** (375 nm) is red-shifted as compared to **MC1** (355 nm), as a result of the electron-donating methoxy groups at the 1- and 4-positions of the outer aryl rings. However, the same effect is not seen in the less intense band in the visible region, where the absorbance maximum of **MC1** (434 nm) is nearly the same as that of **MC2** (435 nm). **MC1** and **MC2** are relatively non-emissive, with quantum yields (Φ_f) of less than 0.01, and they show broad, featureless emission centered near 490 nm.

When thoroughly degassed with bubbling nitrogen, both **MC1** and **MC2** show an additional sharp, red-shifted emission peak (**MC1**, 560 nm; **MC2**, 580 nm) and a vibronic shoulder above 600 nm (see Figure A1 in Section 5.17). Exposure of the samples to air causes the peak to completely disappear. Quenching of the emission by oxygen indicates that the emissive process involves an excited triplet state (phosphorescence) rather than a singlet state (fluorescence). Room temperature phosphorescence is unusual for organic compounds of this type, and it indicates that the four thioether substituents on the central aromatic ring promote intersystem crossing from the singlet excited state to triplet excited state.²³

For both **MC1** and **MC2**, oxidation to the mono-sulfoxide causes an increase in Φ_f rela-

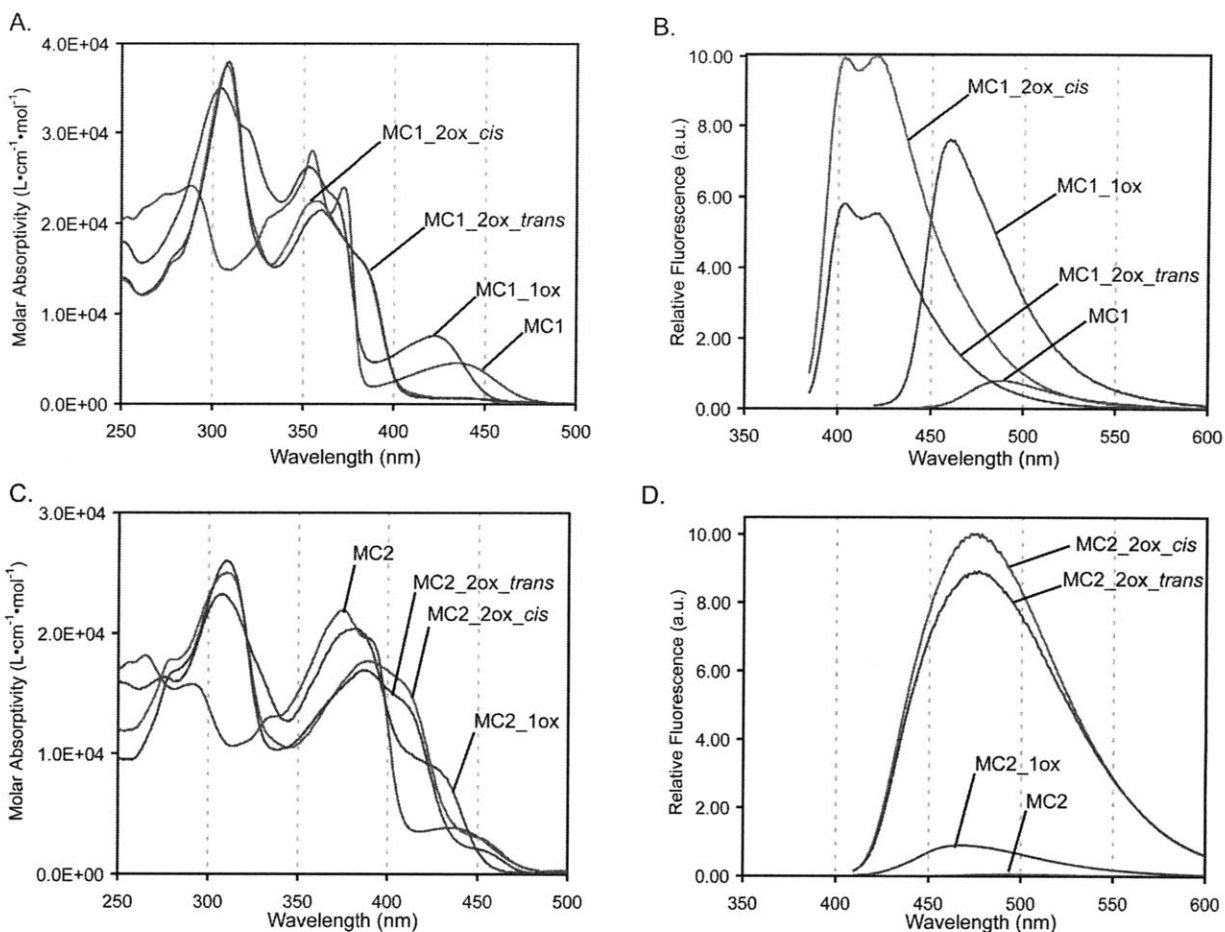


Figure 1. Model compound oxidation.

(a and c) The absorption spectra of **MC1**, **MC2**, and oxidation products. (b and d) The fluorescence spectra of **MC1**, **MC2**, and oxidation products. Within each plot, the fluorescence intensity is scaled to reflect the relative emissivity of each fluorophore as determined by its absolute quantum yield (see Table 1. for values). λ_{ex} : 420 nm (**MC1**, **MC2**), 390 nm (**MC1_1ox**, **MC2_1ox**, **MC2_2ox**), 370 nm (**MC1_2ox**). All spectra were taken in CH_2Cl_2 and all fluorescence spectra are corrected for PMT response.

tive to the parent compound, with the effect being more dramatic for **MC2**. This increase in Φ_{F} is accompanied by a blue-shift in emission, which is more pronounced for **MC1**. The emission maximum of **MC1** shifts from 489 nm for the unoxidized version to 458 nm for the monosulfoxide (**MC1_1ox**). The emission maximum of **MC2** shifts from 493 nm for the unoxidized version to 467 nm for the monosulfoxide (**MC2_1ox**). Further oxidation of **MC1_1ox** to **MC1_2ox** does not cause a significant change in Φ_{F} ; however it is accompanied by a shift in emission maximum from

Compound	$\lambda_{\text{max}}(\text{nm}) / \epsilon(\text{M}^{-1}\cdot\text{cm}^{-1})$	$\lambda_{\text{em}}(\text{nm})$	Φ_{F}^a	$\tau_{\text{F}}(\text{ns})$	$k_{\text{F}}^e(\text{ns}^{-1})$
MC1	355 (28,000), 372 (24,000), 434 (4,600)	489	0.0030	0.094 ^b	0.032
MC1_1ox	304 (35,000), 353 (26,000), 422 (7,600)	458	0.029	<0.4 ^{b,c}	>0.07 ^c
MC1_2ox_cis	308 (38,000), 358 (22,000)	403	0.038	<0.5 ^{b,c}	>0.08 ^c
MC1_2ox_trans	309 (38,000), 360 (21,000)	403	0.022	<0.4 ^{b,c}	>0.06 ^c
MC2	375 (22,000), 435 (4,500)	493	0.0030	0.099 ^b	0.030
MC2_1ox	308 (23,000), 381 (20,000)	467	0.055	2.7 ^d	0.020
MC2_2ox_cis	310 (25,000), 387 (18,000)	473	0.62	2.9 ^d	0.21
MC2_2ox_trans	310 (26,000), 387 (17,000)	473	0.52	2.9 ^d	0.18

^aAbsolute quantum yields were determined by comparison with 9,10-diphenylanthracene in cyclohexane ($\Phi_{\text{F}} = 0.90$). ^bFluorescence lifetimes were measured using a pulsed-femtosecond laser (350 nm) and were fit to monoexponential decays with $R^2 > 0.99$. ^cObtained lifetimes could be fit to monoexponential decays, but the emission profile suggested that photodegradation via deoxygenation to the sulfide occurred during excitation. Therefore, only an upper bound is placed on the lifetime, and a minimum k_{F} is calculated. ^dFluorescence lifetimes were measured using a pulsed-picosecond laser (415 nm) and were fit to monoexponential decays with $R^2 > 0.99$. ^e $\Phi_{\text{F}}/\tau_{\text{F}}$.

Table 1. Model Compound Photophysics in CH_2Cl_2

458 nm to 403 nm and a change in the structure of the emission. Conversely, further oxidation of **MC2_1ox** to **MC2_2ox** results in a 10-fold increase in fluorescence quantum yield, and is accompanied by a small red-shift of the emission maximum from 467 nm to 474 nm. As discussed in the previous section, *cis*- and *trans*-isomers of **MC1_2ox** and **MC2_2ox** were isolated and characterized separately. There appears to be no significant difference in the photophysical properties of the *cis*- and *trans*-isomers. However, it should be noted that in all cases the *cis*- and *trans*-isomers were isolated as a mixture of regioisomers. Because the compounds were not separated, we cannot comment on how the *meta*- versus *para*-orientation of the sulfoxides affects the photophysical properties.

To investigate the effect of further oxidation, the absorbance and emission changes caused by adding increasing amounts of *m*-CPBA to dilute solutions of **MC1** and **MC2** were observed (see Figure A2 in Section 5.17). Increasing oxidation of **MC1** is accompanied by blue-shifted absorbance and emission, and a general increase in emission. Comparison of the spectrum with isolated compounds indicates that after the initial formation of **MC1_1ox**, a significant amount of **MC1_2ox** is formed. Additionally, a peak emerges at 422 nm that we attribute to sulfone-containing compounds with significantly higher quantum yields than the sulfoxides. To understand the

effect of sulfone formation, **MC1** was treated with 8.0 equiv of *m*-CPBA in refluxing CH₂Cl₂ overnight. The least polar fractions were separated by chromatography. The mixture obtained showed strong sulfone signals in FT-IR (see Figure A3), an absorption maximum at 392 nm, and a broad emission with a maximum near 414 nm. The sulfone-containing compounds are also much more emissive than the sulfoxides, with an average quantum yield of 0.40 measured at several excitation wavelengths between 350 nm and 380 nm.

When **MC2** is titrated with oxidant, there is an initial blue shift in absorbance and emission, also accompanied by a substantial increase in emission. However, as the compound is further oxidized the donor-acceptor interaction that develops between the electron-rich terminal aromatic rings and the increasingly electron-poor center ring causes a red-shift in absorbance and emission. The red-shift in emission is accompanied by a decrease in emission efficiency, however the resulting fluorophores are still substantially more emissive than the parent compound.

5.5 Oxidation of Polymers

Polymers **P1** and **P2** were oxidized with 2.10, 3.15, 4.20, 6.30, and 8.40 equivalents of *m*-CPBA overnight at room temperature in a CH₂Cl₂ solution (Figure 2, **P1A-D** and **P2A-D**). The oxidation products of **P1** did not show substantial changes in color; however the reaction mixtures became noticeably green fluorescent under ambient light. Conversely, the color of **P2** changed from yellow to red with increasing amounts of oxidation. The effect of the oxidation on molecular weight was monitored with GPC and is summarized in Table 2. The M_n of the polymers decreased with greater amounts of oxidation. The addition of 8.4 equiv of oxidant caused the molecular weight of **P1** to decrease by half. This suggests that oxidation at the alkyne linkages becomes more competitive with sulfur oxidation with higher amounts of oxidant. It has been reported that diphenylacetylene slowly reacts with *m*-CPBA in chloroform at room temperature to give a variety of oxidation products resulting from the initial formation of an oxirene.²⁴ Some of the oxidation products reported result in cleavage of the diphenylacetylene into two molecules, while others contain linkages that are susceptible to cleavage.²⁵

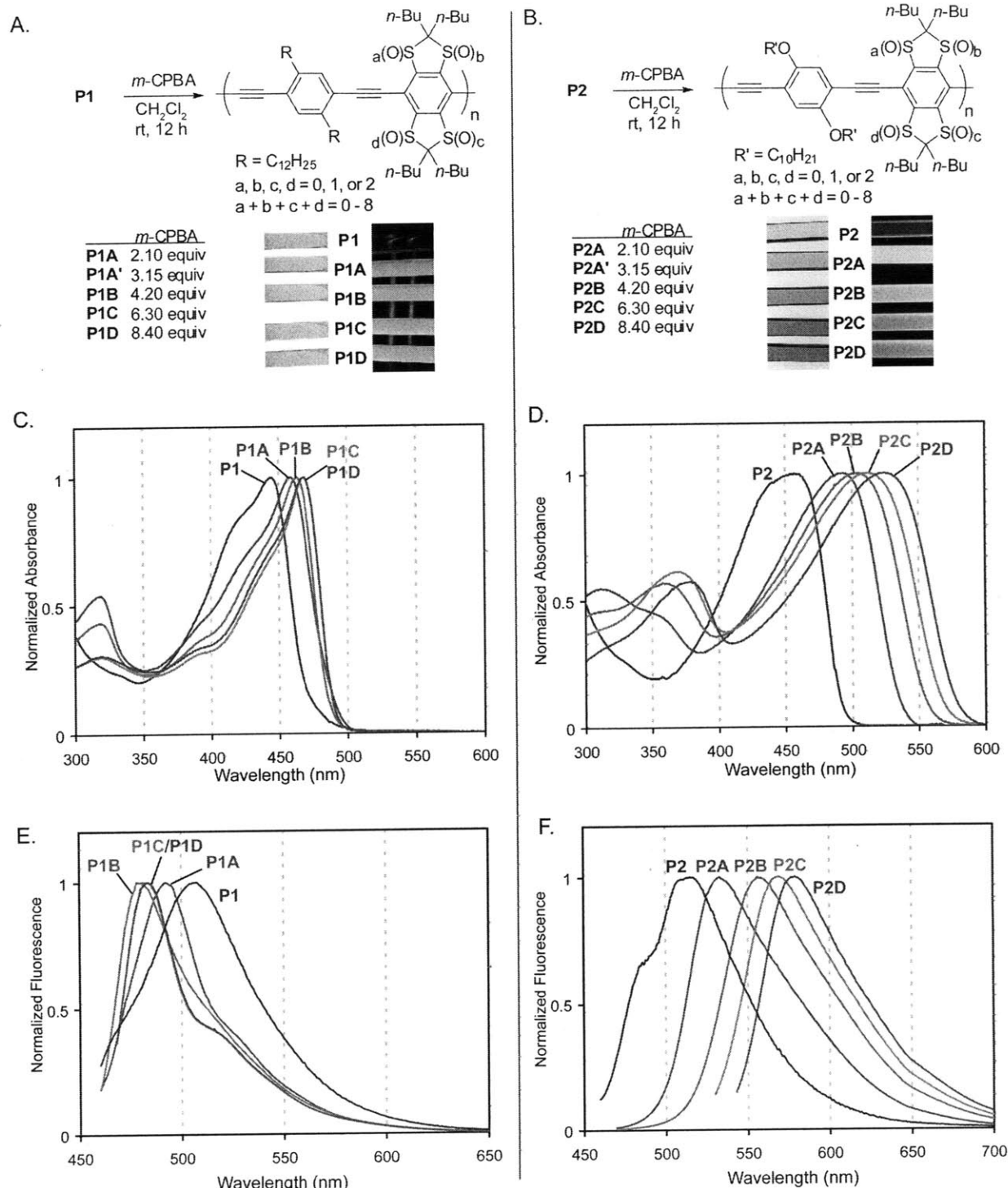


Figure 2. Polymer oxidation.

(a and b) The oxidation of **P1** and **P2** with increasing amounts of oxidant is shown. Photographs show solutions of the polymers in CDCl_3 (5 mg/mL) under ambient light (left) and irradiated at 365 nm with a handheld lamp (right). (c and d) The absorbance spectra of dilute solutions of **P1**, **P1A-D**, **P2**, and **P2A-D** in CH_2Cl_2 are shown. (e and f) The fluorescence spectra of dilute solutions of **P1**, **P1A-D**, **P2**, and **P2A-D** in CH_2Cl_2 are shown and are corrected for PMT response. λ_{ex} : 440-450 nm (**P1**, **P1A-D**), λ_{max} minus 10 nm (**P2**, **P2A-D**).

The presence and relative abundance of sulfoxides and sulfones in the oxidized samples of **P1** and **P2** were evaluated with infrared spectroscopy and compared to similar spectra for the model compounds (see Figures A3, A4 in section 5.17). Oxidation causes significant changes in the spectra of both polymers between 1600 and 850 cm^{-1} (Figure 3). Initially, **P1** has a relatively featureless spectrum. Oxidation with 2.1 equiv. of *m*-CPBA causes a strong absorption band at 1077 cm^{-1} to appear, indicating sulfoxide formation. This band continues to grow and broaden with further oxidation. Beginning with **P1C** and continuing in **P1D**, two peaks at 1335 and 1160 cm^{-1} belonging to sulfones appear. The IR spectrum of **P2** is more challenging to interpret, because signals between 1150 and 1000 cm^{-1} from the aryl ether groups interfere with the observation of the sulfoxide band in the oxidized polymers. **P2A** shows a strong sulfoxide band at 1081 cm^{-1} , but does not show sulfone bands. Sulfone bands appear in **P2B** and are accompanied by a decrease in the initial signal belonging to sulfoxides, which suggests that some of the sulfoxides have been oxidized to sulfones. Beginning with **P2C** and continuing in **P2D**, the sulfone peaks at 1335 and 1161 cm^{-1} continue to

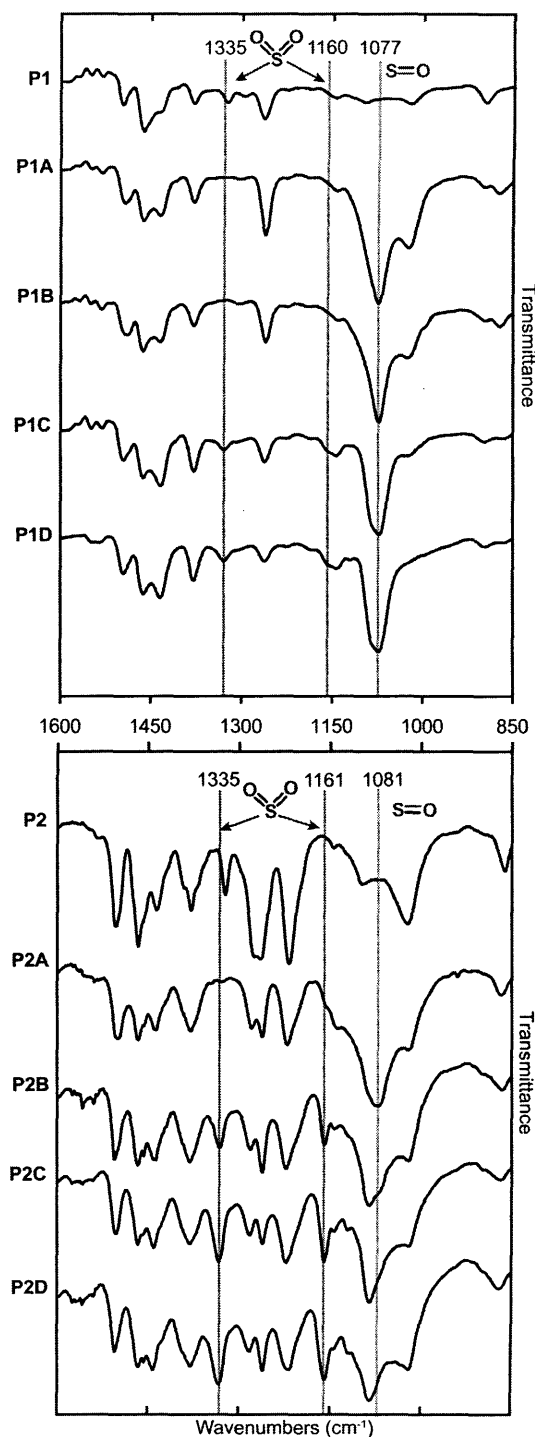


Figure 3. Polymer infrared spectra. A portion of the IR spectra of **P1**, **P1A-D**, **P2**, and **P2A-D** is shown with blue lines indicating sulfone bands and red lines indicating sulfoxide bands. Samples were drop-cast on KBr plates from concentrated CH_2Cl_2 solutions.

grow as the sulfoxide signal weakens.

In summary, IR shows that both **P1** and **P2** are first oxidized to sulfoxides and then oxidized to sulfones. **P2** appears to be more easily oxidized to sulfones relative to **P1**, because of its more electron-rich comonomer. It is difficult to comment quantitatively on the level of oxidation using IR, however the spectra support some important qualitative observations. The **P1A** and **P2A** spectra suggest that most of the thioether-containing aromatic rings have been oxidized to the disulfoxide, which is in accord with the reactivity seen in the model compounds. The weak sulfone bands seen in **P1D** indicate minimal sulfone formation with 8.40 equiv of oxidant, which suggests that most of the thioether repeating units have four or less oxygen atoms. This is in contrast with the strong sulfone bands observed in **P2D**, which suggest that each thioether repeating unit contains at least four oxygen atoms. In both **P1** and **P2**, the oxidized polymers have complex structures. Although this extra-dimension of polydispersity makes characterization challenging, it likely aids in solubility and reduces crystallinity.

5.6 Optical and Photophysical Properties of the Polymers in Solution.

Our primary method of evaluating the effect of oxidation on the polymers is absorption and fluorescence spectroscopy (Figure 2, Table 2). **P1** is relatively nonemissive, with a ΦF less than 0.01. **P1A**'s absorbance ($\lambda_{\text{max}} = 459 \text{ nm}$) is red-shifted as compared to **P1** ($\lambda_{\text{max}} = 444 \text{ nm}$). **P1A**'s emission maximum is blue-shifted from 512 nm to 492 nm relative to the parent polymer, and its quantum yield increases dramatically (35-fold). When **P1** is treated with 4.2 equivalents of oxidant (**P1B**), the absorbance red-shifts and the emission blue-shifts. The spectral changes for **P1B** are accompanied by an increase in quantum yield to 0.53, but the effect of further oxidation is minor.

Similar to **P1**, **P2** is relatively non-emissive in solution, with a quantum yield less than 0.01. The quantum yield of **P2A** is 0.49, which represents a more than 49-fold increase in emission when the polymer is treated with 2.1 equivalents of oxidant. Additional oxidation causes continued red-shifting in absorbance and emission, as can be seen in **P2B**, **P2C**, and **P2D**. How-

Polymer	λ_{\max} (nm)/ ϵ (M ⁻¹ •cm ⁻¹) ^a		λ_{em} (nm)		Φ_F		τ_F^d (ns)	k_F^e (ns ⁻¹)	M_n^f (kDa)	M_w^f (kDa)	PDI ^g
	CH ₂ Cl ₂	film	CH ₂ Cl ₂	film	CH ₂ Cl ₂ ^b	Film ^c	CH ₂ Cl ₂	CH ₂ Cl ₂			
P1	444 (44,000)	457	512	517	0.0096	<0.01	0.13	0.074	236 ^h	1,990	8.40
P1A	459 (38,000)	464	492	500	0.35	<i>n.d.</i>	0.67	0.52	265	2,710	10.2
P1A'	463 (50,000)	<i>n.d.</i>	480	<i>n.d.</i>	0.61	<i>n.d.</i>	0.68	0.90	<i>n.d.</i>	<i>n.d.</i>	<i>n.d.</i>
P1B	463 (54,000)	467	479	498	0.53	0.57	0.73	0.72	215	2010	9.35
P1C	468 (69,000)	469	483	495	0.59	0.70	0.71	0.83	112	587	5.24
P1D	468 (48,000)	468	483	495	0.48	<i>n.d.</i>	0.80	0.60	102	384	3.76
P2	457 (43,000)	489	526	503	0.0085	<0.01	0.17	0.050	18.9 ^h	31.1	1.65
P2A	494 (29,000)	500	532	551	0.49	0.56	1.35	0.36	18.8	32.3	1.72
P2A'	497 (30,000)	<i>n.d.</i>	540	<i>n.d.</i>	0.42	<i>n.d.</i>	1.34	0.31	<i>n.d.</i>	<i>n.d.</i>	<i>n.d.</i>
P2B	503 (25,000)	503	556	580	0.28	<0.10	1.51	0.19	15.9	23.6	1.48
P2C	513 (29,000)	512	568	594	0.25	<0.10	1.66	0.15	13.0	20.3	1.56
P2D	524 (23,000)	520	579	599	0.19	<0.10	1.72	0.11	14.3	22.4	1.57

^a Molar absorptivity based on molecular weight of repeat unit. ^b Absolute quantum yields were determined for **P1**, **P1A-D**, **P2**, and **P2A-B** by comparison with coumarin-6 in ethanol ($\Phi_F = 0.76$). **P2C** and **P2D** were compared to rhodamine B in ethanol ($\Phi_F = 0.49$). ^c Thin film quantum yields of **P1B**, **P1C**, and **P2A** were determined using an integrating sphere and monochromatic light of several wavelengths near the λ_{\max} . Thin-film quantum yields of **P1**, **P2**, **P2B**, **P2C**, **P2D** were determined by comparison with thin-films of perylene in PMMA ($\Phi_F = 0.78$). ^d Fluorescence lifetimes were measured using a pulsed-femtosecond laser (350 nm, **P1**, **P2**) or pulsed-picosecond (415 nm, **P1A-D**, **P2A-D**) laser and were fit to monoexponential decays with $R^2 > 0.99$. ^e Φ_F/τ_F . ^f Determined with GPC(THF) against polystyrene standards. ^g M_w/M_n . ^h Degree of polymerization (DP) based on polymer repeat unit is 260 for **P1** and 21 for **P2**.

Table 2. Polymer Photophysics

ever, greater oxidation is accompanied by a decrease in quantum yield, which appears to be at least partially a result of a decrease in the rate of fluorescence (k_F).

5.7 Response to Hydrogen Peroxide in Solution

The model compounds and polymers did not react with hydrogen peroxide in solution at room temperature. To facilitate a reaction, the oxidation catalyst methylrheniumtrioxide (MTO)²⁵ was added as described by Malashikin and Finney.^{4a} The absorbance and emission of dilute solutions of **MC2** and **P2** in quartz cuvettes were recorded after the addition of catalyst ([MTO] = 0.5 mM), but before the addition of oxidant.²⁶ Following the addition of hydrogen peroxide, the stirred solutions were monitored at 15 minutes, 3 hours, and 20 hours. Initially, three solvents were screened (THF, EtOH, DCM), and the extent of reaction was greatest in DCM. Ethanol showed the same response at a slower rate, but no reaction was observed in THF (unstabilized).

The response at 3 hrs of a 5.00 μM solution of **P2** to a range of H₂O₂ concentrations is

shown in Figure 4 (see Figure A5 in section 5.17 for UV-vis and fluorescence spectra at 15 minutes, 3 hours, and 20 hours). At 3 hrs, fluorescence increases in the 1.00 mM, 100 μ M, 10.0 μ M, 1.00 μ M, and 100 nM samples, but not in the 10.0 nM and 1.0 nM H_2O_2 solutions. The response continues to develop over time, and it can be seen by eye under UV-illumination after 20 hours (Figure 4, inset picture) for all concentrations of H_2O_2 except 1.00 nM (see Figure A5 in Section 5.17).

To better understand and characterize the response of **P2** to hydrogen peroxide, a 10.0 μ M solution of **MC2** was subjected to similar conditions (see Figure A6 in section

5.17 for UV-vis and fluorescence spectra at 15 minutes and 3 hours). At 15 minutes, a fluorescence increase is observed in the samples with a H_2O_2 concentration of 1.00 mM, 100 μ M, and 10.0 μ M. Based on the absorbance spectrum, it appears that after 15 minutes **MC2** has been transformed to **MC2_2ox** in the 1.00 mM H_2O_2 solution. After three hours there is no further reaction, indicating that the disulfoxide is a stopping point under these conditions. At 15 minutes, the 100 μ M H_2O_2 solution, which represents 10 equiv of H_2O_2 per molecule of **MC2**, has been oxidized to the monosulfoxide based on the absorbance spectrum. After 3 hours, the sample shows further oxidation, though it has not yet reached the same point as the 1.00 mM H_2O_2 solution. The 10.0 μ M H_2O_2 solution shows a significant increase in fluorescence at 15 minutes, but its absorbance spectrum is relatively unchanged. After 3 hours, the absorbance spectrum of the 10.0 μ M H_2O_2

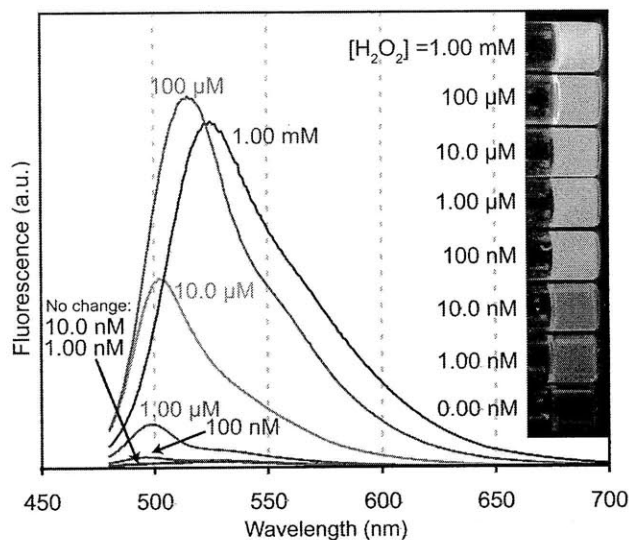


Figure 4. H_2O_2 detection with **P2**.

Fluorescence response of **P2** to hydrogen peroxide. The response of **P2** to H_2O_2 after 3 hours at room temperature is plotted for a series of hydrogen peroxide concentrations. The inset shows the same solutions under UV irradiation (365 nm) at 20 hours. For all solutions: $\lambda_{\text{ex}} = 460 \text{ nm}$, $[\text{P2}] = 5.00 \mu\text{M}$, $[\text{MTO}] = 0.5 \text{ mM}$, $[\text{urea}] = [\text{H}_2\text{O}_2]$ in CH_2Cl_2 with $< 5\%$ ethanol.

appears more like that of the monosulfoxide, and the fluorescence has continued to increase. In the 1.00 μM H_2O_2 sample, there is a significant increase in fluorescence, presumably from the formation of some amount of the monosulfoxide, but the absorbance spectrum changes only slightly. The 100 nM H_2O_2 solution shows no response.

5.8 Thin-film photophysics of polymers

Thin-films of polymers **P1**, **P1A-D**, **P2**, and **P2A-D** were prepared by spin-casting a chloroform solution (1.0 mg/ml) onto silanized glass slides. The films were annealed at 120 $^\circ\text{C}$ for 10 minutes. The films show behavior similar to the dilute solutions, with no signs of aggregation (Table 2, Figure A7 in section 5.17). For **P1**, **P1A**, and **P1B**, the thin-film absorption and emission maxima are red-shifted compared to the solution values. For **P1C** and **P1D**, the absorption maxima are relatively unchanged going from solution to thin-film, however the emission maxima are red-shifted in the solid-state. For **P2** and **P2A**, the thin-film absorption and emission maxima are red-shifted compared to the solution values. **P2B** displays no change in absorption maximum in moving from solution to the solid-state, however its emission does red-shift. **P2C** and **P2D** show a slight blue-shift in absorption when moving from solution to the solid-state, however in both cases the emission is red-shifted.

The films made from the oxidized forms of **P1**, specifically **P1B** and **P1C**, were highly emissive, with quantum yields above 0.50. We compared films of **P1C** to films of a previously

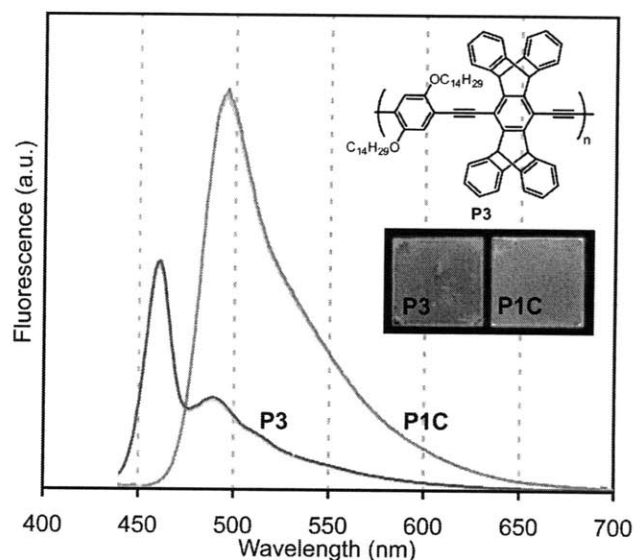


Figure 5. Solid-state emission of **P1C** vs **P1B**. The fluorescence emission at an angle of 22.5 $^\circ$ to the face of the film is shown for **P1B** and **P1C**. The two samples had nearly identical optical densities at the excitation wavelength (420 nm). Representative samples of **P1B** and **P1C** under UV irradiation (365 nm) are shown in the inset.

reported non-aggregating PPE (**P3**) with a fluorescent quantum yield of 0.33 in the solid state.^{2a} In Figure 5, the emission of **P1C** is significantly greater than that of a film of **P3** when both are excited with monochromatic light of 420 nm, a wavelength at which the two films have nearly identical optical densities. Films of **P2A** are also highly fluorescent with a quantum yield of 0.56. Comparatively, films of the more highly oxidized polymers (**P2B-D**) are less emissive, however the fluorescence can be clearly seen by eye under UV irradiation as shown in Figure 6.

5.9 Thin-film photobleaching studies

Films of **P1**, **P1A-D**, **P2**, and **P2A-D** were tested for photostability by comparing the emission before and after the films were irradiated at their absorbance maxima for 30 minutes, using monochromatic light generated from a 450 W steady-state Xe lamp as the irradiation source under aerobic conditions.¹¹ The approximate area of irradiation was 0.25 cm² and the average power density of irradiation was estimated to be 6 mW/cm². Films of **P1** and **P1A-D** had an optical density (OD) of 0.10 ± 0.01. Films of **P2**, **P2A-D**, and **P3** had an OD of 0.05 ± 0.01. The films were not moved during the process to ensure that the measurements reflect the effect of irradiation on one area of the film. All measurements were done in triplicate and the error is reported as the standard deviation. Films of **P1** and **P1A-D** did not show improved photostability as compared to **P3** under identical conditions¹¹ (see Figure A8 in section 5.17). However, films of **P2A-D** proved resistant to photobleaching (Figure 6). **P2A-D** retained more than 95% percent of their

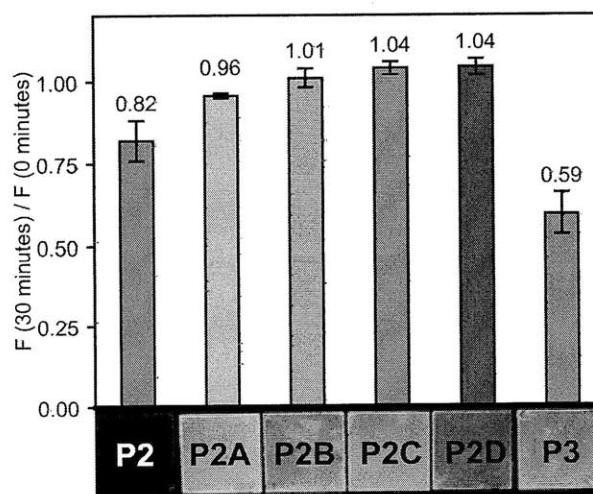


Figure 6. Photostability of **P2** thin films. Thin-films of **P2**, **P2A-D**, and **P3** of the same optical density (OD = 0.05 ± 0.01) were irradiated for 30 minutes at their absorbance maxima with monochromatic light and the ratio of fluorescence at 30 minutes to the initial fluorescence was measured. Representative samples under UV irradiation (365 nm) are shown at the bottom of the plot.

original fluorescence after 30 minutes of irradiation, with **P2B-P2D** even showing a slight increase in emission. They are more photostable than **P3**, which retains only 60% of its initial emission when irradiated at its absorbance maximum (440 nm) at the same OD, in accordance with previously reported results.¹¹

5.10 Understanding the Photophysical Behavior of the Model Compounds

Because of its relatively weak intensity, the absorbance band of **MC1** and **MC2** centered at approximately 435 nm (Figure 1) suggests that the thioethers on the center ring impart intramolecular charge transfer (ICT) character to the HOMO-LUMO optical transition. The ICT character of the transition results from poor spatial overlap of the frontier molecular orbitals (FMOs), which we examined with quantum mechanical calculations (Figure 7a, see Figure A9 in section 5.17 for additional MOs).¹⁹ Qualitatively, for **S1** (a simplified version of **MC1** for ease of computation) the HOMO is primarily located on the center ring with most of the orbital density on the sulfur atoms, while the LUMO is delocalized through

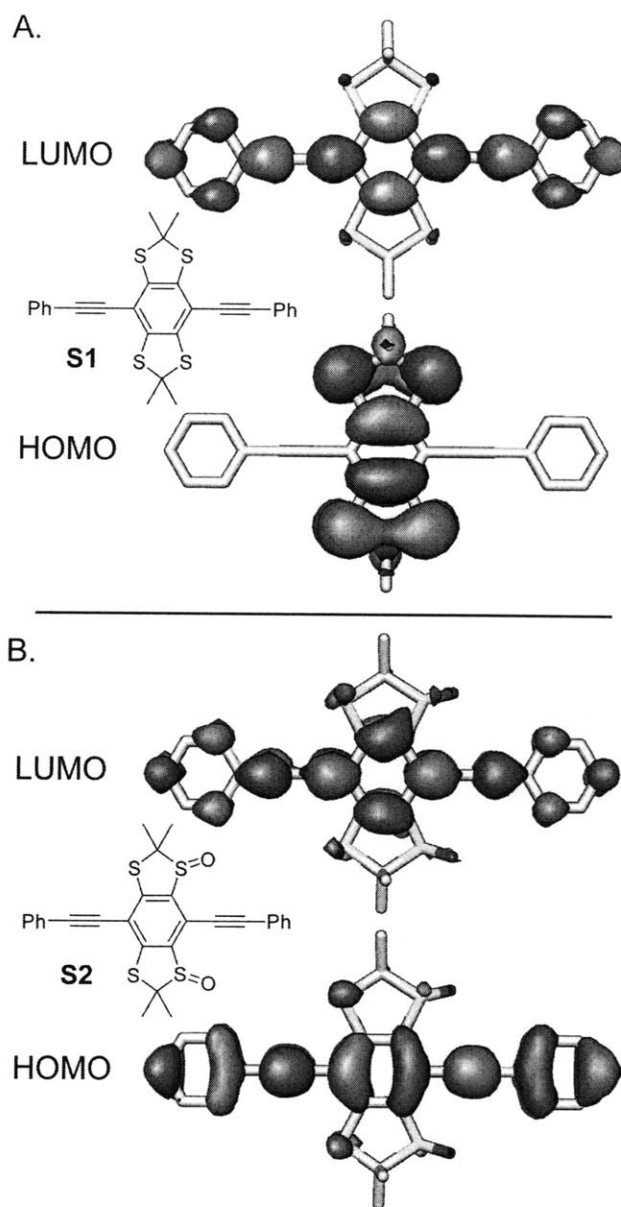


Figure 7. HOMO-LUMO computations. (a and b) Frontier orbital topologies (B3LYP 6-311+G*, Gaussian03) for structures **S1** and **S2**. Structures **S1** and **S2** represent **MC1** and **MC1_2ox_trans**, respectively, with the butyl-groups being replaced with methyl-groups for ease of computation.

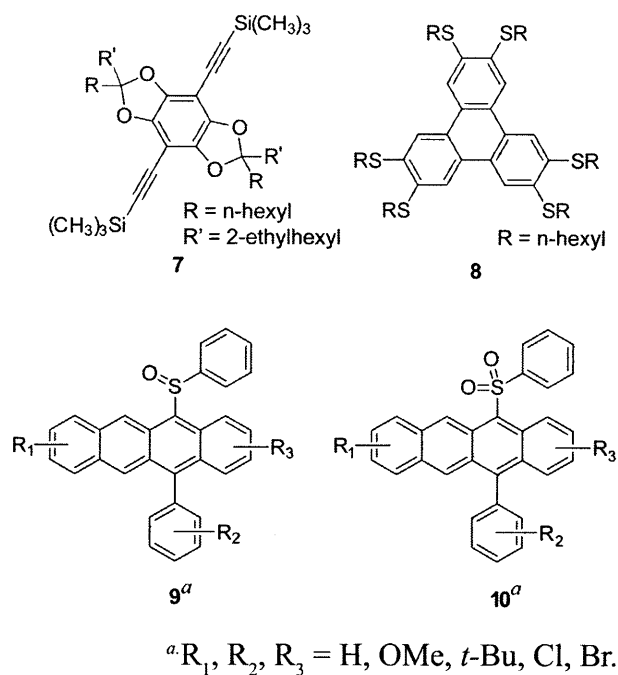
out the molecule's π -system with minimal density on the sulfur atoms. The presence of ICT character has been observed in simple thioether containing aromatic compounds, such as phenyl-*n*-propyl sulfide.²⁷ Additionally, ICT character is observed in compound **7**¹⁹ (Chart 1), which is an oxygen analogue of the thioethers studied here.

Upon oxidation of **MC1** to **MC1_1ox**, the ICT band blue shifts, and with oxidation to the disulfoxide, the ICT band disappears. The computed HOMO and LUMO for **S2** are

in agreement with this observation, as it appears that the spatial overlap of the HOMO and LUMO is significantly greater for **S2** as compared to **S1** (Figure 7). The situation is more complex in the case of **MC2** and its mono- and disulfoxides because the oxidation of the thioethers introduces a donor-acceptor interaction between the electron-rich outer rings and the electron-poor middle ring. However, comparing the absorption spectrum of **MC2** to that of **MC2_1ox** reveals that oxidation to the monosulfoxide causes a blue-shift similar to that seen in **MC1_1ox**. The origin of the weak red-shifted absorbance present in both isomers of **MC2_2ox** may be elucidated by future computational studies.

For **MC1** and **MC2**, the fluorescence quantum yield is low in solution ($\Phi_F = 0.003$, Table 1), for two reasons. First, **MC1** and **MC2** have short fluorescence lifetimes of approximately 100 ps, which indicates that another relaxation process is competing with fluorescence. Based on previous studies of thioethers we suggest that intersystem crossing (ISC) from the singlet excited state to the triplet excited state accounts for the shortened lifetime. In compounds as simple as phenyl-*n*-propyl sulfide, ISC is believed to be the predominant deactivation pathway of the excited state.²⁸ An example of an aromatic chromophore containing more than one thioether is

Chart 1. Literature Compounds.



2,3,6,7,10,11-hexakis(*n*-hexylsulfanyl)triphenylene (Chart 1, Compound **8**), which has a reduced fluorescence quantum yield compared to the parent triphenylene (0.015 vs. 0.066), but displays significant phosphorescence at 77K.²⁸ Compound **8** has a significantly shortened lifetime (0.7 ns) as compared to the parent triphenylene (36.6 ns) or the same compound with the sulfur atoms replaced by oxygen atoms (8.0 ns). For **MC1** and **MC2**, the observation of room temperature phosphorescence (Figure S1, Supporting Information) in degassed samples further supports the argument that ISC is a main deactivation pathway for the singlet excited state.

The second reason that the unoxidized model compounds have low emission is that they have lower rates of fluorescence (k_f) as compared to the oxidized versions. Oxidation of **MC1** to **MC1_1ox** and both isomers of **MC1_2ox** is accompanied by an increase in k_f . The increase in k_f in the disulfoxide as compared to the unoxidized compound appears to be a consequence of better spatial overlap between the HOMO and LUMO (see Figure 7).^{23,29} The oxidation of **MC2** to **MC2_1ox** causes the fluorescence lifetime to increase substantially from 0.099 ns to 2.7 ns, but does not increase k_f . Further oxidation to **MC2_2ox** causes an order of magnitude increase in k_f from 0.020 ns⁻¹ to ~ 0.20 ns⁻¹ and a minor increase in the lifetime.

MC2 shows a more than 150-fold increase in Φ_f when oxidized to the disulfoxide, but the increase is more modest (7- to 13-fold based on the isomer) when **MC1** is oxidized to the disulfoxide. We contend that the sulfoxides in **MC1_2ox** are behaving differently than the sulfoxides in **MC2_2ox**. It has been reported that the fluorescence of aromatic sulfoxides is low because of nonradiative decay pathways involving the sulfoxide. For example, pyrene has a quantum yield of 0.32 in CH₂Cl₂,³⁰ and phenyl 1-pyrenyl sulfide has a quantum yield of 0.34 in CH₂Cl₂.^{4a} Oxidation of the sulfur in phenyl 1-pyrenyl sulfide to a sulfoxide causes the quantum yield to decrease to 0.02, whereas further oxidation causes the quantum yield to increase to 0.76.^{4a} A similar trend, in which the presence of a sulfoxide attached directly to an aromatic core quenches a fluorophore that is relatively unaffected by the presence of a thioether or a sulfone in the same position, is observed for naphthalene, biphenyl, and anthracene sulfides.³¹ However, in the compounds we have exam-

ined sulfoxides do not appear to act as fluorescence quenchers except in **MC1_2ox** (and perhaps in **MC1_1ox**), in which case the emission is blue-shifted towards the near-UV. This suggests that when irradiated at higher energies (shorter wavelengths) sulfoxides may quench fluorescence via a mechanism that is not operative at lower energies (longer wavelengths). The behavior of our model compounds and polymers is not unprecedented. Within a previously reported series of 21 tetracene derivatives (Chart 1), 15 of which are sulfoxides (**9**) and 6 of which are sulfones (**10**), the tetracene derivatives with sulfoxides are more emissive than the tetracene sulfones in nearly every case.³²

5.11 Understanding the Photophysical Behavior of the Polymers

In contrast to the model compounds, the HOMO-LUMO optical transitions of **P1** and **P2** appear to be allowed, thus suggesting that the HOMO is partially delocalized along the polymer's π -backbone and has better spatial overlap with the LUMO. In contrast, when the oxygen-containing monomer **7** is incorporated into PPEs the HOMO remains localized.¹⁹ **P1** and **P2**, which like **MC1** and **MC2** are not very emissive, show large increases in Φ_f when oxidized due to an increase in both k_f and τ_f (Table 2). For example, when **P1** is oxidized to **P1A** with 2.1 equivalents of oxidant, k_f increases from 0.074 ns⁻¹ to 0.52 ns⁻¹ and τ_f increases from 0.13 ns to 0.67 ns. When **P2** is oxidized to **P2A**, k_f increases from 0.050 ns⁻¹ to 0.36 ns⁻¹ and the lifetime increases from 0.17 ns to 1.35 ns. Based on the trends observed for the oxidized model compounds, it appears that the increase in k_f is due to greater spatial overlap of the FMOs due to delocalization of the HOMO along the π -backbone and that the increase in τ_f is due primarily to a decrease in the rate of ISC.

5.12 Understanding the behavior of the polymers in thin films

Because oxidation in solution causes **P1** and **P2** to become emissive, thin-films of the thioether-containing polymers were expected to show a fluorescence turn-on response when irradiated in air. However, this phenomenon was not observed. Instead, the already weak emission further decreased with prolonged irradiation (Figure 6, **P2**), even though thioethers are known to

react with singlet oxygen.³³ There are two possible explanations for this behavior. The first is that the thioethers are not being oxidized to sulfoxides or sulfones under the conditions. The second is that oxidation is so minimal that any oxidized moieties are effectively quenched by the remaining unoxidized segments.

5.13 Blue-shifted versus red-shifted fluorescence turn-on response to H_2O_2

As discussed in the results section, both **MC2** and **P2** show a fluorescence turn-on response to oxidation by hydrogen peroxide in the presence of a catalyst (MTO). However, they differ in that **MC2**'s emission blue-shifts and **P2**'s emission red-shifts under these oxidation conditions. As a conjugated polymer, **P2** offers the opportunity for exciton migration along the polymer backbone to the most highly oxidized, and therefore red-shifted, emissive sites.^{2,34} In contrast, each molecule of **MC2** in dilute solution behaves independently. However, **MC2** offers the opportunity for a dark field fluorescence turn-on response.³⁵ A dark field turn-on is when the emissive species is blue-shifted relative to the initial species, and therefore avoids overlapping emission from the initial species' vibronic manifold of transitions so that there is no initial background signal to subtract. In this situation, the fluorescence turn-on is limited more by the inherent noise in the detector rather than the emissivity of the fluorophore. For example, our instrumentation shows an average turn-on of 900-fold between 430-440 nm for **MC2** in 1.00 mM [H_2O_2] after 15 minutes, even though the emission maximum is above 450 nm. In contrast, when **P2** is oxidized there is still substantial emission from the parent polymer to subtract, even though **P2** does show a slight blue-shift in emission upon initial oxidation. Therefore, **MC2** offers an advantage in situations where the increase in fluorescence intensity is most important, and **P2** offers an advantage in situations where a change in emission color is desired.

5.14 Conclusions

In summary, we have efficiently synthesized model compounds and polymers containing thioethers that show large increases in fluorescence quantum yield when oxidized. We demonstrate

that oxidation is accompanied by a red-shift in emission when the compounds contain electron-rich aromatic rings that act as donor groups. Oxidation with hydrogen peroxide in the presence of an organometallic catalyst points to the potential application of these systems in peroxide sensing. Thin films of the oxidized polymers are shown to be very emissive, and in some cases, to have improved photostability. We conclude that oxidation of the sulfur atoms causes an increase in Φ_F by both increasing the rate of fluorescence (k_f) and decreasing the rate of non-radiative decay, thereby increasing the fluorescence lifetime (τ_f). Based on photophysical studies and computation, we propose that the increase in k_f is caused by greater spatial overlap of the frontier molecular orbitals in the oxidized compounds as compared to the unoxidized compounds.

5.15 Experimental Section

General Methods and Instrumentation. Polymer molecular weights were determined by gel permeation chromatography (GPC) versus polystyrene standards (Agilent Technologies, Inc.) using THF as the eluent. Fluorescence quantum yields were determined against 9,10-diphenylanthracene (cyclohexane, QY = 0.90),³⁶ coumarin-6 (ethanol, QY = 0.76),³⁷ rhodamine B (ethanol, QY = 0.49),³⁸ and perylene (PMMA film, QY = 0.78)³⁹ depending on fluorophore. Compounds **4**,⁴⁰ **5**,⁴¹ and **6**⁴² were prepared according to literature procedures.

2,2,6,6-tetra-*n*-butyl-4,8-diiodo benzo[1,2-*d*;4,5-*d'*]bis[1,3]dithiole (1). To an oven-dried 500 mL flask were added 0.030 g (0.22 mmol, 0.10 equiv) of triethylammonium chloride (as a source of LiCl after deprotonation), 220 mL of anhydrous tetrahydrofuran, 2.62 mL (15.4 mmol, 7.00 equiv) of tetramethylpiperidine, and 8.53 mL (13.6 mmol, 6.20 equiv) of *n*-butyl lithium (1.5 M in hexanes) and the reaction mixture was cooled to -78 °C. After 30 minutes of stirring, 1.00 g (2.20 mmol, 1.00 equiv) of compound **3** was added as a solid. After 30 minutes at -78 °C, 3.35 mL (26.4 mmol, 12.0 equiv) of chlorotrimethylsilane was added. The reaction was held at -78 °C for 2 h, warmed to 0 °C and held for 6 h, and then stirred at 20 °C overnight. The reaction was quenched

with aqueous ammonium chloride and extracted into hexanes, washing three times with 0.1M HCl, once with brine, and drying over sodium sulfate. Removal of the solvent yielded 1.53 g of an off-white solid that was carried through unpurified to the next step. The crude material was dissolved in 140 mL of anhydrous dichloromethane and cooled to 0 °C. To the reaction mixture, 1.07 g (6.60 mmol, 3.00 equiv) of iodine monochloride dissolved in 6 mL of anhydrous dichloromethane was added dropwise over 15 minutes. The reaction mixture was stirred at 0 °C for 2 h and then warmed to room temperature and stirred for 0.5 h. The reaction was quenched by the addition of aqueous sodium thiosulfate and washed three times with 1M sodium thiosulfate, once with 0.1 M sodium hydroxide, once with brine, and dried over sodium sulfate. The crude material was recrystallized from refluxing hexane to yield 1.24 g (1.77 mmol) of a greenish-yellow product in 80% yield. ¹H NMR (500 MHz, CDCl₃, δ) (all coupling constants (*J*) in Hz): 2.04 (4H, pseudo-t, *J* = 7.5), 1.46 (8H, quint, *J* = 7.5), 1.36 (8H, sext, *J* = 7.0), 0.93 (12H, t, *J* = 7.0); ¹³C NMR (126 MHz, CDCl₃, δ): 138.5, 80.5, 68.1, 42.0, 28.1, 22.9, 14.2; HRMS (ESI): 705.9772 [calc'd for M⁺: 705.9784]; IR ν_{max} KBr/cm⁻¹: 2953, 2920, 2848, 1460, 1431, 1374, 1315, 1235, 1069, 734, 676. Mp 149-151°C (hexane).

2,2,6,6-Tetra-*n*-butylbenzo[1,2-*d*;4,5-*d'*]bis[1,3]dithiole (3). To an oven-dried 100 mL flask, 3.00 g (6.90 mmol, 1.00 equiv) of compound **2** and 30 mL of dry toluene were added. To this mixture, 3.56 mL (20.7 mmol, 3.00 equiv) of 5-nonanone and 1.87 mL (13.8 mmol, 2.00 equiv) of tetrafluoroboric acid diethyl ether complex were added and the reaction was refluxed overnight. The reaction was quenched by adding aqueous sodium bicarbonate and then extracted into diethyl-ether and dried over sodium sulfate. The crude material was recrystallized from refluxing methanol to yield 2.51 g (5.52 mmol) of a white powder in 80% yield. ¹H NMR (500 Mz, CDCl₃, δ) (all coupling constants (*J*) in Hz): 6.94 (2H, s), 2.05 (8H, pseudo-t, *J* = 8.0), 1.43 (8H, quint, *J* = 8.0), 1.34 (8H, sext, *J* = 7.5), 0.91 (12H, t, *J* = 7.0); ¹³C NMR (126 Mz, CDCl₃, δ): 135.3, 116.3, 74.9, 41.0, 28.4, 23.0, 14.2; HRMS (ESI): 454.1858 [calc'd for M⁺: 454.1851]; IR ν_{max} KBr/cm⁻¹: 2956,

292s, 2856, 1457, 1428, 1329, 1263, 1103, 870, 739, 649; Mp 123-125 °C (hexane).

2,2,6,6-Tetra-*n*-butylbenzo[*d,d'*]bis[1,3]dithiole-1,1,3,3,5,5,7,7-octone (7). To a 100 mL flask were added 1.00 g (2.20 mmol, 1.00 equiv) of **3**, 4.90 g (19.8 mmol, 9.00 equiv) of *meta*-chloroperbenzoic acid (73% pure by weight), and 30 mL of chloroform. The reaction was heated to reflux and stirred overnight. The chloroform was removed, and the solid was dissolved in diethyl ether (50 mL) and washed with 1M NaOH (3 x 30 mL) and brine. After drying over sodium sulfate, the product was purified via silica gel chromatography (hexane/dichloromethane) to yield 0.820 g (64%) of a white powder. ¹H NMR (500 MHz, CDCl₃, δ) (all coupling constants (*J*) in Hz): 8.53 (s, 2H), 2.23 (t, *J* = 8.5), 1.58 (quint, *J* = 8.0, 8H), 1.43 (sext, *J* = 7.5, 8H), 0.96 (t, *J* = 7.5, 12H); ¹³C NMR (126 MHz, CDCl₃, δ) 142.6, 119.5, 82.1, 28.0, 25.4, 23.2, 13.8; HRMS (ESI): calcd for [M + Na]⁺: 605.1342; found, 605.1353. IR (KBr, thin film) ν_{max} (cm⁻¹): 3080, 2962, 2874, 1467, 1352, 1165, 880, 728, 692.

2,2,6,6-tetra-*n*-butyl-4,8-diiodobenzo[*d,d'*]bis[1,3]dithiole-1,1,3,3,5,5,7,7-octone (8). To a flask were added 0.300 g (0.430 mmol, 1.00 equiv) of compound **1**, 9.4 mL CCl₄, 9.4 mL of acetonitrile, 14.1 mL of water, 0.009 g of RuCl₃·3H₂O (0.03 mmol, 8 mol%), and 0.870 g periodic acid (3.80 mmol, 8.80 equiv). Drops of sat'd sodium bicarbonate solution were added to maintain the pH between 6 and 8. After 3 h, the reaction mixture was extracted with diethyl ether (3 x 20 mL) and the combined organic layers were washed with water and brine. After drying over sodium sulfate, the ether was passed through a silica gel plug and the solvent was removed to yield 0.248 g (70.0%) of a white powder. ¹H NMR (500 MHz, CDCl₃, δ) (all coupling constants (*J*) in Hz): 2.27 (t, *J* = 8.0, 8H), 1.57 (quint, *J* = 8.0, 8H), 1.44 (sext, *J* = 7.5, 8H), 0.97 (t, *J* = 7.5, 12H); ¹³C NMR (126 MHz, CDCl₃, δ) 145.3, 79.3, 78.4, 29.1, 25.7, 23.2, 13.8; HRMS (DART): calcd for [M + H]⁺: 834.9455; found, 834.9462. IR (KBr, thin film) ν_{max} (cm⁻¹): 2960, 2873, 1466, 1352(s), 1160(s), 884, 727.

Model Compound 1 (MC1). In a 100 mL flask, 0.100 g of diiodo **1** (0.141 mmol, 1.00 equiv), 0.008 g of Pd(0)[P(Ph)₃]₄ (5 mol%), and 0.003 g CuI (10 mol%) were dissolved in 30 ml of a degassed 2:1 mixture of toluene and diisopropylamine. The reaction mixture was degassed with bubbling argon for five minutes, and 0.047 mL of phenylacetylene (0.424 mmol, 3.00 equiv) was added. The flask was sealed and heated to 60 °C overnight. After cooling, the reaction mixture was extracted into diethylether and washed with saturated ammonium chloride solution, dilute acid, and brine. After drying over sodium sulfate and removal of solvent, the crude mixture was dry loaded onto a silica column and chromatographed, beginning with hexane and finally eluting with a 4:1 mixture of hexane/DCM. The isolated product was further purified by recrystallization from refluxing hexane to yield 0.067 g (73% yield) of a yellow crystal. ¹H NMR (500 Mz, CDCl₃, δ) (all coupling constants (*J*) in Hz): 7.57 (4H, dd, *J* = 7.0, 3.0), 7.36 (6H, m), 2.09 (8H, pseudo-t, *J* = 8.0 Hz), 1.53 (8H, quint, *J* = 7.5 Hz), 1.36 (8H, sext, *J* = 7.5 Hz), 0.94 (12H, t, *J* = 7.0 Hz); ¹³C NMR (126 Mz, CDCl₃, δ): 137.9, 132.0, 129.0, 128.5, 122.8, 110.4, 99.6, 86.5, 73.2, 42.4, 28.3, 23.0, 14.2; HRMS (ESI): 654.2492 [calc'd for M⁺: 654.2477]; FTIR ν_{max} KBr/cm⁻¹: 2931, 2859, 2217, 1493, 1442, 1323, 1263, 754, 713, 688; Mp 143-145 °C (hexane).

Model Compound 2 (MC2). The same procedure as for **MC1** was used with the substitution of 0.051 g (0.31 mmol, 2.2 equiv) of compound **4** for phenylacetylene. Additionally, **MC2** was eluted with 1:1 hexane/DCM. After hexane recrystallization, 0.730 g (67% yield) of a yellow crystal was obtained. ¹H NMR (500 Mz, CDCl₃, δ) (all coupling constants (*J*) in Hz): 7.05 (2H, d, *J* = 3.0), 6.88 (2H, dd, *J* = 9.0, 3.0 Hz), 6.83 (2H, d, *J* = 9.0 Hz), 3.90 (6H, s), 3.80 (6H, s), 2.09 (8H, pseudo-t, *J* = 8.0 Hz), 1.53 (8H, quint, *J* = 7.5 Hz), 1.36 (8H, sext, *J* = 7.5 Hz), 0.93 (12H, t, *J* = 7.5); ¹³C NMR (126 Mz, CDCl₃, δ): 154.9, 153.4, 137.8, 118.1, 116.5, 112.8, 112.7, 110.5, 96.0, 90.6, 73.0, 57.0, 56.1, 42.4, 28.3, 23.0, 14.2; HRMS (ESI): 774.2885 [calc'd for M⁺: 774.2899]; FTIR ν_{max} KBr/cm⁻¹: 2956, 2933, 2871, 2204, 1604, 1500, 1463, 1322, 1298, 1270, 1226, 1179, 1152, 1046, 1023, 872, 805, 735, 713; Mp 149-152 °C (hexane).

Oxidation of Model Compounds.

General Procedure. In a flask, 0.025 g of the model compound was dissolved in 3.0 mL of dry dichloromethane and cooled to -78 °C. The oxidation of **MC1** with 2.1 equivalents of *m*-CPBA was performed at twice the scale (0.050 g **MC1**, 6.0 mL dichloromethane). The appropriate amount of oxidant, either 1.05 equiv or 2.10 equiv, was measured by volume from a freshly-prepared 0.100 M stock solution of *m*-CPBA in dichloromethane, and added dropwise to the reaction. The reaction was stirred for 30 minutes and then warmed to 0 °C. It was allowed to warm to room temperature and stir overnight. Excess potassium carbonate was added to neutralize any acids, and the reaction mixture was purified with silica gel chromatography, eluting with progressively more polar mixtures of hexanes and dichloromethane. To elute the most polar compounds, 1-10% of ethyl acetate was added to a 1:1 mixture of hexane and dichloromethane.

MC1 oxidation with 1.05 equivalents of oxidant.

MC1_1ox. After recrystallization from hexane, 0.022 g of yellow solid was isolated in 88% yield. ¹H NMR (500 Mz, CDCl₃, δ) (all coupling constants (*J*) in Hz): 7.63 (2H, m), 7.58 (2H, m), 7.38 (6H, m), 2.24 (1H, m), 2.09 (8H, m), 2.05 (1H, m), 1.89 (1H, m), 1.72 (1H, m), 1.6-1.3 (16H, m), 0.98 (3H, t, *J* = 7.5), 0.952 (3H, t, *J* = 7.5), 0.947 (3H, t, *J* = 7.5), 0.92 (3H, t, *J* = 7.5); ¹³C NMR (126 Mz, CDCl₃): δ147.8, 145.0, 139.9, 139.0, 132.3, 132.0, 129.5, 129.4, 128.6(2), 122.4, 122.2, 116.7, 111.3, 101.1, 100.9, 85.7, 85.0, 80.8, 73.7, 43.2, 42.2, 33.5, 30.0, 28.5, 28.4, 28.0, 27.9, 23.3, 23.0(2), 22.9, 14.2 (2), 14.1(2); HRMS (ESI): 670.2425 [calc'd for M⁺: 670.2426]; FTIR ν_{\max} KBr/cm⁻¹: 2957, 2932, 2871, 2219, 1493, 1443, 1303, 1148, 1066, 872, 755, 689; MP: 176-178 °C (hexane).

MC1 oxidation with 2.10 equivalents of oxidant.

MC1_2ox_cis. After chromatography, 0.010 g of a yellow solid was isolated in 19% yield. The

material contains a small amount of the *para*- isomer (8%) as determined by comparing ¹H NMR integrations (see ¹H-NMR spectrum). Shifts are reported for the *meta*-isomer. ¹H NMR (500 Mz, CDCl₃, δ): 7.70 (2H, dd, *J* = 7.5, 2.0 Hz), 7.60 (2H, dd, *J* = 7.5, 2.0 Hz), 7.41 (6H, m), 2.28 (2H, m), 2.09 (2H, m), 1.91 (2H, m), 1.69 (2H, m), 1.65-1.55 (4H, m), 1.48 (8H, m), 1.33 (4H, sextet, *J* = 7.5 Hz), 0.99 (6H, t, *J* = 7.0 Hz), 0.92 (6H, t, *J* = 7.0 Hz); ¹³C NMR (126 Mz, CDCl₃): δ 153.5, 140.5, 132.7, 132.4, 130.2, 129.7, 128.7 (2), 125.4, 121.9, 121.5, 112.7, 102.9, 102.5, 84.8, 83.2, 81.1, 33.5, 29.8, 28.4, 27.9, 23.2, 23.0, 14.1 (2); FTIR ν_{\max} KBr/cm⁻¹: 3058, 2958, 2931, 2871, 2218, 1597, 1530, 1491, 1464, 1443, 1420, 1380, 1305, 1261, 1144, 1069, 1026, 872, 803, 757, 689, 649, 529; HRMS (ESI): 687.2467 [calc'd for M+: 687.2453].

MC1_2ox_trans. After recrystallization from hexane, 0.013 g of a yellow solid was isolated in 25% yield. The material contains only trace amounts of the *para*-isomer (< 5%), which is barely visible in NMR. Shifts are reported for the *meta*-isomer. ¹H NMR (500 Mz, CDCl₃, δ): 7.69 (2H, dd, *J* = 7.5, 2.0), 7.60 (2H, dd, *J* = 7.5, 2.0), 7.42 (6H, m), 2.26 (2H, m), 2.09 (2H, m), 1.92 (2H, m), 1.74 (2H, m), 1.65-1.55 (4H, m), 1.48 (8H, m), 1.35 (4H, sextet, *J* = 7.5), 1.00 (6H, t, *J* = 7.0), 0.93 (6H, t, *J* = 7.0); ¹³C NMR (126 Mz, CDCl₃, δ): 153.8, 140.7, 132.6, 132.1, 130.2, 129.7, 128.7 (2), 125.1, 122.0, 121.5, 113.0, 102.8, 102.0, 84.8, 83.3, 81.5, 33.3, 28.8, 28.4, 27.9, 23.2, 22.9, 14.1 (2); FTIR ν_{\max} KBr/cm⁻¹: 3057, 2958, 2932, 2869, 2218, 1597, 1530, 1490, 1462, 1443, 1420, 1380, 1305, 1261, 1144, 1068, 1026, 873, 803, 757, 689, 650, 529; Mp 182-183 °C (hexane).

Over-oxidation products and mixed fractions. In addition to the materials described above, 0.020 g of material in mixed fractions, with the presence of some sulfone containing compounds, was isolated.

MC2 oxidation with 1.05 equivalents of oxidant.

MC2_1ox. After recrystallization from methanol, 0.015 g of a yellow solid was isolated in 60% yield. ¹H NMR (500 Mz, CDCl₃): δ 7.09 (1H, *J* = 3.0 Hz), 7.04 (1H, *J* = 3.0 Hz), 6.91 (1H, dd, *J* =

9, 3 Hz), 6.90 (1H, dd, $J = 9, 3$ Hz), 6.85 (2H, d, $J = 9$ Hz), 3.91 (3H, s), 3.90 (3H, s), 3.81 (6H, s), 2.24 (1H, m), 2.10 (4H, m), 2.05 (1H, m), 1.87 (1H, m), 1.72 (1H, m), 1.53 (4H, m), 1.45 (4H, m), 1.37 (4H, m), 1.31 (4H, sextet, $J = 7.5$ Hz), 0.95 (3H, t, $J = 7.5$ Hz), 0.94 (3H, t, $J = 7.5$ Hz), 0.93 (3H, t, $J = 7.5$), 0.90 (3H, t, $J = 7.5$); ^{13}C NMR (125 Mz, CDCl_3 , δ): 155.4, 155.1, 153.4, 147.6, 145.0, 139.8, 139.0, 118.2, 118.1, 117.4, 116.9, 116.8, 112.8, 112.7, 112.4, 112.2, 111.4, 97.6, 97.4, 89.7, 89.0, 80.7, 73.4, 57.0, 56.9, 56.2, 56.1, 43.0, 42.3, 33.5, 30.0, 28.4, 28.0, 27.9, 23.3, 23.0(2), 22.9, 14.2, 14.1(1); FTIR ν_{max} $\text{KBr}/\text{cm}^{-1}$: 2956, 2933, 2871, 2205, 1605, 1579, 1499, 1463, 1302, 1273, 1225, 1180, 1069, 1045, 1022, 872, 807, 735; HRMS (ESI): 790.2864 [calc'd for M^+ : 790.2849]; Mp 165-168 °C (methanol).

MC2 oxidation with 2.10 equivalents of oxidant.

MC2_2ox_cis. After chromatography, 0.014 g of a yellow solid was isolated in 54% yield. The material contains both the *meta*- and *para*-isomer in a 3:1 ratio as determined by ^1H NMR integrations. *meta*-Isomer: ^1H NMR (500 Mz, CDCl_3 , δ): 7.15 (1H, d, $J = 3$), 7.05 (1H, d, $J = 3$), 6.94 (2H, dd, $J = 9, 3$), 6.86 (2H, d, $J = 9$), 3.92 (3H, s), 3.90 (3H, s), 3.81 (6H, s), 2.28 (2H, m), 2.06 (2H, m), 1.86 (2H, m), 1.66 (2H, m), 1.65-1.55 (4H, m), 1.47 (8H, m), 1.30 (4H, sextet, $J = 7.5$), 0.98 (6H, t, $J = 7.0$), 0.91 (6H, t, $J = 7.0$); *para*-Isomer non-overlapping signals: 7.10 (2H, d, $J = 3$), 3.91 (6H, s); Both isomers: ^{13}C NMR (126 Mz, CDCl_3): δ 155.9, 155.5, 155.1, 153.6, 153.5 (3), 140.5, 125.5, 119.5, 118.5, 118.2, 118.1 (2), 117.9, 117.3, 113.0, 112.9, 112.8, 112.7, 111.9, 111.7, 111.5, 99.6, 99.5, 99.0, 88.8, 88.1, 87.3, 81.0, 80.6, 57.1, 57.0, 56.9, 56.3, 56.2, 56.1, 33.5 (2), 29.8 (2), 28.4 (2), 27.9 (2), 23.2 (2), 23.0 (2), 14.1 (2); IR ν_{max} $\text{KBr}/\text{cm}^{-1}$: 2956, 2931, 2870, 2204, 1605, 1576, 1498, 1462, 1390, 1302, 1274, 1226, 1180, 1151, 1068, 1045, 1022, 872, 808, 736; HRMS (ESI): 807.2854 [calc'd for M^+ : 807.2876].

MC2_2ox_trans. After chromatography, 0.011 g of a yellow solid was isolated in 42% yield. The material contains both the *meta*- and *para*-isomer in a 4:1 ratio as determined by ^1H NMR integrations. *meta*-Isomer: ^1H NMR (500 Mz, CDCl_3 , δ): 7.12 (1H, d, $J = 3$ Hz), 7.05 (1H, d, $J = 3$ Hz),

6.94 (2H, dd, $J = 9, 3$), 6.86 (2H, d, $J = 9$), 3.92 (3H, s), 3.90 (3H, s), 3.82 (6H, s), 2.27 (2H, m), 2.09 (2H, m), 1.91 (2H, m), 1.75 (2H, m), 1.65-1.55 (4H, m), 1.47 (8H, m), 1.34 (4H, sextet, $J = 7.5$ Hz), 0.99 (6H, t, $J = 7.0$), 0.92 (6H, t, $J = 7.0$); *para*-Isomer non-overlapping signals: 7.09 (2H, d, $J = 3$), 3.91 (6H, s); Both isomers: ^{13}C NMR (126 Mz, CDCl_3 , δ): 156.1, 155.6, 155.2, 153.7, 153.4(2), 153.3, 140.6, 125.1, 119.8, 118.3, 118.1, 118.0(2), 117.8, 117.2, 113.1, 112.8, 112.7, 112.0, 111.7, 111.5, 99.2, 98.7, 88.9, 88.2, 87.4, 81.3, 81.0, 56.9(3), 56.2(2), 56.1, 33.3, 32.8, 29.8, 29.7, 28.4(2), 27.9(2), 23.2, 23.0, 14.1(3); IR ν_{max} $\text{KBr}/\text{cm}^{-1}$: 2956, 2933, 2870, 2205, 1605, 1576, 1498, 1462, 1391, 1303, 1275, 1226, 1180, 1151, 1065, 1045, 1022, 872, 810, 736.

Note: It is likely that some of the *para*-isomers of **MC1_2ox** are lost during chromatography as the yields for the disulfoxides are lower as compared to the yields of **MC2_2ox** after purification. The loss of some of the **MC1_2ox** *para*-isomers during chromatographic separation likely accounts for the difference in the reported *meta*-to-*para* ratios for **MC1_2ox** versus **MC2_2ox**.

Polymer 1 (P1). To an oven-dried 10 mL flask, 0.0400 g of diiodo **1** (0.0566 mmol, 1.00 equiv) and 0.0270 g (0.0583 mmol, 1.03 equiv) of dialkyne **5** were added. The flask was moved into a nitrogen glove box, where 0.001 g CuI (5 mol%), 0.002 Pd(0)[P(Ph)₃]₄ (3 mol%), 1.5 mL of toluene, and 0.5 mL diisopropylamine were added and the reaction was heated to 60 °C for 48 h. Upon cooling, the reaction was removed from the glove box and extracted into dichloromethane. The organic layer was washed with aqueous ammonium chloride, dilute hydrochloric acid, and brine. The organic layer was dried with sodium sulfate and removed. The crude polymer was dissolved in a minimal amount of dichloromethane and precipitated into a rapidly stirring excess of methanol and the solid was collected by filtration. This process was repeated twice to obtain 0.043 g of a rubbery yellow solid in 83% yield. ^1H NMR (500 Mz, CDCl_3 , δ): 7.37(2H, br), 2.86 (4 H, br), 2.12 (8H, br), 1.86 (4H, br), 1.70 (8H, br), 1.55 (8H, br), 1.46 (4H, s), 1.38 (8H, br), 1.26 (32H, br), 0.96 (12H, br), 0.88 (6H, t, $J = 7.0$); ^{13}C NMR (126 Mz, CDCl_3): 142.6, 137.8, 132.8, 73.3, 53.7, 42.3, 34.6, 32.2, 31.8, 31.3, 30.2, 30.1, 30.0, 29.9, 29.6, 28.3, 23.0, 22.9(2), 14.4, 14.3; IR ν_{max} $\text{KBr}/\text{cm}^{-1}$: 2925, 2854, 2195, 1493, 1462, 1431, 1378, 1320, 1259, 1018, 892, 796, 713.

Polymer 2 (P2). To an oven-dried 10 mL flask, 0.0400 g of diiodo **1** (0.0570 mmol, 1.00 equiv), 0.001 g CuI (5 mol%), 0.002 g Pd(0)[P(Ph)₃]₄ (3 mol%), and 0.0260 g of dialkyne **6** (0.0580 mmol, 1.03 equiv) were added. A degassed mixture of 1.5 mL of toluene, and 0.5 mL diisopropylamine was added and the flask was heated to 45 °C under argon for 24 hours. Upon cooling, the reaction mixture was extracted into dichloromethane and washed with aqueous ammonium chloride, dilute hydrochloric acid, and brine. The organic layer was dried with sodium sulfate and the solvent was removed. The crude polymer was dissolved in a minimal amount of dichloromethane and precipitated into a rapidly stirring excess of methanol and the solid was collected by filtration. This process was repeated twice to obtain 0.049 g of an orange solid in 98% yield. ¹H NMR (500 Mz, CDCl₃, δ): 7.00 (2H, br), 4.07 (4 H, br), 2.10 (8H, br), 1.92 (4H, br), 1.70 (8H, br), 1.55 (12H, br), 1.40 (12H, br), 1.29 (24H, br), 0.95 (12H, t, *J* = 7.0), 0.90 (6H, t, *J* = 7.0); ¹³C NMR (126 Mz, CDCl₃, δ): 153.8, 140.5, 137.9, 135.7, 117.0, 73.1, 70.8, 70.0, 42.6, 32.2, 29.9, 29.7, 29.4, 28.3, 28.2, 26.3, 26.2, 23.0, 22.9, 14.4, 14.2; IR ν_{max} KBr/cm⁻¹: 2926, 2855, 2200, 1501, 1464, 1431, 1379, 1268, 1217, 1090, 1024, 862, 801, 715.

General Procedure for Polymer Oxidation. To a 20-mL vial equipped with a stir-bar, 0.0050 g of polymer and 3 mL of dichloromethane were added. From a stock solution of *m*-CPBA dissolved in dichloromethane, the appropriate volume of oxidant was added dropwise and the solution was stirred at room temperature overnight. To the vial was then added excess potassium carbonate and basic alumina to remove any excess peracid and the *m*-chlorobenzoic acid formed during the reaction. The reaction mixture was filtered through a 4-micron teflon syringe filter and the solvent was removed. In all cases, mass recovery was quantitative or nearly quantitative.

General Procedure for Oxidation with Hydrogen Peroxide. To a 1-cm quartz cuvette equipped with a stir-bar, 3.00 mL of a solution of either **MC2** (10.0 μM) or **P2** (5.0 μM) in dichloromethane was added. Next, 40.0 μL of a 0.040 M methyltrioxorhenium(VII) (MTO) ethanol solution was added. Stock solutions of 0.0100 M to 0.000,001,00 M hydrogen peroxide in ethanol were pre-

pared by dissolving urea hydrogen peroxide complex in absolute ethanol followed by serial dilution. The appropriate stock solution was chosen for each sample so that between 3 and 30 μL could be added to the cuvette, therefore causing a negligible effect on concentration. Once hydrogen peroxide was added to each of the cuvettes, the absorption and emission spectra were collected at 15 minutes, 3.0 hours, and 20 hours and compared to the spectra obtained before the addition of oxidant.

5.16 References

- (1) Grimsdale, A. C.; Chan, K. L.; Martin, R. E.; Jokisz, P. G.; Holmes, A. B. *Chem. Rev.* **2009**, *109*, 897-1091.
- (2) (a) Yang, Y-S.; Swager, T. M. *J. Am. Chem. Soc.* **1998**, *120*, 5321-5322, 11864-11873.)
(b) Thomas III, S. W.; Joly, G. D.; Swager, T. M. *Chem. Rev.* **2007**, *107*, 1339-1386. (c) McQuade, D. T.; Pullen, A. E.; Swager, T. M. *Chem. Rev.* **2000**, *100*, 2537-2574.
- (3) (a) Scurlock, R. D.; Wang, B.; Ogilby, P. R.; Sheats, J. R.; Clough, R. L. *J. Am. Chem. Soc.* **1995**, *117*, 10194-10202. (b) Dam, N.; Scurlock, R. D.; Wang, B.; Ma, L.; Sundahl, M.; Ogilby, P. R. *Chem. Mater.* **1999**, *11*, 1302-1305.
- (4) (a) Malashikhin, S.; Finney, N. S. *J. Am. Chem. Soc.* **2008**, *130*, 12846-12847. (b) Schulte-Ladbeck, R.; Vogel, M.; Karst, U. *Anal. Bioanal. Chem.* **2006**, *386*, 559-565.
- (5) Molecular Biology of Free Radicals in Human Diseases; Aruoma, O. I., Halliwell, B. B., Eds.; OICA International: Micoud, St. Lucia, 1998.
- (6) (a) Romaner, L.; Pogantsch, A.; de Freitas, P. S.; Scherf, U.; Gaal, M.; Zojer, E.; List, E. J. W. *Adv. Funct. Mater.* **2003**, *13*, 597-601. (b) Cho, S. Y.; Grimsdale, A. C.; Jones, D. J.; Watkins, S. E.; Holmes, A. B. *J. Am. Chem. Soc.* **2007**, *129*, 11910-11911.
- (7) Bunz, U. H. F. *Chem. Rev.* **2000**, *100*, 1605-1644.
- (8) McIlroy, S. P.; Cló, E.; Nikolajsen, L.; Frederiksen, P. K.; Nielsen, C. B.; Mikkelsen, K. V.; Gothelf, K. V.; Ogilby, P. R. *J. Org. Chem.* **2005**, *70*, 1134-1146.
- (9) Park, S.-J.; Gesquiere, A. J.; Yu, J.; Barbara, P. F. *J. Am. Chem. Soc.* **2004**, *126*, 4116-4117.

- (10) (a) Yan, M.; Rothberg, L. J.; Papadimitrakopoulos, F.; Galvin, M. E.; Miller, T. M. *Phys. Rev. Lett.* **1994**, *73*, 744-747. (b) Kocher, C.; Montali, A.; Smith, P.; Weder, C. *Adv. Funct. Mater.* **2001**, *11*, 31-35.
- (11) Andrew, T. L.; Swager, T. M. *Macromolecules* **2008**, *41*, 8306-8308.
- (12) (a) Kim, Y.; Swager, T. M. *Chem. Comm.* **2005**, 372-374. (b) Kim, Y.; Whitten, J. E.; and Swager T. M. *J. Am. Chem. Soc.* **2005**, *127*, 12122-12130.
- (13) Chen, R.-F.; Zhu, R.; Fan, Q.; Huang, W. *Org. Lett.* **2008**, *10*, 2913-2916.
- (14) Roncali, J. *Chem. Rev.* **1992**, *92*, 711-738.
- (15) Gingras, M.; Raimundo, J.-M.; Chabre, Y. M. *Angew. Chem. Int. Ed.* **2006**, *45*, 1686-1712.
- (16) Mayor, M.; Lehn, J.-M.; Fromm, K. M.; Fenske, D. *Angew. Chem. Int. Ed. Engl.* **1997**, *36*, 2370-2372.
- (17) (a) Yoon, C.-B.; Kang, I.-N.; Shim, H.-K. *J. Polym. Sci., Part A: Polym. Chem.* **1997**, *35*, 2253-2258. (b) Shim, H. K.; Yoon, C. B.; Ahn, T.; Hwang, D. H.; Zyung, T. *Synth. Met.* **1999**, *101*, 134-135. (c) Reisch, H. A.; Scherf, U. *Macromol. Chem. Phys.* **1999**, *200*, 552-561. (d) Hou, J.; Fan, B.; Huo, L.; He, C.; Yang, C.; Li, Y. *J. Polym. Sci., Part A: Polym. Chem.* **2006**, *44*, 1279-1290. (e) Gutierrez, J. J.; Luong, N.; Zepeda, D.; Ferraris, J. P. *Polym. Prepr. (Am. Chem. Soc., Div. Polym. Chem.)* **2004**, *45*, 172-173.
- (18) Dutta, T.; Woody, K. B.; Parkin, S. R.; Watson, M. D.; Gierschner, J. *J. Am. Chem. Soc.*, **2009**, *131*, 17321-17327.
- (19) Reddy, T. J.; Iwama, T.; Halpern, H. J.; Rawal, V. H. *J. Org. Chem.* **2002**, *67*, 4635-4639.
- (20) Krizan, T. D.; Martin, J. C. *J. Am. Chem. Soc.* **1983**, *105*, 6155-6157.
- (21) Rodriguez, C. M.; Ode, J. M.; Palazon, J. M.; Martin, V. S. *Tetrahedron*, **1992**, *48*, 3571-3576.
- (22) Aggarwal, V. K.; Davies, I. W.; Franklin, R.; Maddock, J.; Mahon, M. F.; Molloy, K. C. *J. Chem. Soc. Perkin Trans. 1* **1994**, 2363-2368.
- (23) Turro, N. J. *Modern Molecular Photochemistry*; University Science Books: Sausalito, CA, 1991.
- (24) Stille, J. K.; Whitehurst, D. D. *J. Am. Chem. Soc.* **1964**, *86*, 4871-4876.

- (25) (a) Herrmann, W. A.; Kühn, F. E. *Acc. Chem. Res.* **1997**, *30*, 169-180. (b) Vassell, K. A.; Espenson, J. H. *Inorg. Chem.* **1994**, *33*, 5491-5498. (c) Yamazaki, S. *Bull. Chem. Soc. Jpn.* **1996**, *69*, 2955-2959.
- (26) **MC1** and **P1** were not investigated because it was anticipated they would respond more slowly to hydrogen peroxide than the more electron-rich **MC2** and **P2**.
- (27) Becker, R. S.; Jordan, A. D.; Kolc, J. *J. Chem. Phys.* **1973**, *59*, 4024-4028.
- (28) (a) Baunsgaard, D.; Larsen, M.; Harrit, N.; Frederiksen, J.; Wilbrandt, R.; Stapelfeldt, H. *J. Chem. Soc., Faraday Trans.* **1997**, *93*, 1893-1901. (b) Marguet, S.; Markovitsi, D.; Millie, P.; Sigal, H. *J. Phys. Chem. B.* **1998**, *102*, 4697-4710.
- (29) Zuccherro, A. J.; Wilson, J. N.; Bunz, U. H. F. *J. Am. Chem. Soc.* **2006**, *128*, 11872-11881.
- (30) Berlman, I. B. *Handbook of Fluorescence Spectra*; Academic Press: New York, 1965.
- (31) (a) Lee, W.; Jenks, W. *J. Org. Chem.* **2001**, *66*, 474-480. (b) Jenks, W. S.; Matsunaga, N.; Gordon, M. *J. Org. Chem.* **1996**, *61*, 1275-1283.
- (32) Lin, Y.; Lin, C. *Org. Lett.* **2007**, *9*, 2075-2078.
- (33) Clennan, E. L. *Acc. Chem. Res.* **2001**, *34*, 875-884.
- (34) Kim, T.-H.; Swager, T. M. *Angew. Chem. Int. Ed.* **2003**, *42*, 4803-4806.
- (35) Thomas, S. W., III.; Venkatesan, K.; Müller, P.; Swager, T. M. *J. Am. Chem. Soc.* **2006**, *128*, 16641-16648.
- (36) Eaton, D. F. *Pure Appl. Chem.* **1988**, *60*, 1107-1114.
- (37) Reynolds, G. A.; Drexhage, K. H. *Opt. Commun.* **1975**, *13*, 222-225.
- (38) Casey, K. G.; Quitevis, E. L. *J. Phys. Chem.* **1988**, *92*, 6590-6594.
- (39) Melhuish, W. H. *J. Opt. Soc. Am.* **1964**, *52*, 183-186.
- (40) Mu, F.; Hamel, E.; Lee, D. J.; Pryor, D. E.; Cushman, M. *J. Med. Chem.* **2003**, *46*, 1670-1682.
- (41) Huang, S.; Tour, J. M. *Tet. Lett.* **1999**, *40*, 3347-3350.

(42) Shirai, Y.; Zhao, Y.; Cheng, L.; Tour, J. M. *Org. Lett.* **2004**, *6*, 2129-2132.

5.17 Additional Figures

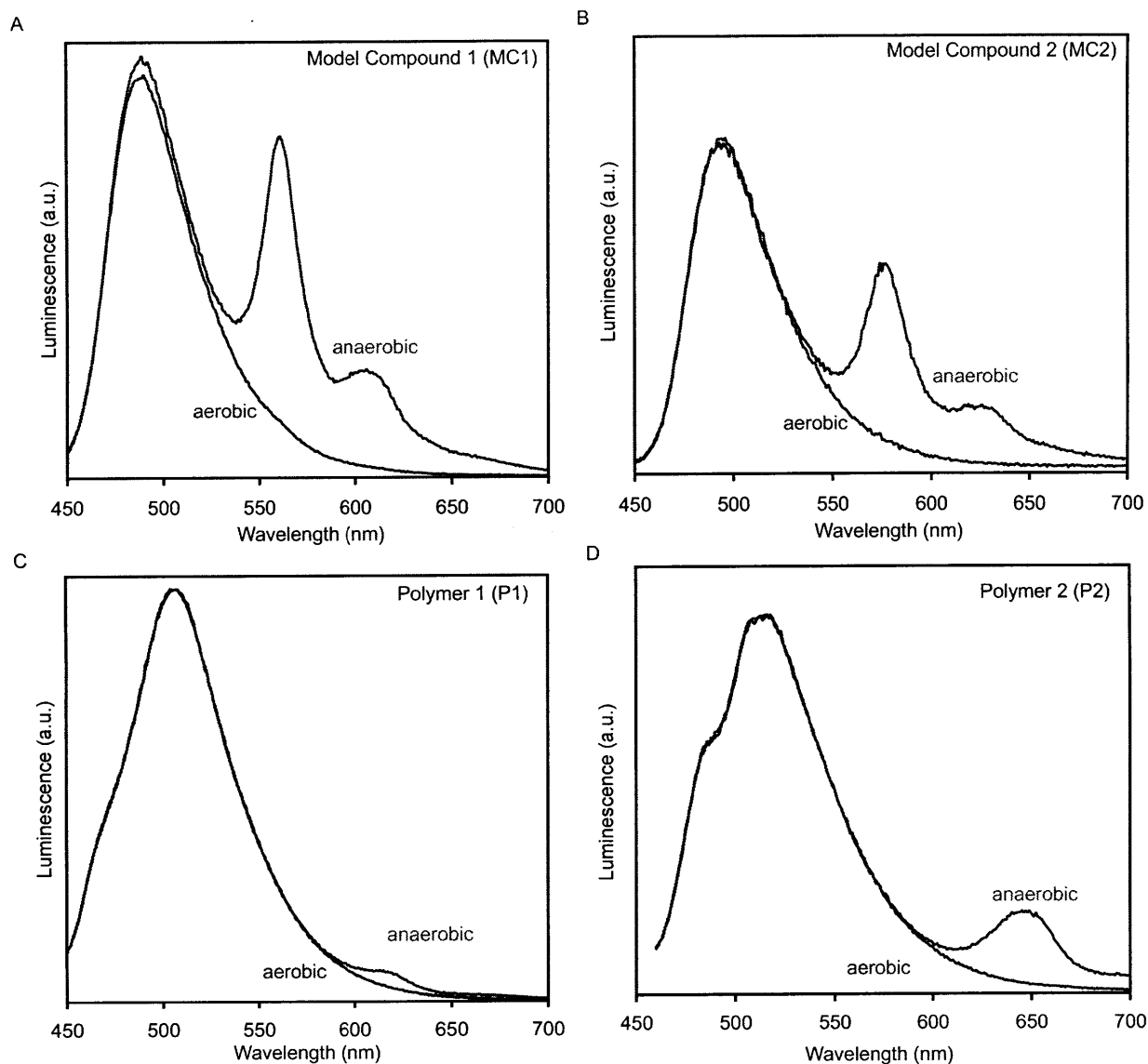


Figure A1. *Effect of Oxygen on Emission.*

(a, b, c, and d) Luminescence spectra of **MC1**, **MC2**, **P1**, and **P2** at room temperature in CHCl_3 under aerobic and anaerobic conditions. Anaerobic samples were prepared by bubbling nitrogen through a septum-capped quartz vial for a minimum of 10 minutes. After recording the anaerobic spectrum, the septum was removed from the vial and the aerobic spectrum was recorded. λ_{ex} : 420 nm (**MC1**, **MC2**), 440 nm (**P1**, **P2**). All spectra are corrected for PMT response.

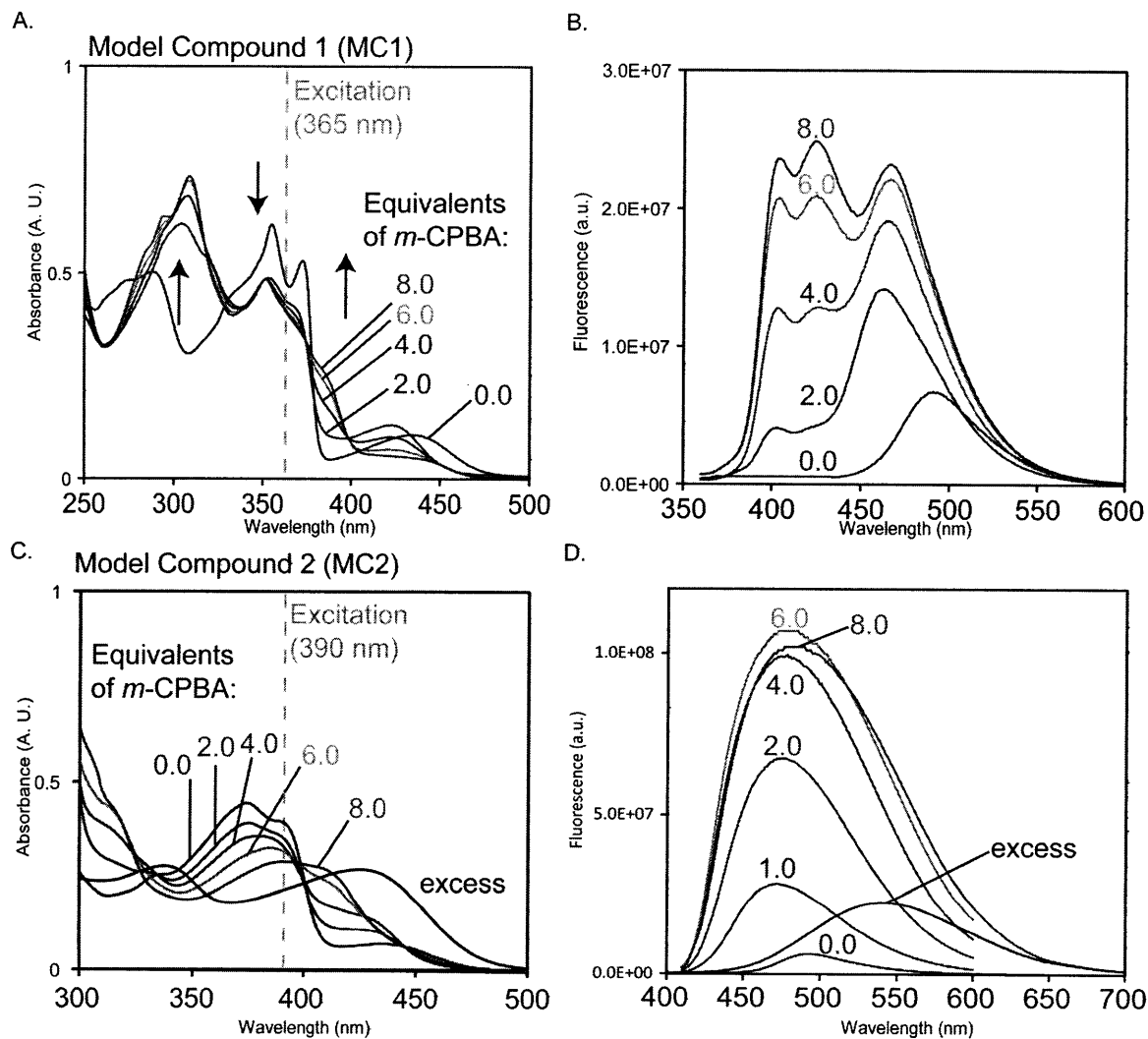


Figure A2. Titration of Model Compounds with *m*-CPBA.

(a and b) Absorption and fluorescence spectra of **MC1** in CH_2Cl_2 before and after the addition of increasing amounts of *m*-CPBA. The sample was allowed to stir for a minimum of 30 minutes per 1.0 equivalent of oxidant added before the spectrum was recorded. All spectra were taken from the same cuvette and the volume of CH_2Cl_2 was adjusted for evaporative losses. (c and d) Absorption and fluorescence spectra of **MC2** in CH_2Cl_2 before and after the addition of increasing amounts of *m*-CPBA. The experimental details are the same as in a and b. Excess refers to >20 equivalents of oxidant.

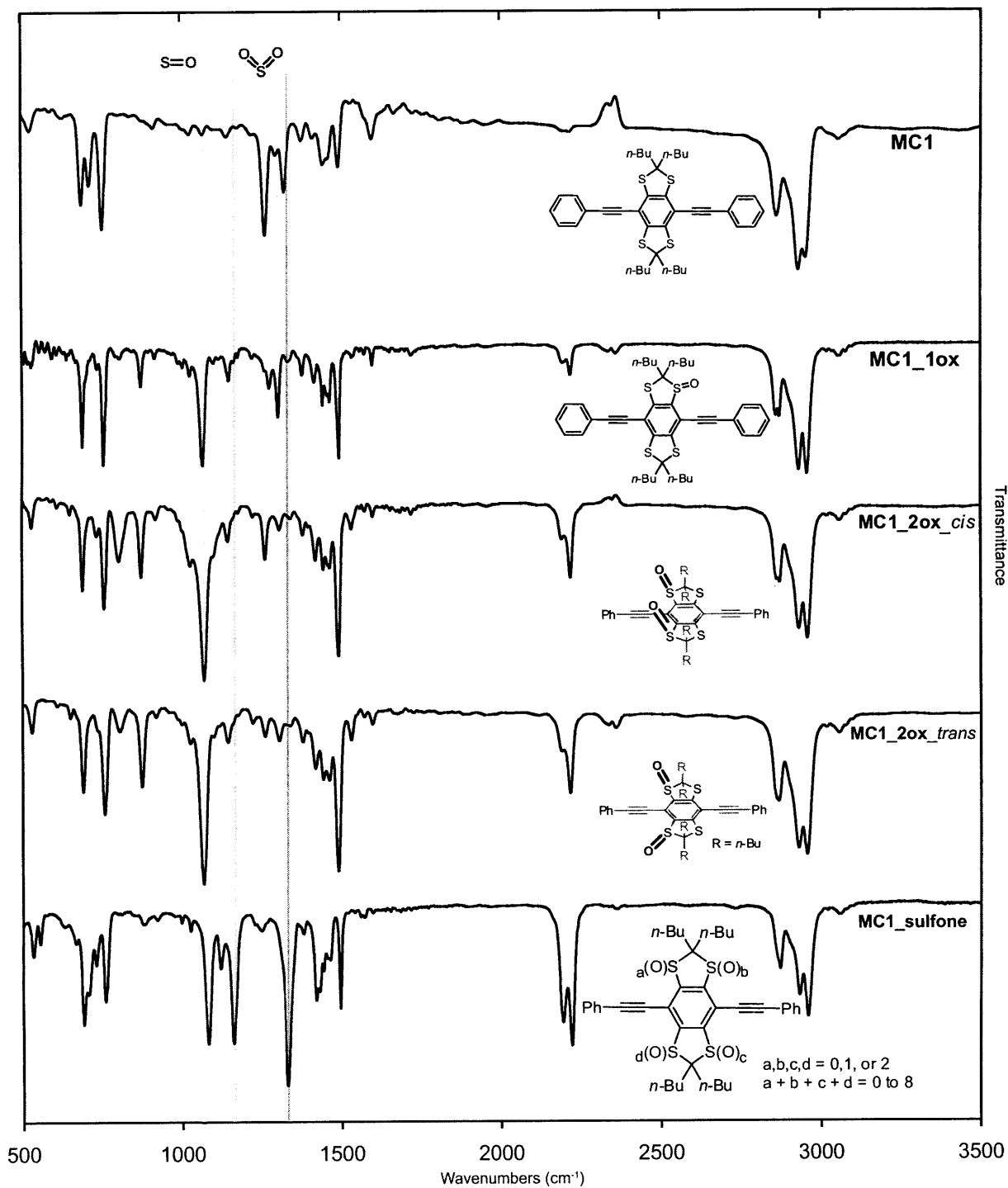


Figure A3. MC1 IR.

MC1_sulfone was prepared as described in footnote 24 of the text.

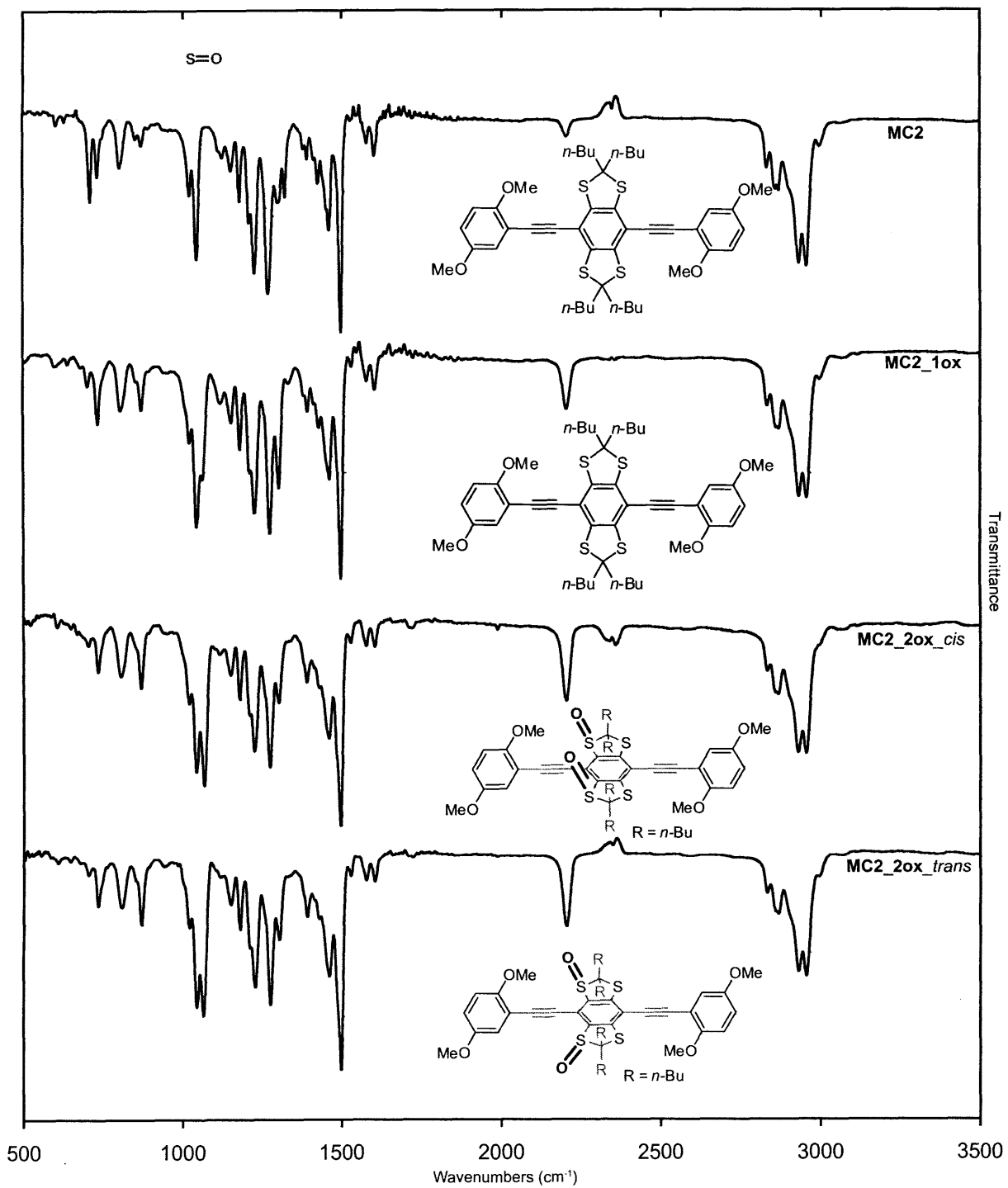


Figure A4. MC2 IR.

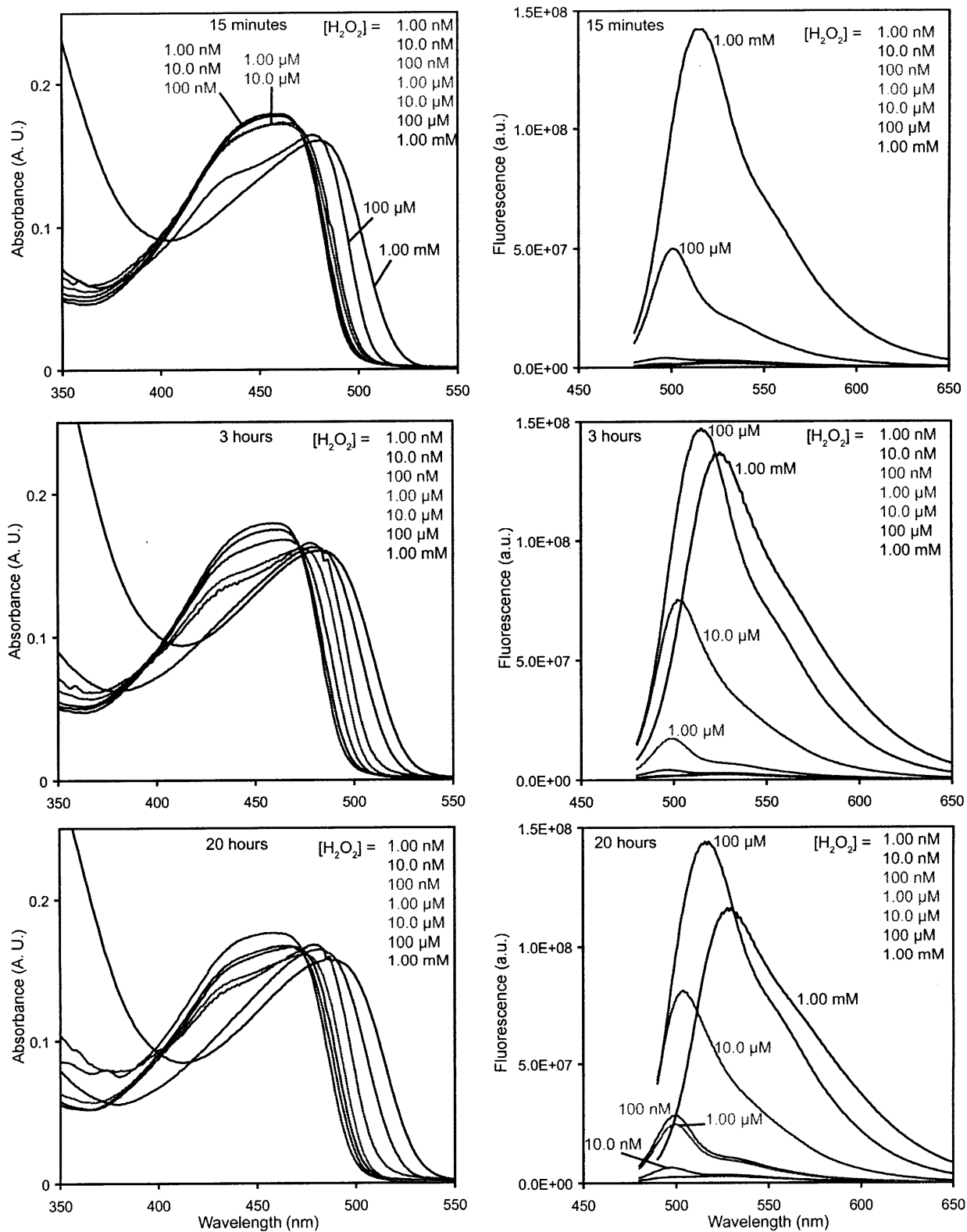


Figure A5. Oxidation of P2 with H₂O₂.
 For all solutions: $\lambda_{\text{ex}} = 460 \text{ nm}$, [P2] = 5.00 μM, [MTO] = 0.5 mM, [urea] = [H₂O₂] in CH₂Cl₂ with < 5% ethanol.

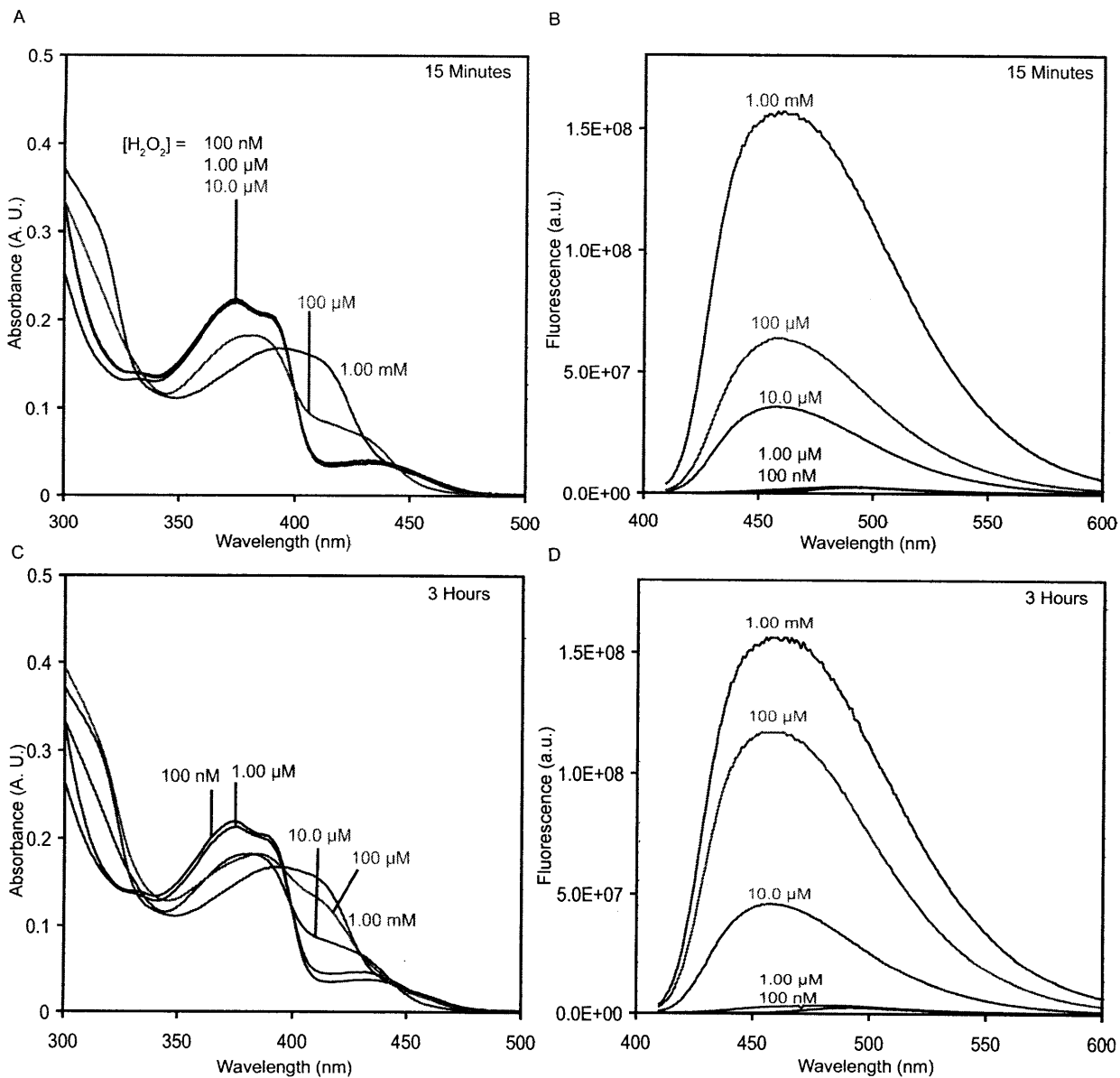


Figure A6. Oxidation of **MC2** with H_2O_2 .

For all solutions: $\lambda_{ex} = 390$ nm, $[MC2] = 10.00$ μM, $[MTO] = 0.5$ mM, $[urea] = [H_2O_2]$ in CH_2Cl_2 with < 5% ethanol.

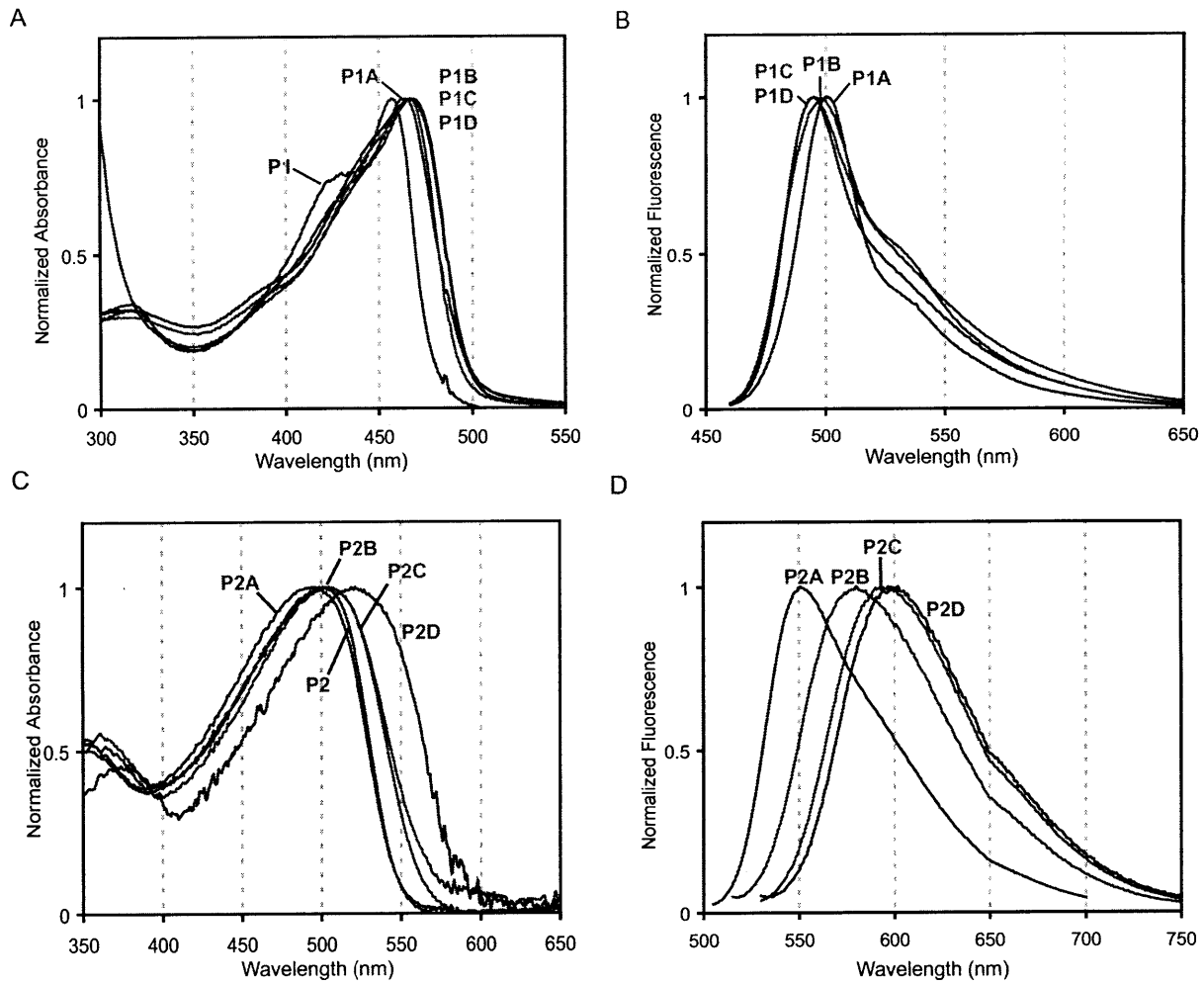


Figure A7. *Thin-film Spectra of Polymers.*

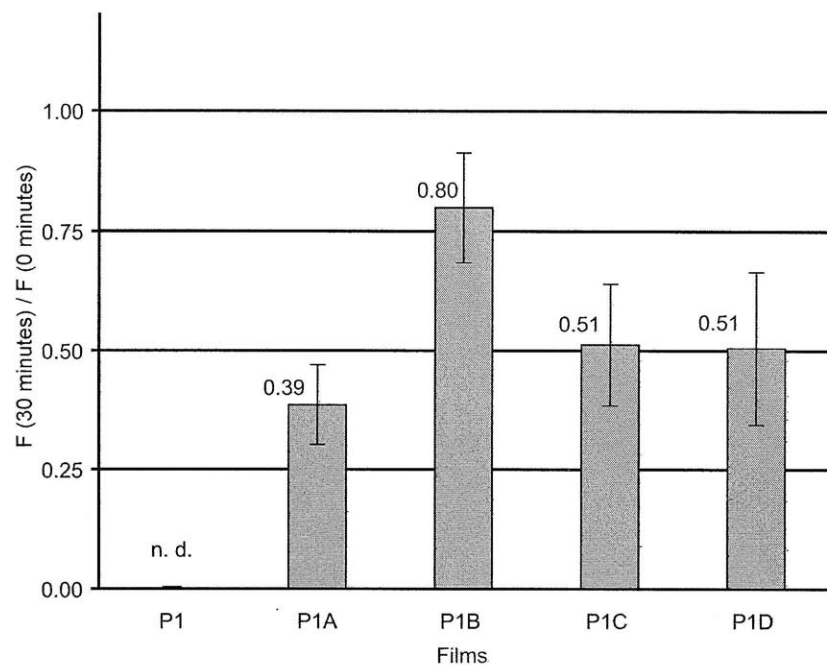


Figure A8. *Photostability of PI thin-films.*

Thin-films of **PI** were irradiated for 30 minutes at their absorbance maxima with monochromatic light and the ratio of fluorescence at 30 minutes to the initial fluorescence was measured. All films had an optical density of 0.10 ± 0.01 .

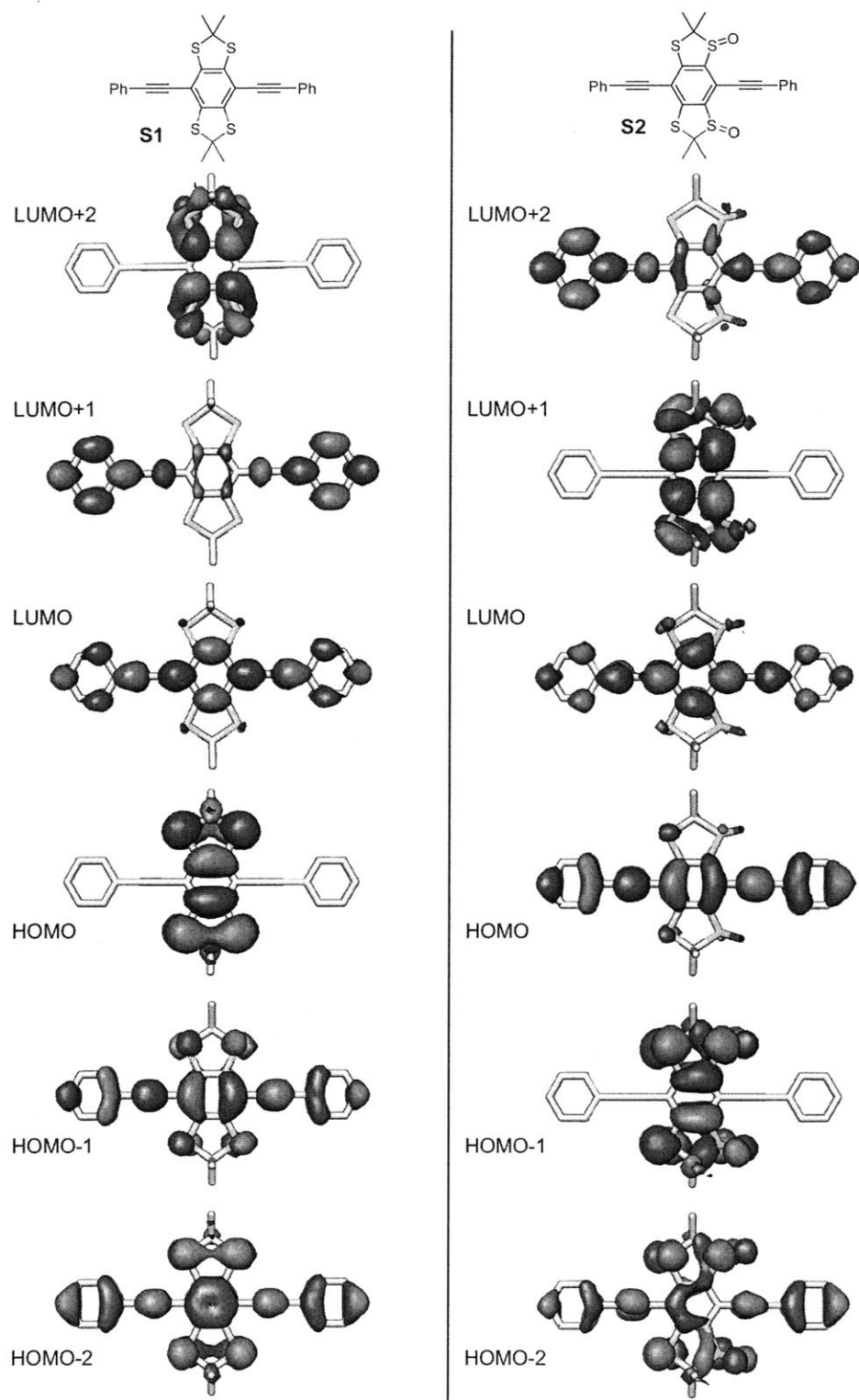
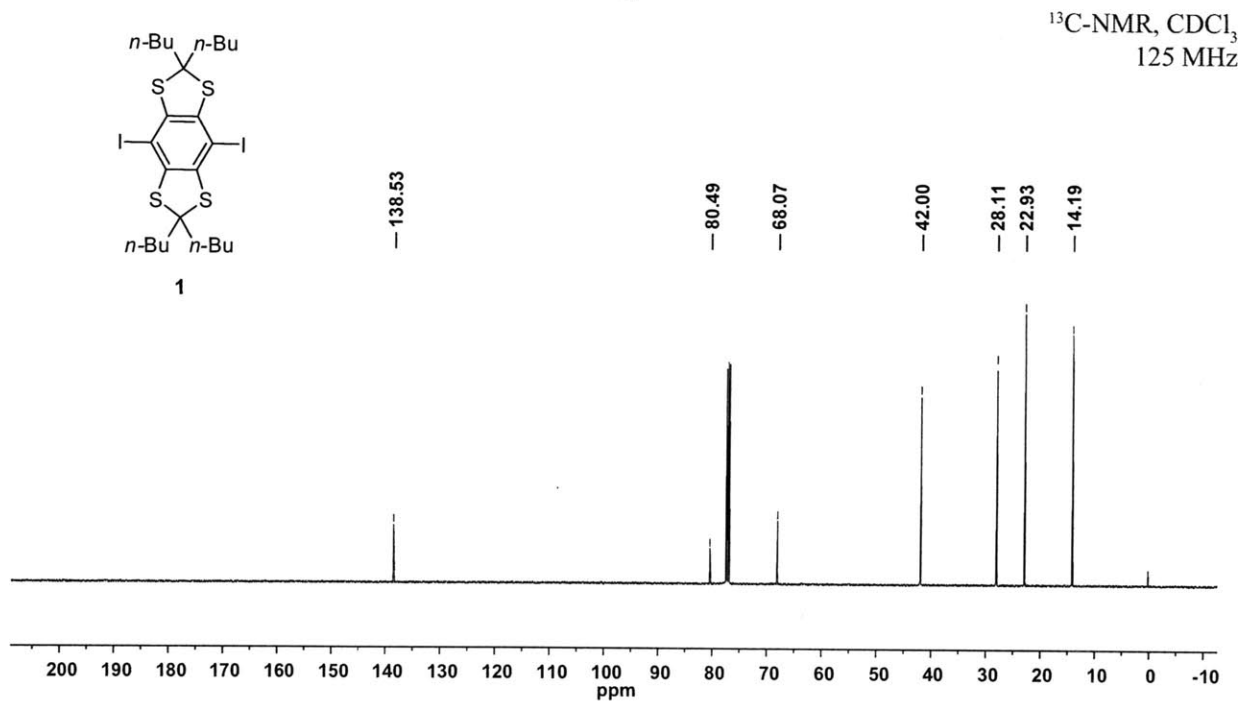
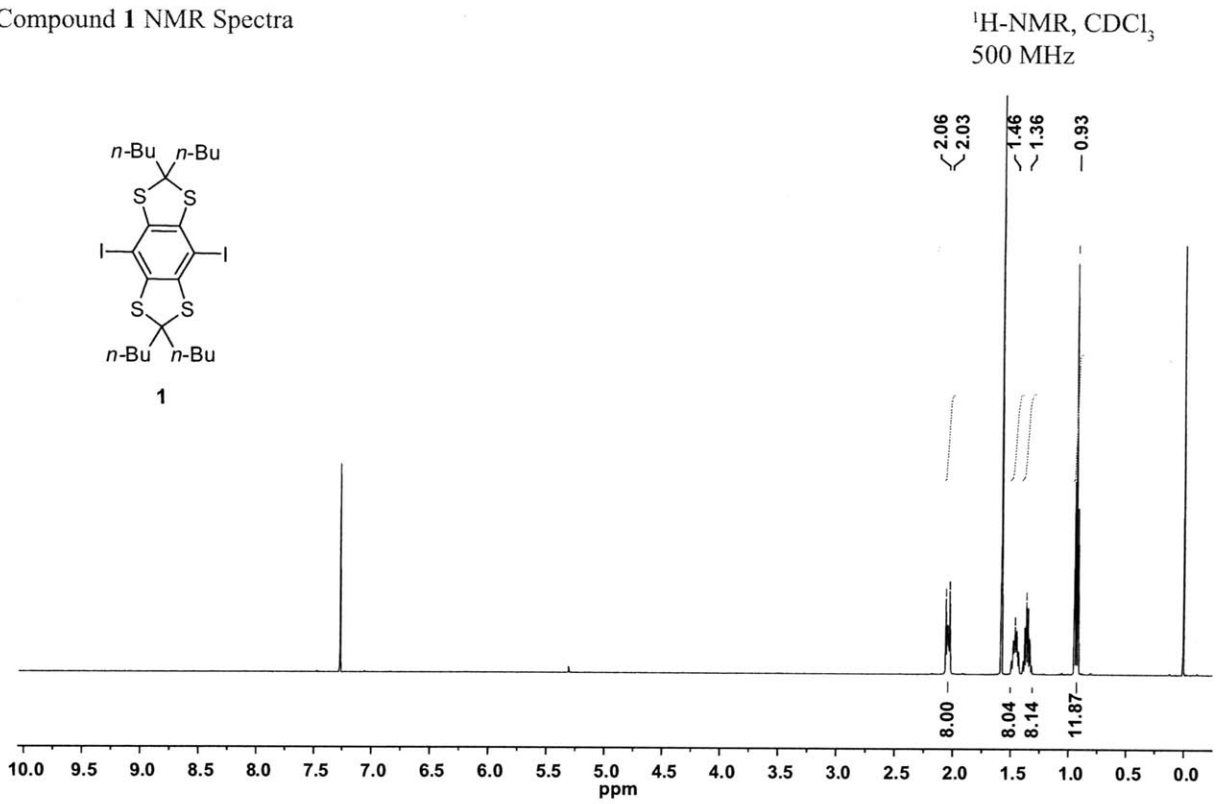


Figure A9. Frontier Molecular Orbitals of **S1** and **S2**.

Frontier orbital topologies (DFT, B3LYP 6-311+G*, Gaussian03) for structures **S1** and **S2**, which are similar to **MC1** and **MC1_2ox_trans**, respectively, except that the butyl-groups have been replaced with methyl-groups for ease of computation.

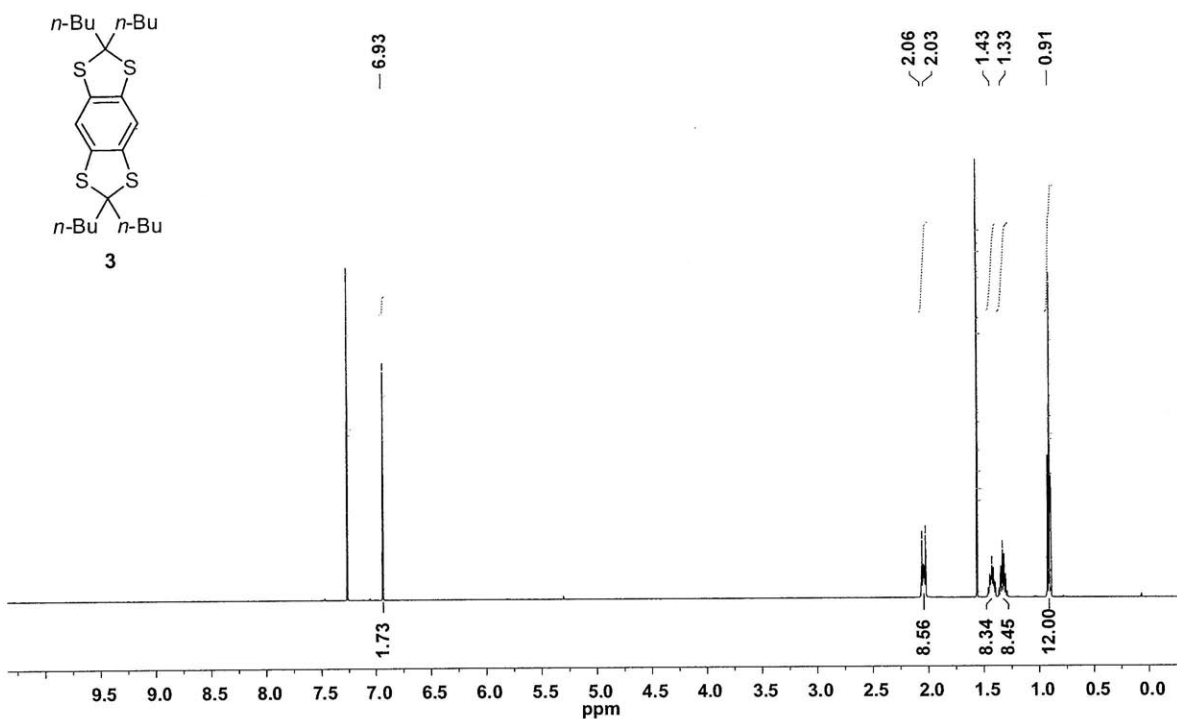
5.18 NMR Spectra

Compound **1** NMR Spectra

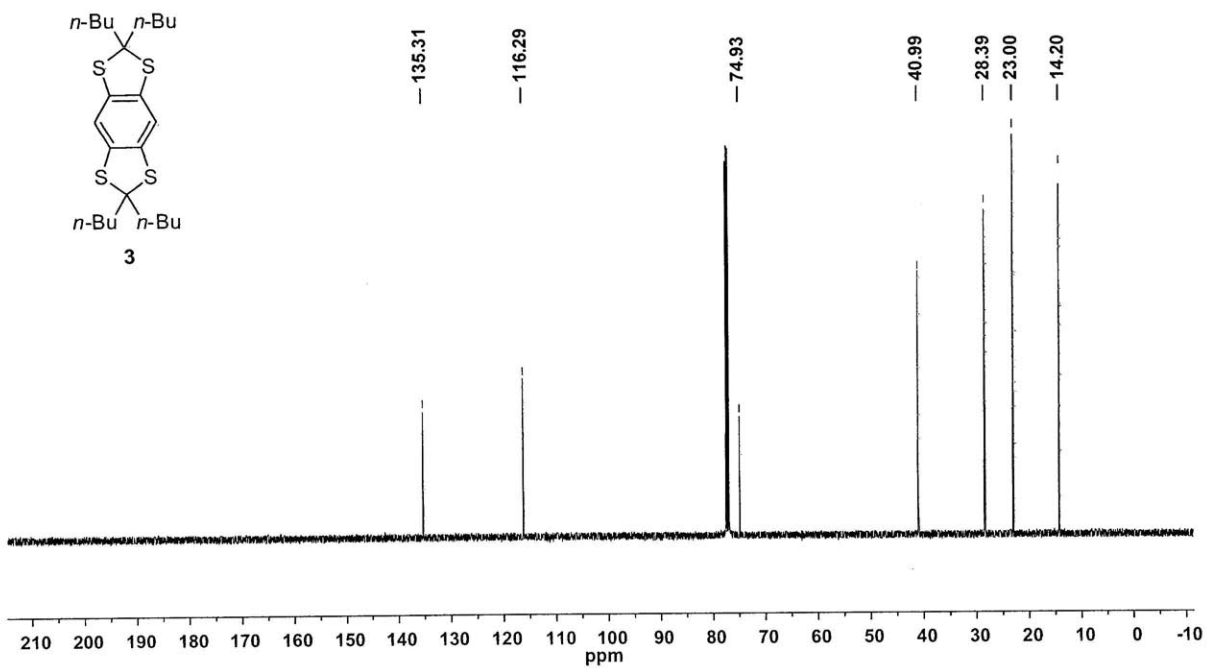


Compound 3 NMR Spectra

$^1\text{H-NMR}$, CDCl_3
500 MHz

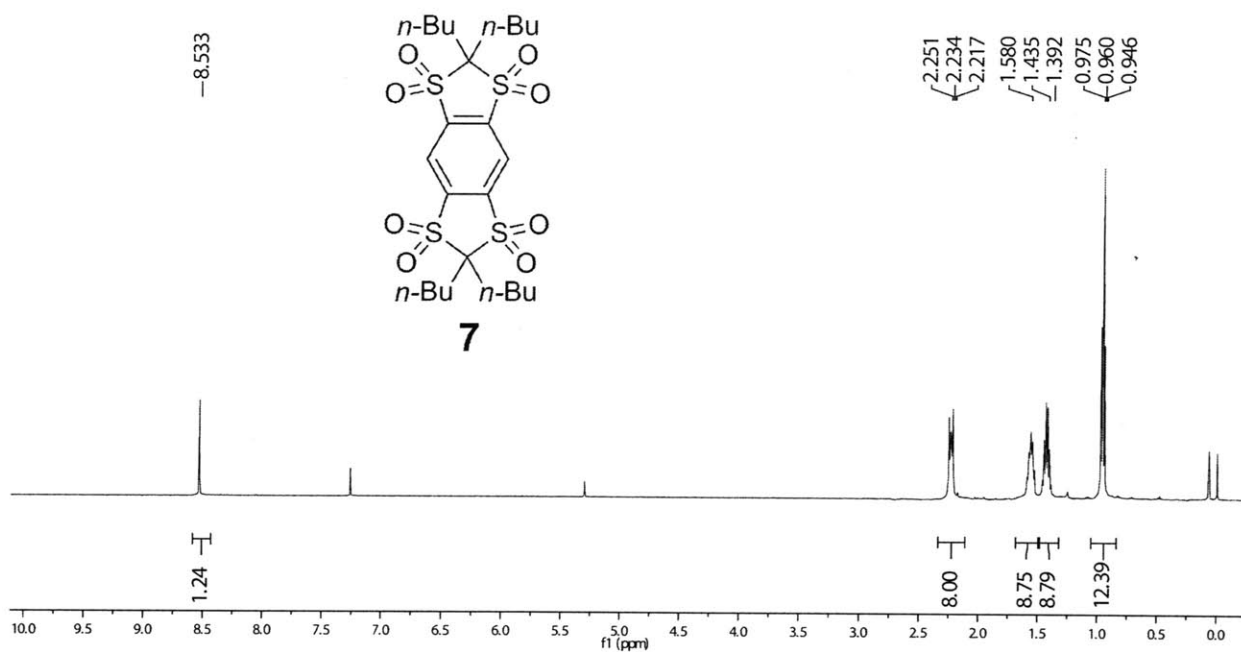


$^{13}\text{C-NMR}$, CDCl_3
125 MHz

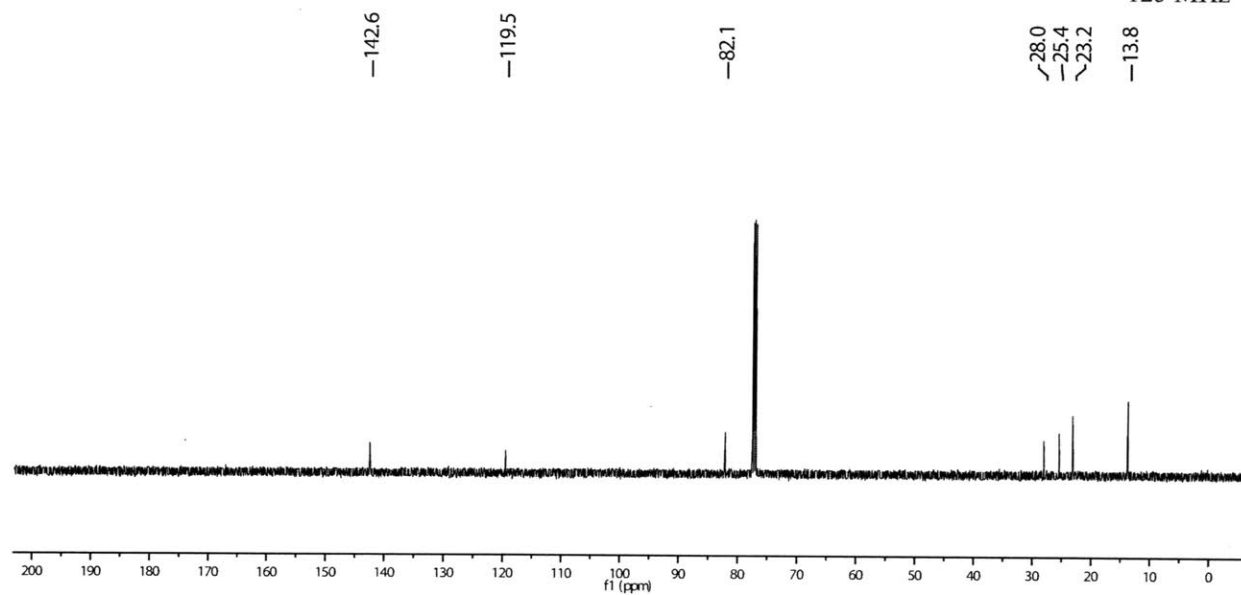


Compound 7 NMR Spectra

¹H-NMR, CDCl₃
500 MHz

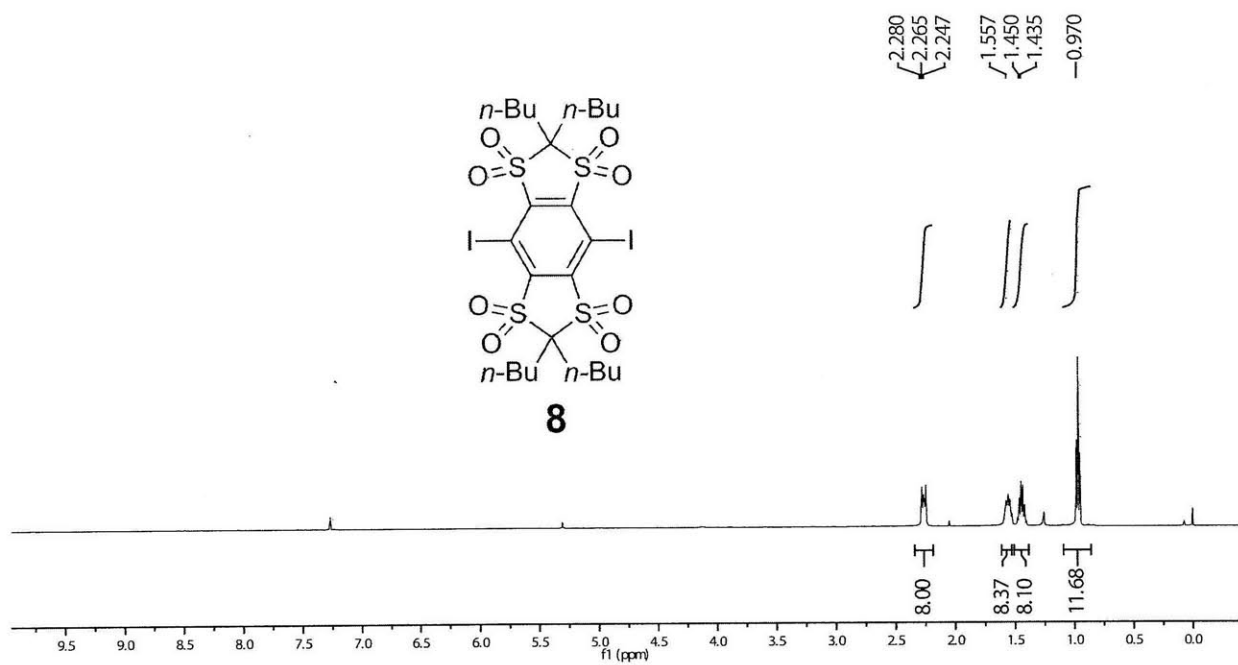


¹³C-NMR, CDCl₃
125 MHz

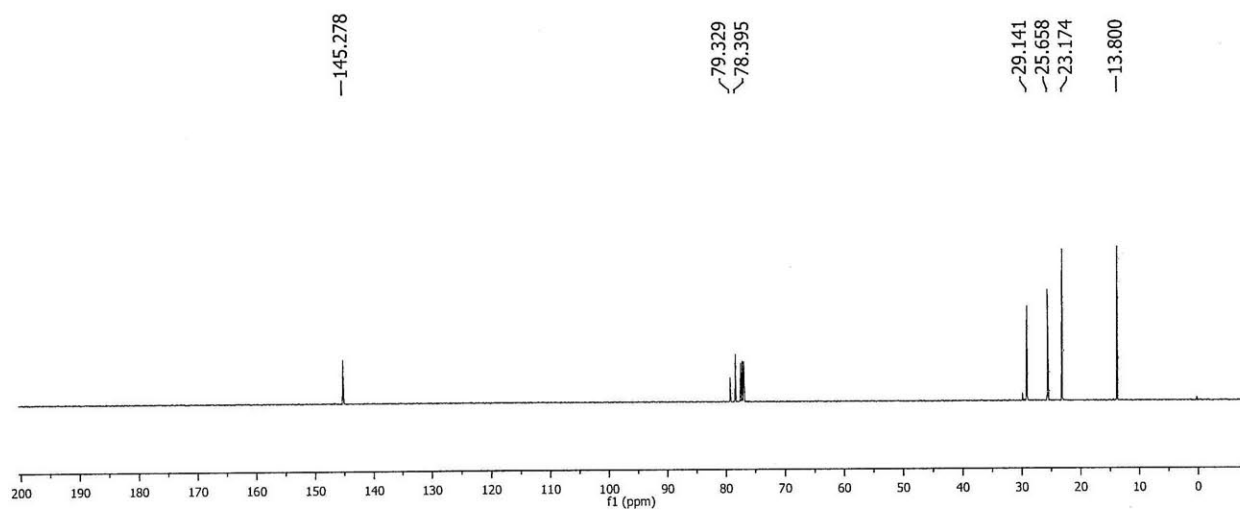


Compound **8** NMR Spectra

¹H-NMR, CDCl₃
500 MHz

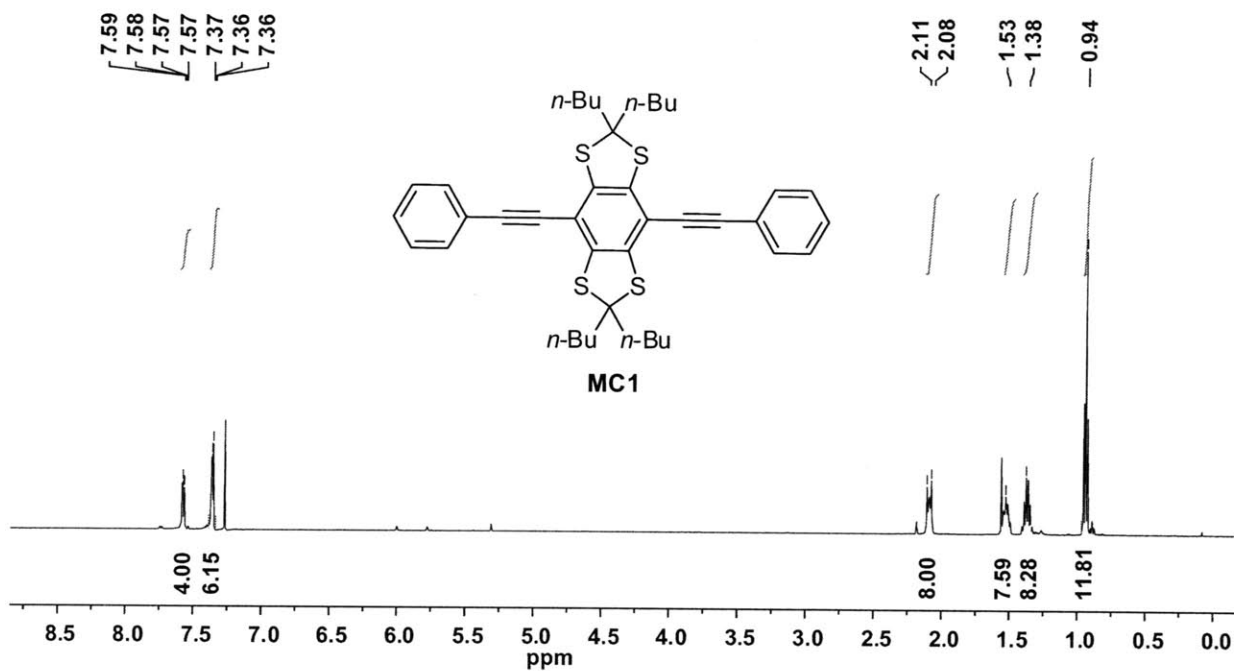


¹³C-NMR, CDCl₃
125 MHz

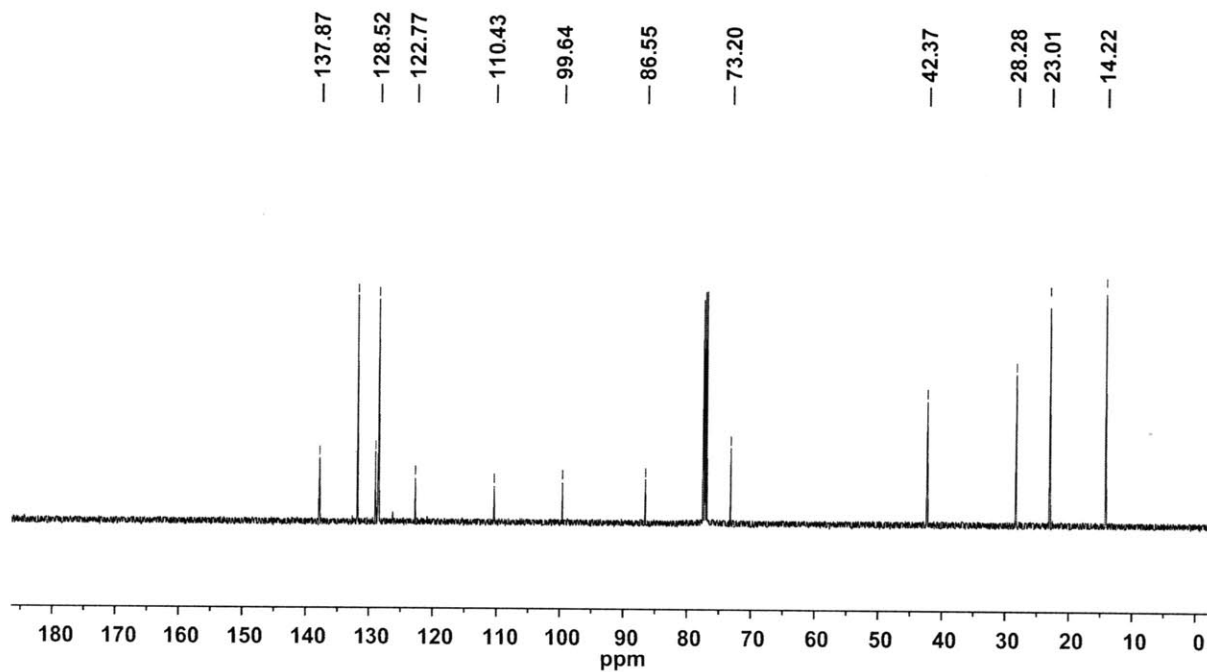


Model Compound **1** NMR Spectra

$^1\text{H-NMR}$, CDCl_3
500 MHz

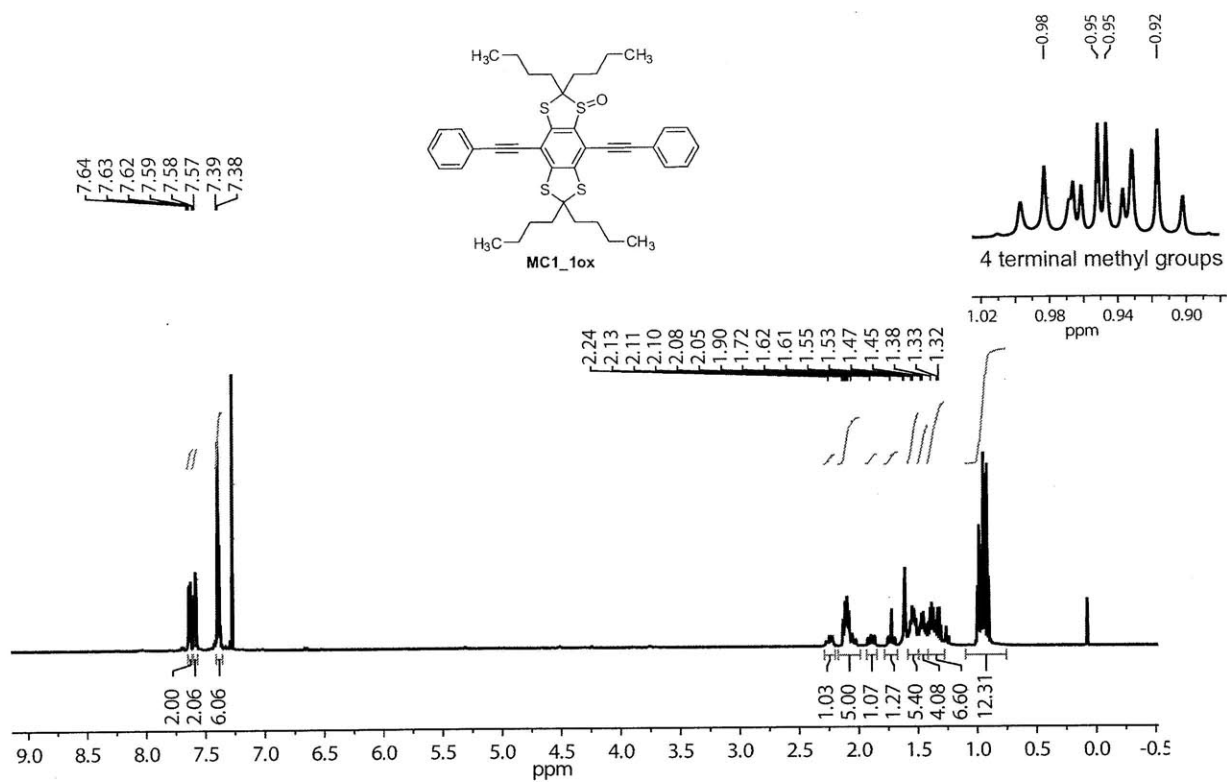


$^{13}\text{C-NMR}$, CDCl_3
126 MHz

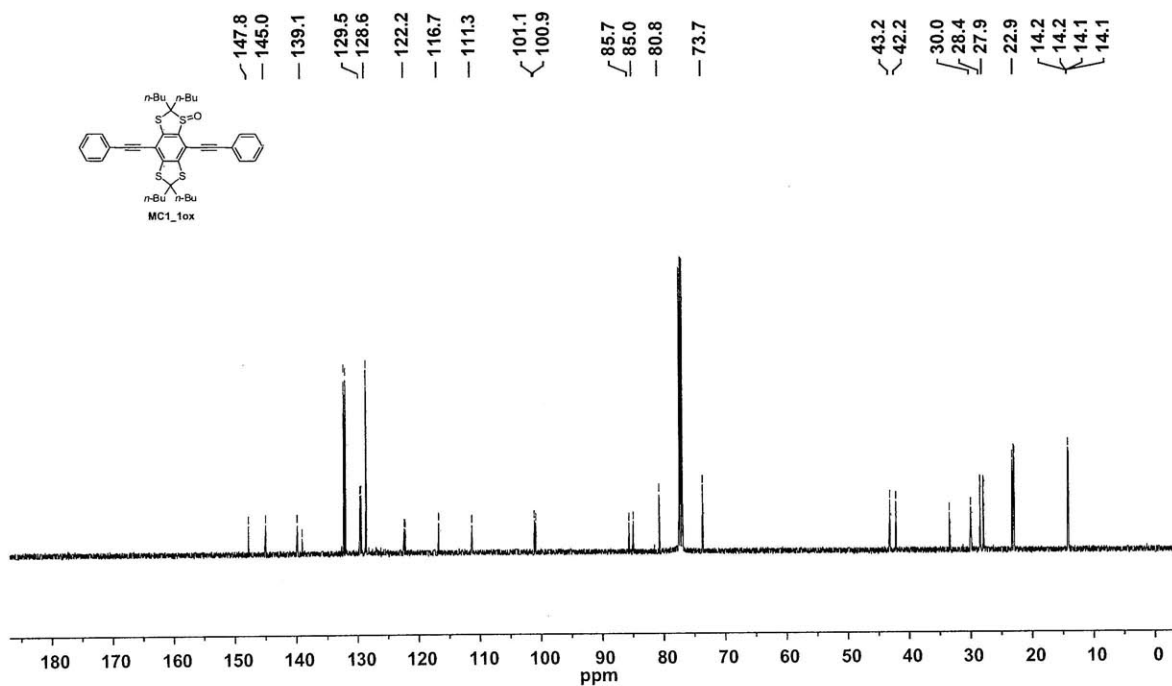


MC1_1ox NMR Spectra

¹H-NMR, CDCl₃
500 MHz

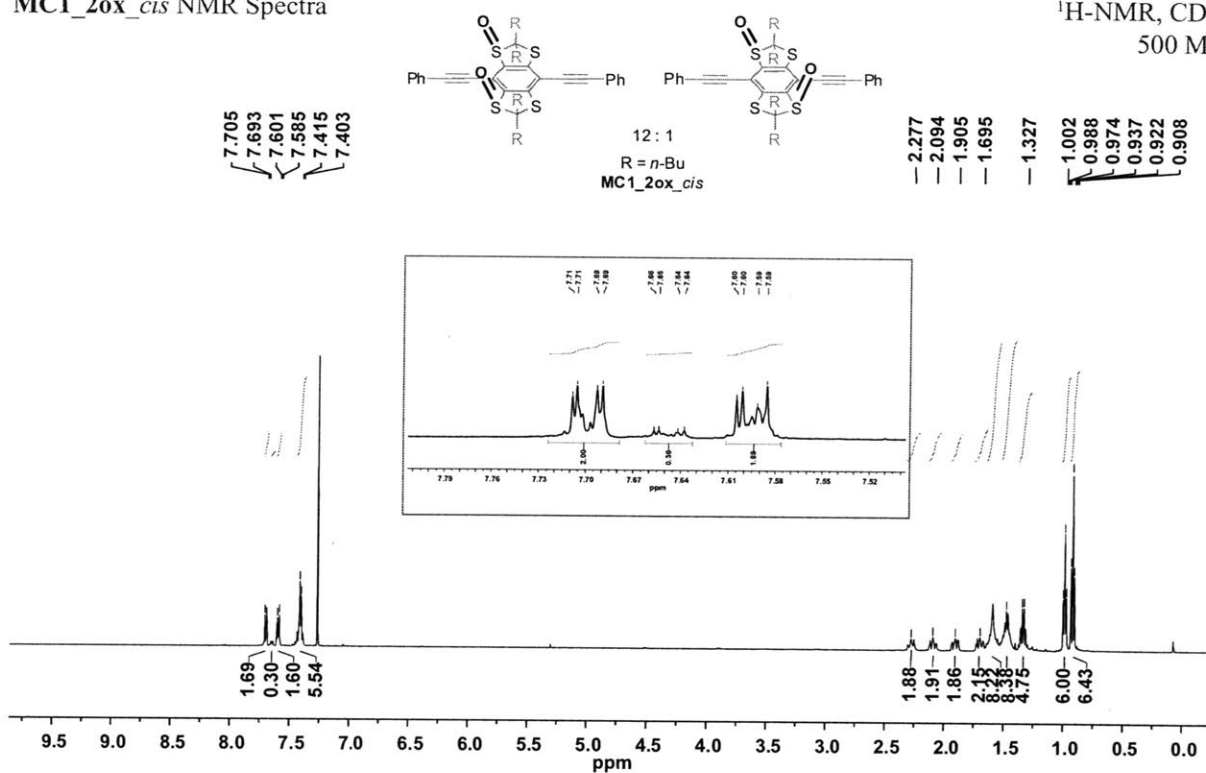


¹³C-NMR, CDCl₃
126 MHz

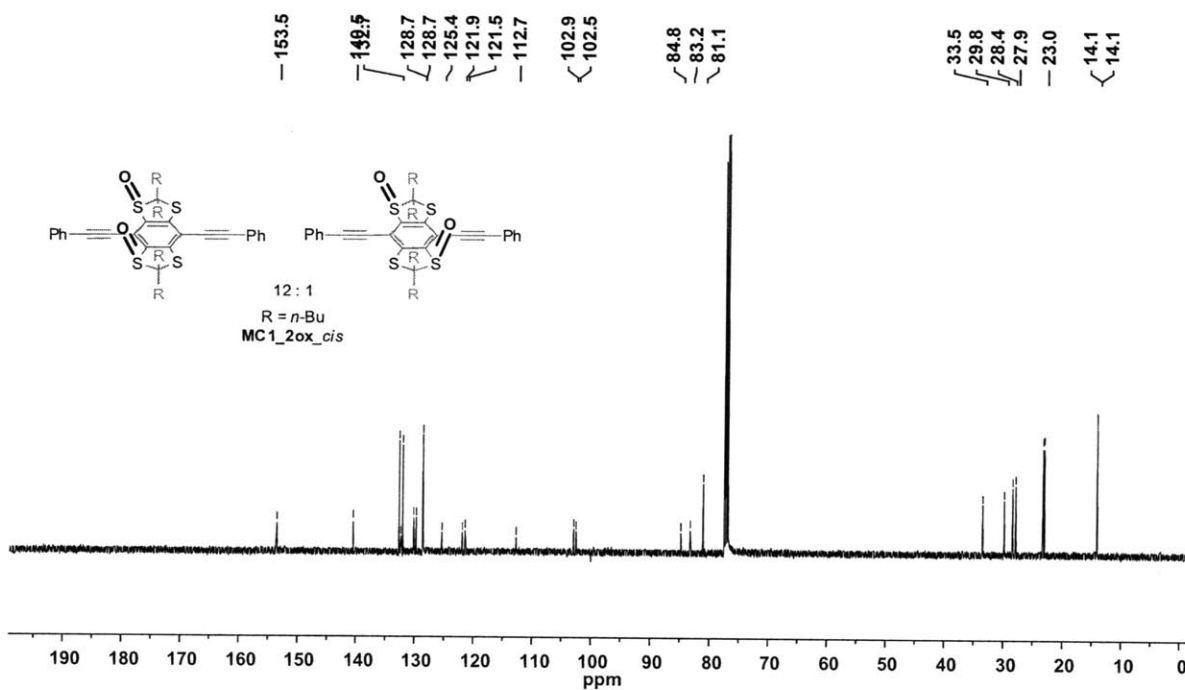


MC1_2ox_cis NMR Spectra

¹H-NMR, CDCl₃
500 MHz

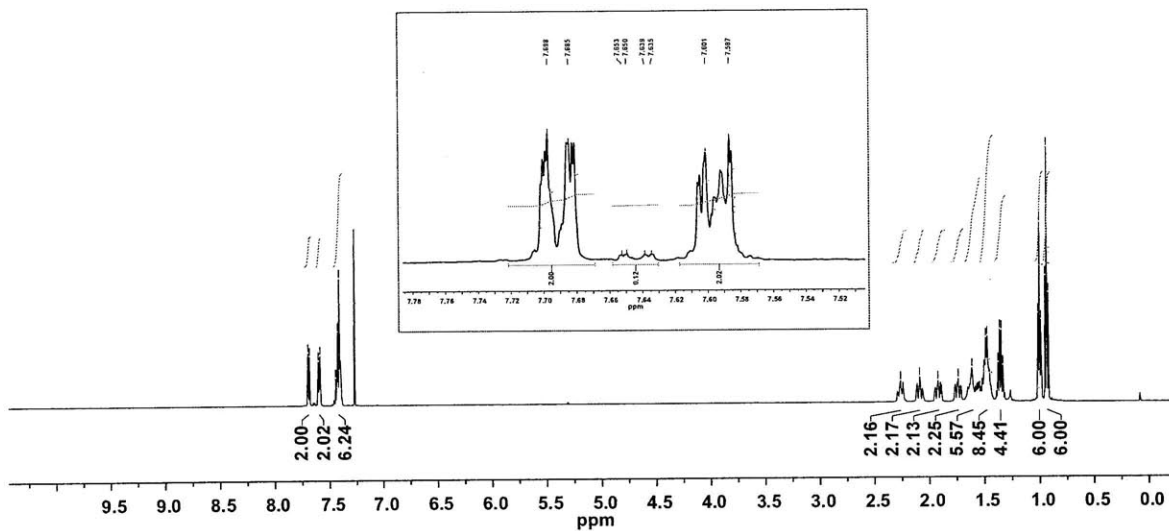
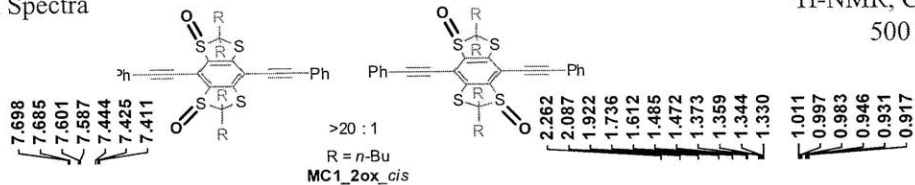


¹³C-NMR, CDCl₃
126 MHz

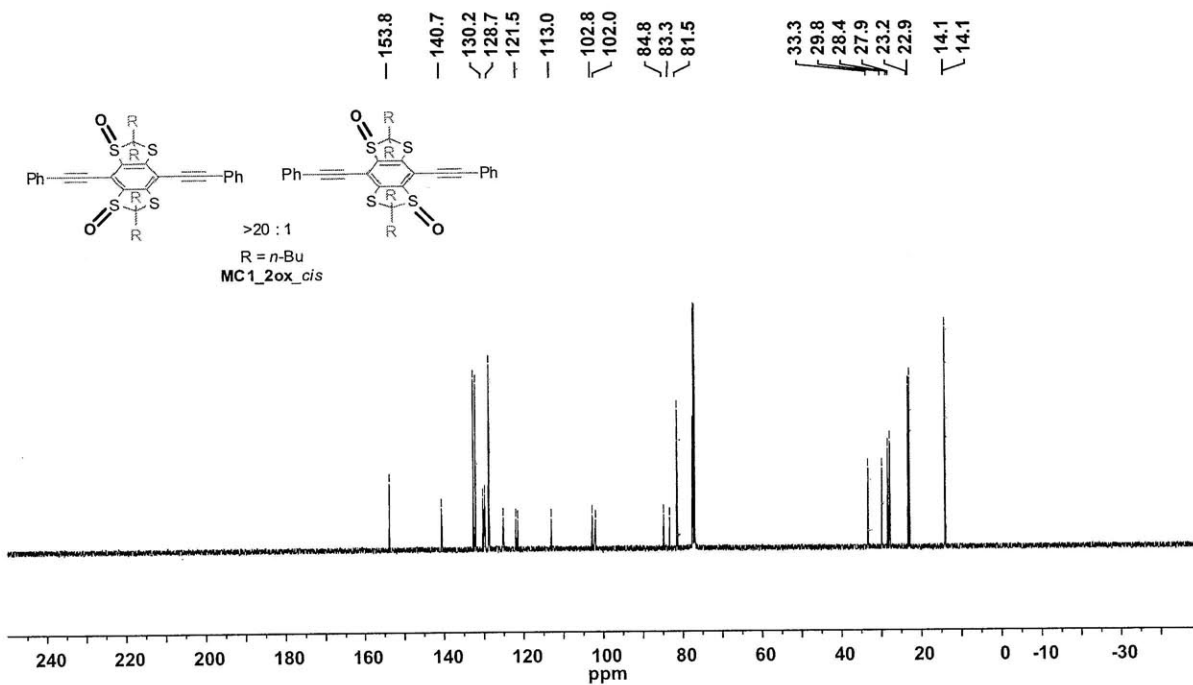
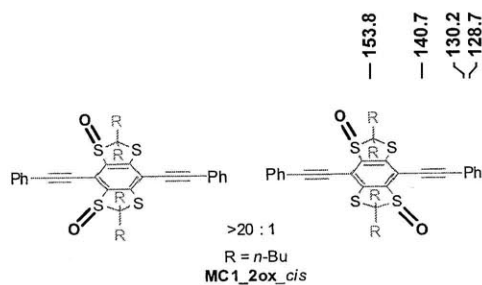


MC1_2ox_trans NMR Spectra

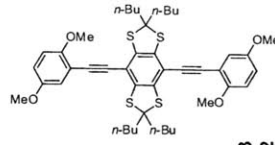
¹H-NMR, CDCl₃
500 MHz



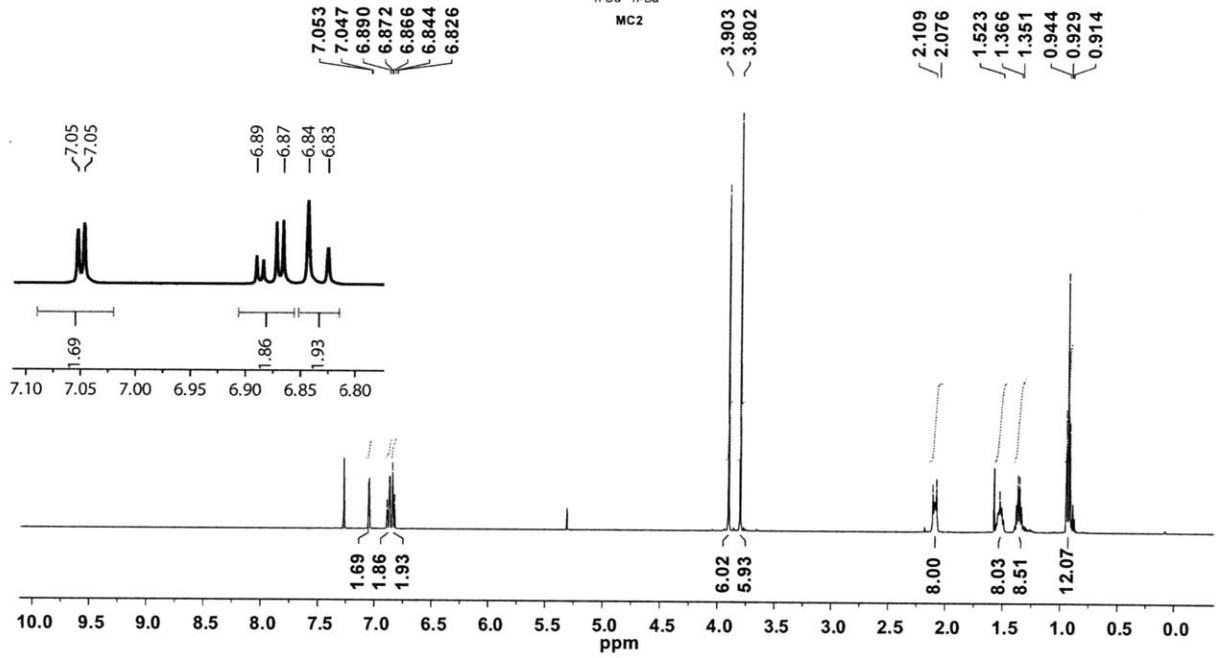
¹³C-NMR, CDCl₃
126 MHz



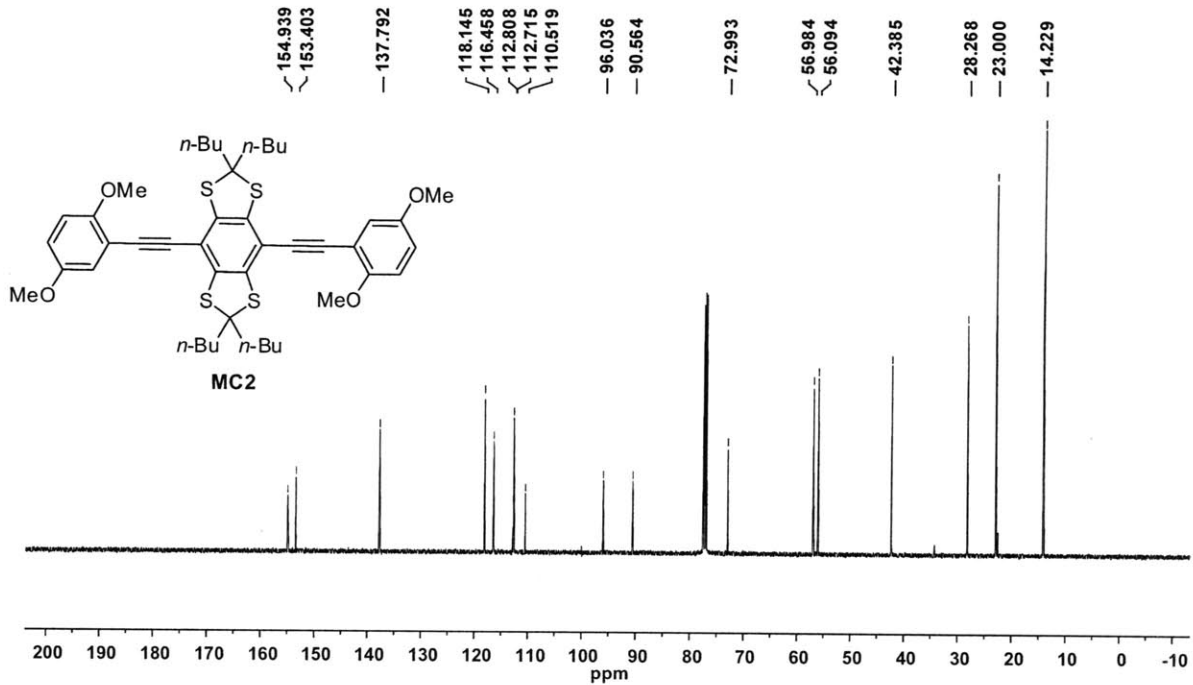
Model Compound 2 NMR Spectra



$^1\text{H-NMR}$, CDCl_3
500 MHz

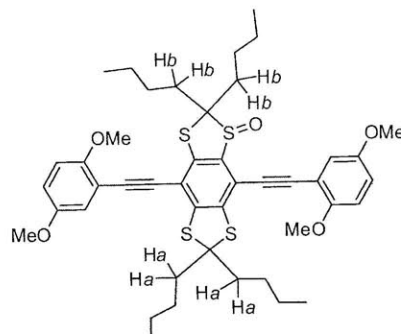
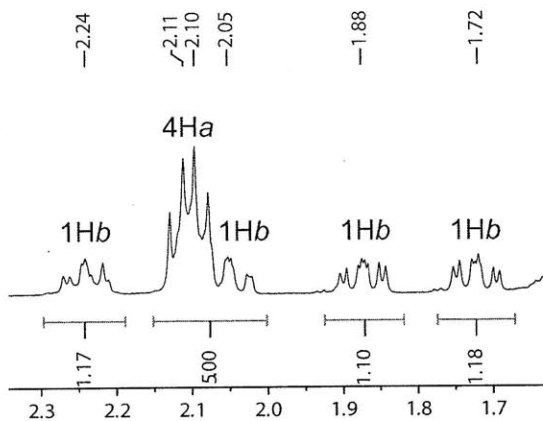


$^{13}\text{C-NMR}$, CDCl_3
126 MHz

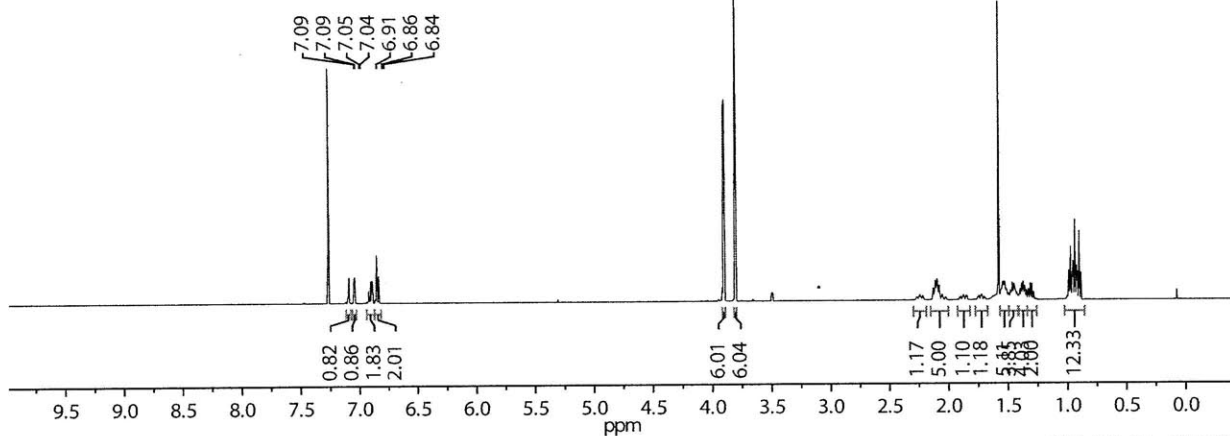
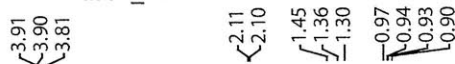


MC2_1ox NMR Spectra

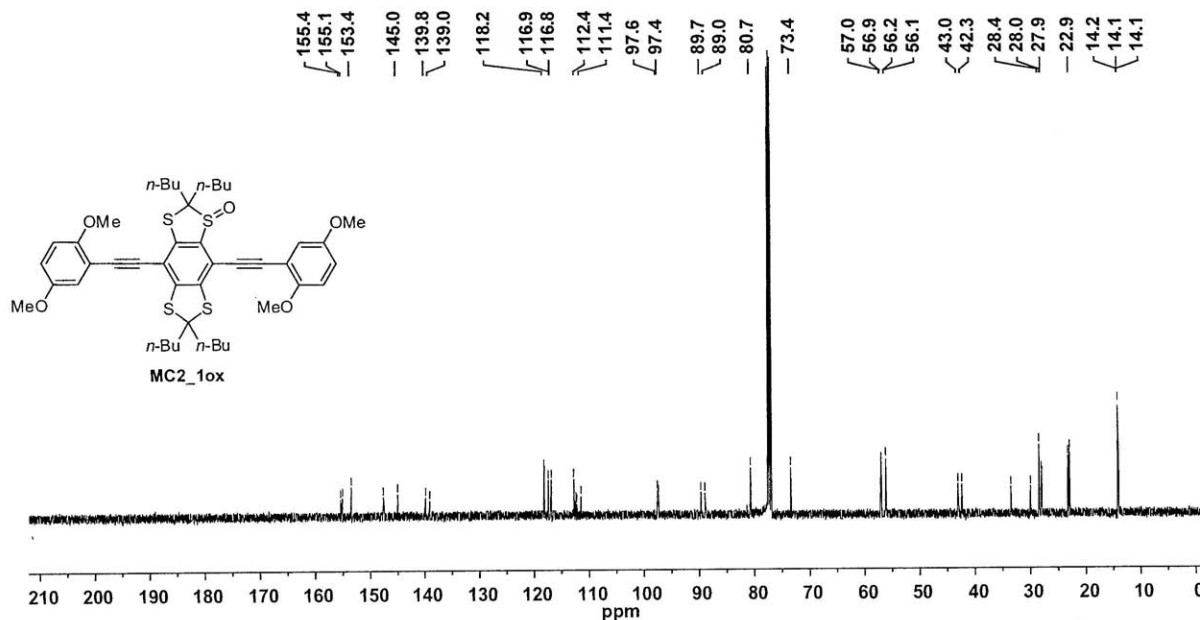
¹H-NMR, CDCl₃
500 MHz



MC2_1ox

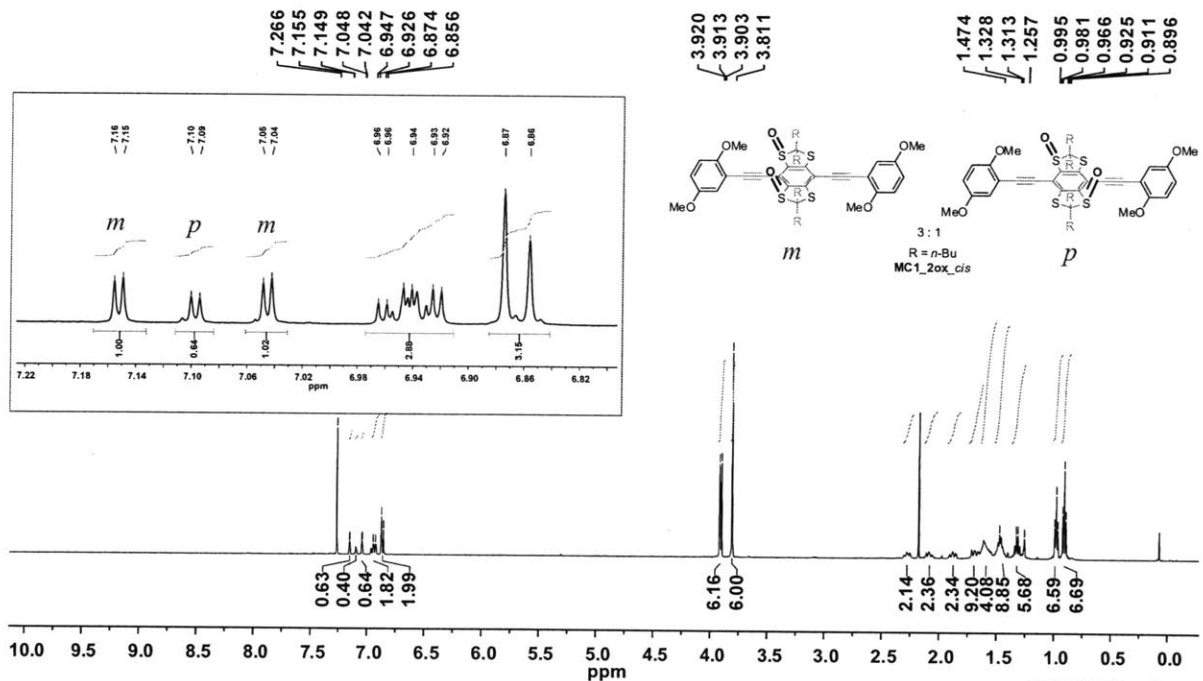


¹³C-NMR, CDCl₃
125 MHz

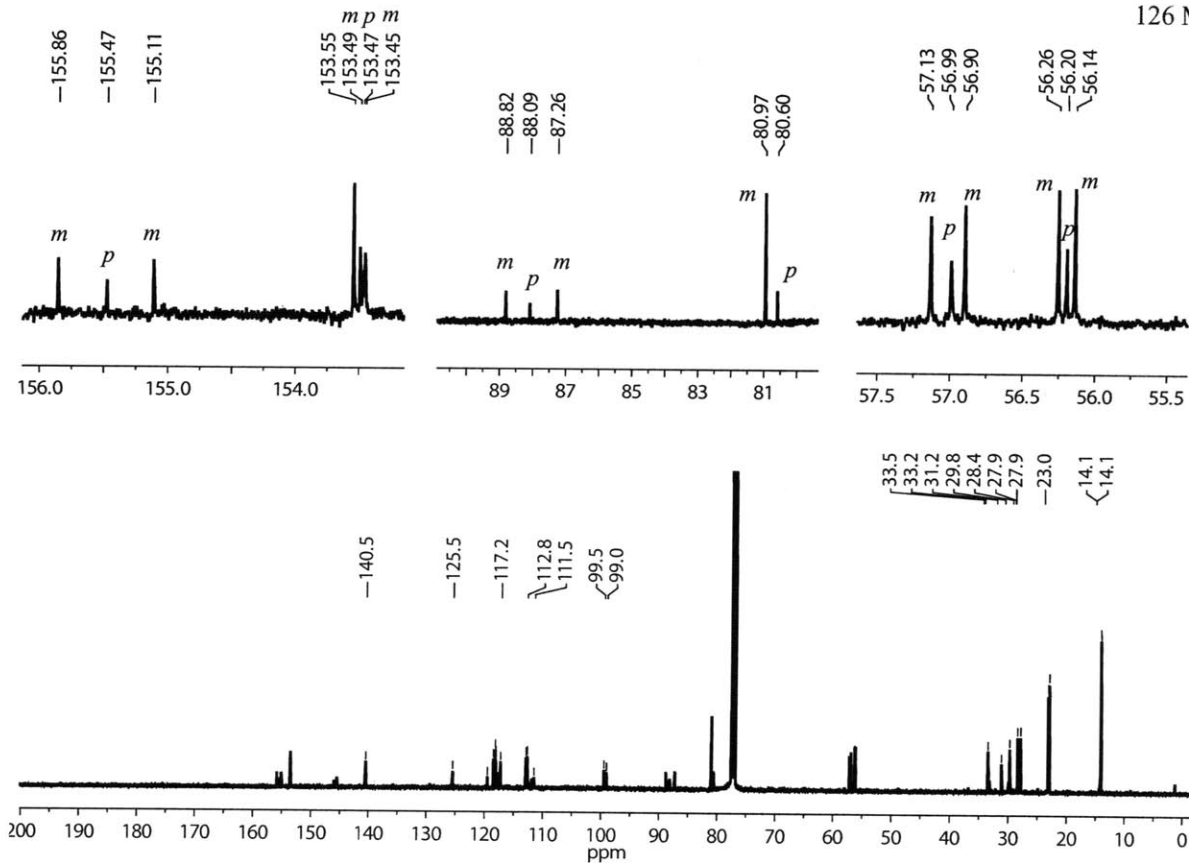


MC2_2ox_cis NMR Spectra

¹H-NMR, CDCl₃
500 MHz

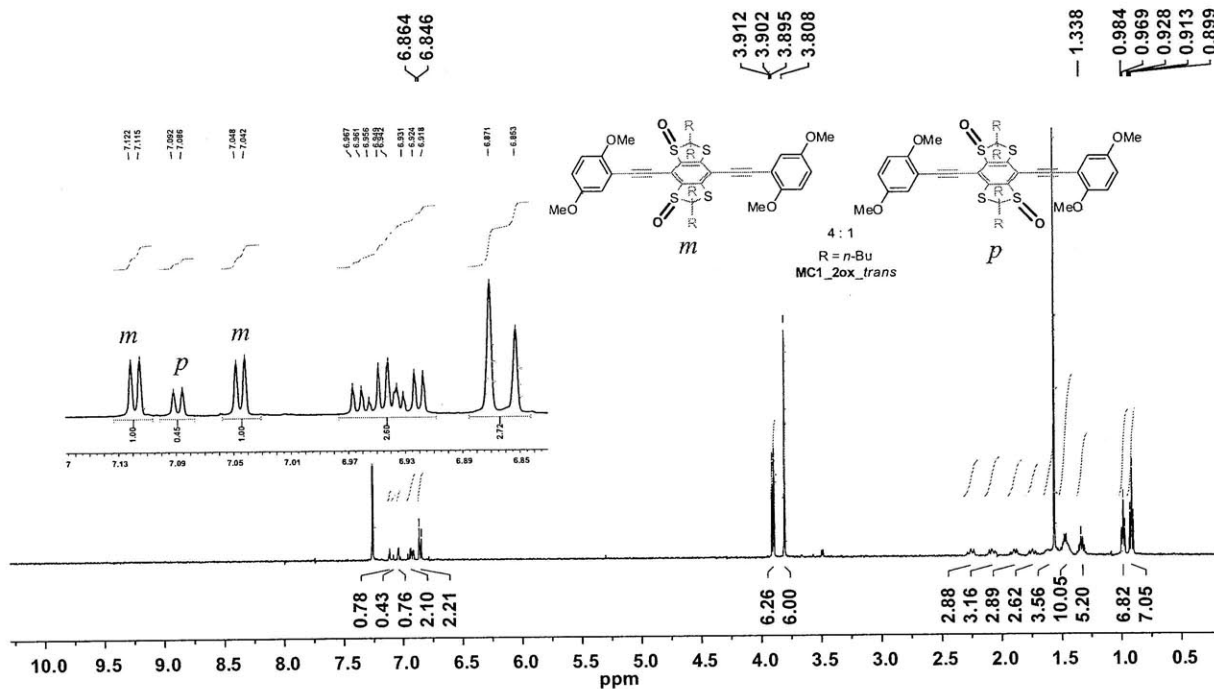


¹³C-NMR, CDCl₃
126 MHz

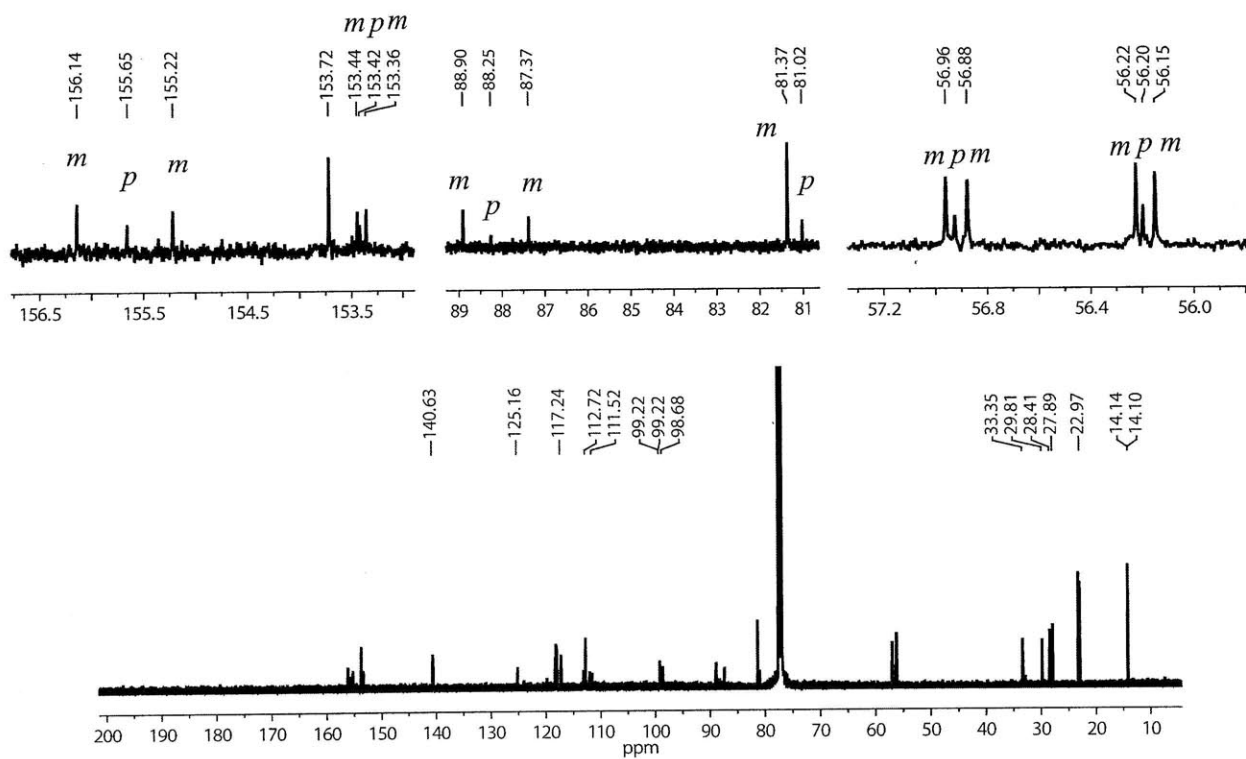


MC2_2ox_trans NMR Spectra

¹H-NMR, CDCl₃
500 MHz

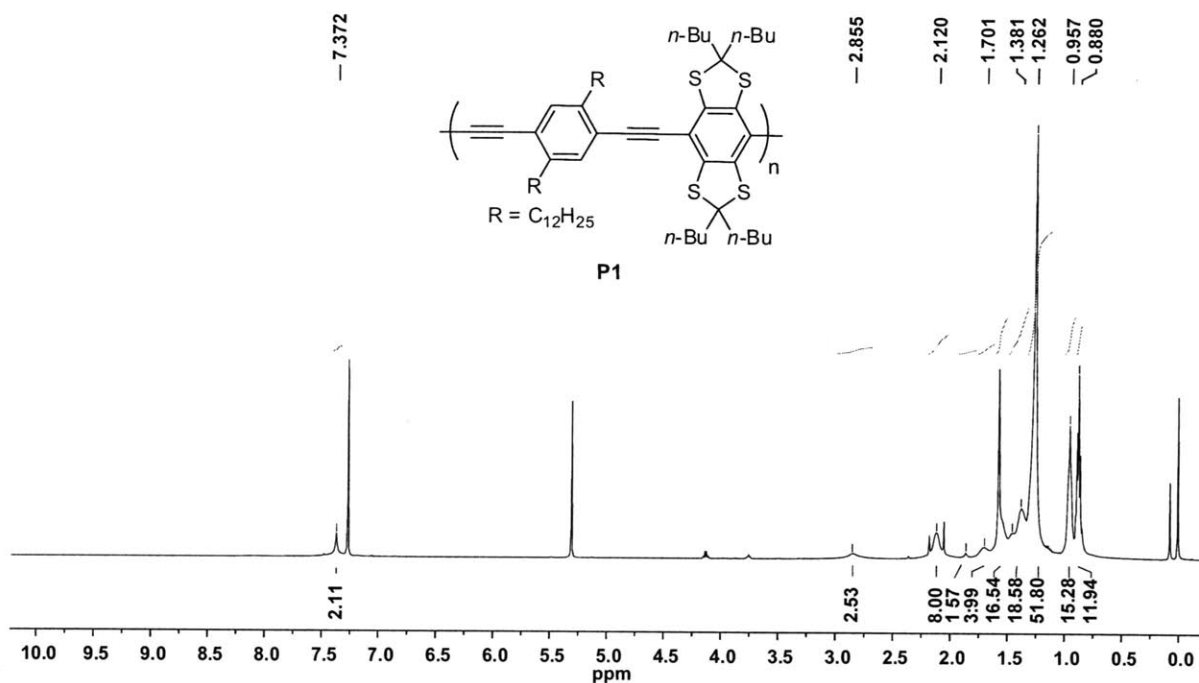


¹³C-NMR, CDCl₃
126 MHz

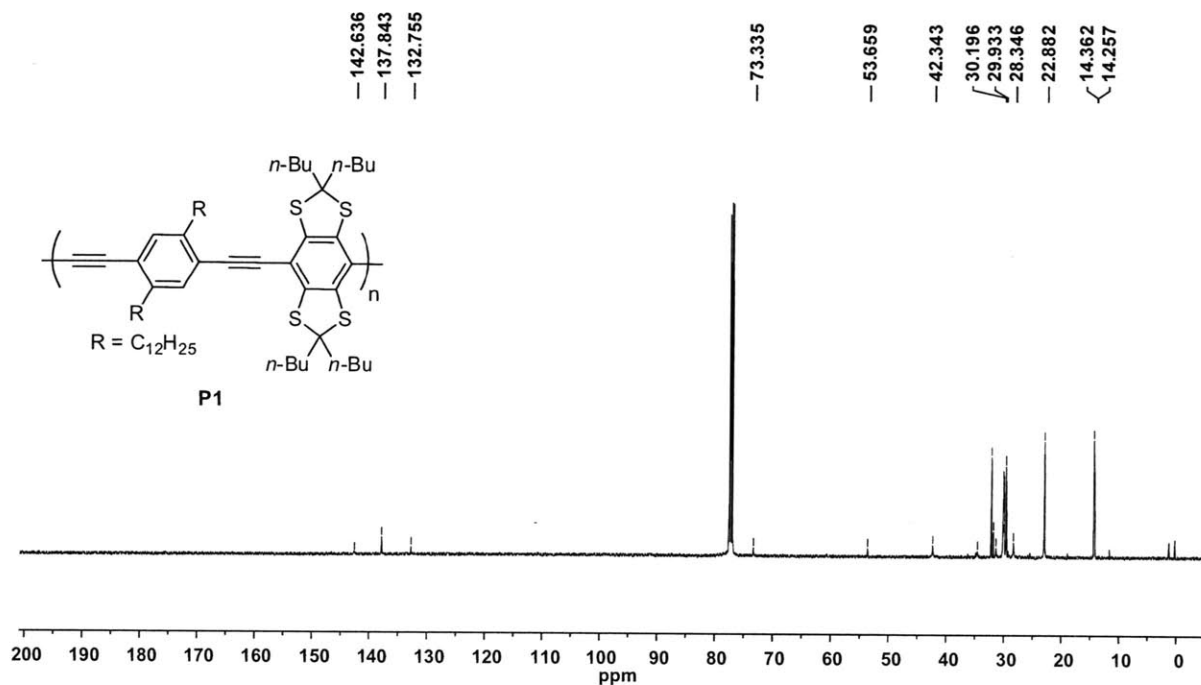


Polymer 1 NMR Spectra

¹H-NMR, CDCl₃
500 MHz

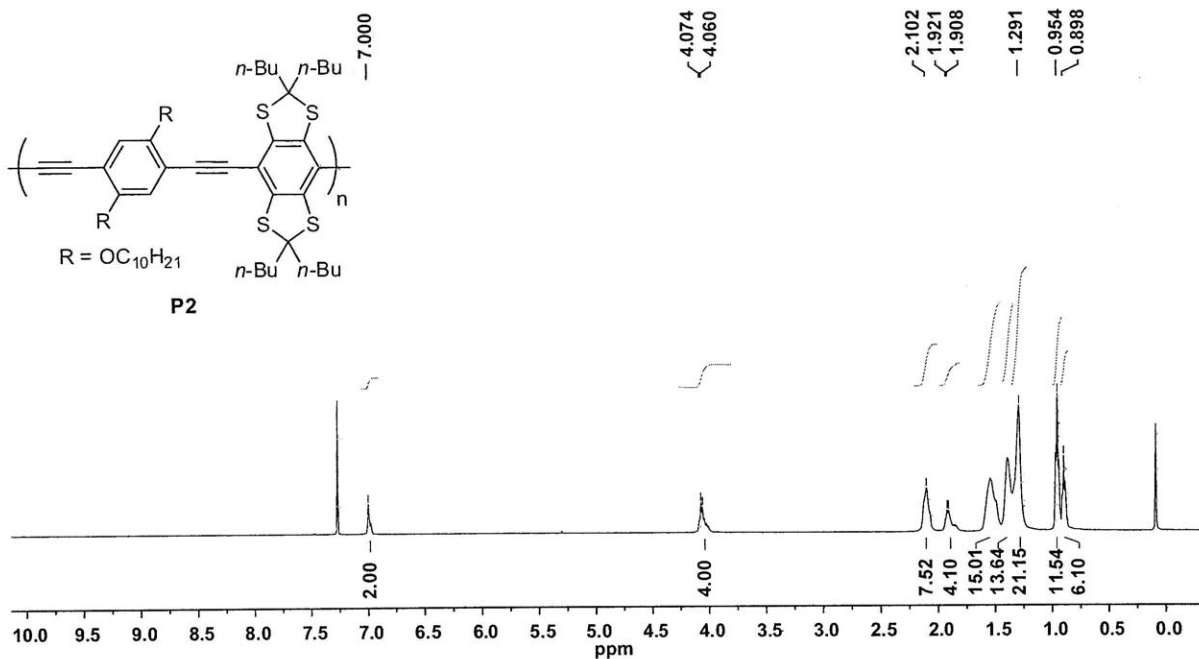


¹³C-NMR, CDCl₃
125 MHz

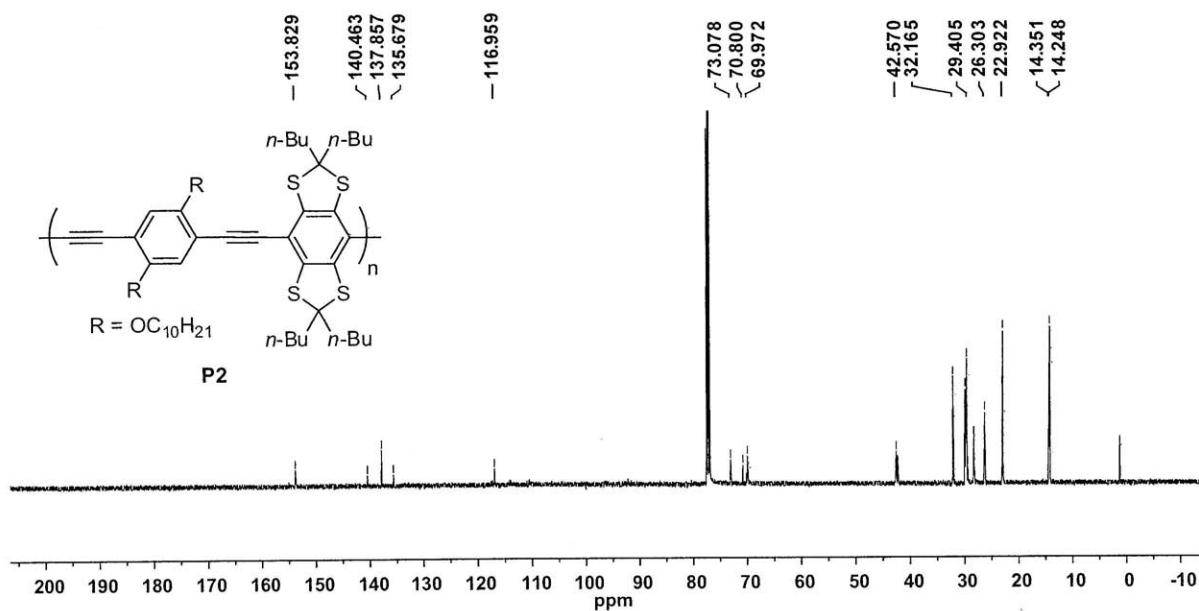


Polymer **2** NMR Spectra

¹H-NMR, CDCl₃
50 °C, 500 MHz



¹³C-NMR, CDCl₃
125 MHz



CHAPTER 6

Work Towards the Synthesis and Characterization of Electroactive Conjugated Polymers Based on the BDPA Free Radical

6.1 Introduction

The synthesis of an electroactive conjugated polymer containing a stabilized carbon-centered radical based on the 1,3-bisdiphenylene-2-phenylallyl (BDPA) radical,¹ first reported by Koelsch, is described. The BDPA radical is an interesting functionality to introduce into the main-chain of a conjugated polymer because it can be reduced to a stabilized, delocalized carbanion, therefore making the polymer *n*-dopable.² Conjugated polymer semiconductors that are *p*-dopable are well-known, but there has been less success in developing *n*-dopable materials.³ The electrochemical behavior of BDPA in solution is shown in Figure 1. BDPA displays a reversible one-electron reduction to its carbanion and a reversible one-electron oxidation under the experimental conditions.² In reality, the BDPA carbocation can be reactive, likely because of its partial antiaromatic character, and when generated under chemical conditions it readily cyclizes to a spiro product (Figure 1c).^{2c,4} In contrast, the BDPA carbanion is relatively stable (persisting for days under 1 atm oxygen) in polar aprotic solvents such as dimethylformamide (DMF) and dimethylsulfoxide (DMSO) when generated either electrochemically or by deprotonation of the hydrocarbon precursor.^{2a} The predominant decomposition pathway of the BDPA carbanion under ambient conditions is via oxidation to the radical.^{2a} Previous electrochemical studies have found that the BDPA radical and closely related derivatives with substitution at the 4-position of

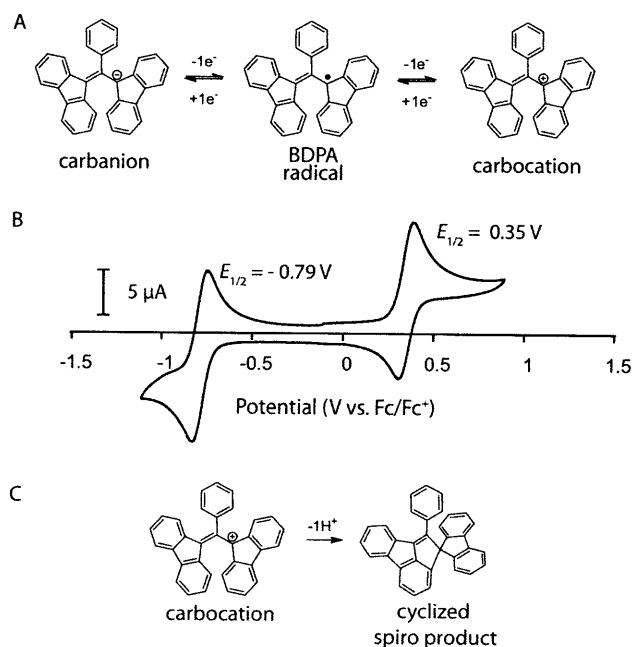
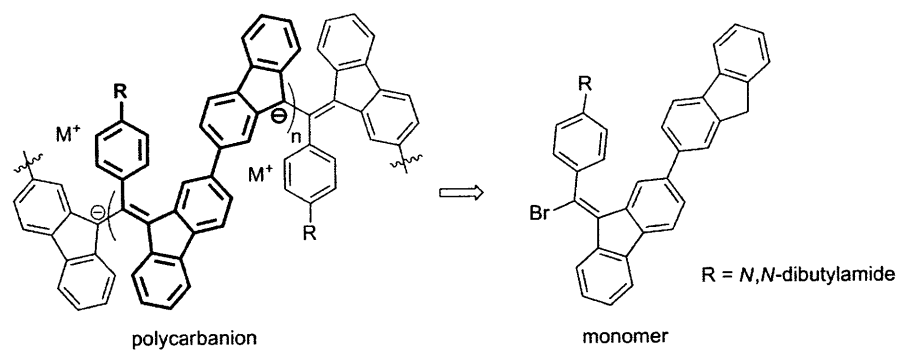
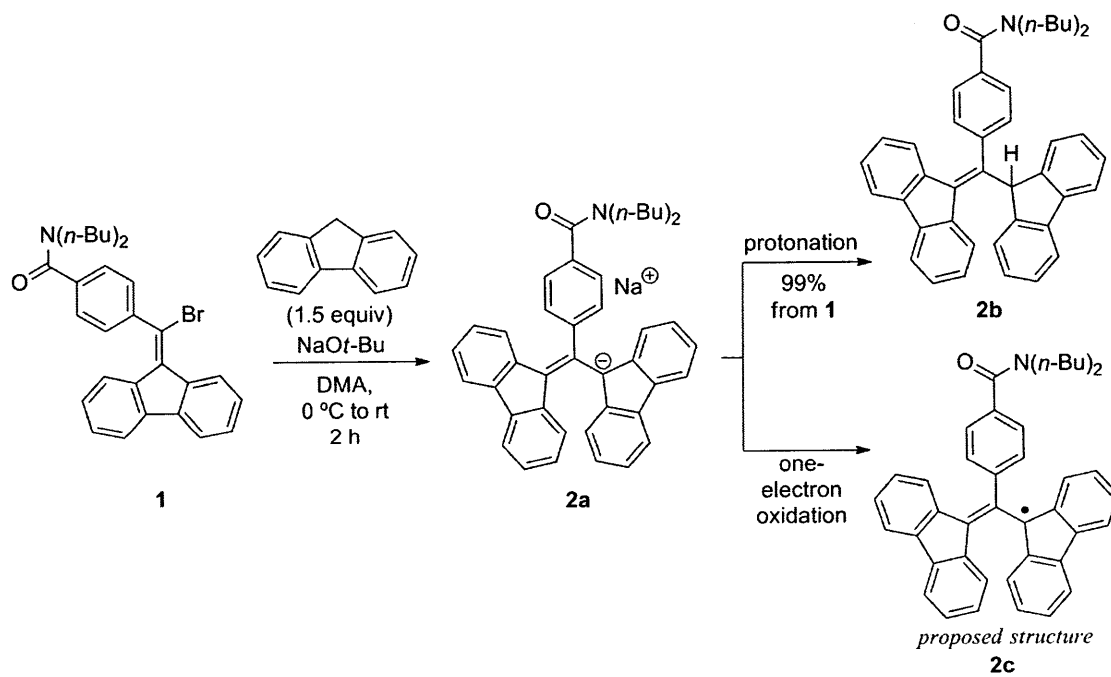


Figure 1. BDPA Electrochemistry

(a) The BDPA radical's reversible one-electron reduction to its carbanion and oxidation to its carbocation is shown. (b) A cyclic voltammogram of the BDPA radical performed in acetonitrile with 0.10 M $(n\text{-Bu})_4\text{NPF}_6$ with a Pt-button electrode is shown. (c) The irreversible cyclization of the carbocation to a spiro product is shown.



Scheme 1. Retrosynthetic analysis



Scheme 2.

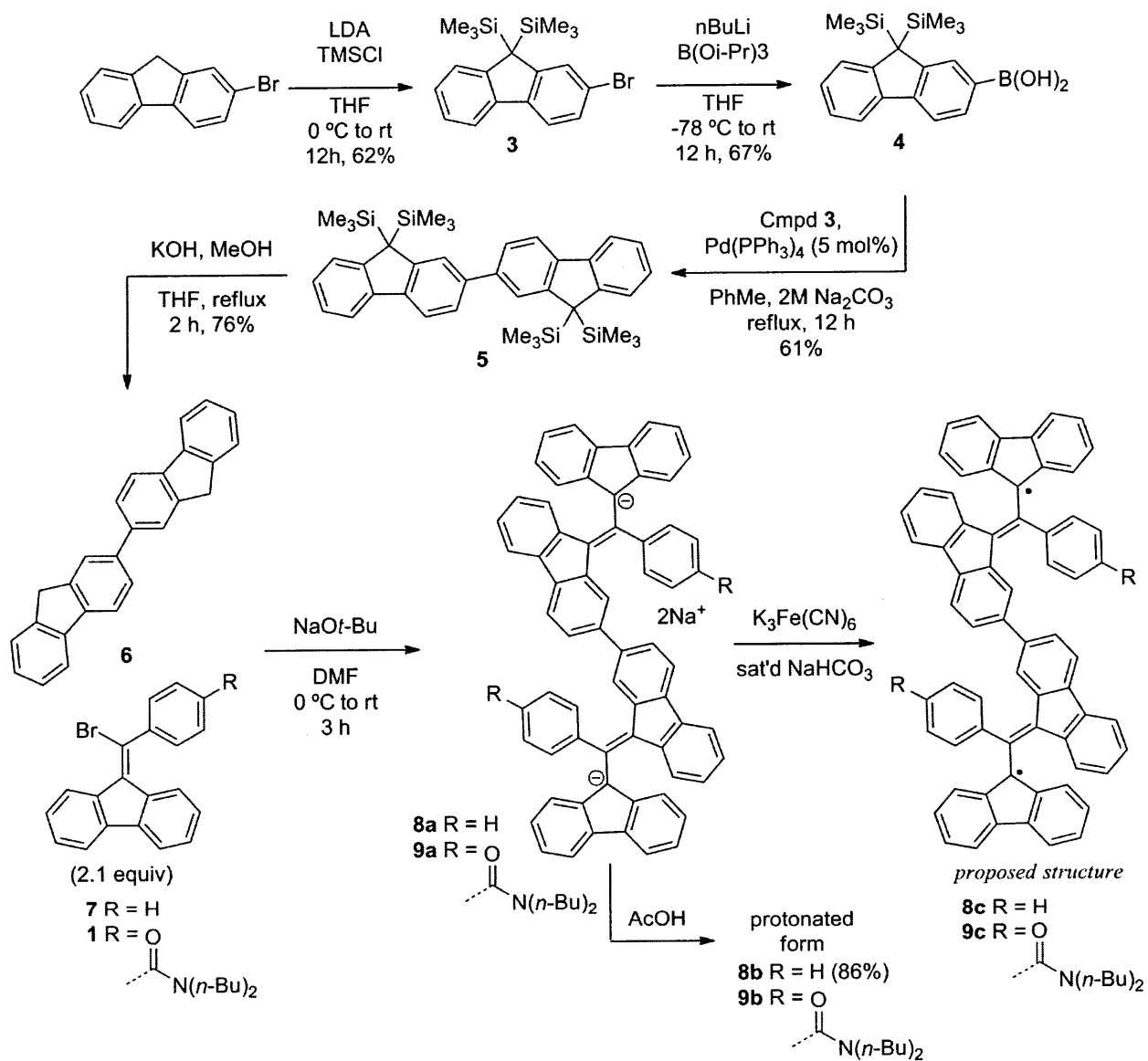
the phenyl ring behave as semiconductors with energy gaps of 1.5-1.7 eV in the solid state.⁵

6.2 Synthesis

Building on Kuhn and Neugebauer's synthesis of BDPA,^{1b} an anionic polymerization method in which the BDPA polymer is synthesized as a polycarbanion and then oxidized to the polyradical was pursued (Scheme 1). To our knowledge, the incorporation of the BDPA radical into the main chain of a conducting polymer has not been described previously. However, a polyacetylene polymer with a pendant BDPA connected through the 4-position of the phenyl ring has been previously reported.⁶

As seen in Scheme 1, the monomer contains a di-*n*-butylamide at the 4-position of the phenyl ring designed to provide several useful properties both for the monomer and the final material. It was anticipated that the flexible *n*-butyl groups would impart additional solubility to the polymer. Secondly, the amide was predicted to promote solubility of the monomer and the growing polymer in the polar aprotic solvents used for the polymerization. Additionally, the moderate electron-withdrawing ability of the amide was seen as desirable in stabilizing the carbanion, although the effect was expected to be modest. In reality, the di-*n*-butyl amide also facilitated the characterization of the synthetic intermediates and the desired monomers by allowing for facile chromatographic separation of the *E*- and *Z*-isomers. As shown in Scheme 2, the amide does not negatively affect the conjugate addition of a fluorene anion to a vinyl-bromide (**1**) electrophile to form the stabilized carbanion (**2a**). Protonation of **2a** results in the formation of **2b**, a stable hydrocarbon that can be purified and characterized using standard techniques. The complete characterization of **2c** using IR, UV-vis, EPR, elemental analysis, HRMS, and electrochemistry is underway but has not yet been completed.

In order to test the viability of an anionic polymerization strategy and to study the effect of linking two BDPA radicals through the 2-position of a fluorene ring, BDPA dimers were synthesized as model systems (Scheme 3). The synthesis began with the protection of the 9,9'-posi-



Scheme 3.

tions of 2-bromofluorene with trimethylsilyl groups (**3**) and the introduction of a boronic acid at the 2-position (**4**) via lithiation. In both cases, purification did not require chromatography. In addition to allowing lithium-halogen exchange to take place selectively without the interference of deprotonation at the 9-position, the trimethylsilyl groups provide enhanced solubility for the resulting bifluorene (**5**), which is obtained by palladium-catalyzed coupling of **3** and **4**. After deprotection, bifluorene **6** was reacted with 2.1 equivalents of bromides **7** and **1** to obtain the dianions **8a** and **9a**, respectively, which can be quenched with excess acetic acid to isolate the protonated BDPA-precursors **8b** and **9b**. Bifluorene **6** has been previously synthesized using a one-step dimerization of fluorene in the presence of a mixture of aluminum chloride and cupric chloride^{7a} and via the reduction of the bifluorenone,^{7b} which itself is available in two-steps from fluorenone. Although the one-step procedure using fluorene is attractive, the purification of the crude reaction mixture is challenging due to the insolubility of **6** in most solvents.^{7a} The authors use sublimation at 190-220 °C under high vacuum and subsequent recrystallization from chlorobenzene to isolate modest quantities of pure material (< 0.3 g). The synthetic strategy we report provides an alternative route to **6** and may be useful in synthesizing similar structures.

Protonation of carbanions **8a** and **9a** results in a complex mixture of tautomers, *E/Z*-double bond isomers, and rotamers, which makes **8b** and **9b** challenging to characterize using NMR (¹H and ¹³C NMR spectra for **8b** are included in Section 6.7). However, the carbanions (**8a**, **9a**) offer simplified ¹H and ¹³C NMR spectra due to their extensive delocalization. Carbanions for NMR study were generated by adding 2.0 equivalents of potassium *tert*-butoxide per acidic proton to a *d*₆-DMSO solution of the protonated precursor.^{2e} Figure 2 (*top*) shows a portion of the ¹H NMR spectrum of the carbanion of a previously reported BDPA derivative with a bromide at the 4-position of the phenyl ring (Br-BDPA).^{1b} The structure has six unique proton signals between 6.0 and 8.0 ppm. The signal farthest upfield (Hc) is noticeably broadened, although its doublet splitting is still discernable. Broadening is also apparent in He at close inspection when it is compared to

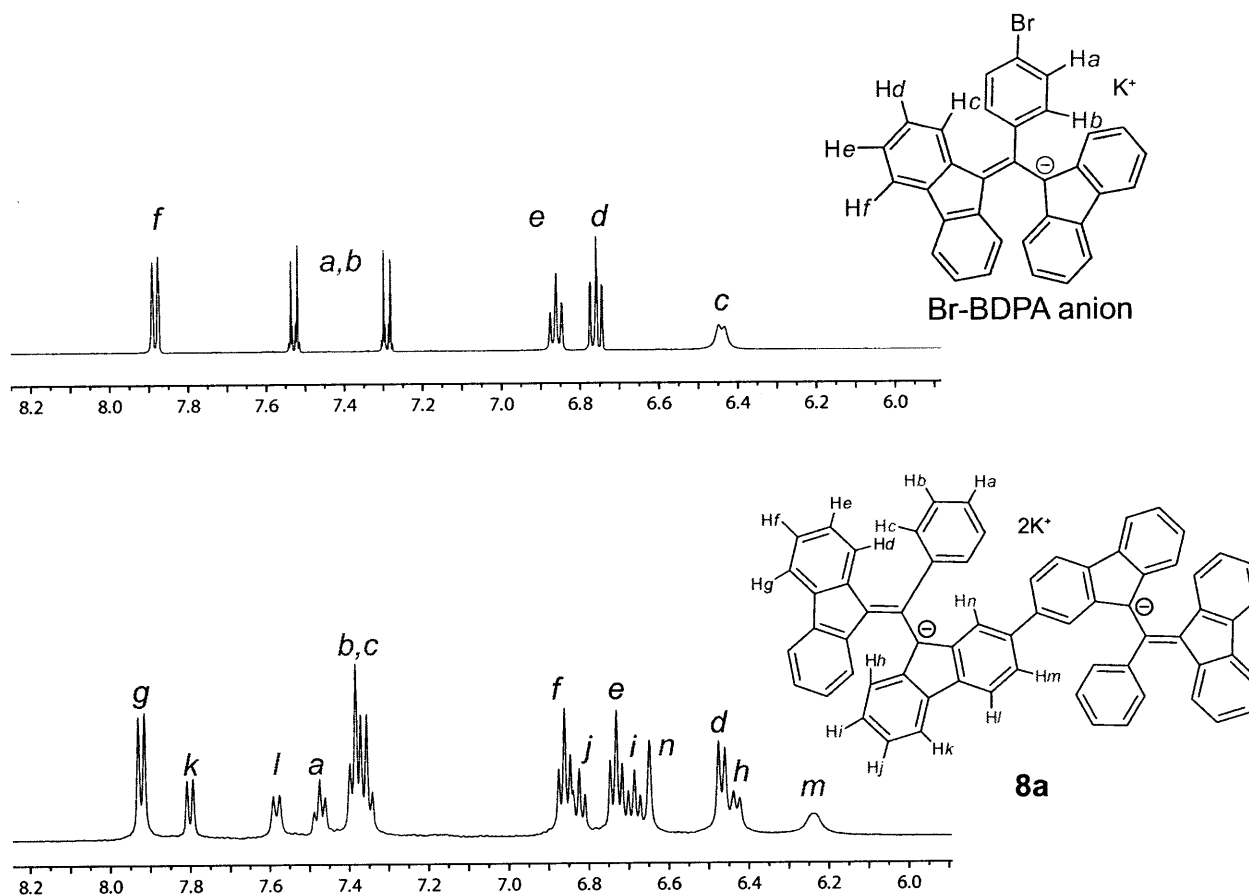


Figure 2. ^1H NMR of carbanions
 (top) The ^1H NMR of the Br-BDPA carbanion in d_6 -DMSO at 20 °C is shown. (bottom)
 The ^1H NMR of **8a** in d_6 -DMSO at 40 °C is shown.

Hd, although the effect is more subtle. Because the broadening appears to occur on those carbons with the higher proportion of the HOMO, we hypothesize that it is due to an interaction with the potassium counterion (all three of potassium's naturally occurring isotopes are NMR active and quadrupolar). Figure 2 (bottom) shows the ^1H NMR spectrum of **8a** and the proton assignments, which were deduced using gCOSY 2D NMR. To decrease the line-broadening due to slow rotational tumbling the sample was heated to 40 °C. The signal for Hm is noticeably broadened, but it is unclear whether this is a result of an interaction with the counterion or a result of the proton's location within the compound. The ^{13}C NMR spectra of the Br-BDPA anion, **8a**, and **9a** are also well-resolved and informative (see Section 6.7). Br-BDPA shows one signal at 110.8 that we attribute to the two symmetric carbons at the 9-positions of the fluorene ring systems. As would be

expected due to the decrease in symmetry, the spectra of **8a** and **9a** both show two signals in the same region (**8a**: 110.3, 111.4; **9a**: 111.2, 112.5 ppm). It should be noted that well-resolved spectra for **9a** were obtained with a lithium counterion in a mixture of d_7 -DMF and d_6 -DMSO, because the same spectra with a potassium counterion in pure DMSO were broadened. In general, the presence of the amide causes the NMR spectra to be less well-resolved. Increasing the acquisition temperature (70 °C was the highest temperature investigated) had minimal effects on the spectrum. The addition of D_2O in small quantities (5-10% by volume) was beneficial, presumably because it affected the solvation of the potassium counterions.

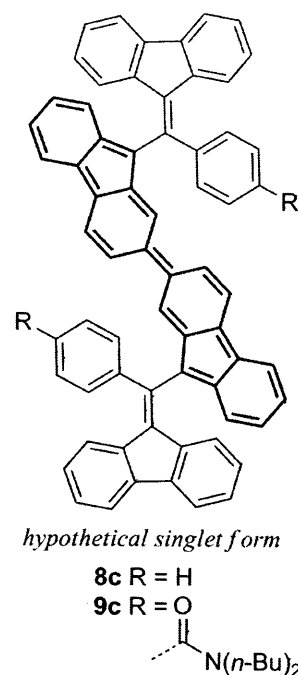
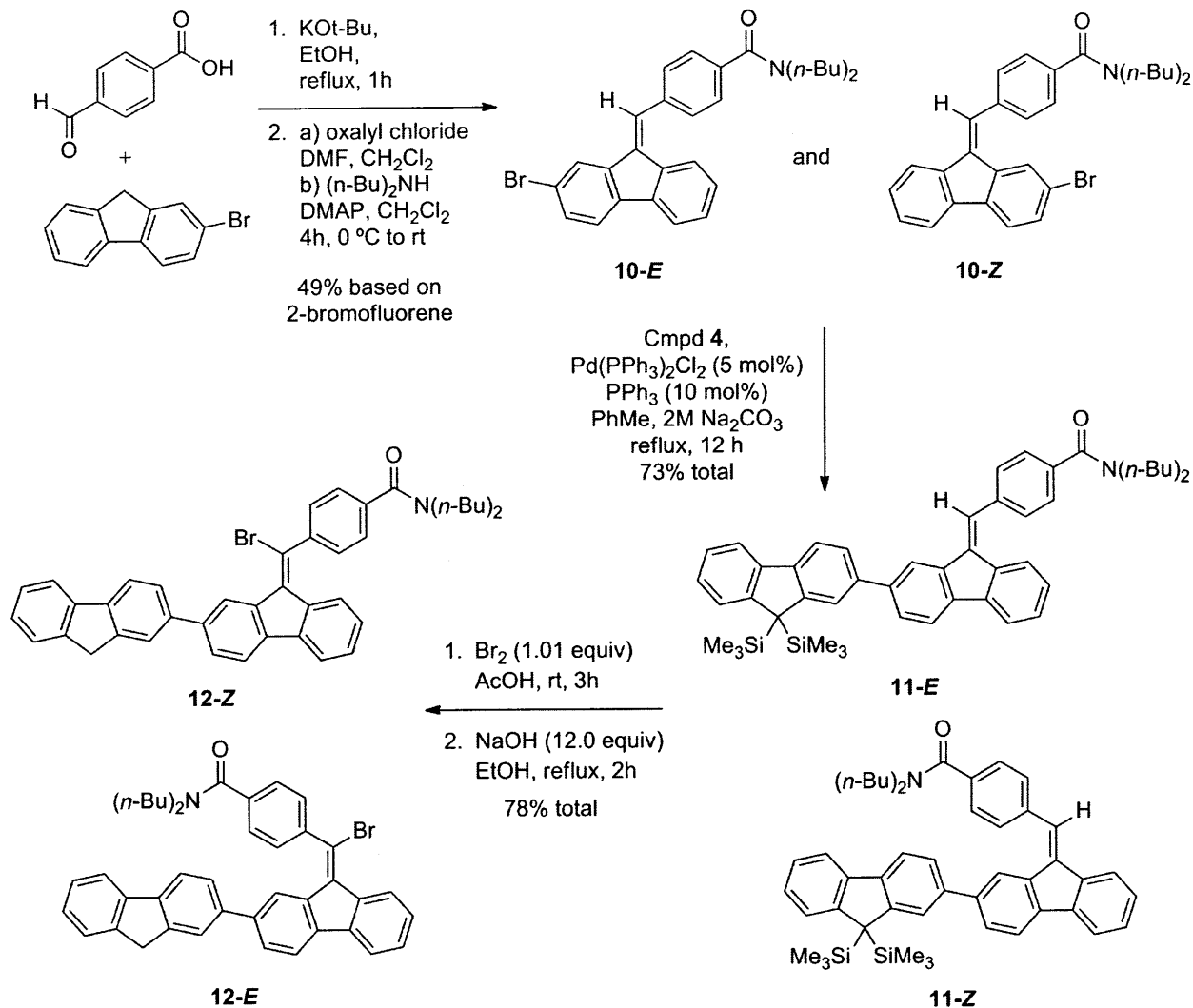


Chart 1.

The complete characterization of **8c** and **9c** using IR, UV-vis, EPR, elemental analysis, HRMS, and electrochemistry is underway but has not yet been completed. In general, we have found that at room temperature the compounds exist as weakly interacting biradicals. A resonance structure in which the two electrons form a bond can be drawn (Chart 1), but this structure requires the disruption of four aromatic rings. If such a structure were the biradical's ground state, a red-shifted absorbance band, in comparison with the monomeric radical, would be expected. Instead, the absorbance spectra of samples of crude biradical appear similar to that of the monomeric species. Additionally, we observe an EPR signal at room temperature in solution. Finally, cyclic voltammetry of **8c** displays two closely spaced reduction peaks of equal intensity, which agrees with the view that **8c** and **9c** behave as two proximate, yet mostly electronically independent, π -systems. Initial results from low-temperature EPR (MeTHF, 77 K) indicate coupling between the radicals in **9c**, the nature of which has not yet been determined. Previously reported BDPA biradicals, joined through the phenyl ring, have shown both singlet and triplet ground states in low temperature EPR, depending



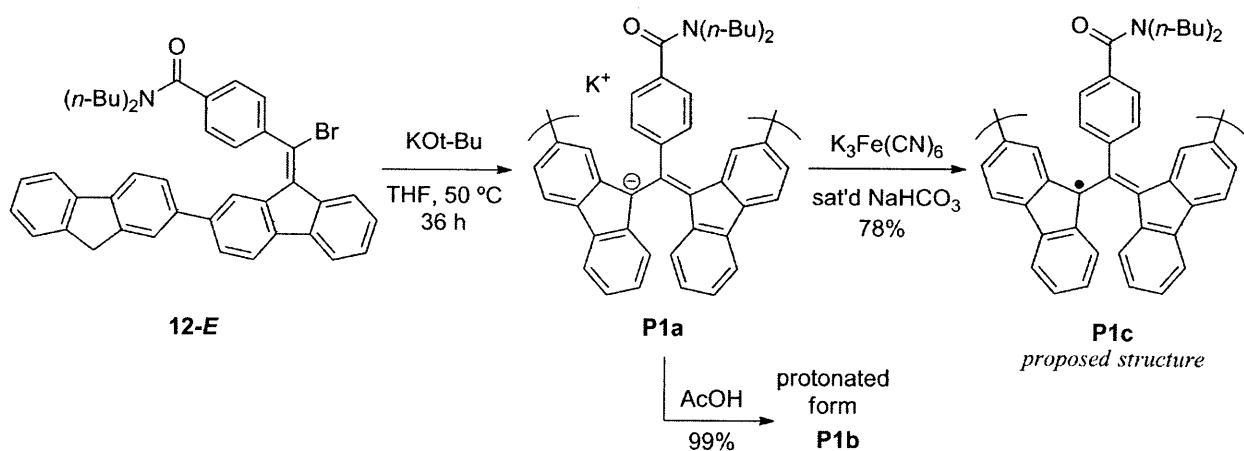
Scheme 4.

on the connectivity.⁸ In either case, based on examples of triphenylmethyl radicals with similar connectivity, we expect the coupling between the radicals to be modest.⁹

The synthesis of monomer 12 began with condensation of 2-bromofluorene and 4-carboxybenzaldehyde (Scheme 4). The reaction product was isolated as the potassium salt via filtration and used in the next step without purification. The carboxylate salt was converted to a di-*n*-butylamide via the acid chloride, and chromatography allowed for the separation of the *E* and *Z* isomers for characterization. A 1:1 mixture of bromide isomers was then coupled with boronic acid **4**. The

E and *Z* isomers of amide **11** could not successfully be separated by chromatography. To obtain pure samples of **11-E** and **11-Z**, samples of **10-E** and **10-Z** were reacted separately. Compound **11-E/Z** was brominated with a slight excess of bromine in acetic acid. Additional bromine led to electrophilic bromination of the aromatic rings. The dibromide was isolated via filtration. Hydrogen bromide was eliminated with sodium hydroxide in refluxing ethanol. Bromide monomers **12-E** and **12-Z** could be separated by chromatography, with **12-E** eluting first.

Several conditions for polymerization (Scheme 5) were screened, but in all cases *tert*-butoxide was used as the base. The *tert*-butoxide anion is basic enough to deprotonate fluorene at the 9-position but does not attack the alkenyl bromide electrophile. The reactions were performed in a nitrogen glove box and heated to 50 °C in a sand bath for 36 hours in sealed vessels. The effect of solvent and counterion were screened as shown in Table 1. Both monovalent (Li, Na, K) and divalent (Mg, Ba, Zn) counterions were investigated. The monovalent counterions produced longer oligomers based on the *M_n*, as determined by GPC (DMF) of the crude polyanions. GPC of the polyanions using DMF consistently gave significantly lower *M_n*'s when compared to GPC performed on the protonated and radical forms of the same oligomers in THF. Because GPC determines molecular weight based on comparison with polystyrene standards, we suspect that these standards are less relevant to the polyanions, due to their unusual structure, as compared to the



Scheme 5.

Table 1. Polymerization conditions

Monomer	Solvent ^a	Base/Additive ^b	M _n (kDa) ^c	M _w (kDa) ^c	M _w /M _n
12- <i>E</i>	DMF	LiOt-Bu	4.3	6.4	1.5
12- <i>E</i>	THF	LiOt-Bu	1.8	2.3	1.3
12- <i>E</i>	THF	NaOt-Bu	3.9	4.9	1.3
12- <i>E</i>	THF	KOt-Bu	4.7	6.2	1.3
12- <i>E</i>	THF	Mg(Ot-Bu) ₂	NR	****	****
12- <i>E</i>	THF	Ba(Ot-Bu) ₂	2.0	2.8	1.4
12- <i>E</i>	THF	KOt-Bu/ZnCl ₂	3.2	4.6	1.4
12- <i>E</i>	DMA	LiOt-Bu	3.3	4.3	1.3
12- <i>E</i>	DMA	NaOt-Bu	4.4	6.0	1.4
12- <i>E</i>	DMA	KOt-Bu	4.3	5.6	1.3
12- <i>E</i>	DMA	Mg(Ot-Bu) ₂	1.9	2.0	1.1
12- <i>E</i>	DMA	Ba(Ot-Bu) ₂	3.1	3.9	1.3
12- <i>E</i>	DMA	KOt-Bu/ZnCl ₂	2.7	5.3	2.0
12- <i>Z</i>	DMA	KOt-Bu	3.8	5.0	1.3
12- <i>E/Z</i> (1:1)	DMA	KOt-Bu	4.3	6.1	1.4

^aReactions were performed with a monomer concentration of 10 mM. ^b4.0 equivalents of base were used; 2.0 equivalents of ZnCl₂. ^cDetermined using GPC(DMF) against polystyrene standards.

protonated and radical forms. However, comparing the GPC results obtained from the polyanions on a relative basis to determine the effect of varying the solvent and counterion seems valid for screening reaction conditions. In THF, potassium provided the longest oligomers, whereas in DMA, sodium and potassium gave similar results. Only in the case of magnesium di-*tert*-butoxide did the monomer solution not turn from yellow to deep blue. Based on these results, the polymerization was performed on a larger scale using potassium *tert*-butoxide as the base and THF as the solvent. The use of THF as the solvent necessitates that the reactions be kept oxygen free, as the BDPA carbanion is much more easily oxidized in THF as compared to DMF or DMSO.^{2a} After 36 hours, the reaction mixture was either treated with acetic acid to isolate the protonated form of the polymer (**P1b**) or with an excess of potassium ferricyanide in saturated sodium bicarbonate solution to isolate the radical form of the polymer (**P1c**). **P1b** is a light yellow powder that is readily soluble in DCM, THF, and chloroform, and which has a M_n of 6.5 kDa (degree of polymerization = 11) based on GPC using THF as eluent. The proton NMR of **P1b** shows a broadened signal that is in agreement with the proposed structure. The most convincing evidence for the proposed struc-

ture of **P1b**, and hence the success of the polymerization, is the ^{13}C NMR (see the end of Section 6.7), which shows the presence of a broad peak centered at 52.7 ppm. This signal is specific to the carbon attached to the acidic proton of the BDPA-precursor and, for comparison, similar peaks can be observed in the ^{13}C spectra of **2b** and **8b** (see Section 6.7). In addition, a ^1H and ^{13}C NMR spectrum of **P1a** was obtained by deprotonating **P1b** with potassium *tert*-butoxide in d_6 -DMSO, as previously described for the dimer **8a** and **9a**. The spectra obtained at 50 °C are broad but are in general agreement with those observed for **2a**, **8a**, and **9a**. **P1c** was purified by precipitation into methanol and collected by filtration as a dark red powder that has a M_n of 9.4 kDa (degree of polymerization = 16) based on GPC (THF). The higher molecular weight of the radical form of the polymer (**P1C**) is likely in part due to the fractionation of the polymer.

6.3 Electrochemistry

Figure 3 shows the results of cyclic voltammetry performed on thin-films of the polymer on platinum electrodes in acetonitrile with organic electrolyte (0.10 M $(n\text{-Bu})_4\text{NPF}_6$). Figure 3b shows the reversible reduction peak of **P1c** from a sample prepared by drop-casting a chloroform solution of the polymer on a platinum wire.

6.4 Conclusion

In conclusion, work towards the synthesis of BDPA bi- and polyradicals joined through the 2-position of a fluorene ring is presented. The dianionic form of the biradicals has been characterized using ^1H and ^{13}C NMR. In addition, a monomer containing a 9H,9'H-fluorene and a vinyl bromide joined through the 2-position of each fluorene ring has been prepared. In polar aprotic solvent under basic conditions this monomer forms BDPA carbanion oligomers, which have been investigated using NMR. Treatment of these polyanions with acid leads to the isolation a protonated BDPA precursor, whereas treatment with a one-electron oxidant presumably leads to the isolation of poly BDPA radicals. Cyclic voltammetry of films of the polyradicals show a reversible reduction peak and an irreversible oxidation peak. Future work will include further characterization of the bi- and polyradicals using UV-vis spectroscopy, elemental analysis, electrochemistry,

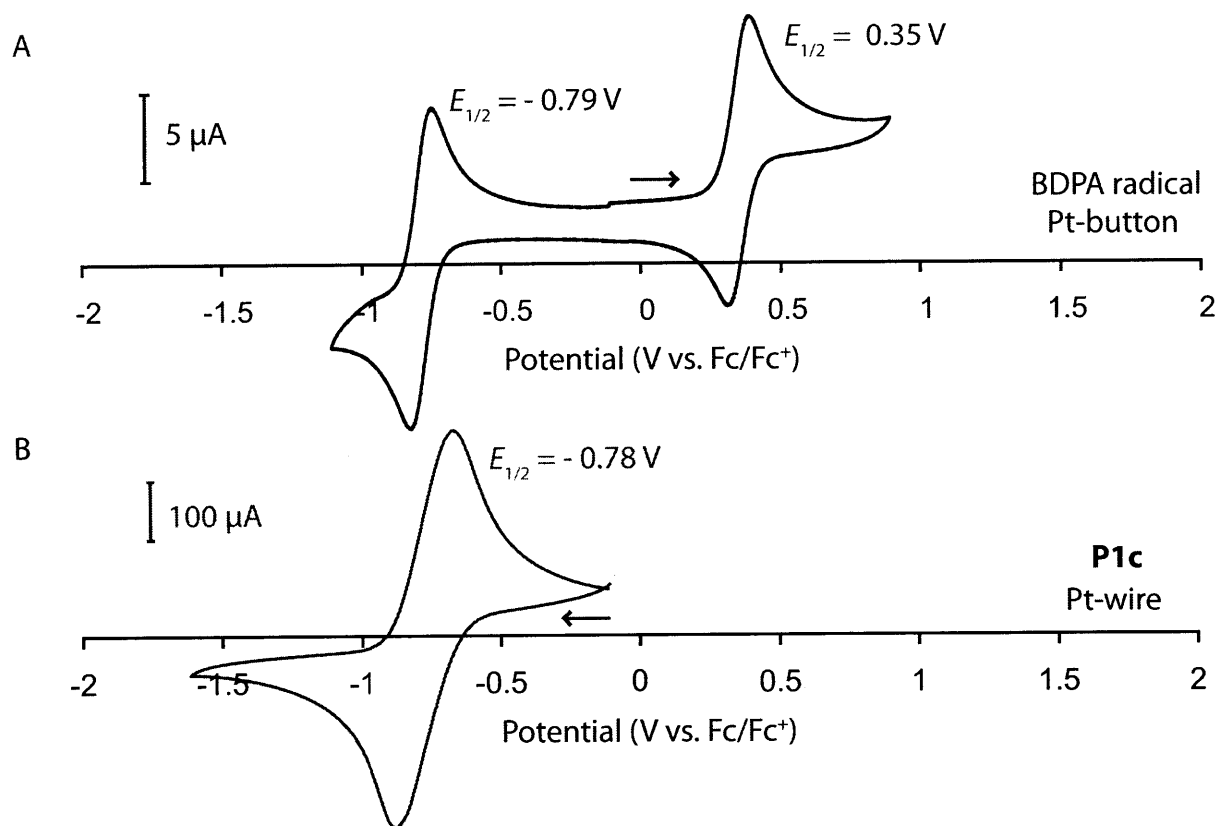


Figure 3. Cyclic voltammetry

(a) A cyclic voltammogram (CV) of the BDPA radical on a Pt-button electrode is shown (0.0 V to 1.5 V to -1.5 V, 100 mV/s). (b) A CV of a **P1c** film dropcast on a Pt-wire electrode is shown (0.0 V to -1.5 V, 100 mV/s). All CVs were obtained in MeCN with 0.10 M (*n*-Bu)₄NPF₆.

HRMS, and IR. In addition, the nature of the interaction between the unpaired electrons will be investigated using EPR. Finally, films of the polyradicals will be investigated for their ability to act as *n*-dopable semiconductors in organic field effect transistors.

6.5 Experimental Section

4-(bromo(9H-fluoren-9-ylidene)methyl)-N,N-dibutylbenzamide (1). To a 200 mL flask cooled in an ice bath were added 0.600 g of 4-(bromo(9H-fluoren-9-ylidene)methyl)benzoic acid (see

Chapter 2 for synthesis), 30 mL of dry dichloromethane, 0.21 mL oxalyl chloride (0.30 g, 0.0024 mol, 1.5 equiv), and 1 drop of DMF. The reaction mixture was allowed to warm to room temperature until bubbling ceased. The solvent and excess reagent were distilled off, and the remaining solid was dissolved in 20 mL of dichloromethane. To this solution were added 1.10 mL of di-*n*-butylamine (0.822 g, 0.00636 mol, 4.0 equiv) and catalytic 4-dimethylaminopyridine. The solution was stirred for 4 h and then moved to a separatory funnel where it was washed with 0.1 M HCl (3 X 20 mL), sat'd sodium bicarbonate (3 X 20 mL), and brine. The solution was dried over sodium sulfate. After removal of the solvent, the crude reaction mixture was purified with silica gel chromatography using hexane with increasing amounts of ethyl acetate. The product was isolated as a light yellow crystal (0.629 g, 81%). ¹H NMR (500 MHz, CDCl₃, δ) (all coupling constants (*J*) in Hz): 8.86 (d, *J* = 7.5, 1H), 7.74 (d, *J* = 7.5, 1H), 7.66 (d, *J* = 7.5, 1H), 7.51 (s, 4H), 7.47 (td, *J* = 7.5, 1.5, 1H), 7.40 (td, *J* = 7.5, 1.5, 1H), 6.85 (td, *J* = 7.5, 1.5, 1H), 6.34 (d, *J* = 7.5, 1H), 3.55 (t, *J* = 7.5, 2H), 3.30 (t, *J* = 7.5, 2H), 1.69 (m, 2H), 1.56 (m, 2H), 1.44 (m, 2H), 1.23 (m, 2H), 1.01 (t, *J* = 7.5, 3H), 0.87 (t, *J* = 7.5, 3H); ¹³C NMR (126 MHz, CDCl₃, δ) 171.0, 143.6, 141.4, 140.1, 138.3, 138.2, 138.0, 136.6, 129.5, 129.0, 128.5, 127.7, 127.4, 127.0, 126.3, 124.9, 123.5, 119.8, 119.6, 49.2, 44.9, 31.1, 29.9, 20.5, 20.1, 14.2, 13.9; FT-IR (KBr, thin film) ν_{\max} (cm⁻¹): 3045, 2960, 2858, 1626, 1506, 1466, 1380, 1304, 1266, 1188, 1106, 1023, 950, 853, 782, 731; mp 162-164 °C (methanol).

4-((9H-fluoren-9-yl)(9H-fluoren-9-ylidene)methyl)-*N,N*-dibutylbenzamide (2b). To an oven-dried 100 mL flask cooled in an ice bath were added 0.250 g of 4-(bromo(9H-fluoren-9-ylidene)methyl)-*N,N*-dibutylbenzamide (**1**) (0.000512 mol, 1.00 equiv), 0.127 g of fluorene (0.000768 mol, 1.50 equiv), 0.197 g of sodium *tert*-butoxide (0.00205 mol, 4.00 equiv), and 20 mL of anhydrous dimethylacetamide. The solution was stirred at 0 °C for 30 minutes and then stirred at room temperature for 2 h. The reaction was quenched by adding 5.0 mL of glacial acetic acid followed by 50 mL of water. The quenched reaction mixture was extracted with diethyl ether (2 x 10 mL). The combined organic layers were washed several times with water and once with brine, before being

dried over sodium sulfate. After removal of the ether, the crude product was dissolved in toluene and heated to reflux for 30 minutes in order to convert the product into one rotamer. After removal of the toluene, the crude product was purified with silica gel chromatography. The column was eluted with hexane, 3:1 hexane/DCM, and finally 5:4:1 hexane/DCM/ethyl acetate to obtain 0.290 g (99%) of product as an amorphous solid. Attempts at recrystallization from both polar and non-polar solvents failed and heating while drying under high vacuum lead to partial decomposition. ¹H NMR (500 MHz, CDCl₃, δ) (all coupling constants (*J*) in Hz): 8.45 (d, *J* = 8.0, 1H), 7.89 (d, *J* = 7.5, 1H), 7.76 (d, *J* = 7.5, 1H), 7.64 (d, *J* = 7.5, 2H), 7.59 (d, *J* = 7.5, 2H), 7.49 (t, *J* = 7.5, 1H), 7.38 (t, *J* = 7.5, 1H), 7.34 (t, *J* = 7.5, 2H), 7.26 (m, 3H), 7.00 (d, *J* = 8.0, 2H), 6.84 (t, *J* = 7.5, 1H), 6.71 (d, *J* = 8.0, 2H), 6.50 (s, 1H), 6.14 (d, *J* = 8.0, 1H), 3.42 (t, *J* = 7.5, 2H), 2.93 (t, *J* = 7.5, 2H), 1.58 (m, 2H), 1.35 (m, 4H), 1.02 (m, 2H), 0.96 (t, *J* = 8.0, 3H), 0.81 (t, *J* = 8.0, 3H); ¹³C NMR (126 MHz, CDCl₃, δ) 171.6, 144.2, 144.1, 142.1, 141.5, 140.0, 139.5, 138.8 (2), 136.2, 136.1, 128.5, 127.8, 127.7, 127.5, 127.1, 126.8, 126.1, 125.7, 125.3, 120.2, 120.1, 119.3, 52.8, 43.9, 44.6, 30.9, 29.8, 20.4, 19.9, 14.1, 14.0; FT-IR (KBr, thin film) ν_{max} (cm⁻¹): 3061, 2958, 2930, 2871, 1633, 1507, 1446, 1423, 1378, 1297, 1269, 1184, 1101, 1020, 941, 840, 783, 732, 649, 621.

4-((9H-fluoren-9-yl)(9H-fluoren-9-ylidene)methyl)-*N,N*-dibutylbenzamide carbanion (2a).

To generate the anion for NMR, 0.040 g of (2b), 0.016 g of potassium *tert*-butoxide (2.0 equiv), 0.95 mL of *d*₆-DMSO, and 0.05 mL of D₂O were stirred under argon for 30 minutes and then transferred to an NMR tube, which was subsequently flushed with argon and capped. ¹H NMR (500 MHz, *d*₆-DMSO, 50 °C, δ) (all coupling constants (*J*) in Hz): 7.84 (br, 4H), 7.33 (d, *J* = 8.0, 2H), 7.22 (d, *J* = 8.0, 2H), 7.0 – 6.0 (br, 12H (signal too broad to accurately integrate), 3.38 (t, *J* = 7.5, 2H), 3.26 (t, *J* = 7.5, 2H), 1.53 (m, 2H), 1.43 (m, 2H), 1.29 (m, 2H), 1.09 (m, 2H), 0.87 (t, *J* = 7.5, 3H), 0.74 (t, *J* = 7.5, 3H).

(2-bromo-9H-fluorene-9,9-diyl)bis(trimethylsilane) (3). To an oven-dried 1000 mL flask were added 30.00 g of 2-bromofluorene (0.1224 mol, 1.00 equiv) and 200 mL of dry THF. In a separate flask, an LDA solution was prepared by adding 196.0 mL of a 1.50 M *n*-butyllithium solution in hexane (0.294 mol, 2.40 equiv) to a solution of 50.0 mL of diisopropylamine in 50.0 mL of THF. Half of the LDA solution (approximately 150 mL) was slowly added to the flask containing 2-bromofluorene, which was maintained at 0 °C in an ice bath during the addition. The flask was allowed to warm to room temperature. The flask was cooled with an ice bath to 0 °C and 20.2 mL of trimethylsilylchloride (17.3 g, 0.171 mol, 1.40 equiv) was added. After stirring for 0.5 h at 0 °C, the flask was allowed to warm to room temperature. The flask was cooled to 0 °C and the remaining LDA solution was added. The flask was warmed to room temperature and then cooled to 0 °C before adding 20.2 mL of trimethylsilylchloride and stirring for 0.5 h at 0 °C. The flask was allowed to warm to room temperature overnight and quenched with excess sat'd ammonium chloride. The reaction mixture was extracted with diethyl ether (3 x 50 mL) and the organic layers were combined and washed with 0.1 M HCl, sat'd sodium bicarbonate, and brine. The diethylether solution was dried over sodium sulfate. After removal of solvent, the crude material was recrystallized from refluxing ethanol (approximately 500 mL). After filtration, 28.00 g (62%) of product was isolated as clear, rectangular prisms. ¹H NMR (500 MHz, CDCl₃, δ) (all coupling constants (*J*) in Hz): 7.89 (multiplet with second-order splitting, 1H), 7.79 (dd, *J* = 8.0, 0.50, 1H), 7.70 (dd, *J* = 1.5, 0.50, 1H), 7.57 (multiplet with second-order splitting, 1H), 7.48 (dd, *J* = 8.0, 1.5, 1H), 7.36 (multiplet with second-order splitting, 2H), -0.07 (s, 16H); ¹³C NMR (126 MHz, CDCl₃, δ) 149.8, 147.6, 139.4(2), 127.6, 127.5, 125.8, 124.7, 124.6, 121.2, 120.1, 119.7, 44.8, -0.7; HRMS (EI): calcd for C₁₉H₂₅BrSi₂ [M]⁺: 388.06733; found, 388.0674. FT-IR (KBr, thin film) ν_{\max} (cm⁻¹): 3050, 2952, 2892, 1589, 1554, 1456, 1436, 1397, 1261, 1248, 1171, 1105, 1063, 941, 901, 873, 857, 821, 734, 684; mp 169-170 °C (ethanol).

(9,9-bis(trimethylsilyl)-9H-fluoren-2-yl)boronic acid (4). To an oven-dried 200 mL flask were

added 5.00 g of (2-bromo-9H-fluorene-9,9-diyl)*bis*(trimethylsilane) (**1**) (0.0128 mol, 1.00 equiv) and 80 mL of dry THF. The solution was cooled to -78 °C with dry ice in acetone, and 12.0 mL of a 1.5 M solution of *n*-butyllithium in hexane (0.0167 mol, 1.3 equiv) was added. The solution was stirred at -78 °C for 1 h. To the reaction mixture was added 4.81 g (0.0256 mol, 2.00 equiv) of triisopropylborate. The solution was allowed to warm to room temperature and stir overnight. The reaction was quenched with 50 mL of 1 M HCl and then extracted into diethyl ether (3 X 30 mL). The combined organic layers were washed with brine and dried over sodium sulfate. After removal of the ether, the crude mixture was purified by recrystallization from refluxing hexane to yield 3.02 g (67%) of a white powder. ¹H NMR (500 MHz, CDCl₃/CD₃OD, δ) (all coupling constants (*J*) in Hz): 7.99 (s, 1H), 7.90 (m, 2H), 7.71 (d, *J* = 7.5, 1H), 7.57 (m, 1H), 7.32 (m, 2H), -0.12 (s, 18H); ¹³C NMR (126 MHz, CDCl₃/CD₃OD, δ) 148.3, 146.9, 142.5, 140.2, 130.1, 129.6, 126.1, 124.6, 124.3, 120.2, 119.4, 119.1, 44.1, -0.9; FT-IR (KBr, thin film) ν_{\max} (cm⁻¹): 3206, 3050, 2954, 2892, 1607, 1560, 1446, 1401, 1347, 1328, 1261, 1250, 926, 883, 840, 741; mp 85-90 °C (hexane).

9,9,9',9'-tetrakis(trimethylsilyl)-9H,9'H-2,2'-bifluorene (5). To an oven-dried 100 mL flask were added 1.00 g of (2-bromo-9H-fluorene-9,9-diyl)*bis*(trimethylsilane) (**1**) (0.00257 mol, 1.00 equiv), 1.09 g of (9,9-*bis*(trimethylsilyl)-9H-fluorene-2-yl)boronic acid (**2**) (0.00308 mol, 1.20 equiv), 0.150 g of Pd(PPh₃)₄ (5 mol%), 30 ml toluene, and 20 mL of aqueous 2M Na₂CO₃. The solution was degassed with bubbling argon and then heated to reflux for 12 h under argon. After cooling to room temperature, the reaction mixture was moved to a separatory funnel and 50 mL of diethyl ether were added. The organic layer was washed with brine. After drying over sodium sulfate, the organic layer was removed and the mixture was purified with silica gel chromatography eluting with 95:5 hexane/dichloromethane. A total of 0.975 g (61%) of product was isolated as a white powder. ¹H NMR (500 MHz, CDCl₃, δ) (all coupling constants (*J*) in Hz): 8.02 (d, *J* = 8.0, 2H), 7.97 (m, 4H), 7.76 (dd, *J* = 8.0, 1.5, 2H), 7.62 (d, *J* = 8.0), 7.38 (m, 4H), 0.00 (s, 36H); ¹³C

NMR (126 MHz, CDCl_3 , δ) 148.4, 148.1, 140.2, 139.6, 139.1, 125.8, 124.7, 124.6, 123.8, 123.1, 120.3, 120.1, 44.4, -0.6; HRMS (EI): calcd for $\text{C}_{38}\text{H}_{50}\text{Si}_4$ $[\text{M}]^+$: 618.2984; found, 618.2998; FT-IR (KBr, thin film) ν_{max} (cm^{-1}): 3058, 2954, 2899, 1609, 1442, 1396, 1249, 1173, 1124, 1105, 941, 905, 860, 821, 780, 752, 738, 685, 622; mp 243-245 °C (hexane).

9H,9'H-2,2'-bifluorene (6). To a 200 mL flask were added 0.500 g of 9,9,9',9'-tetrakis (trimethylsilyl)-9H,9'H-2,2'-bifluorene (**5**) (0.000807 mol, 1.00 equiv), 0.034 g KOH flake (0.00061, 0.75 equiv), 50 mL of tetrahydrofuran, and 25 mL of methanol. The solution was degassed with bubbling argon for 5 minutes and then heated to reflux for 2 h under argon. The solution was cooled and filtered to isolate 0.202 g (76%) of product as a white crystal. ^1H NMR (500 MHz, CDCl_3 , δ) (all coupling constants (J) in Hz): 7.88 (d, $J = 8.0$, 2H), 7.86 (m, 2H), 7.84 (d, $J = 8.0$, 2H), 7.70 (dd, $J = 8.0$, 2.0, 2H), 7.59 (d, $J = 8.0$, 2H), 7.41 (t, $J = 8.0$, 2H), 7.33 (td, $J = 8.0$, 2.0, 2H), 4.00 (s, 4H); ^{13}C NMR (126 MHz, CDCl_3 , δ) 144.1, 143.7, 141.7, 141.0, 140.3, 127.0, 126.9, 126.2, 125.3, 124.0, 120.4, 120.2, 127.0, 126.9, 126.2, 125.3, 124.0, 120.4, 120.2, 37.2; HRMS (EI): calcd for $\text{C}_{26}\text{H}_{18}$ $[\text{M}]^+$: 330.1403 ; found, 330.1405; FT-IR (KBr, thin film) ν_{max} (cm^{-1}): 3064, 3014, 2921, 1590, 1146, 1403, 1234, 1180, 947, 817, 761, 728; mp 316-318 °C (tetrahydrofuran, methanol), lit. mp 316-318 °C (toluene).^{7b}

Protonated BDPA dimer (8b). To an oven-dried 50 mL flask cooled in an ice bath were added 0.080 g of 9H,9'H-2,2'-bifluorene (**6**) (0.000240 mol, 1.00 equiv), 0.170 g of 9-(bromo(phenyl)methylene)-9H-fluorene (0.000510 mol, 2.10 equiv), 0.210 g of sodium *tert*-butoxide (0.00220 mol, 9.00 equiv), and 30 mL of anhydrous, degassed dimethylformamide. The solution was stirred at 0 °C for 30 minutes and at room temperature for 3.5 h. The reaction was quenched by adding 5.0 mL of glacial acetic acid followed by 50 mL of water. The quenched reaction mixture was extracted with diethyl ether (2 x 10 mL) and the combined organic layers were washed several times with water and once with brine, before being dried over sodium sulfate. The crude product was

purified by silica gel chromatography eluting with 3:1 hexane/DCM. The isolated material (0.172 g, 86%) is a complex mixture of tautomers, E/Z-double bond isomers, and rotamers. HRMS (EI): calcd for $C_{66}H_{42} [M]^+$: 834.3281; found, 834.3282; FT-IR (KBr, thin film) ν_{\max} (cm^{-1}): 3059, 1615, 1593, 1572, 1146, 1342, 1268, 1155, 1024, 908, 825, 782, 731, 703, 674, 620.

BDPA dimer dianion (8a). To generate the dianion for NMR, 0.035 g of **8b**, 0.019 g of potassium *tert*-butoxide (4.0 equiv), and 1.0 mL of d_6 -DMSO were stirred under argon for 30 minutes and then transferred to an NMR tube, which was subsequently flushed with argon and capped. ^1H NMR (500 MHz, d_6 -DMSO, 40 °C, δ) (all coupling constants (J) in Hz): 7.92 (d, $J=7.5$, 4H), 7.80 (d, $J=7.5$, 2H), 7.58 (d, $J=7.5$, 2H), 7.45 (m, 2H), 7.37 (m, 8H), 6.86 (t, $J=7.5$, 4H), 6.82 (t, $J=7.5$, 2H), 6.73 (t, $J=7.5$, 4H), 6.69 (t, $J=7.5$, 2H), 6.65 (s, 2H), 6.47 (d, $J=7.5$, 4H), 6.43 (d, $J=7.5$, 2H), 6.24 (br, 2H); ^{13}C NMR (126 MHz, d_6 -DMSO, 40 °C, δ) 145.1, 143.5, 139.2, 138.9, 137.4, 132.5, 132.2, 132.1, 130.8, 127.6, 127.4, 122.8, 122.6, 120.7 (2), 119.6, 118.1, 117.9, 117.8 (2), 117.3, 117.2, 111.4, 110.3.

Protonated *N,N*-dibutylbenzamide BDPA dimer (9b). To an oven-dried 50 mL flask cooled in an ice bath were added 0.030 g of 9H,9'H-2,2'-bifluorene (**6**) (0.000098 mol, 1.0 equiv), 0.093 g of 9-(bromo(phenyl)methylene)-9H-fluorene (0.00019 mol, 2.1 equiv), 0.078 g of sodium *tert*-butoxide (0.00082 mol, 9.0 equiv), and 8 mL of anhydrous, degassed dimethylformamide. The solution was stirred at 0 °C for 30 minutes and at room temperature 3.5 h. The reaction was quenched by adding 5.0 mL of glacial acetic acid followed by 50 mL of water. The quenched reaction mixture was extracted with diethyl ether (2 x 10 mL). The combined organic layers were washed several times with water and once with brine, before being dried over sodium sulfate. The crude product was purified by silica gel chromatography eluting with 45:45:10 hexane/DCM/ethyl acetate. The isolated material (0.083 g, 80%) is a complex mixture of tautomers, E/Z-double bond isomers, and rotamers. Based on preliminary NMR data (not included) further purification may be necessary.

FT-IR (KBr, thin film) ν_{\max} (cm⁻¹): 3060, 2957, 2930, 2871, 1633, 1447, 1425, 1297, 1101, 826, 782, 732.

***N,N*-dibutylbenzamide BDPA dimer dianion (9a).** To generate the dianion for NMR, 0.020 g of (9b), 0.006 g of lithium *tert*-butoxide (4.0 equiv), 0.7 mL of *d*₆-DMSO, and 0.5 mL of *d*₇-DMF were stirred under argon for 30 minutes and then transferred to an NMR tube, which was subsequently flushed with argon and capped. ¹H NMR (500 MHz, *d*₆-DMSO/*d*₇-DMF, 50 °C, δ) (all coupling constants (*J*) in Hz): 8.00 (br, 4H), 7.85 (br, 2H), 7.65 (br, 2H), 7.51 (d, *J* = 7.5, 4H), 7.35 (d, *J* = 7.5, 4H), 7.1 – 6.0 (br, 22H (signal too broad to accurately integrate), 3.5-3.3 (signal overlaps with water peak, 4H), 1.7-0.7 (br, signals overlap with *tert*-butanol signal, 14H); ¹³C NMR (126 MHz, *d*₆-DMSO/*d*₇-DMF, 40 °C, δ) 171.7, 146.4, 143.3, 139.7, 138.6, 137.1, 133.7, 133.1, 133.0, 131.7, 131.0, 129.2, 127.8, 126.6, 123.6, 123.4, 121.6, 120.4, 119.0, 118.8 (2), 118.5, 118.2, 112.5, 111.2, 49.3(br), 30.6(br), 20.3, 14.5.

(*E/Z*)-4-((2-bromo-9H-fluoren-9-ylidene)methyl)-*N,N*-dibutylbenzamide (10). To a 500 mL flask equipped with a reflux condenser were added 3.68 g of 2-bromofluorene (0.0150 mol, 1.00 equiv), 2.70 g of 4-carboxybenzaldehyde (0.0180 mol, 1.2 equiv), 4.62 g potassium *tert*-butoxide (0.0413 mol, 2.75 equiv), and 150 mL of absolute ethanol. The reaction mixture was heated to reflux. After 1 h of reflux a yellow precipitate formed, and the reaction was allowed to cool to room temperature overnight. The precipitate, which is the potassium salt of the condensation product, was isolated by vacuum filtration and washed with ethanol and hexanes. After drying under high vacuum at 100 °C overnight, 5.15 g of yellow powder was isolated. A portion of this material was carried on to the next step without further purification. To a 200 mL flask cooled in an ice bath were added 3.93 g of the potassium salt of the crude condensation product (assumed to be 0.0095 mol, 1.0 equiv), 30 mL of dry dichloromethane, 1.24 mL oxalyl chloride (1.80 g, 0.0140 mol, 1.50 equiv), and 1 drop of DMF. The reaction mixture was allowed to warm to room temperature until bubbling ceased. The solvent and excess reagent were distilled off, and the remaining solid was

dissolved in 50 mL of dichloromethane. To this solution were added 6.40 mL of di-*n*-butylamine (4.91 g, 0.038 mol, 4.00 equiv) and catalytic 4-dimethylaminepyridine. The solution was stirred for 4 h and then moved to separatory funnel where it was washed with 0.1 M HCl (3 X 20 mL), sat'd sodium bicarbonate (3 X 20 mL), and brine. The solution was dried over sodium sulfate. After removal of the solvent, the crude reaction mixture was purified with silica gel chromatography. The *E* and *Z* isomers could be eluted separately using 80% hexane, 10% dichloromethane, and 10% ethyl acetate. The *E* isomer elutes before the *Z* isomer. In total, 3.61 g (49% based on 2-bromofluorene) of product was isolated (*E* isomer, 1.31 g; *Z* isomer, 1.53 g; mixed fractions, 0.770 g). The *E* isomer was isolated as an amorphous yellow solid and the *Z* isomer was isolated as a viscous yellow oil. Subsequently, the reaction was performed on approximately 3X this scale and the product was isolated as a 1:1 mixture of *E* and *Z* isomers. *E* isomer: ¹H NMR (500 MHz, CDCl₃, δ) (all coupling constants (*J*) in Hz): 7.91 (d, *J* = 2.0, 1H), 7.69 (d, *J* = 7.5, 1H), 7.6 (m, 5H), 7.51 (dd, *J* = 8.0, 2.0, 1H), 7.47 (d, *J* = 8.0, 2H), 7.33 (td, *J* = 7.5, 1.0, 1H), 7.08 (td, *J* = 7.5, 1.0, 1H), 3.54 (t, *J* = 7.5, 2H), 3.28 (t, *J* = 7.5, 2H), 1.69 (m, 2H), 1.56 (m, 2H), 1.45 (m, 2H), 1.21 (m, 2H), 1.01 (t, *J* = 7.5, 3H), 0.85 (t, *J* = 7.5, 3H); ¹³C NMR (126 MHz, CDCl₃, δ) 171.4, 141.4, 140.5, 138.2, 137.4, 137.3, 136.3, 136.2, 131.3, 129.4, 129.2, 127.6, 127.3, 127.0, 124.6, 123.8, 121.1, 121.0, 120.0, 49.1, 44.8, 31.0, 29.9, 20.5, 20.0, 14.2, 13.8; FT-IR (KBr, thin film) ν_{\max} (cm⁻¹): 3059, 2958, 2930, 2872, 1633, 1508, 1448, 1425, 1412, 1378, 1297, 1257, 1234, 1187, 1101, 1064, 955, 869, 820, 771, 728. *Z* isomer: ¹H NMR (500 MHz, CDCl₃, δ) (all coupling constants (*J*) in Hz): 7.79 (d, *J* = 7.5, 1H), 7.69 (m, 3H), 7.61 (d, *J* = 8.0, 2H), 7.58 (d, *J* = 8.0, 1H), 7.49 (d, *J* = 8, 2H), 7.44 (dd, *J* = 8.0, 2.0, 1H), 7.40 (td, *J* = 7.5, 1.0, 1H), 7.37 (td, *J* = 7.5, 1.0, 1H), 3.54 (t, *J* = 7.5, 2H), 3.31 (t, *J* = 7.5, 2H), 1.69 (m, 2H), 1.56 (m, 2H), 1.43 (m, 2H), 1.23 (m, 2H), 1.01 (t, *J* = 7.5, 3H), 0.86 (t, *J* = 7.5, 3H); ¹³C NMR (126 MHz, CDCl₃, δ) 171.4, 140.4, 139.2, 138.5, 138.3, 137.5, 137.2, 136.3, 131.7, 129.5, 128.8, 127.9, 127.7, 127.5, 127.2, 121.3, 120.6(2), 119.9, 49.2, 44.8, 31.2, 29.9, 20.6, 20.1, 14.2, 14.1; FT-IR (KBr, thin film) ν_{\max} (cm⁻¹): 3050, 2958, 2930, 2872, 1633, 1508, 1464, 1440, 1421, 1378, 1296, 1268, 1186, 1101, 1064, 955, 831, 776, 734.

(*E/Z*)-4-((9',9'-bis(trimethylsilyl)-9H,9'H-[2,2'-bifluoren]-9-ylidene)methyl)-*N,N*-dibutylbenzamide (11). To an oven-dried 500 mL flask were added 8.40 g of a (*E/Z*)-4-((2bromo-9H-fluoren-9-ylidene)methyl)-*N,N*-dibutylbenzamide (1:1 mixture of isomers) (0.00123 mol, 1.00 equiv), 6.70 g of (9,9-bis(trimethylsilyl)-9H-fluoren-2-yl)boronic acid (2) (0.00147 mol, 1.20 equiv), 0.604 g of Pd(PPh₃)₂Cl₂ (5 mol%), 0.450 g of triphenylphosphine (10 mol%), 100 ml toluene, and 50 mL of aqueous 2M Na₂CO₃. The solution was degassed with bubbling argon and then heated to reflux for 12 h under argon. After cooling to room temperature, the reaction mixture was moved to a separatory funnel and 100 mL of diethyl ether were added. The organic layer was washed with sat'd sodium bicarbonate and brine. After drying over sodium sulfate, the organic layer was removed and the mixture was purified with silica gel chromatography using mixtures of hexane, dichloromethane, and ethyl acetate. The product was eluted with 10:9:1 hexane, dichloromethane, and ethyl acetate as a 1:1 mixture of *E* and *Z* isomers and obtained in 73% yield (8.96 g) as a yellow powder. The *E* and *Z* isomers could not be resolved in our hands using chromatography, unlike in the case of the bromide starting material. In order to isolate pure samples of the *E* and *Z* isomers for characterization, the same reaction was performed twice on a smaller scale with pure samples of the *E* and *Z* isomers, respectively. *E* isomer: ¹H NMR (500 MHz, CDCl₃, δ) (all coupling constants (*J*) in Hz): 8.08 (d, *J* = 1.0, 1H), 8.02 (d, *J* = 7.5, 1H), 7.97 (m, 1H), 7.89 (d, *J* = 1.0, 1H), 7.83 (d, *J* = 7.5, 1H), 7.77 (s, 1H), 7.76 (d, *J* = 7.5, 1H), 7.71 (ddd, *J* = 7.5, 2.5, 1.5, 2H), 7.66 (d, *J* = 7.5, 2H), 7.62 (d, *J* = 7.5, 1H), 7.58 (d, *J* = 7.5, 1H), 7.49 (d, *J* = 7.5, 1H), 7.37 (m, 3H), 7.07 (td, *J* = 7.5, 1.0, 1H), 3.55 (t, *J* = 7.5, 2H), 3.30 (t, *J* = 7.5, 2H), 1.70 (m, 2H), 1.57 (m, 2H), 1.45 (m, 2H), 1.22 (m, 2H), 1.02 (t, *J* = 7.5, 3H), 0.86 (t, *J* = 7.5, 3H), -0.01 (s, 18H); ¹³C NMR (126 MHz, CDCl₃, δ) 171.5, 148.4, 148.1, 141.5, 141.4, 140.1 (2), 139.8, 139.1, 138.3, 138.0, 137.4, 137.1, 136.9, 129.5, 129.1, 128.0, 127.0, 126.9, 126.5, 125.9, 124.7(2), 124.6, 124.0, 123.3, 120.3, 120.2, 120.1 (2), 119.5, 49.1, 44.8, 44.5, 31.1, 29.9, 20.6, 20.0, 14.2, 13.9, -0.6; FT-IR (KBr, thin film) ν_{\max} (cm⁻¹): 3050, 2957, 2863, 1633, 1452, 1424, 1297, 1250, 1104, 915, 834,

822, 732. *Z* isomer: ^1H NMR (500 MHz, CDCl_3 , δ) (all coupling constants (J) in Hz): 8.10 (d, $J = 1.0$, 1H), 7.90 (d, $J = 7.5$, 1H), 7.87 (d, $J = 8.0$, 1H), 7.83 (d, $J = 8.0$ Hz, 1H), 7.82 (d, $J = 7.5$, 1H), 7.76 (m, 4H), 7.71 (s, 1H), 7.64 (dd, $J = 8.0$, 1.5, 1H), 7.59 (m, 1H), 7.51 (d, $J = 8.0$, 2H), 7.42 (td, $J = 7.5$, 1.0, 1H), 7.35 (m, 4H), 3.53 (t, $J = 7.5$, 2H), 3.29 (t, $J = 7.5$, 2H), 1.69 (m, 2H), 1.45 (m, 4H), 1.05 (m, 2H), 1.01 (t, $J = 7.5$, 3H), 0.68 (t, $J = 7.5$, 3H), -0.08 (s, 18H); ^{13}C NMR (126 MHz, CDCl_3 , δ) 171.3, 148.4, 148.1, 140.9, 140.5, 140.1, 140.0, 139.7, 139.2, 138.8, 137.9, 137.2(2), 137.1, 129.7, 128.7, 128.2, 127.3, 127.2, 126.7, 125.9, 124.7, 124.5, 123.5, 123.4, 123.0, 120.5, 120.4, 120.2, 120.0, 119.9, 49.2, 44.9, 44.4, 31.0, 29.9, 20.6, 19.8, 14.2, 13.9, -0.06; FT-IR (KBr, thin film) ν_{max} (cm^{-1}): 3050, 2957, 2871, 1633, 1457, 1443, 1424, 1296, 1250, 1104, 902, 884, 842, 822, 737.

(*E/Z*)-4-(9H,9'H-[2,2'-bifluoren]-9-ylidenebromomethyl)-N,N-dibutylbenzamide (12). To a 500 mL oven-dried flask were added 4.36 g (*E/Z*)-4-((9',9'-bis(trimethylsilyl)-9H,9'H-[2,2'-bifluoren]-9-ylidene)methyl)-N,N-dibutylbenzamide (**11**) (0.00607 mol, 1.00 equiv) and 280 mL of glacial acetic acid. To this solution, 0.320 mL of bromine (0.980 g, 0.00610 mol, 1.01 equiv) was added dropwise over 10 minutes. The reaction was stirred for 3 h at room temperature and 200 mL of water were added. The crude dibromide was isolated by filtration and allowed to thoroughly dry on the filter pad. To a 1000 mL flask containing the dibromide (approx 4.8 g, 0.0055 mol) was added 500 mL of absolute ethanol. To this flask was added a solution of 2.64 g of NaOH (pellet form) (0.066 mol, 12.0 equiv) in the minimum amount of water needed for dissolution. The reaction mixture was heated to reflux for 2 h and then cooled to room temperature. The yellow precipitate formed was isolated by filtration and then subsequently purified by silica gel chromatography eluting with mixtures of hexane, dichloromethane, and ethyl acetate. The elution solvent was ramped from 50:50 hexane/DCM to 45:45:10 hexane/DCM/ethyl acetate with the *E*-isomer eluting before the *Z*-isomer. A total of 3.08 g (78%) of pure material was isolated (*E* isomer, 1.62 g; *Z* isomer, 1.46 g). *E* isomer: ^1H NMR (500 MHz, CDCl_3 , δ) (all coupling constants (J) in Hz):

8.88 (d, $J = 7.5$, 1H), 7.75 (m, 4H), 7.58 (s, 4H), 7.56 (d, $J = 7.5$, 1H), 7.55 (dd, $J = 8.0, 2.0$, 1H), 7.48 (td, $J = 7.5, 1.5$, 1H), 7.42 (td, $J = 7.5, 1.5$, 1H), 7.39 (m, 2H), 7.32 (td, $J = 7.5, 1.5$, 1H), 7.23 (dd, $J = 7.5, 1.5$, 1H), 6.61 (d, $J = 1.5$), 3.93 (s, 2H), 3.48 (t, $J = 7.5, 2H$), 3.02 (t, $J = 7.5, 2H$), 1.64 (m, 2H), 1.41 (m, 4H), 1.01 (t, $J = 7.5, 3H$), 0.88 (m, 2H), 0.64 (t, $J = 7.5, 3H$); ^{13}C NMR (126 MHz, CDCl_3 , δ) 170.6, 144.2, 143.8 (2), 141.5, 141.2, 141.1, 140.3, 139.7, 139.0, 138.8, 138.5, 138.3, 136.7, 129.6, 129.1, 127.9, 127.4, 127.3, 126.9 (2), 126.3, 125.7, 125.3, 124.0, 123.5 (2), 120.4, 120.1, 119.9, 119.8, 49.1, 44.8, 37.1, 30.9, 29.8, 20.6, 19.7, 14.2, 13.8; FT-IR (KBr, thin film) ν_{max} (cm^{-1}): 3043, 2957, 2927, 2856, 1624, 1446, 1417, 1295, 1098, 822, 769, 733. Z isomer: ^1H NMR (500 MHz, CDCl_3 , δ) (all coupling constants (J) in Hz): 9.21 (d, $J = 1.5$, 1H), 7.90 (m, 2H), 7.85 (d, $J = 7.5$, 1H), 7.81 (d, $J = 8.0$, 1H), 7.76 (td, $J = 7.5, 1.5$, 2H), 7.69 (d, $J = 8.0$, 1H), 7.59 (d, $J = 7.5$, 1H), 7.54 (multiplet with second-order splitting, 4H), 7.42 (td, $J = 7.5, 1.5$, 1H), 7.34 (td, $J = 7.5, 1.5$, 1H), 7.27 (td, $J = 7.5, 1.5$, 1H), 6.87 (td, $J = 7.5, 1.5$, 1H), 6.37 (d, $J = 7.5$, 1H), 4.02 (s, 2H), 3.56 (t, $J = 7.5, 2H$), 3.32 (t, $J = 7.5, 2H$), 1.70 (m, 2H), 1.58 (m, 2H), 1.45 (m, 2H), 1.24 (m, 2H), 1.02 (t, $J = 7.5, 3H$), 0.88 (t, $J = 7.5, 3H$); ^{13}C NMR (126 MHz, CDCl_3 , δ) 171.0, 144.2, 143.7, 143.6, 141.6, 141.2, 140.9, 140.4, 140.3, 139.9, 138.7, 138.5, 138.3, 136.6, 129.1, 128.7, 128.6, 127.7, 127.1, 127.0(2), 126.3, 125.3, 125.2, 125.0, 124.1, 123.8, 120.4, 120.2, 120.1, 119.6, 49.2, 44.9, 37.3, 31.1, 29.9, 20.6, 20.1, 14.2, 13.9; FT-IR (KBr, thin film) ν_{max} (cm^{-1}): 3058, 2957, 2930, 2871, 1633, 1448, 1425, 1297, 1101, 825, 770, 734.

Protonated form of Polymer 1 (P1b). To an oven-dried 100 mL flask was added 0.280 g of (*E*)-4-(9H,9'H-[2,2'-bifluoren]-9-ylidenebromomethyl)-N,N-dibutylbenzamide (**12-E**) (0.000429 mol, 1.00 equiv). The flask was flushed with argon and sealed under vacuum and then moved into a nitrogen glove box. In the glove box, 0.192 g of sublimed potassium *tert*-butoxide (0.00171 mol, 4.00 equiv) and 40 mL of anhydrous tetrahydrofuran were added. The reaction was heated to 50 °C in a sandbath for 36 h within the glovebox. After cooling, the reaction flask was removed from the glove box and 5.0 mL of glacial acetic acid was added with stirring. Additional water was added and the precipitate was isolated by filtration, washing with methanol and hexane. After

drying under vacuum, 0.244 g (99%) of a light yellow material was isolated. GPC (THF) M_n = 6.5 kDa, PDI (M_n/M_w) = 2.1, DP (based on M_n) = 11; FT-IR (KBr, thin film) ν_{\max} (cm^{-1}): 3060, 2957, 2930, 2871, 1634, 1506, 1447, 1424, 1378, 1297, 1265, 1184, 1101, 1020, 908, 824, 769, 735, 650.

Anionic form of Polymer 1 (P1a). To generate the polyanion for NMR, 0.035 g of **P1b**, 0.014 g of potassium *tert*-butoxide, and 1.0 mL of d_6 -DMSO were stirred under argon for 30 minutes and then transferred to an NMR tube, which was subsequently flushed with argon and capped. Spectra are available in Section 6.7.

Radical form of Polymer 1 (P1c). To an oven-dried 100 mL flask was added 0.280 g of (*E*)-4-(9H,9'H-[2,2'-bifluoren]-9-ylidenebromomethyl)-*N,N*-dibutylbenzamide (**12-E**) (0.000429 mol, 1.00 equiv). The flask was flushed with argon and sealed under vacuum and then moved into a nitrogen glove box. In the glove box, 0.192 g of sublimed potassium *tert*-butoxide (0.00171 mol, 4.00 equiv) and 40 mL of anhydrous tetrahydrofuran were added. The reaction was heated to 50 °C in a sandbath for 36 h within the glovebox. After cooling, the reaction flask was removed from the glove box and 1.40 g of potassium ferricyanide (0.00429 mol, 10.0 equiv) dissolved in 10 mL of sat'd aqueous sodium bicarbonate was added. The reaction mixture immediately turned brown. After stirring for 2 minutes, additional water was added and the reaction mixture was transferred to a separatory funnel where it was extracted with DCM (3 x 50 mL). The combined organic layers were washed with water and brine and then dried over sodium sulfate. After removal of the solvent, the crude product was dissolved in the minimum amount of DCM needed (approx 5 mL) and then added drop-wise to a beaker of rapidly stirring methanol (100 mL). The resulting precipitate was isolated by filtration and washed with hexane to obtain 0.190 g (78 %) of a dark red solid. GPC (THF) M_n = 9.4 kDa, PDI (M_n/M_w) = 2.1, DP (based on M_n) = 16; FT-IR (KBr, thin film) ν_{\max} (cm^{-1}): 3059, 2957, 2930, 2871, 1721 (fluorenone end-group), 1633, 1504, 1445, 1424, 1378, 1297, 1261, 1184, 1100, 1020, 953, 823, 779, 736.

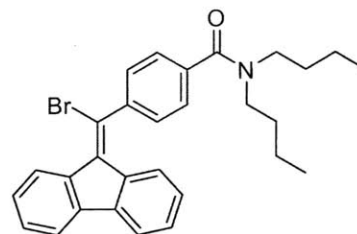
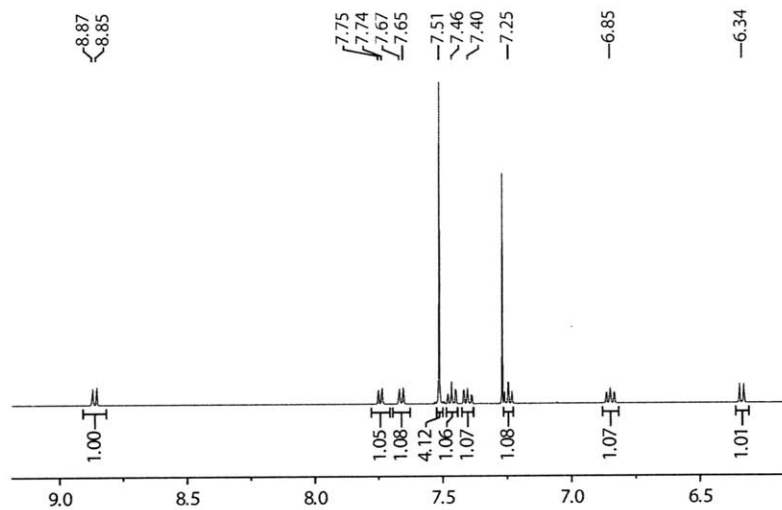
6.6 References

- (1) (a) Koelsch, C. F. *J. Amer. Chem. Soc.* **1957**, *79*, 4439. (b) Kuhn, R.; Neugebauer, F. A. *Monatsh. Chem.* **1964**, *95*, 3. (c) Azuma, N.; Ozawa, T.; Yamauchi, J. *Bull. Chem. Soc. Jpn.* **1994**, *67*, 31.
- (2) (a) Pacifici, J. G.; Garst, J. F.; Jansen, E. G. *J. Am. Chem. Soc.*, **1965**, *87*, 3014. (b) Kuhn, R.; Fischer, H.; Neugebauer, F. A. *Liebigs Ann. Chem.* **1972**, *654*, 64. (c) Andrieux, C. P.; Merz, A.; Saveant, J.-M.; Tomahogh, R. *J. Am. Chem. Soc.* **1984**, *106*, 1957. (d) Breslin, D. T.; Fox, M. A. *J. Phys. Chem.* **1993**, *97*, 13341. (e) Plater, M. J.; Kemp, S.; Lattmann, E. *J. Chem. Soc., Perkin Trans. 1*, **2000**, 971.
- (3) (a) Babel, A.; Jenekhe, S. A. *J. Am. Chem. Soc.* **2003**, *125*, 13656. (b) Newman, C. R.; Frisbie, C. D.; da Silva Filho, D. A.; Brdas, J.-L.; Ewbank, P. C.; Mann, K. R. *Chem. Mater.* **2004**, *16*, 4436. (c) Zhan, X.; Tan, Z.; Domercq, B.; An, Z.; Zhang, X.; Barlow, S.; Li, Y.; Zhu, D.; Kippelen, B.; Marder, S. R. *J. Am. Chem. Soc.* **2007**, *129*, 7246. (d) Letizia, J. A.; Salata, M. R.; Tribout, C. M.; Facchetti, A.; Ratner, M. A.; Marks, T. J. *J. Am. Chem. Soc.* **2008**, *130*, 9679. (e) Usta, H.; Facchetti, A.; Marks, T. J. *J. Am. Chem. Soc.* **2008**, *130*, 8580.
- (4) (a) Koelsch, C. F. *J. Am. Chem. Soc.* **1932**, *54*, 4744. (b) Nojima, M.; Takagi, M.; Morinaga, M.; Nagao, G.; Tokura, N. *J. Chem. Soc. Perkin I* **1978**, 488.
- (5) Eley, D. D.; Jones, K. W.; Littler, J. G. F.; Willis, M. R. *Trans. Faraday Soc.* **1967**, 902.
- (6) Nishide, H.; Yoshioka, N.; Saitoh, Y.; Gotoh, R.; Miyakawa, T.; Tsuchida, E. *J. Macromol. Sci., Part A: Pure Appl. Chem.* **1992**, *29*, 775.
- (7) (a) Wen, L.-S.; Kovacic, P. *Tetrahedron* **1978**, *34*, 2723. (b) Barnett, M. D.; Daub, G. H.; Hayes, F. N.; Ott, D. G. *J. Am. Chem. Soc.* **1959**, *81*, 4583.
- (8) (a) Tukada, H. *J. Am. Chem. Soc.* **1991**, *113*, 8991. (b) Tukada, H.; Mutai, K. *Tetrahedron Lett.* **1992**, *33*, 6665.
- (9) Rajca, A. *Chem. Rev.* **1994**, *94*, 871.

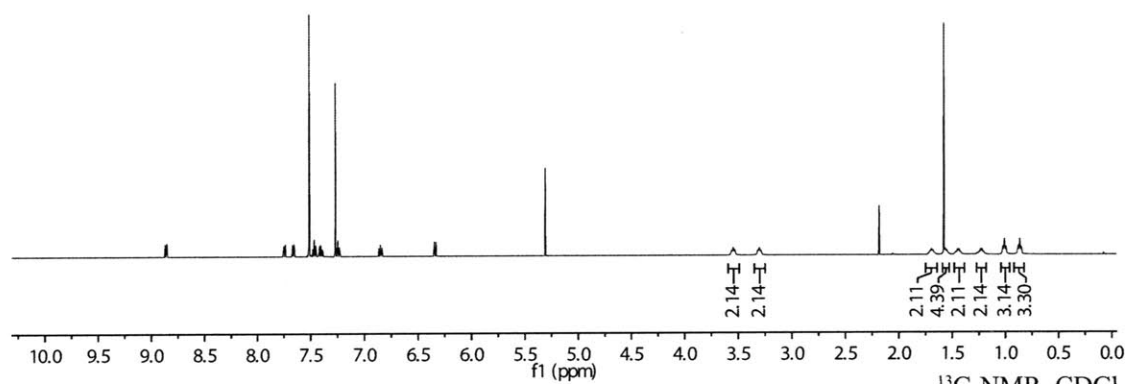
6.7 NMR Spectra

Compound 1 NMR Spectra

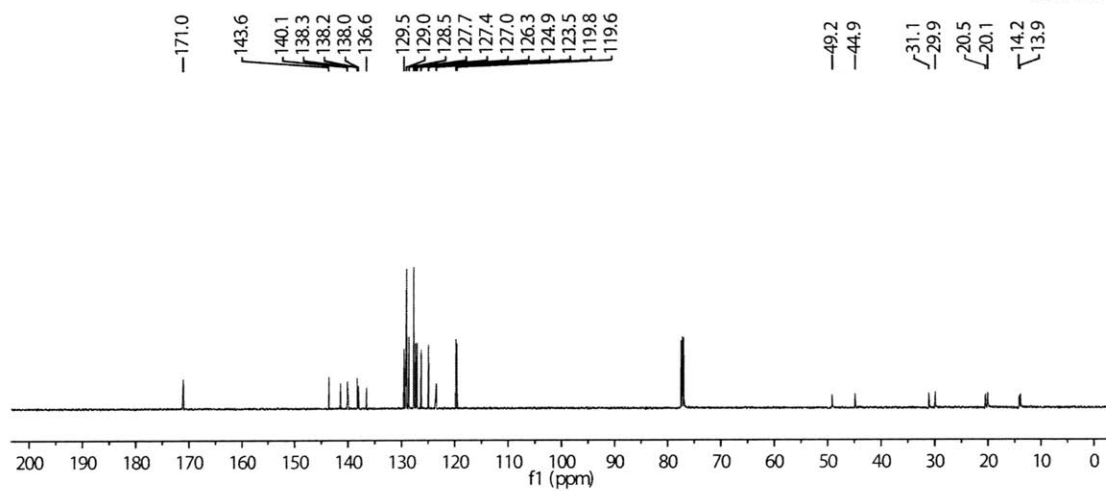
¹H-NMR, CDCl₃
500 MHz



3.55
3.30
1.69
1.44
1.23
1.01
0.87

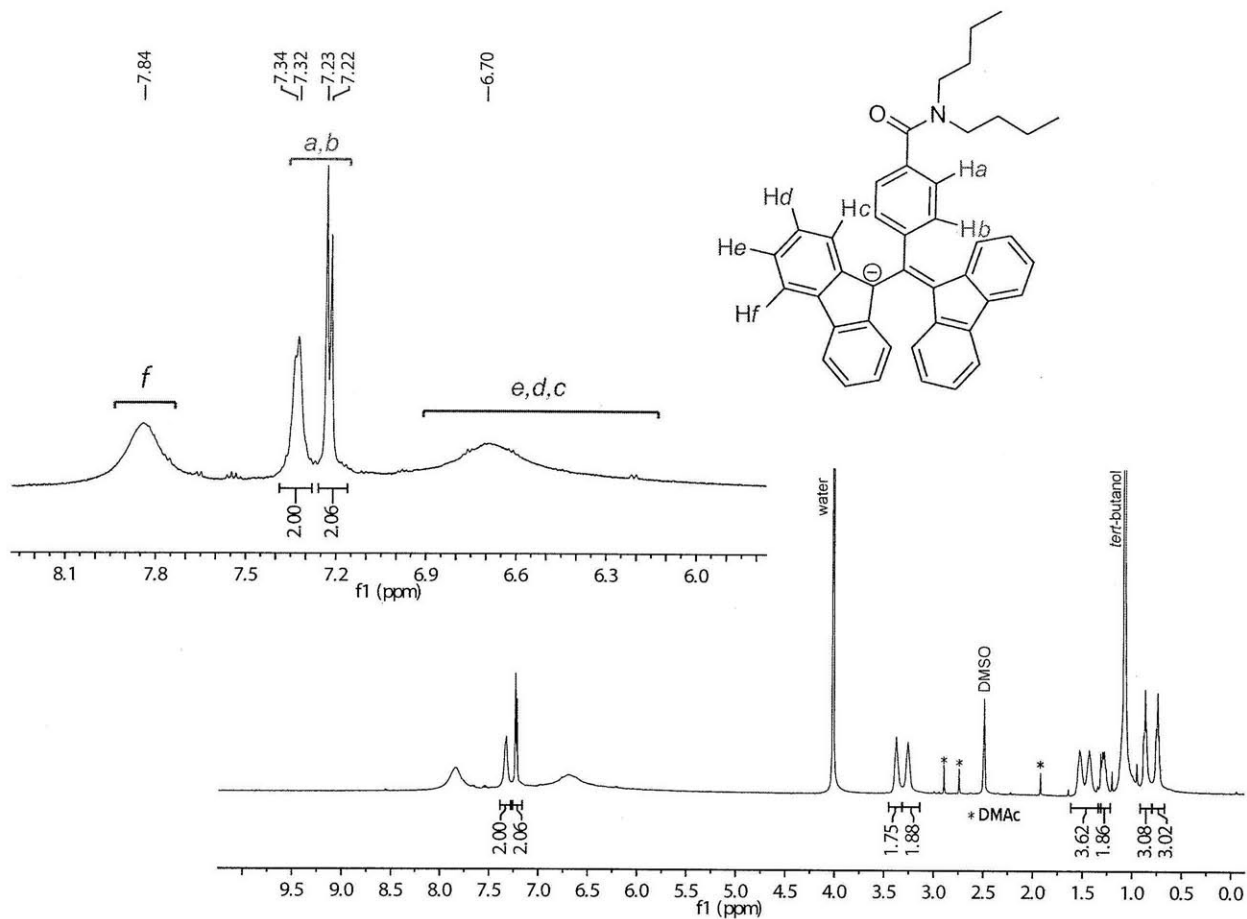


¹³C-NMR, CDCl₃
126 MHz



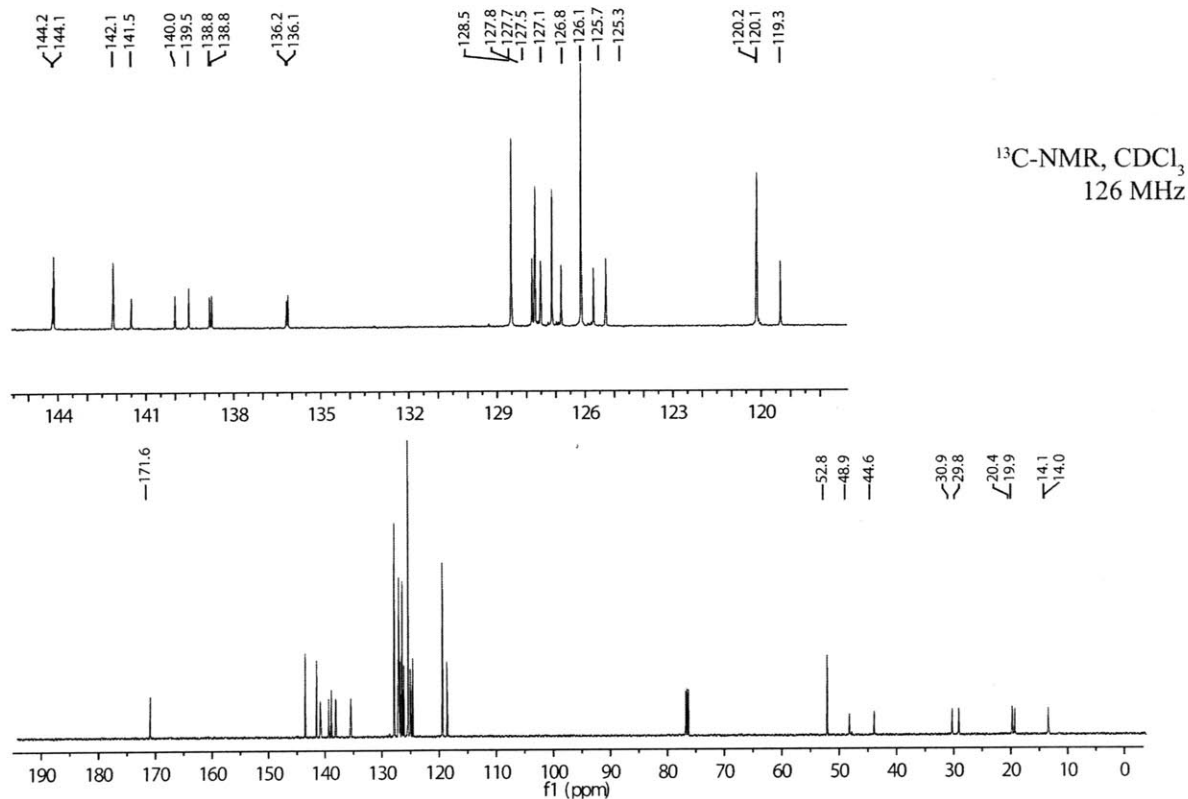
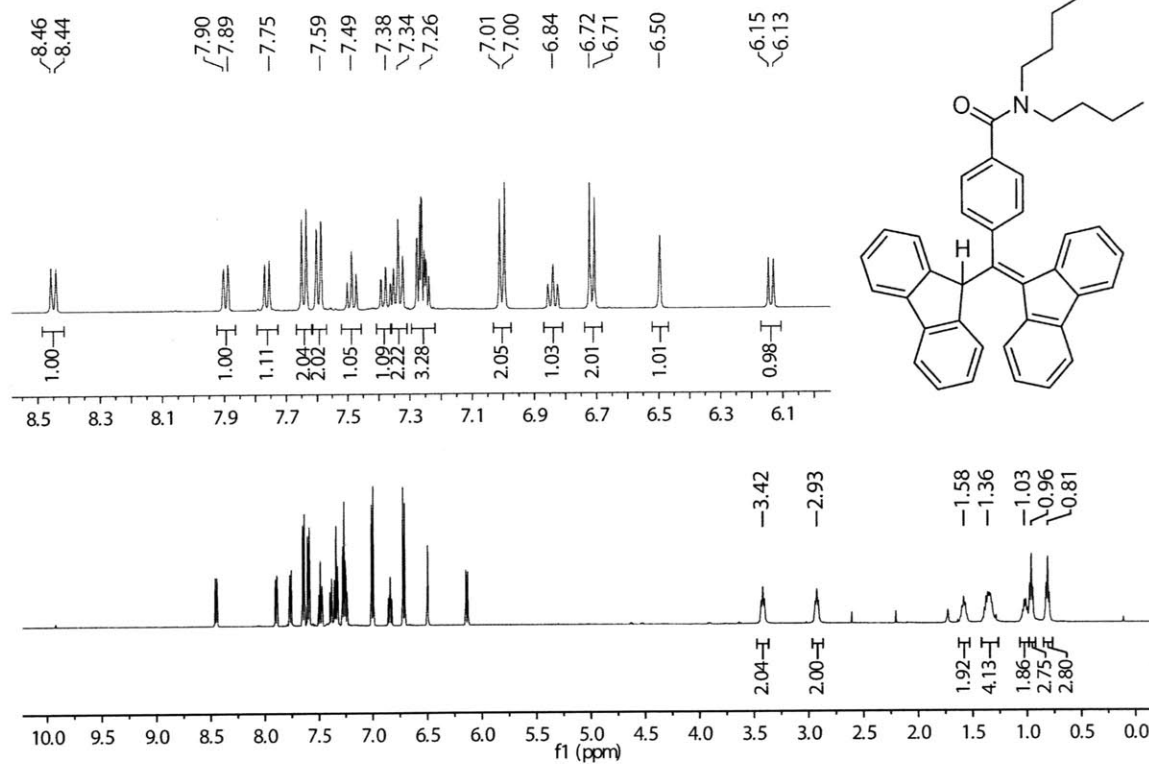
Compound 2a NMR Spectra

$^1\text{H-NMR}$, $d_6\text{-DMSO}$
 40 °C, 500 MHz



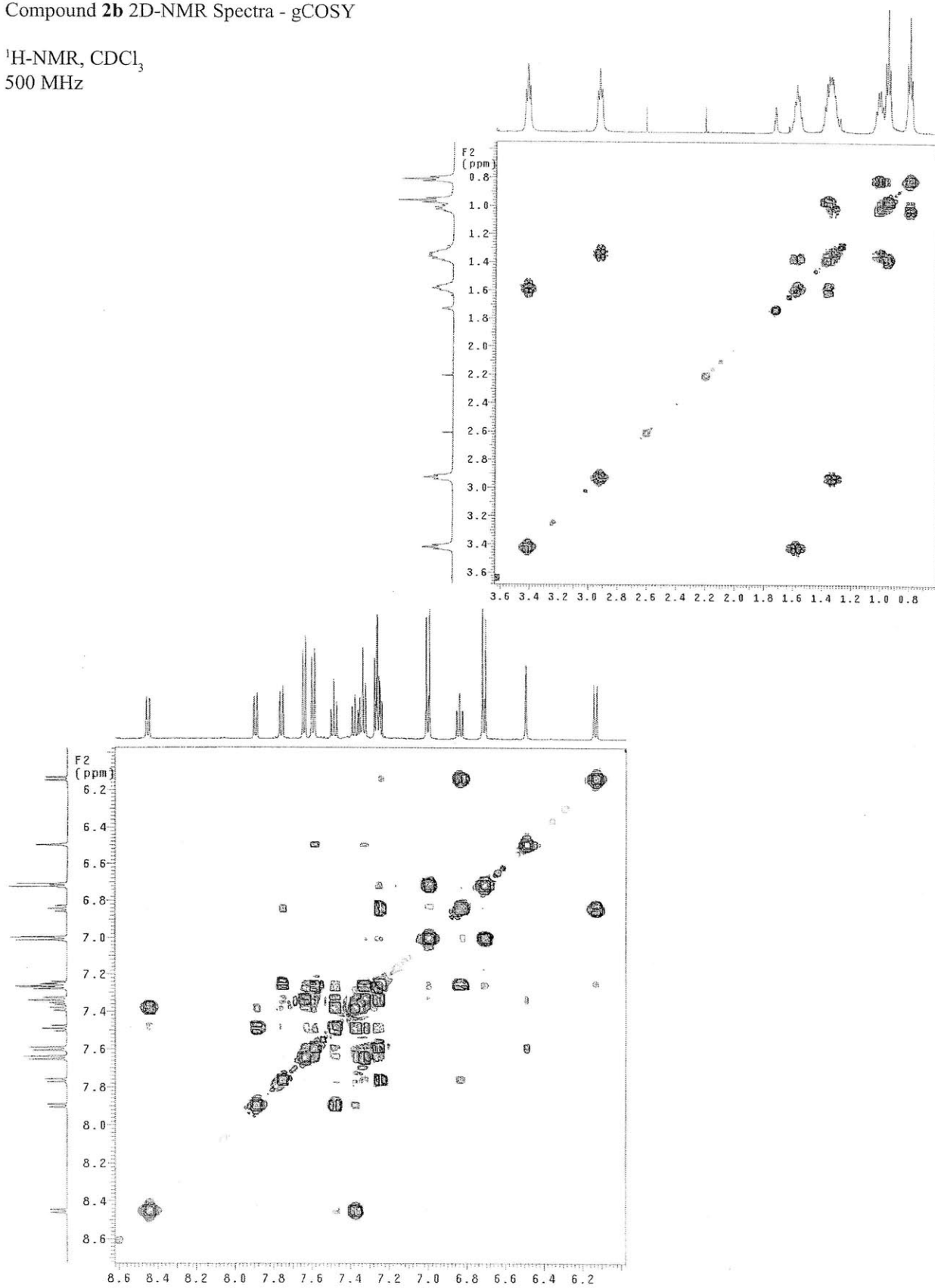
Compound **2b** NMR Spectra

¹H-NMR, CDCl₃
500 MHz



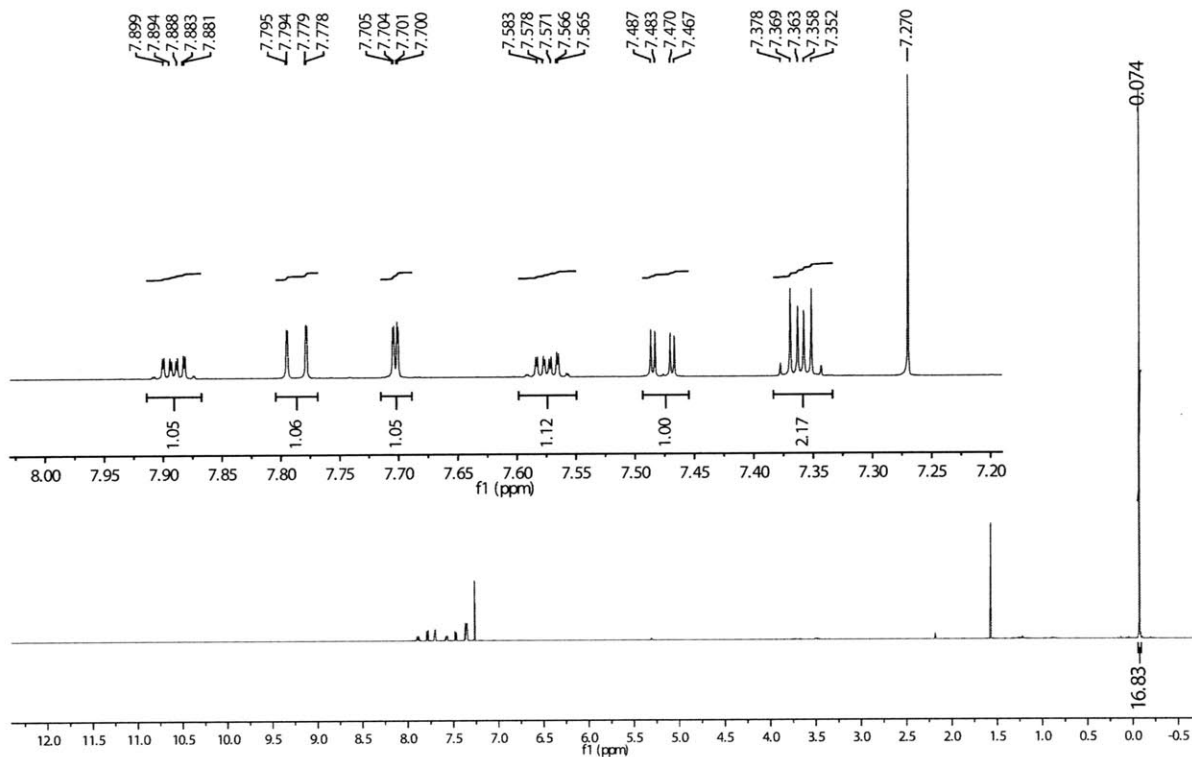
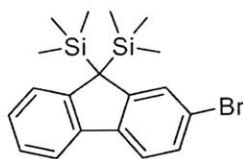
Compound **2b** 2D-NMR Spectra - gCOSY

$^1\text{H-NMR}$, CDCl_3
500 MHz

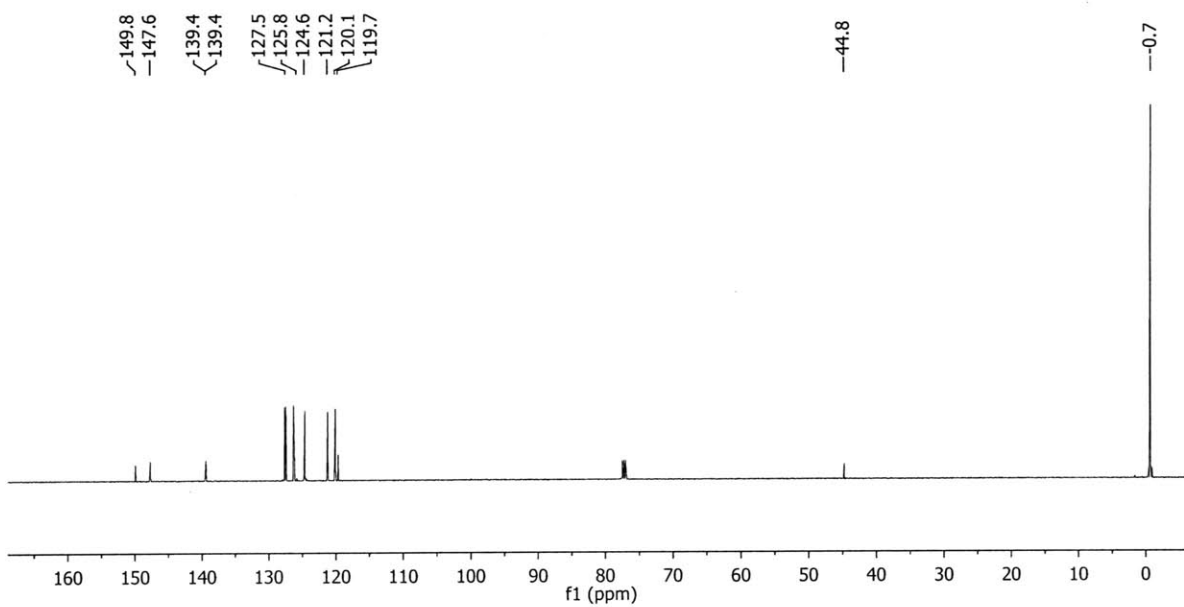


Compound 3 NMR Spectra

¹H-NMR, CDCl₃
500 MHz

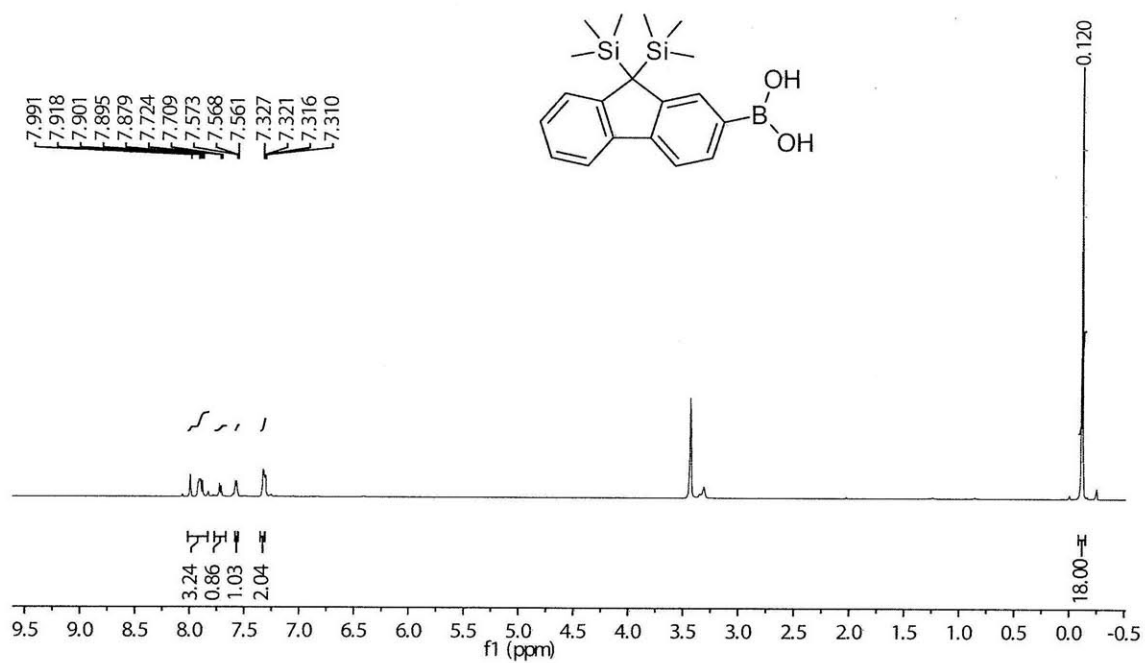


¹³C-NMR, CDCl₃
126 MHz

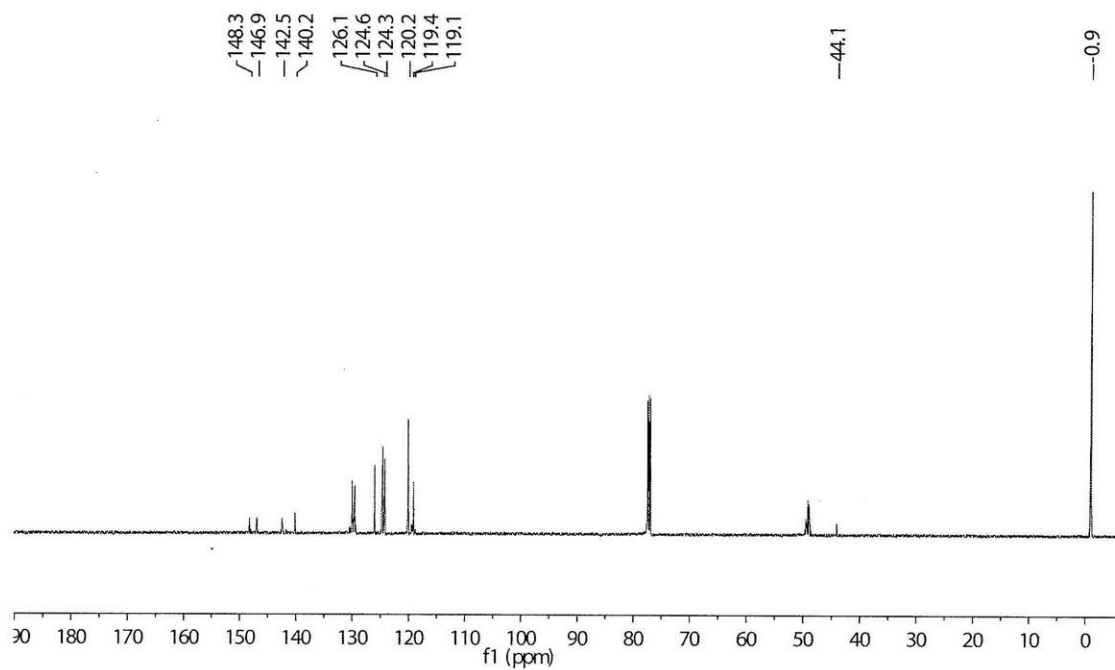


Compound 4 NMR Spectra

$^1\text{H-NMR}$, CD_3OD
500 MHz

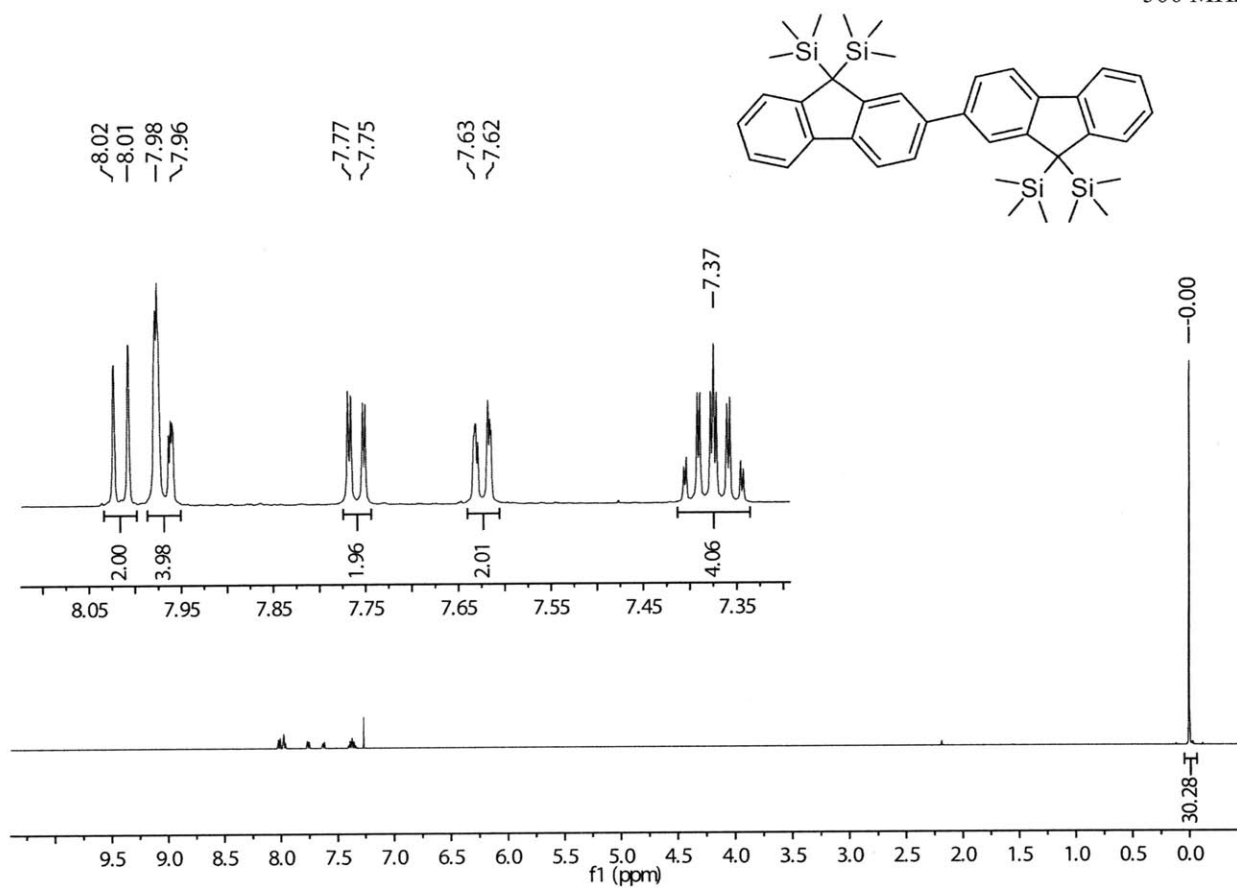


$^{13}\text{C-NMR}$, $\text{CD}_3\text{OD}/$
 CDCl_3 126 MHz

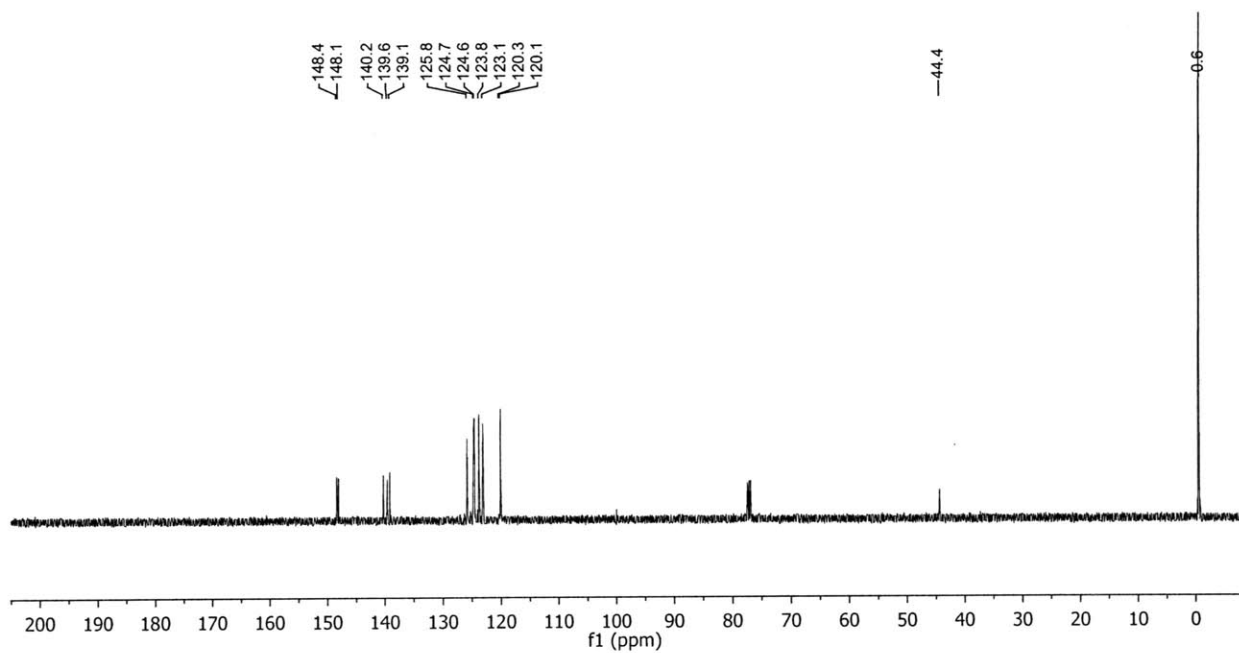


Compound 5 NMR Spectra

¹H-NMR, CDCl₃
500 MHz

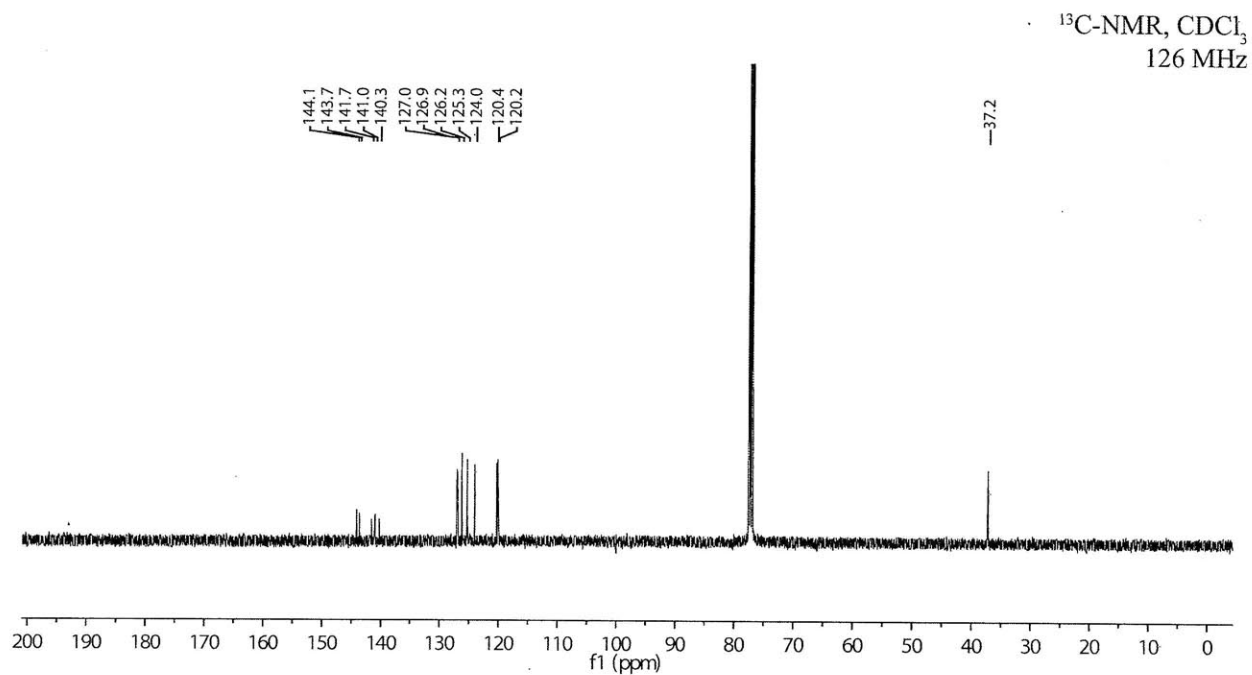
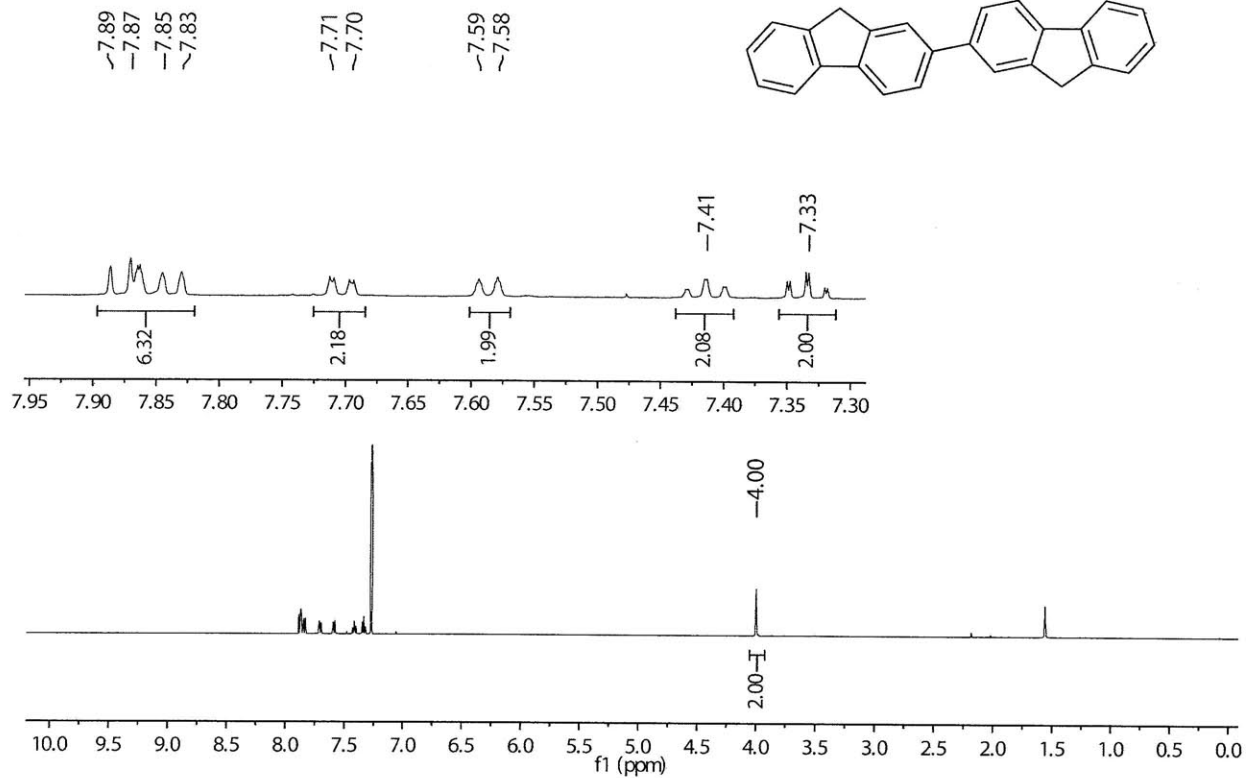


¹³C-NMR, CDCl₃
126 MHz



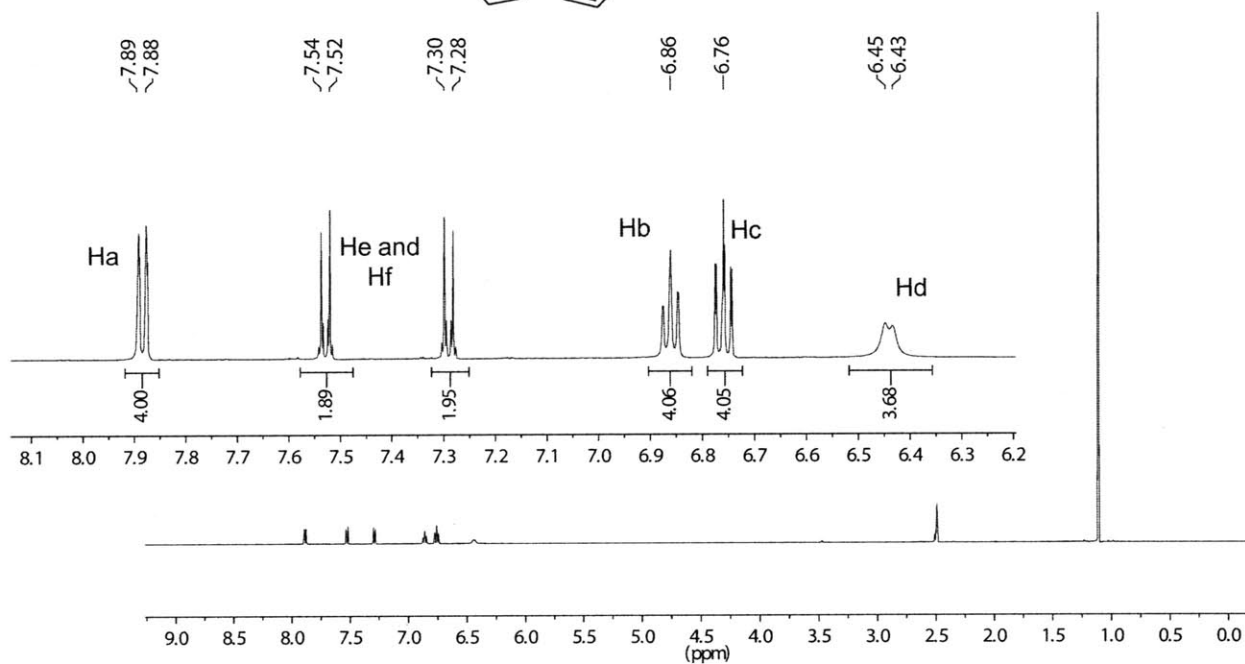
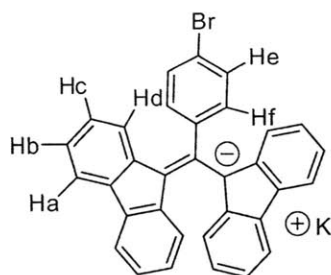
Compound 6 NMR Spectra

$^1\text{H-NMR}$, CDCl_3
500 MHz

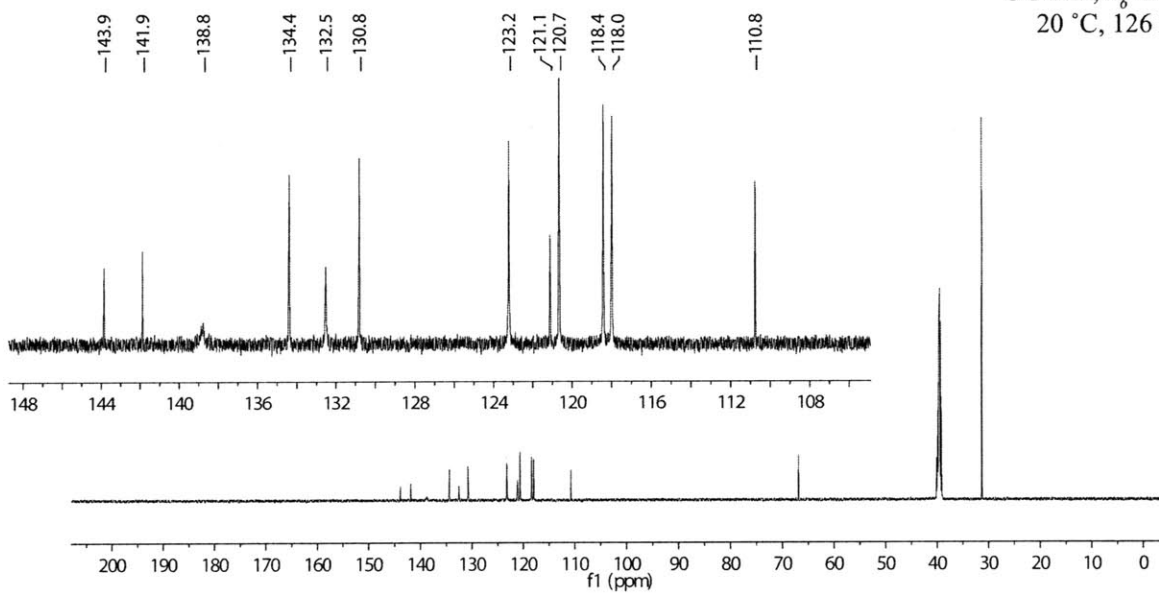


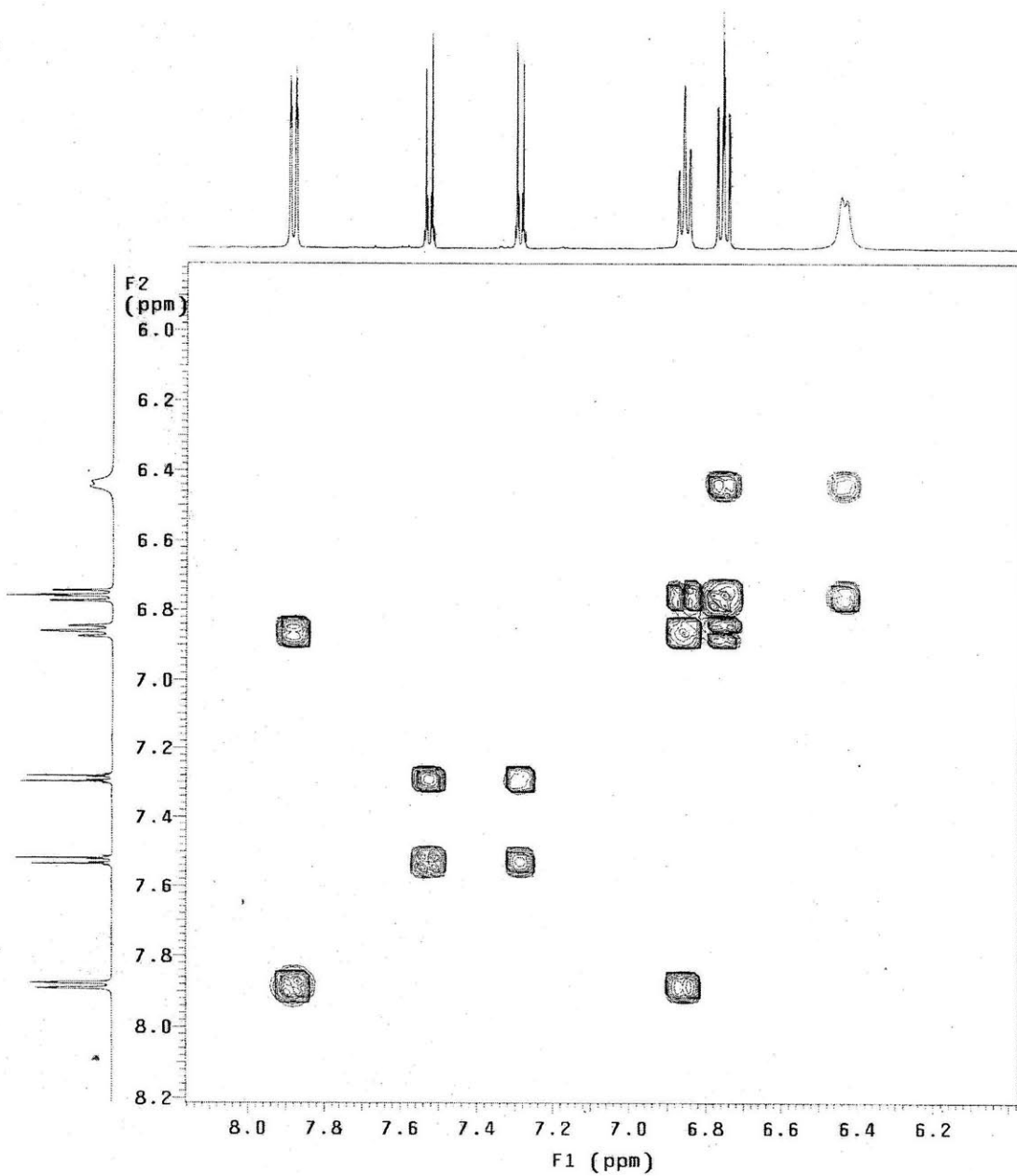
Br-BDPA NMR Spectra

$^1\text{H-NMR}$, $d_6\text{-DMSO}$
20 °C, 500 MHz



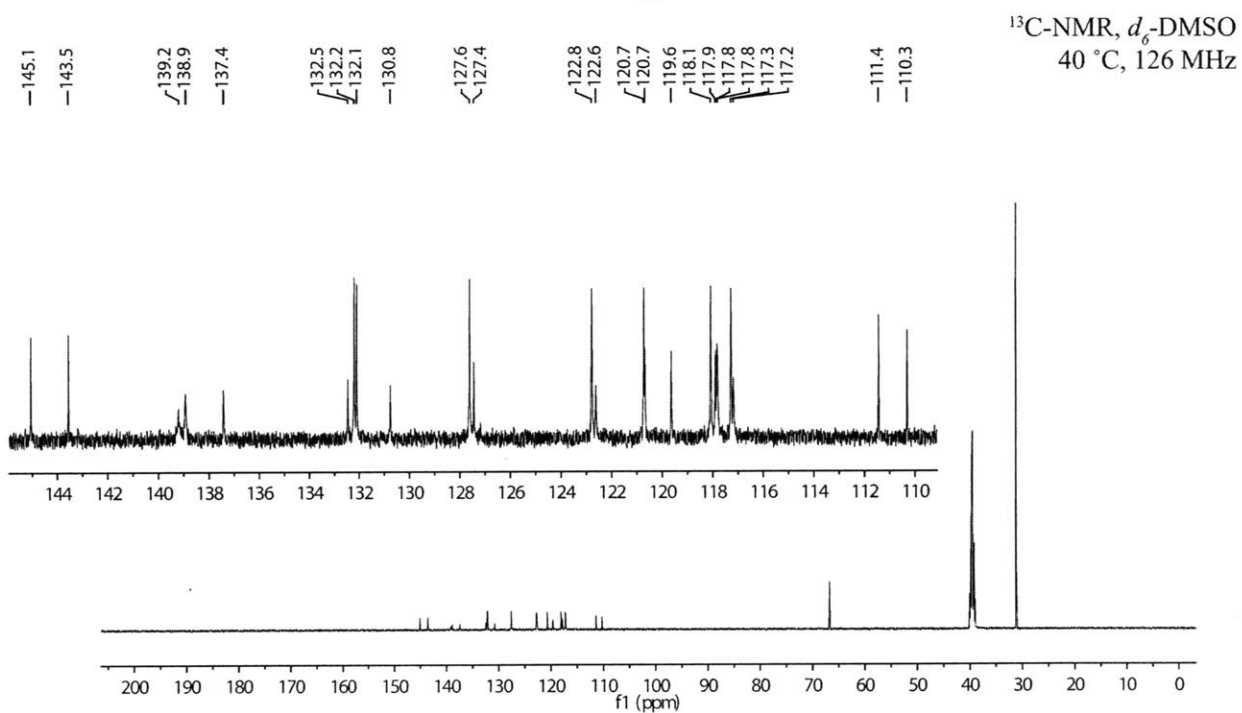
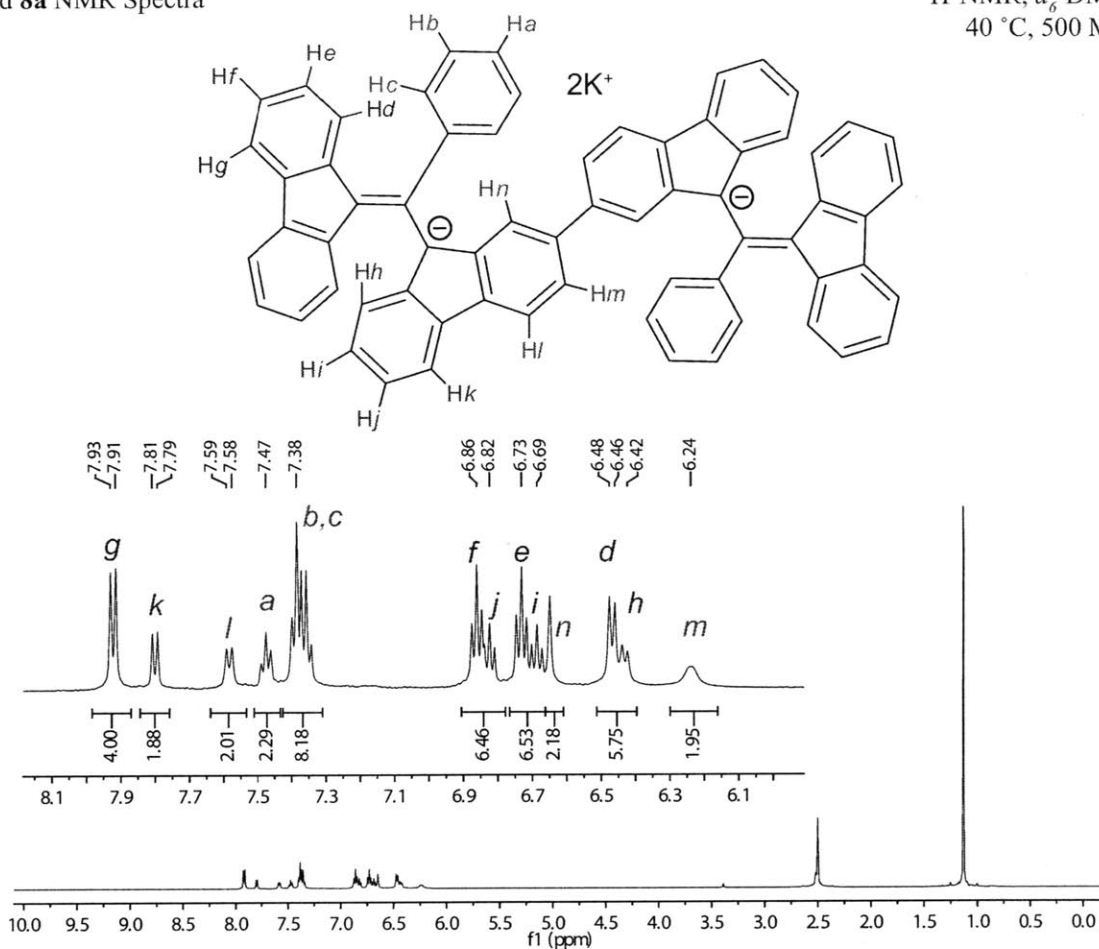
$^{13}\text{C-NMR}$, $d_6\text{-DMSO}$
20 °C, 126 MHz





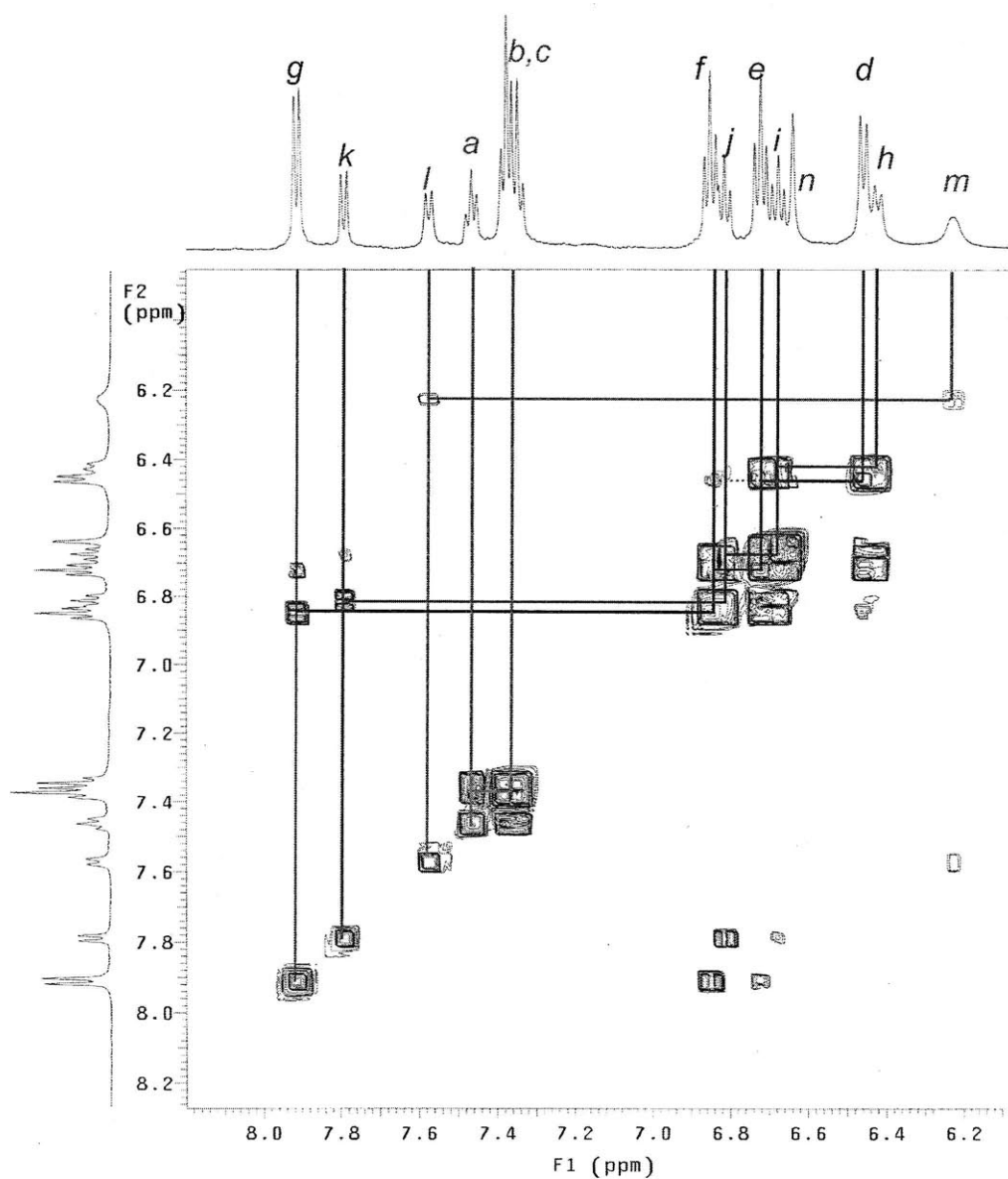
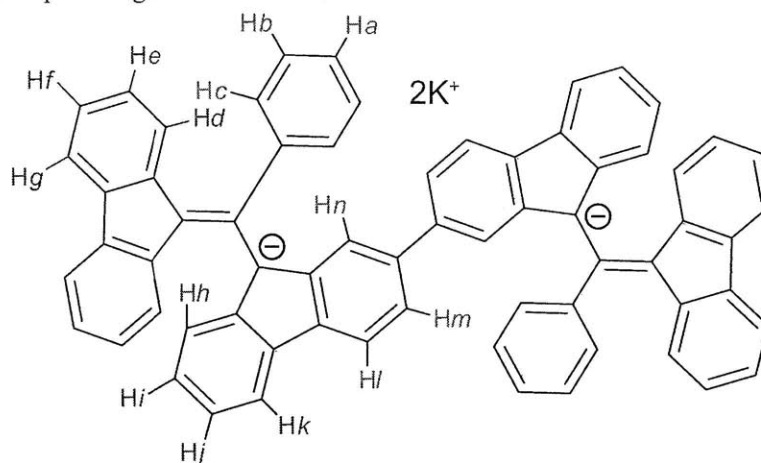
Compound **8a** NMR Spectra

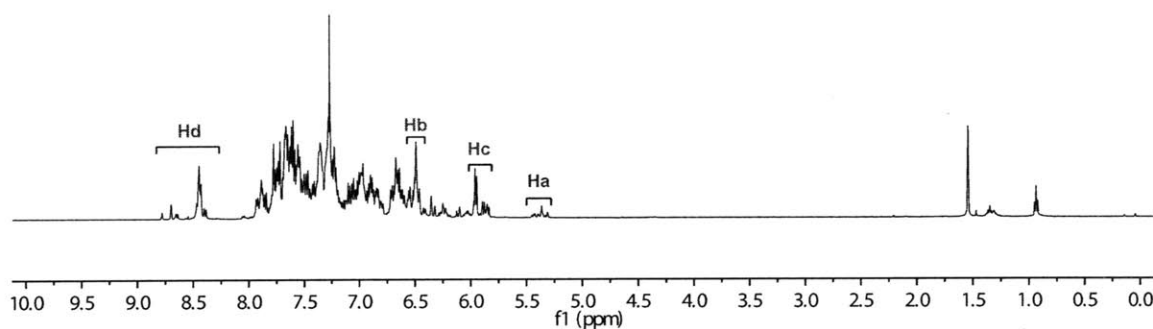
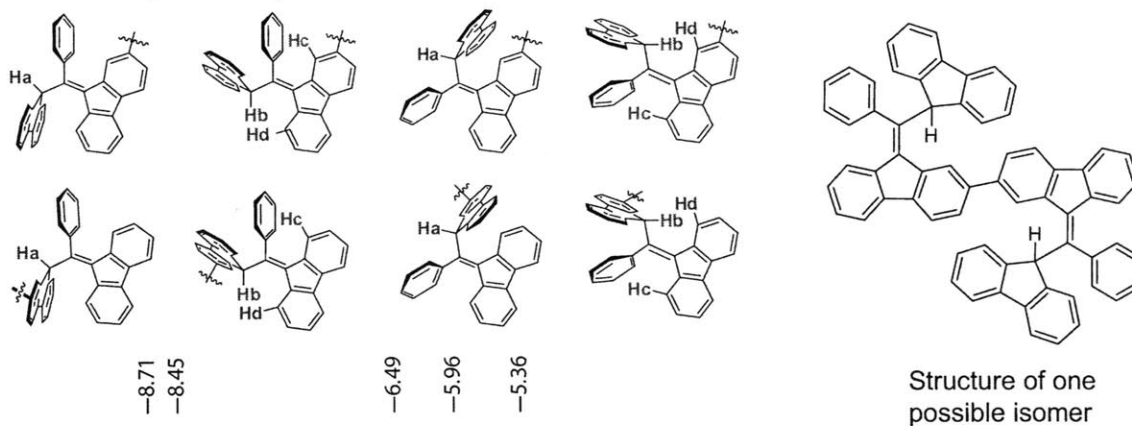
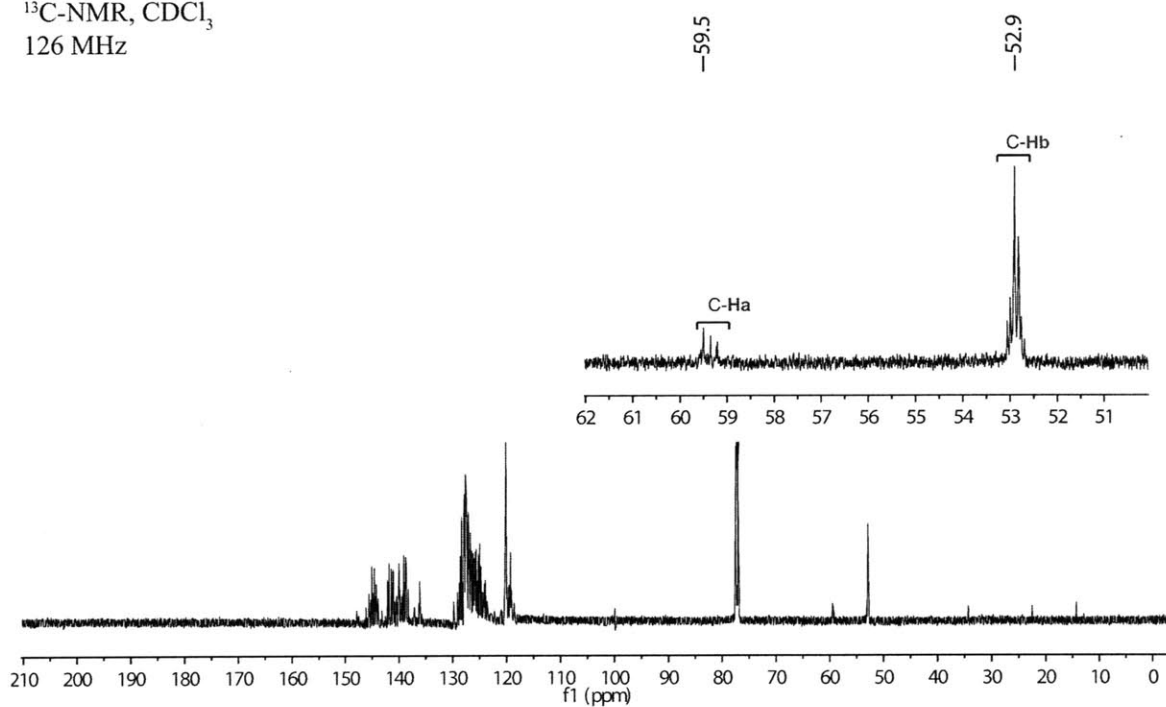
$^1\text{H-NMR}$, $d_6\text{-DMSO}$
40 °C, 500 MHz



Compound **8a** 2D-NMR Spectra - gCOSY

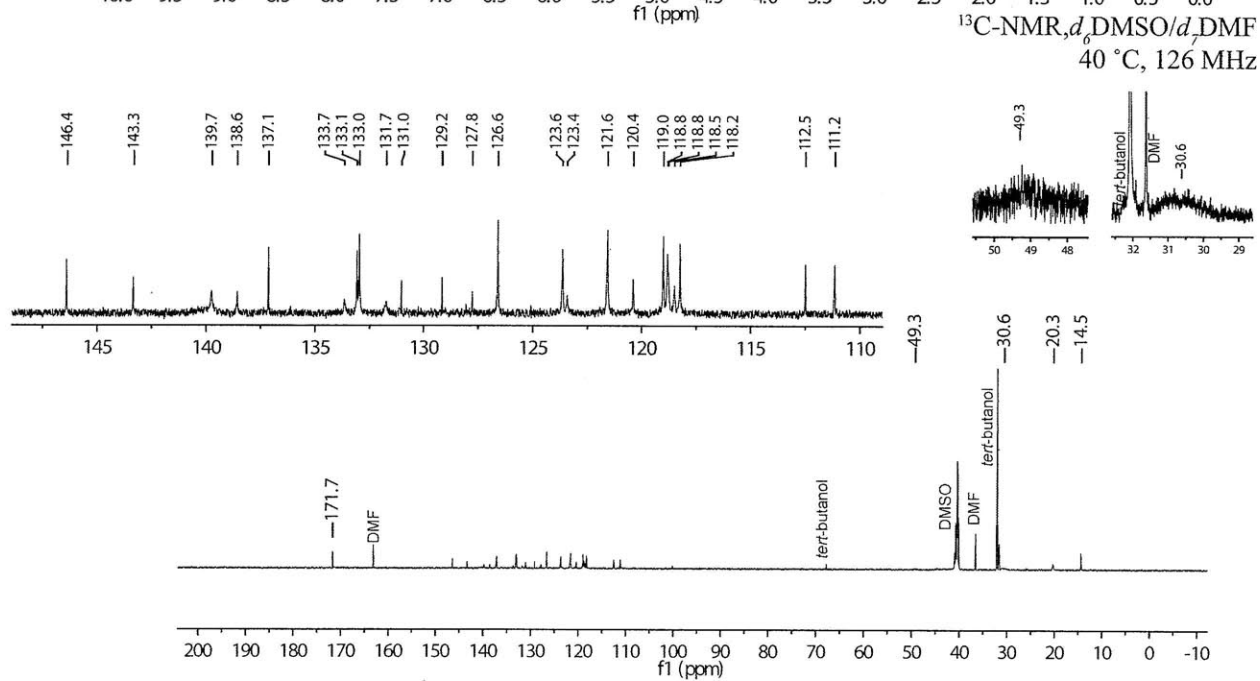
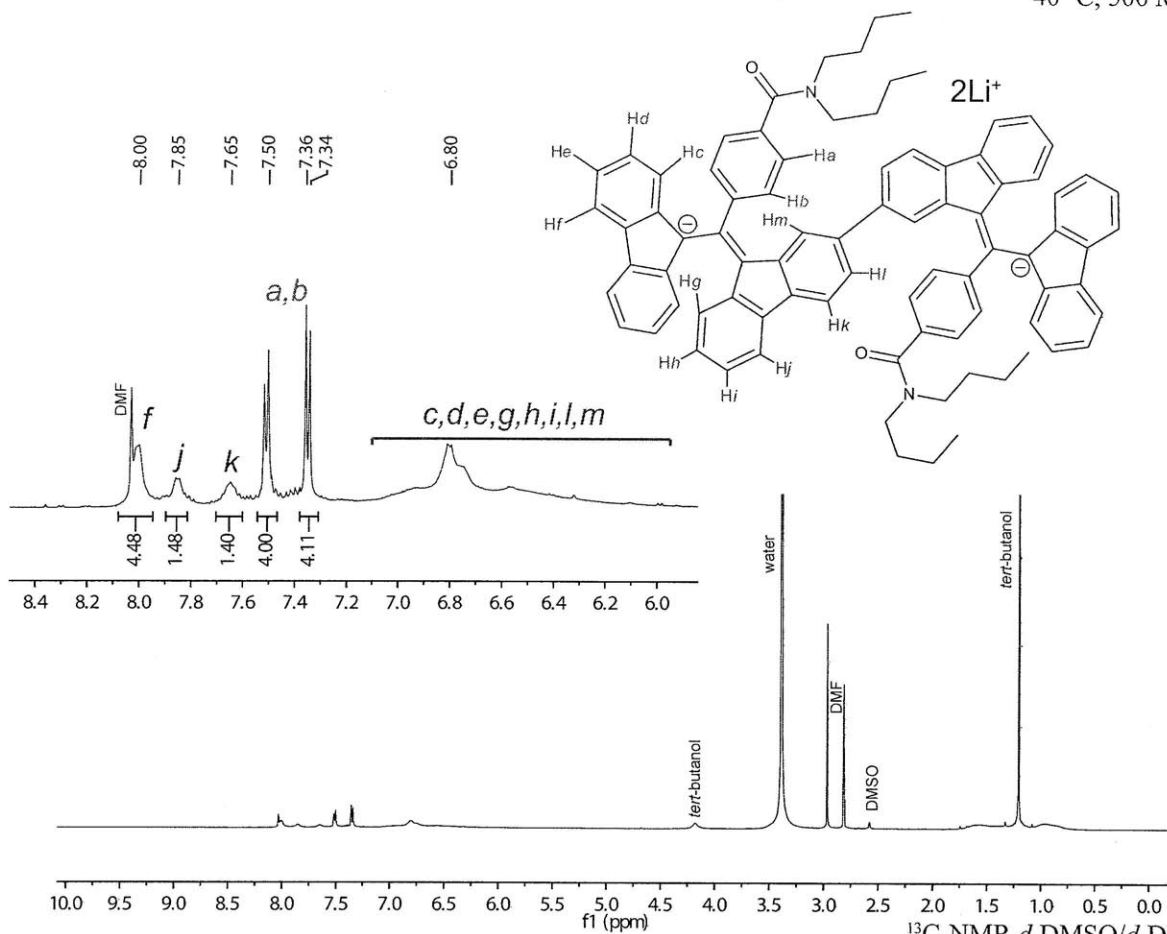
¹H-NMR, *d*₆-DMSO
40 °C, 500 MHz



General proton chemical shifts for proposed
tautomers, isomers, and rotamers $^{13}\text{C-NMR}$, CDCl_3
126 MHz

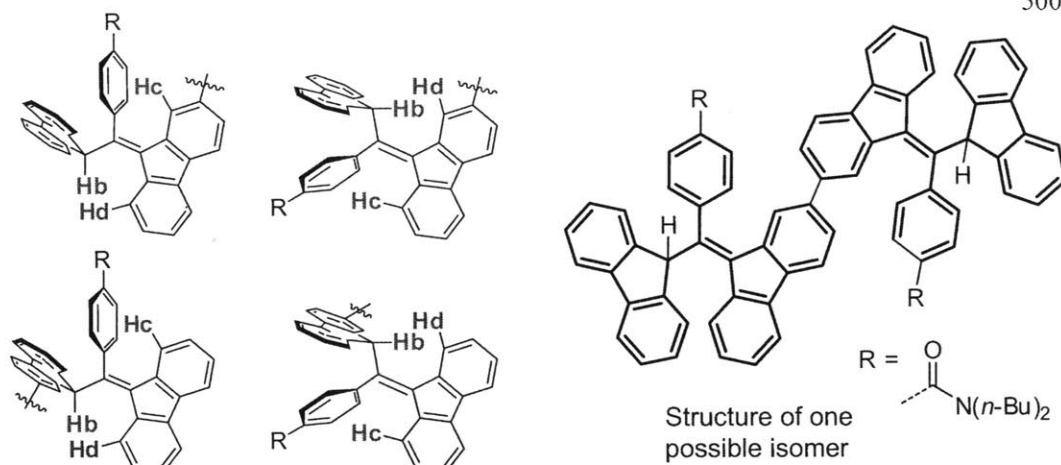
Compound **9a** NMR Spectra

$^1\text{H-NMR}$, d_6 -DMSO/ d_7 -DMF
40 °C, 500 MHz

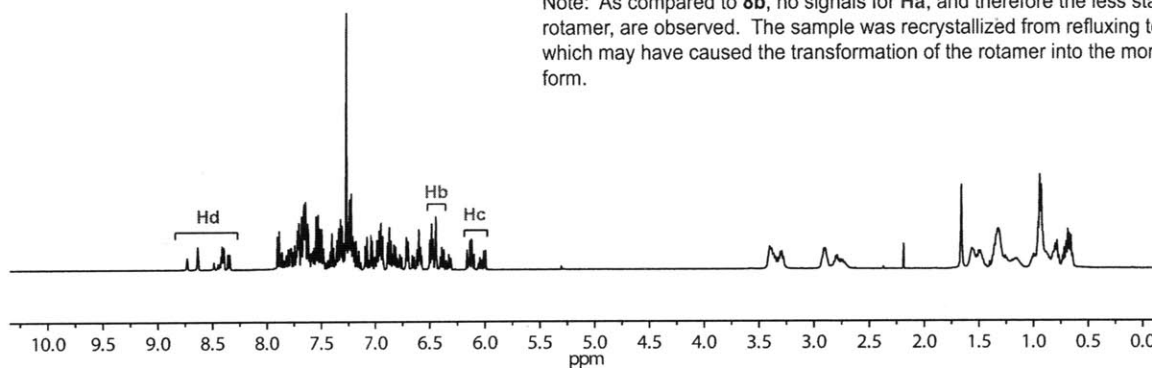


Compound **9c** NMR Spectra

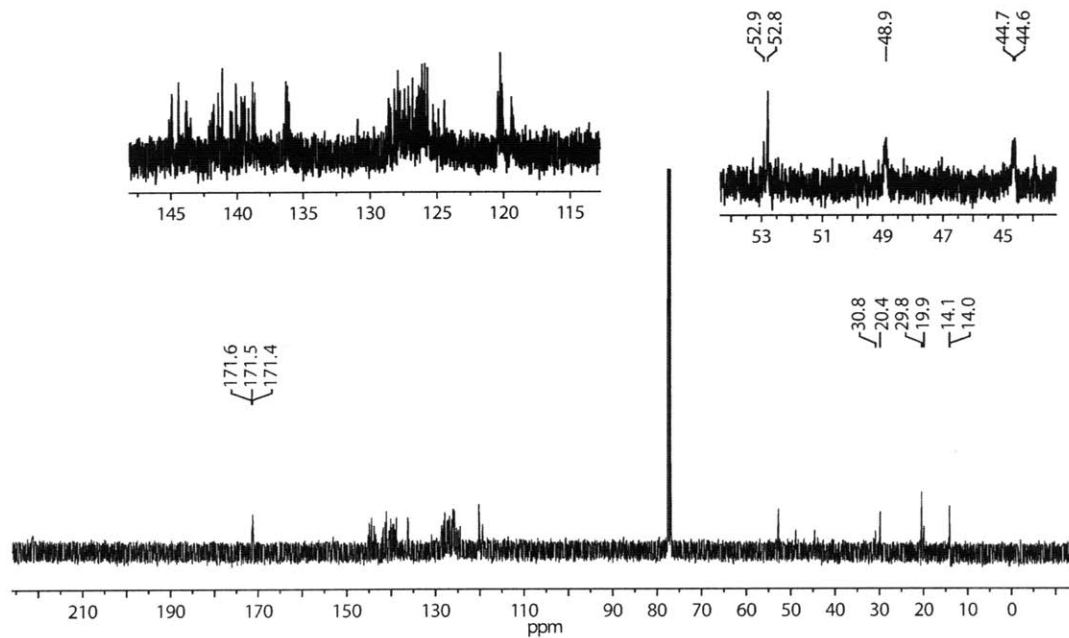
$^1\text{H-NMR}$, CDCl_3
500 MHz



Note: As compared to **8b**, no signals for Ha, and therefore the less stable rotamer, are observed. The sample was recrystallized from refluxing toluene, which may have caused the transformation of the rotamer into the more stable form.

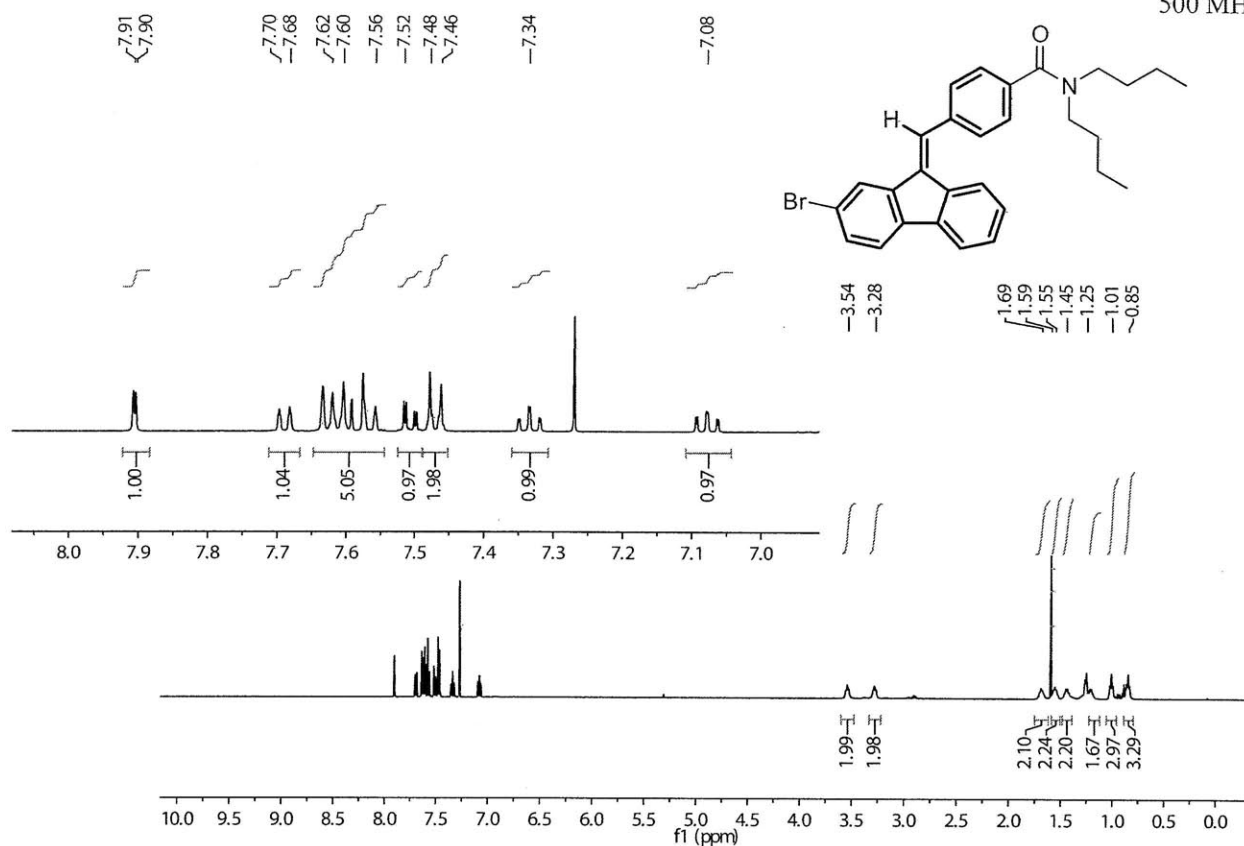


$^{13}\text{C-NMR}$, CDCl_3
126 MHz

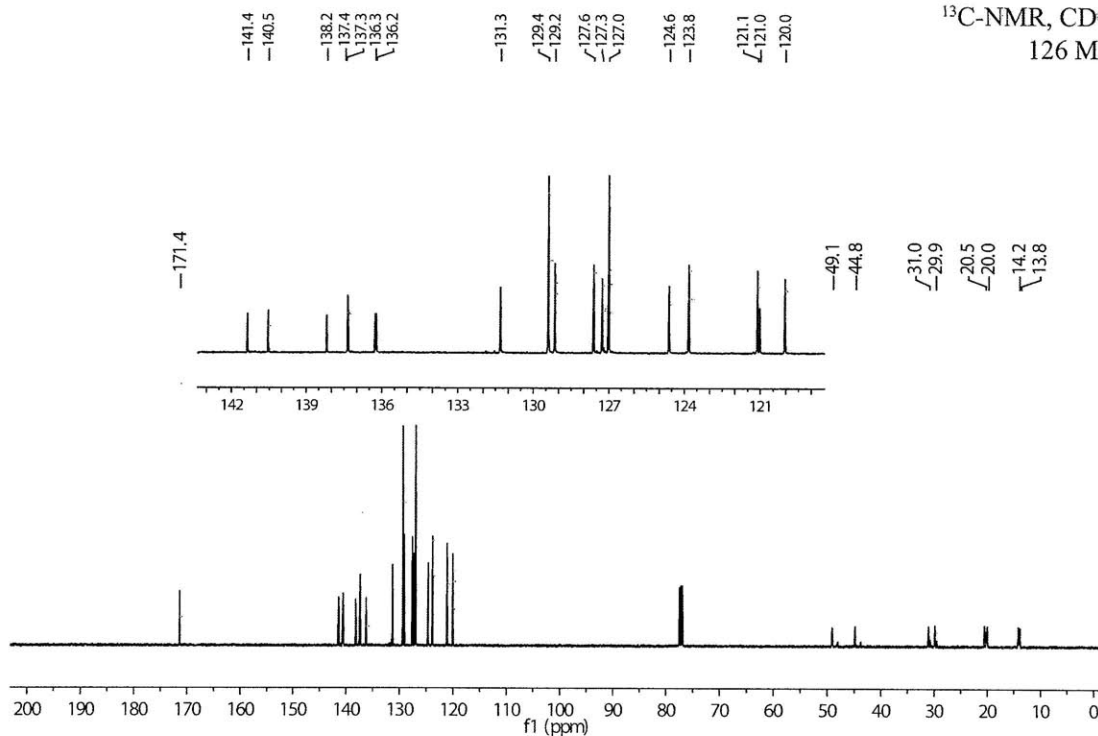


Compound **10-E** NMR Spectra

¹H-NMR, CDCl₃
500 MHz

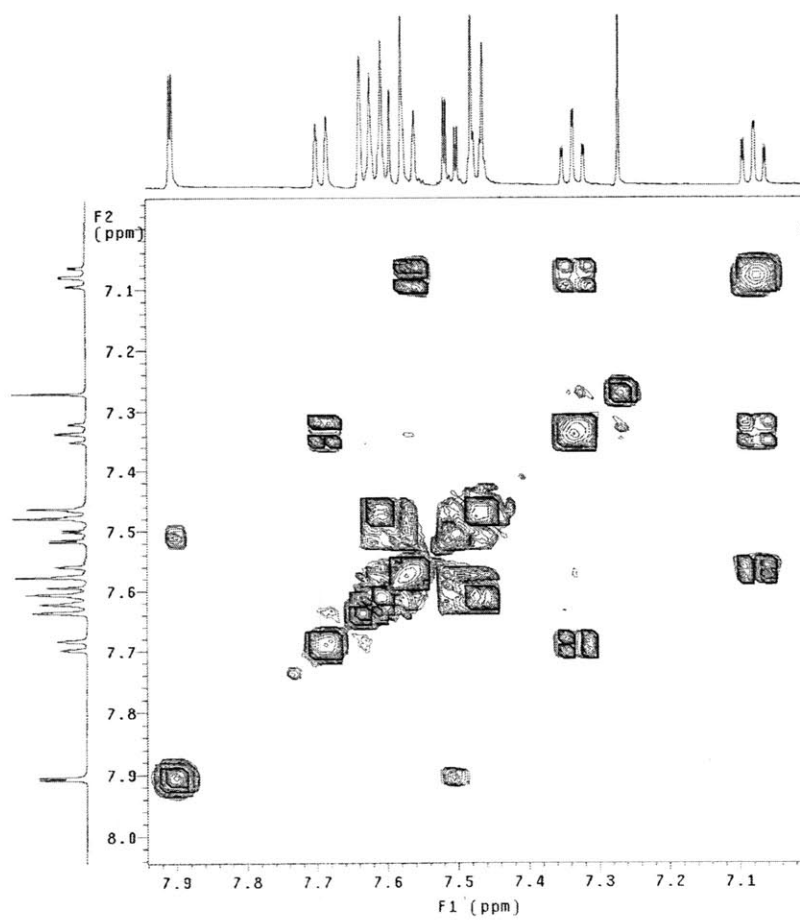
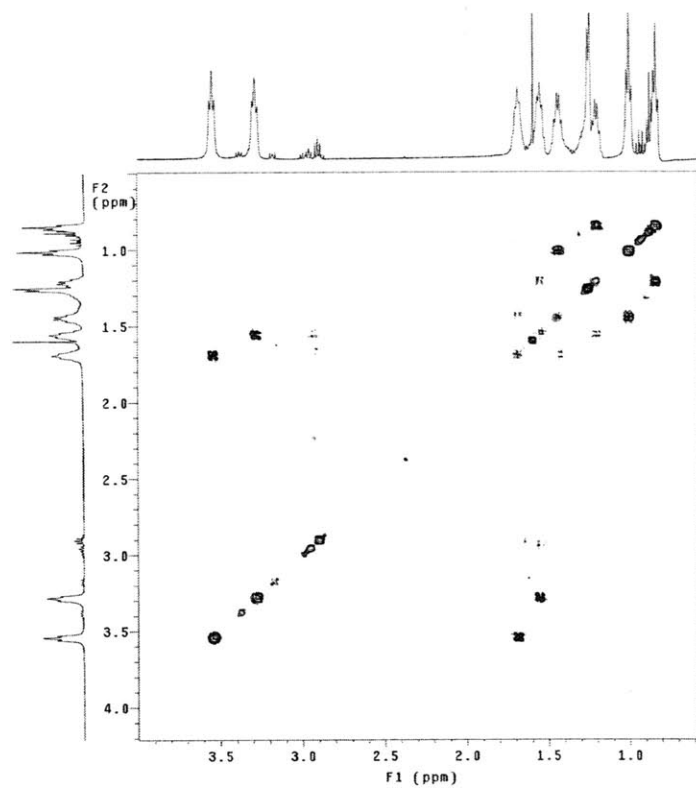


¹³C-NMR, CDCl₃
126 MHz

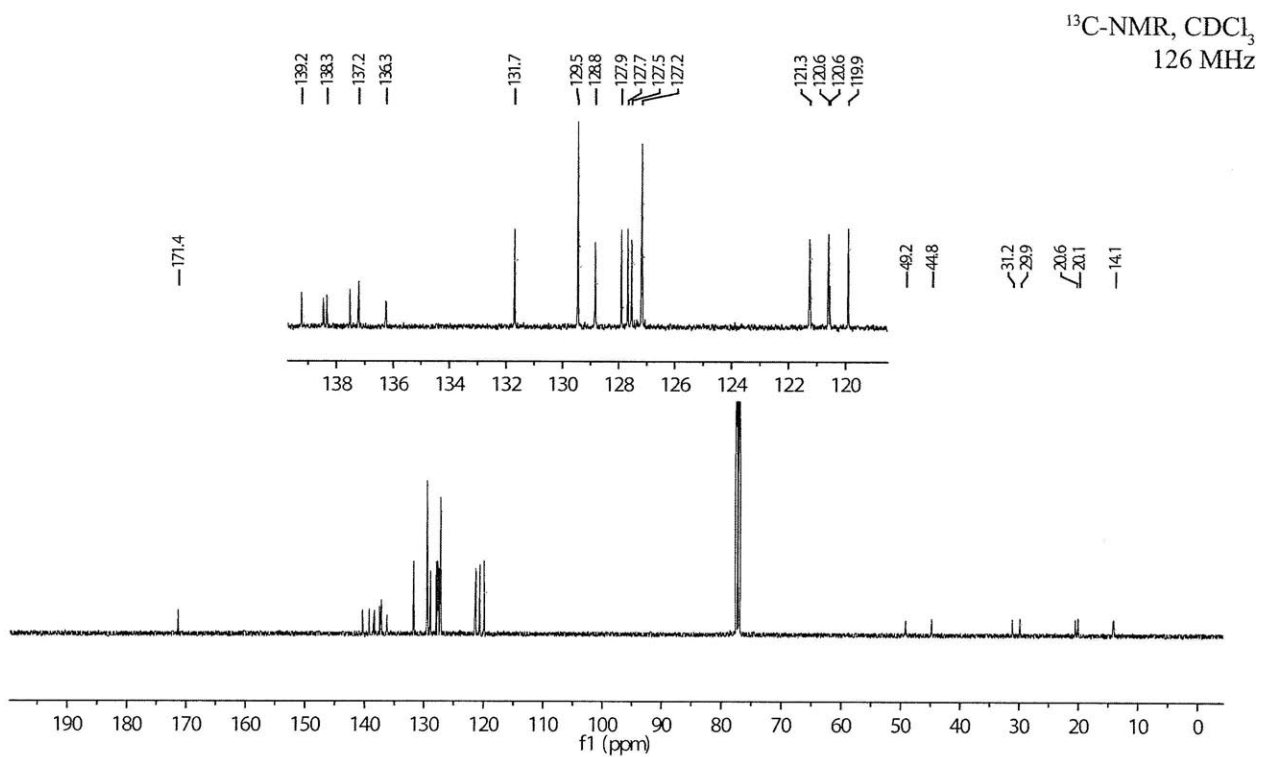
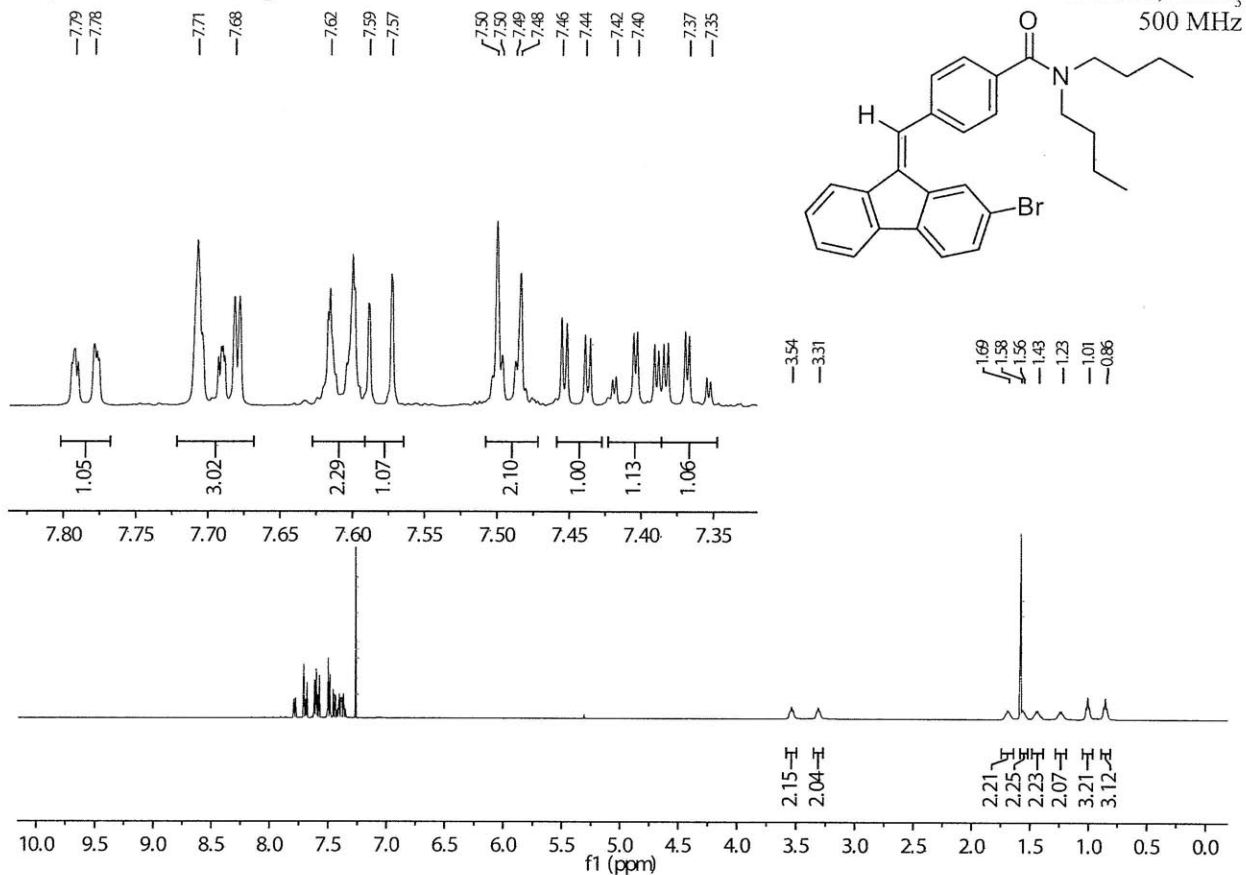


Compound 10-E 2D-NMR Spectra - gCOSY

$^1\text{H-NMR}$, CDCl_3
500 MHz

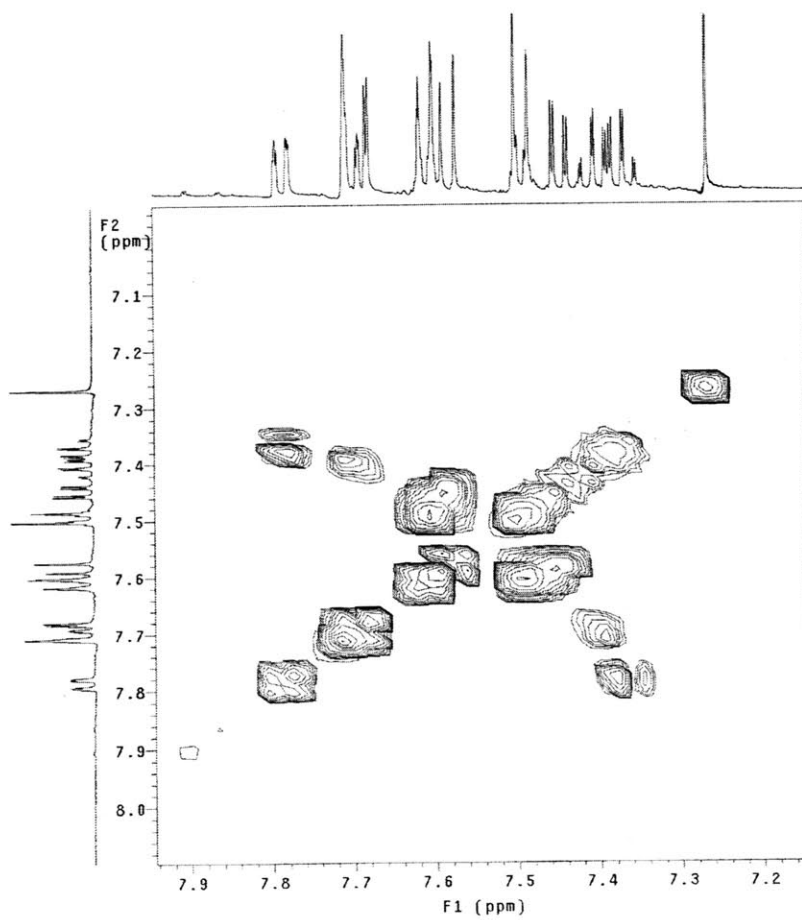
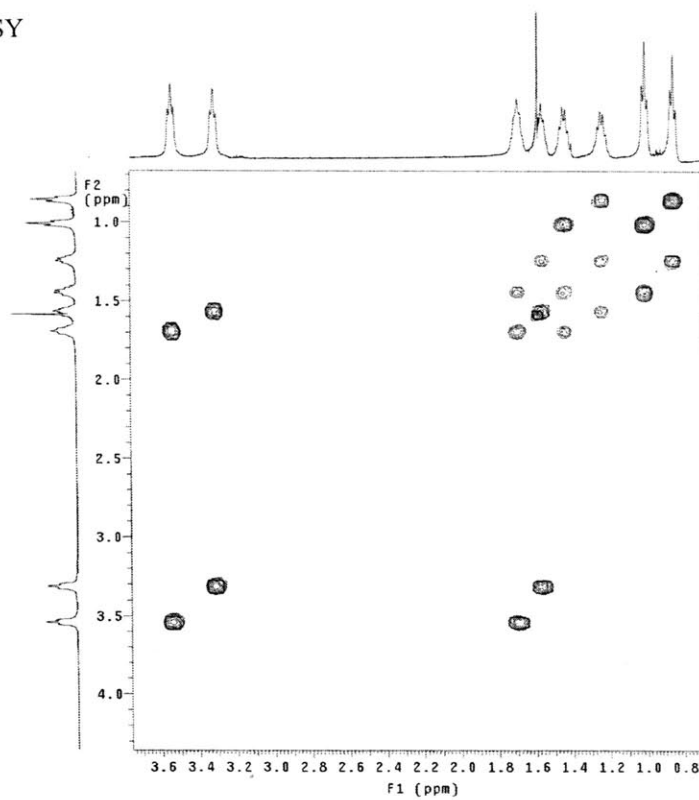


Compound **10-Z** NMR Spectra

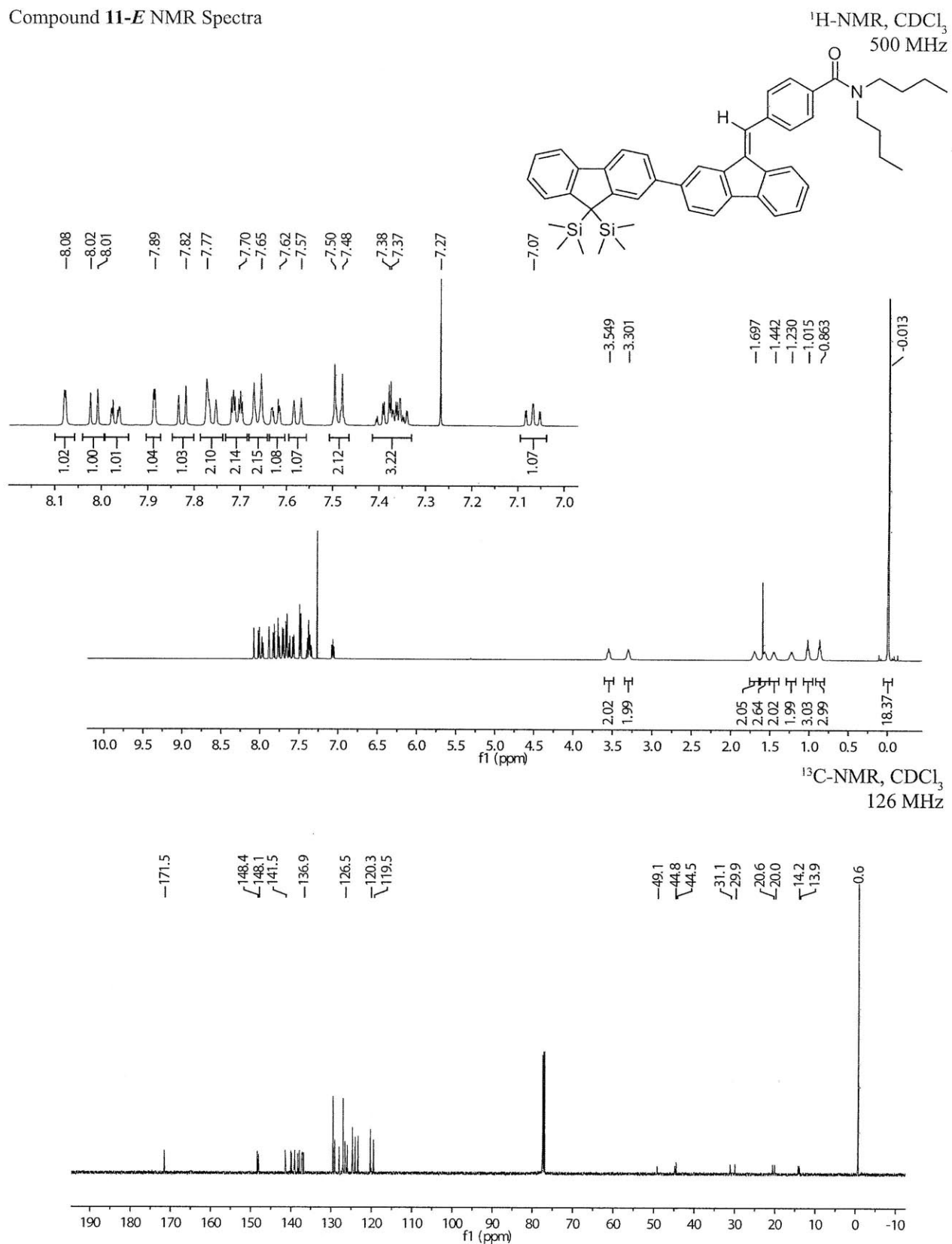


Compound **10-Z** 2D-NMR Spectra - gCOSY

$^1\text{H-NMR}$, CDCl_3
500 MHz

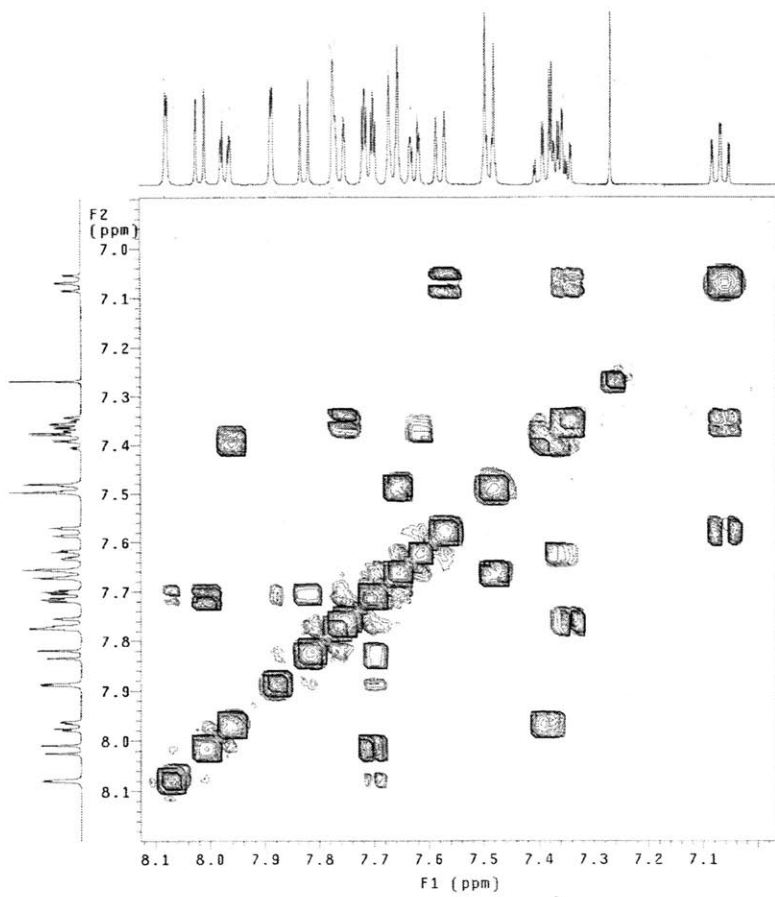
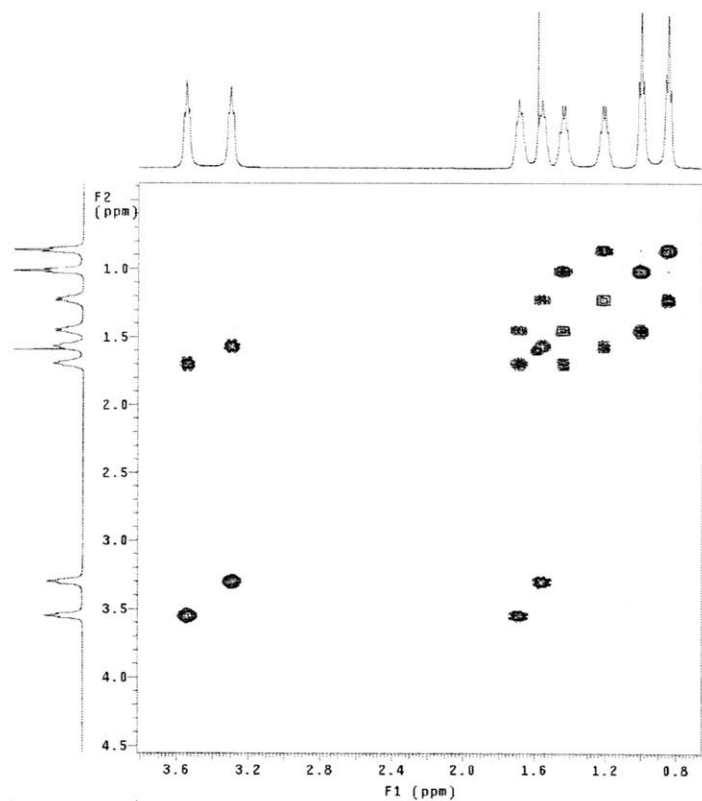


Compound **11-E** NMR Spectra



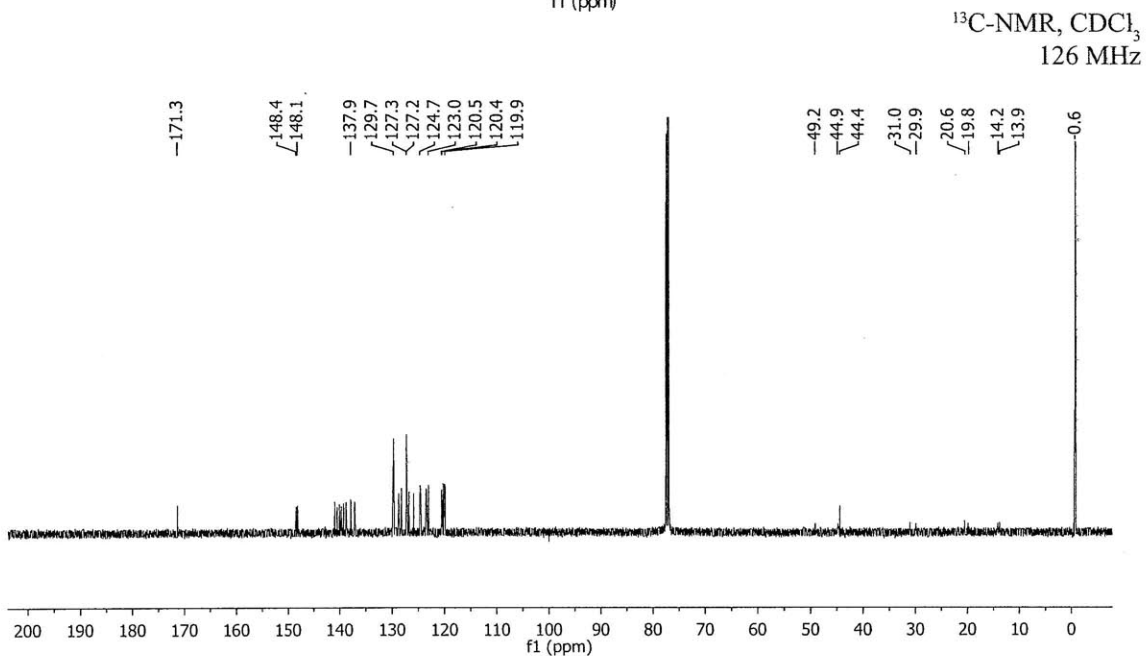
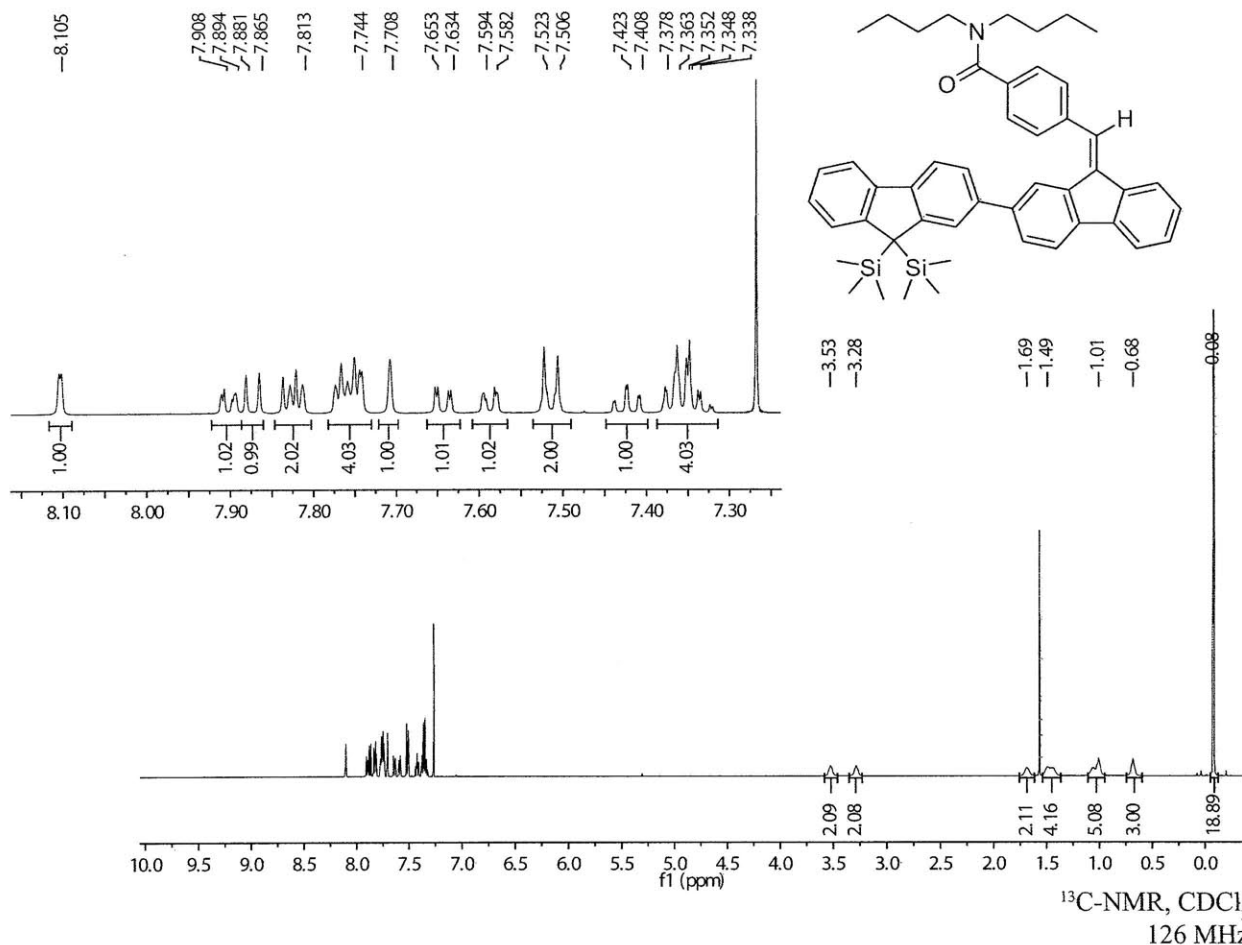
Compound **11-E** 2D-NMR Spectra - gCOSY

$^1\text{H-NMR}$, CDCl_3
500 MHz



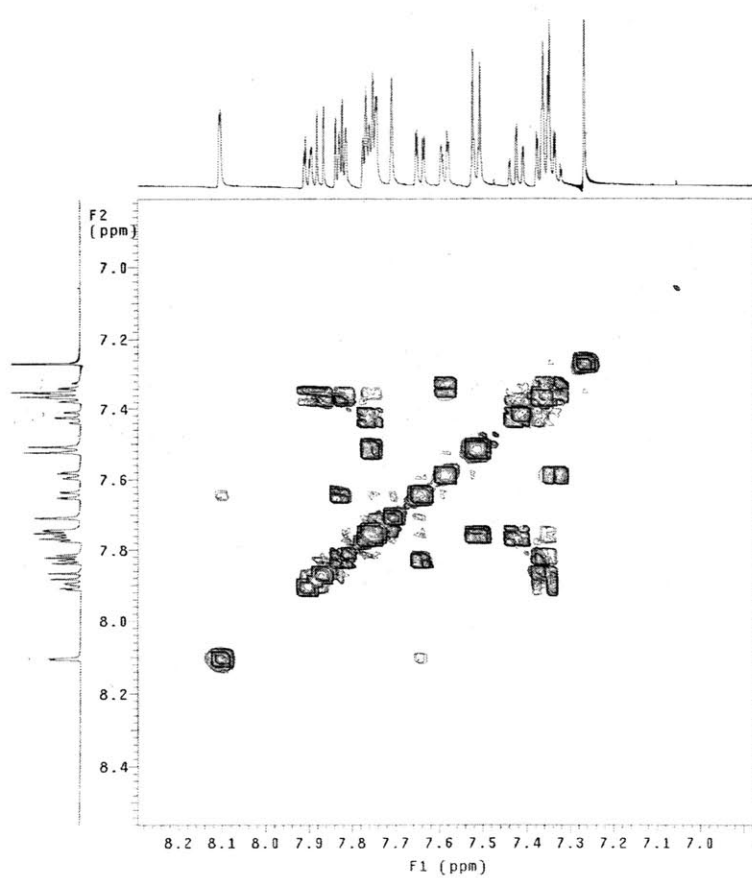
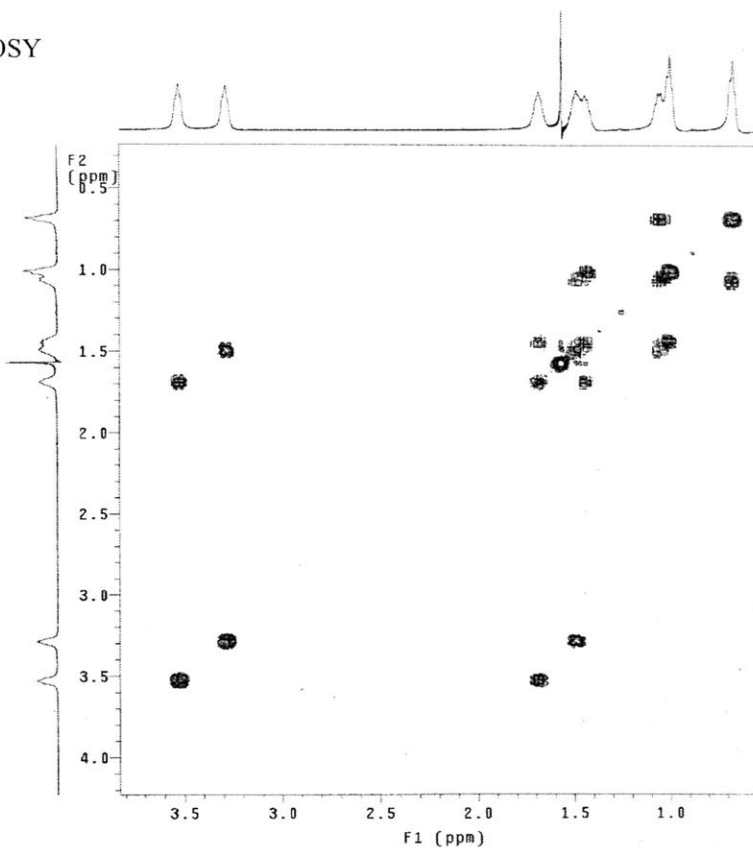
Compound **11-Z** NMR Spectra

$^1\text{H-NMR}$, CDCl_3
500 MHz



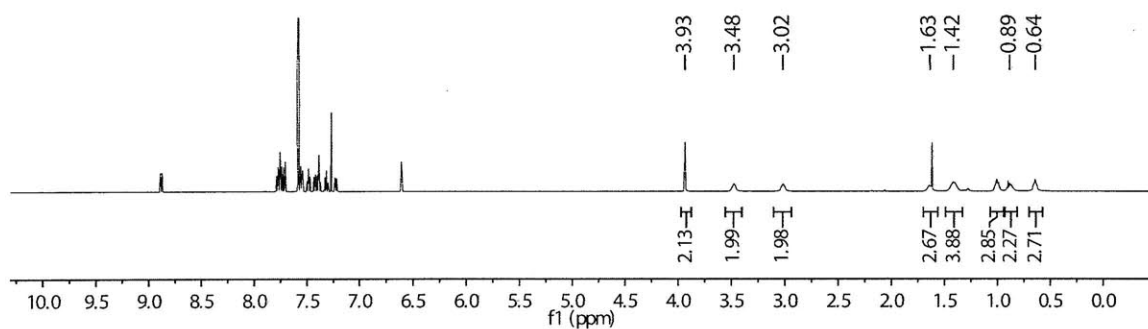
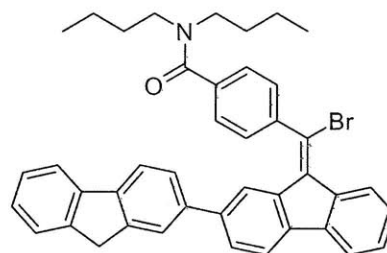
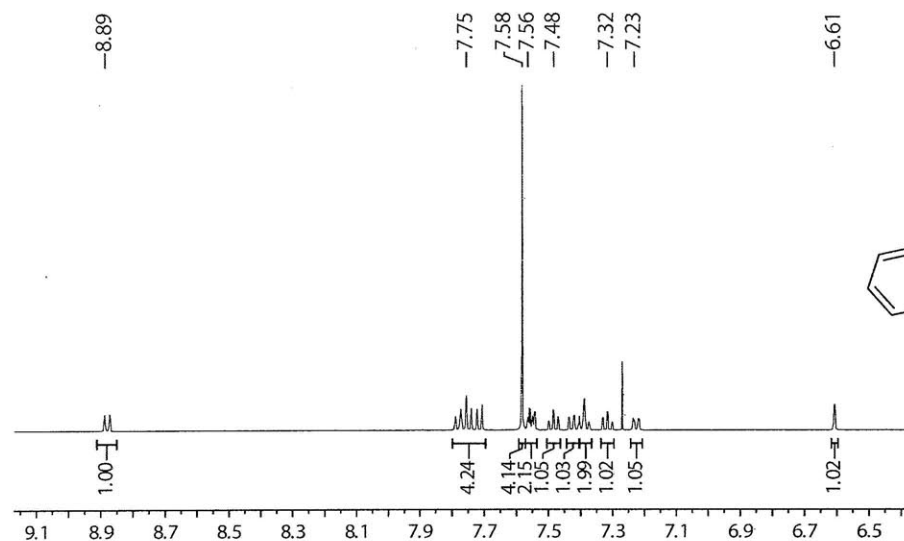
Compound 11-Z 2D-NMR Spectra - gCOSY

$^1\text{H-NMR}$, CDCl_3
500 MHz

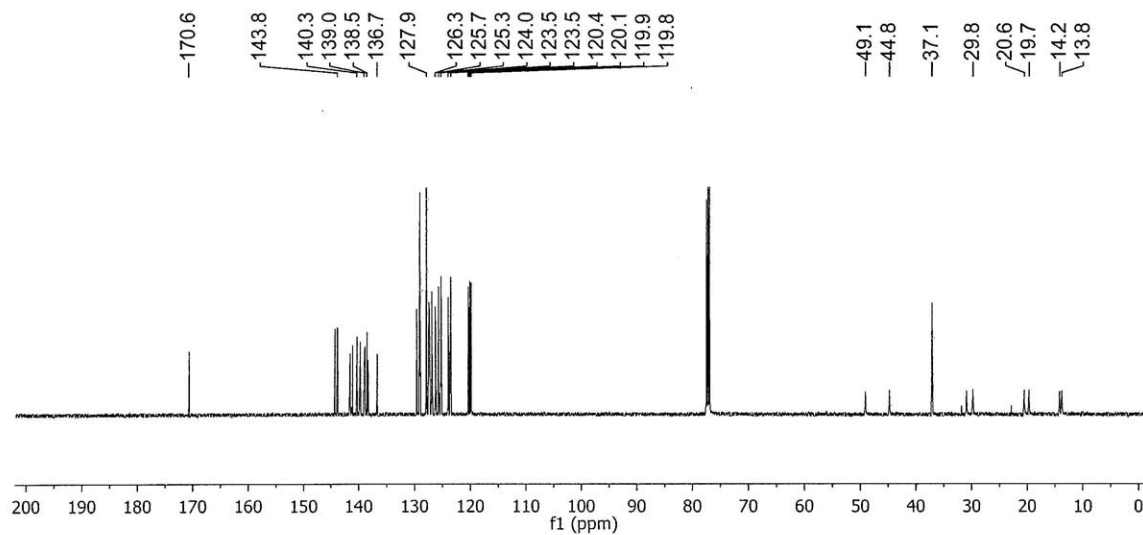


Compound **12-E** NMR Spectra

¹H-NMR, CDCl₃
500 MHz

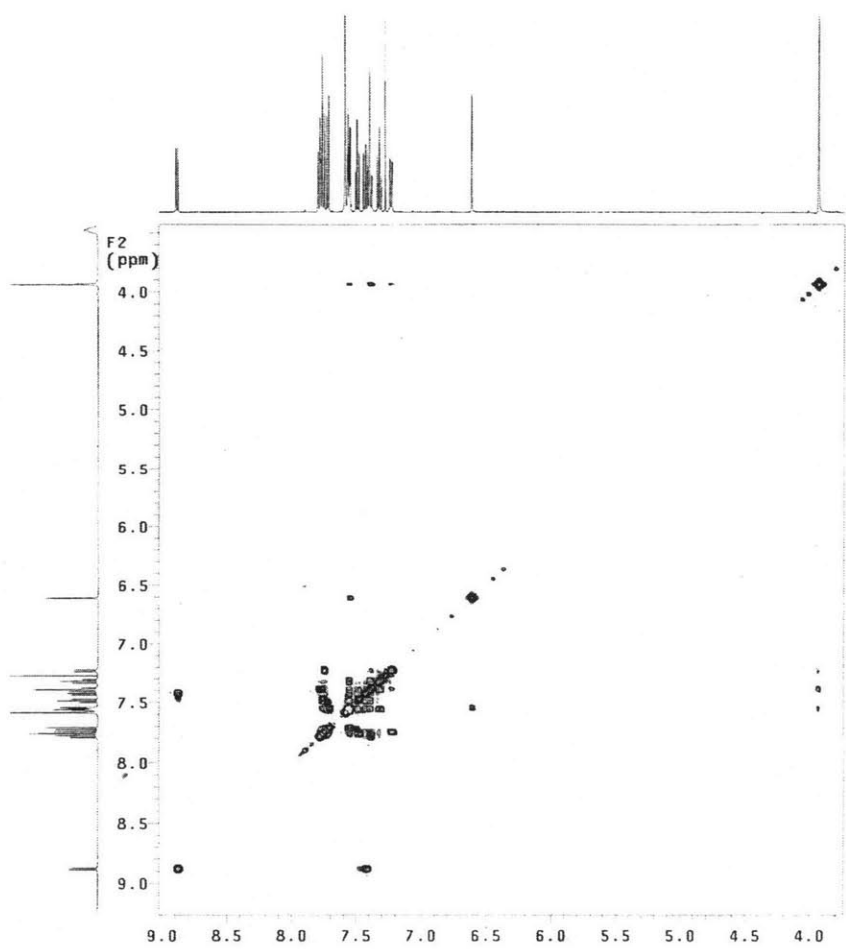
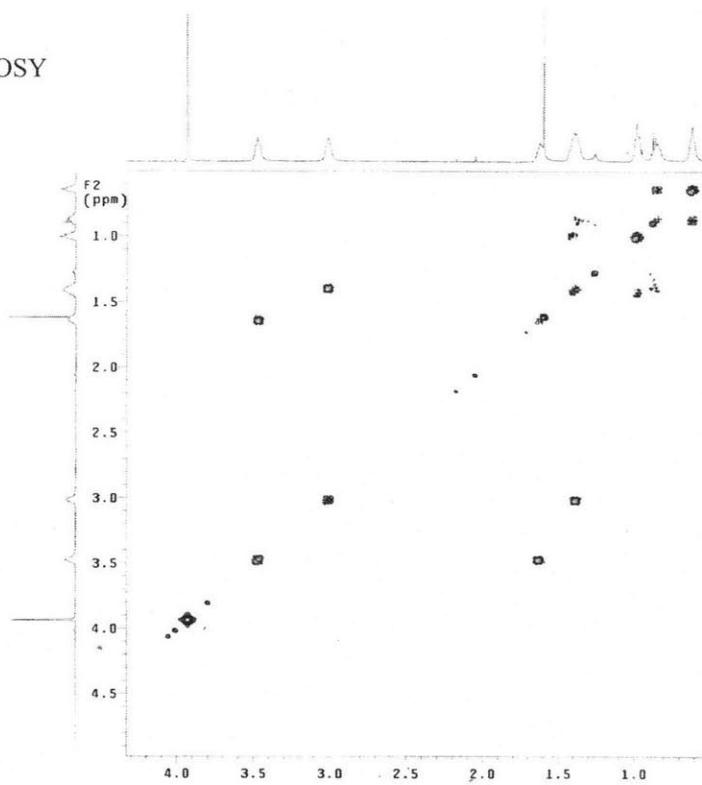


¹³C-NMR, CDCl₃
126 MHz



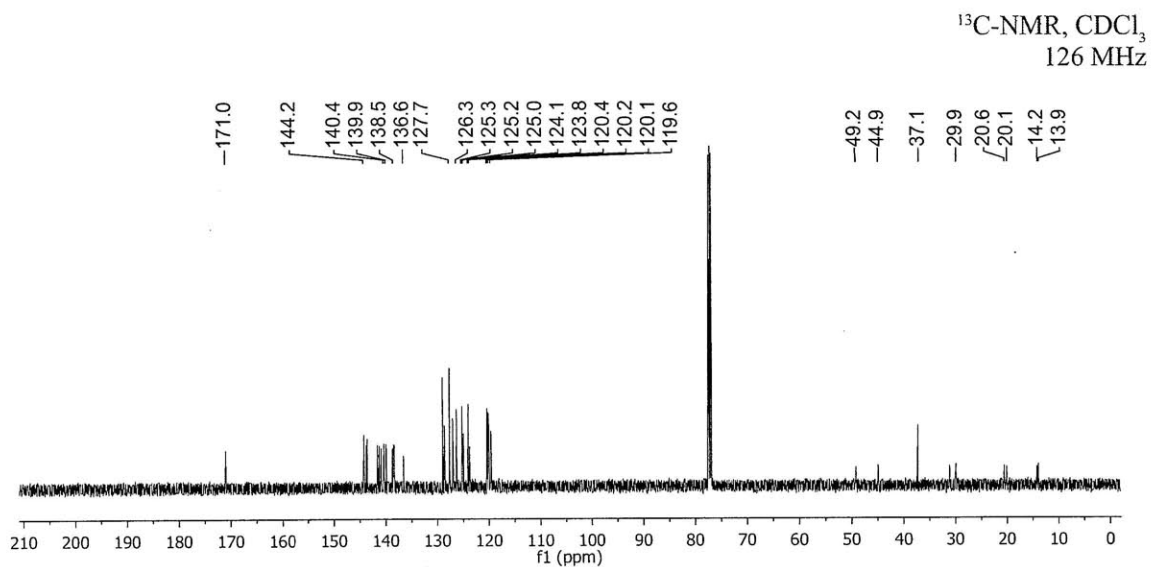
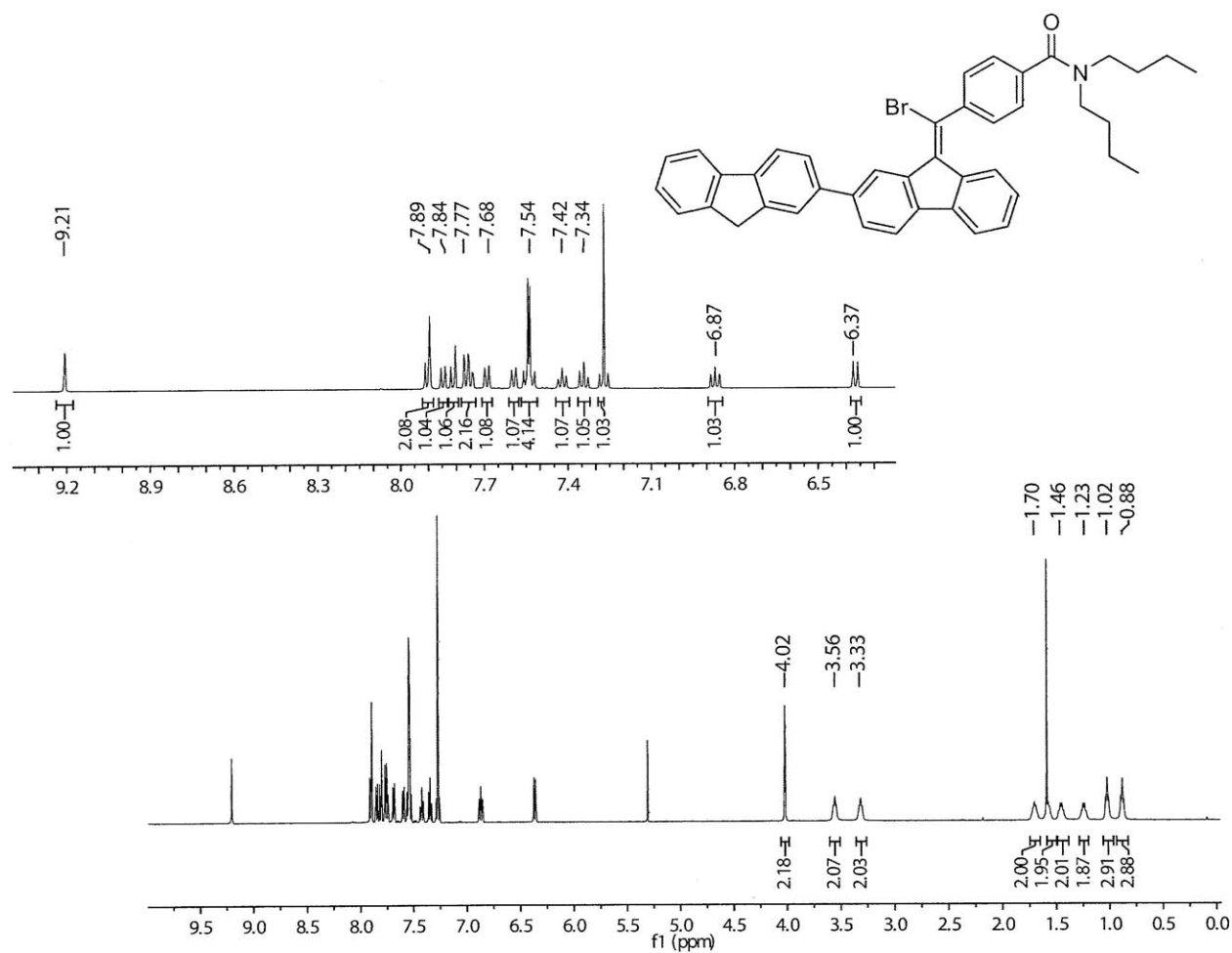
Compound **12-E** 2D-NMR Spectra - gCOSY

$^1\text{H-NMR}$, CDCl_3
500 MHz



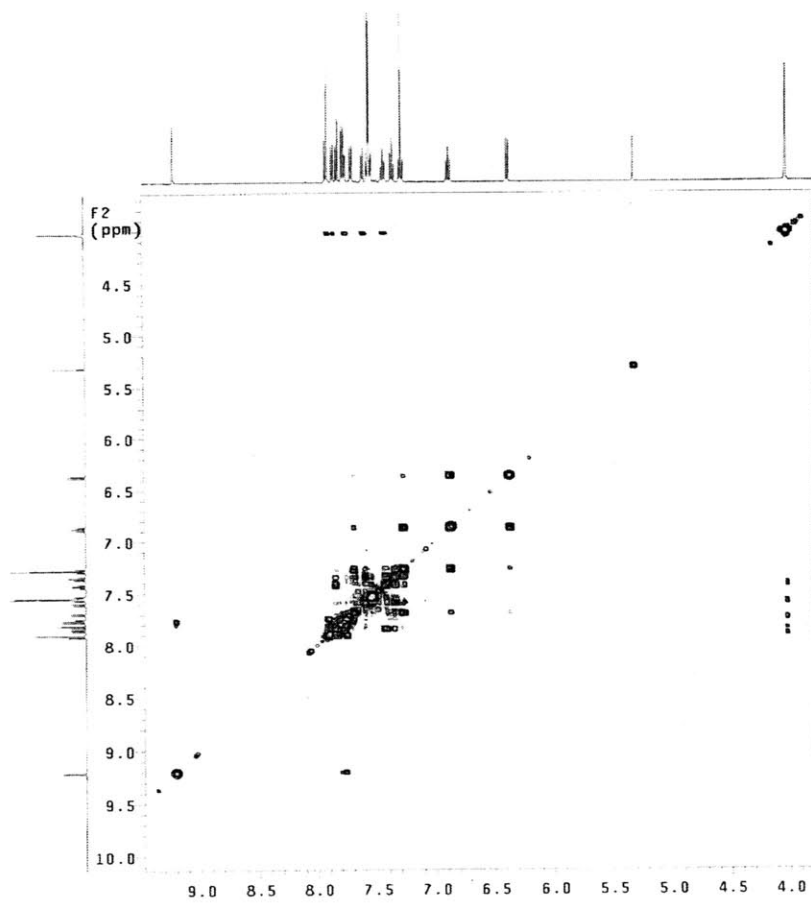
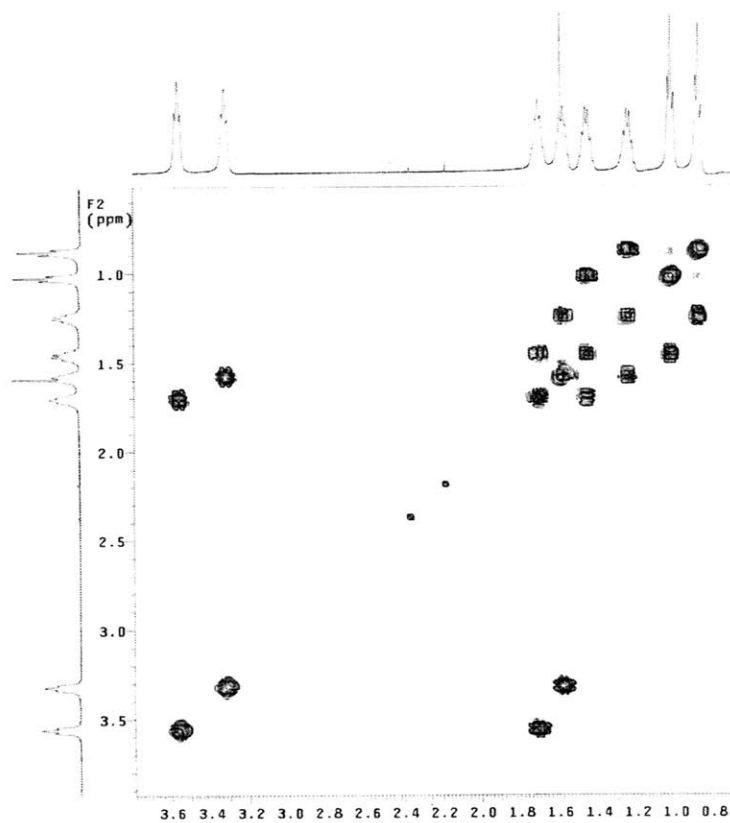
Compound 12-Z NMR Spectra

¹H-NMR, CDCl₃
500 MHz

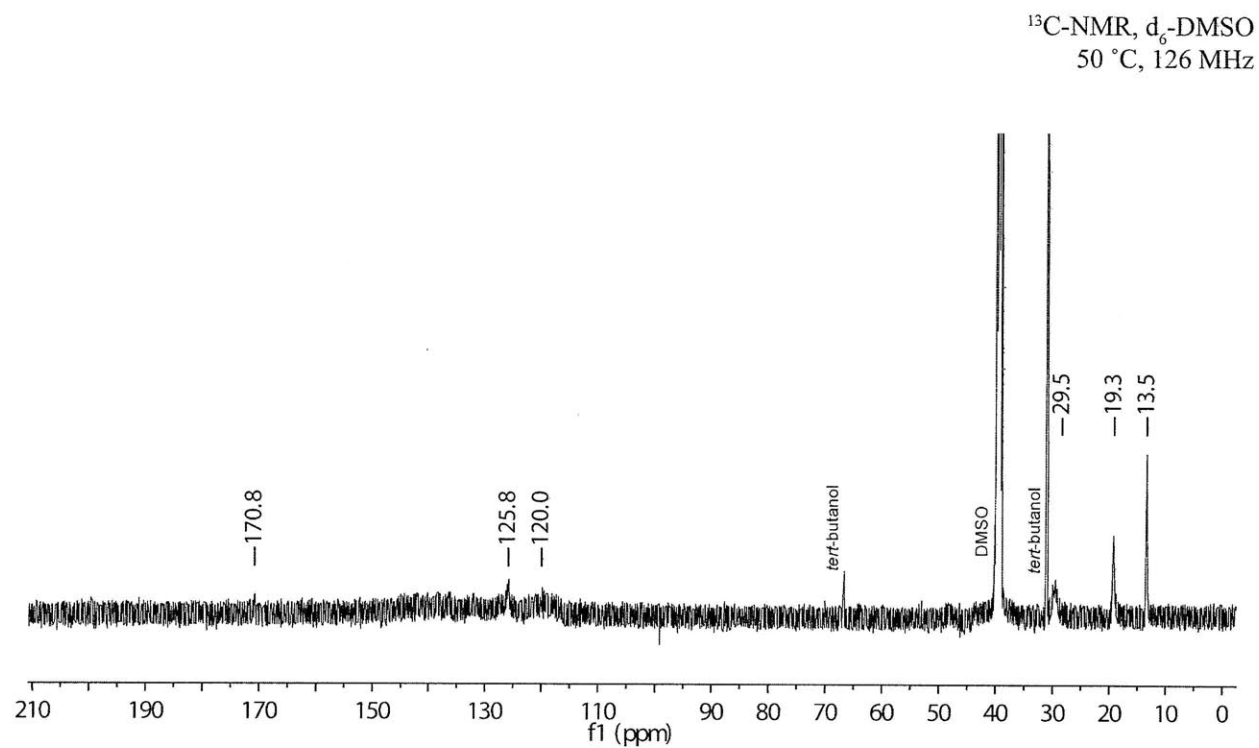
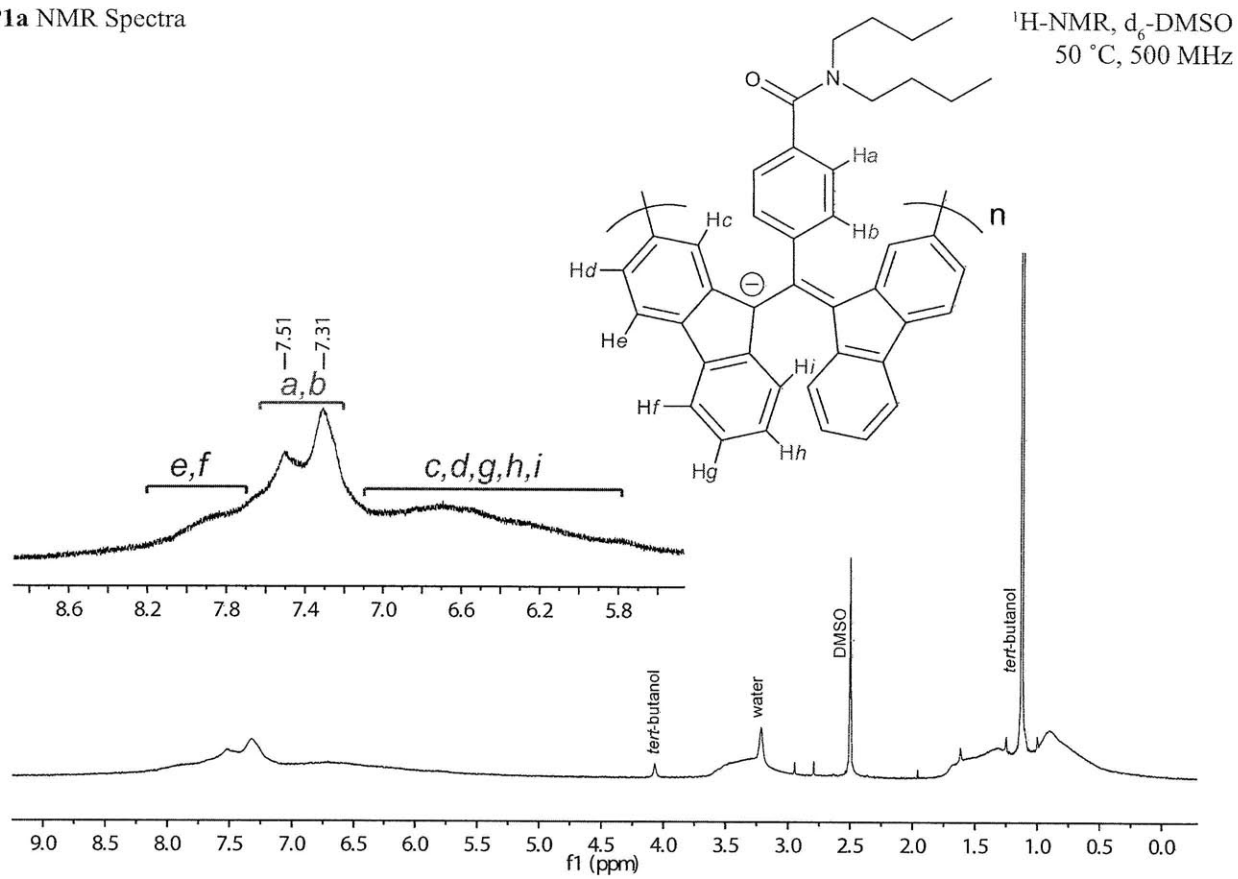


Compound 12-Z 2D-NMR Spectra - gCOSY

$^1\text{H-NMR}$, CDCl_3
500 MHz

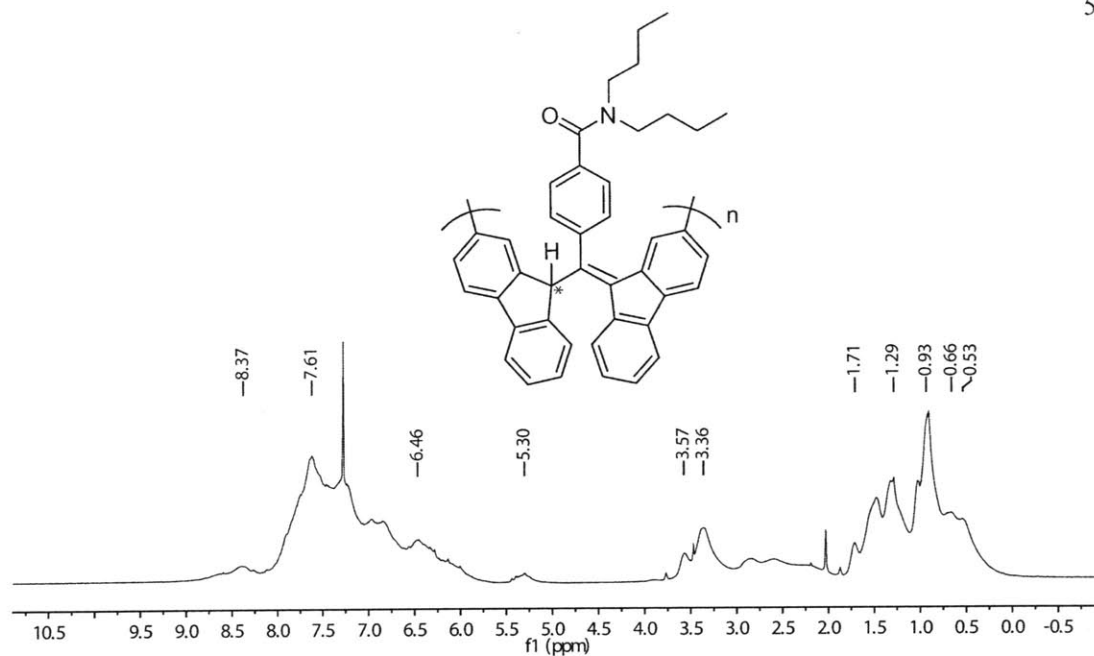


P1a NMR Spectra

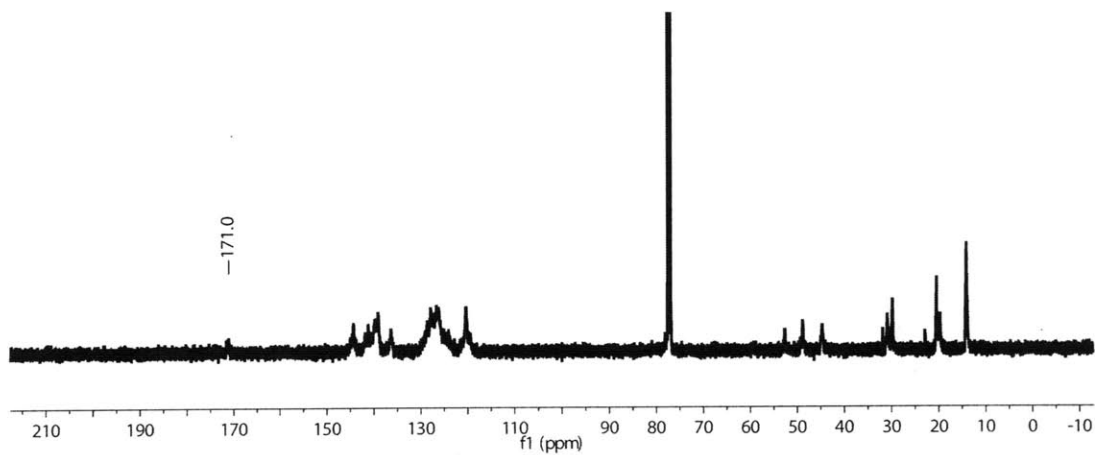
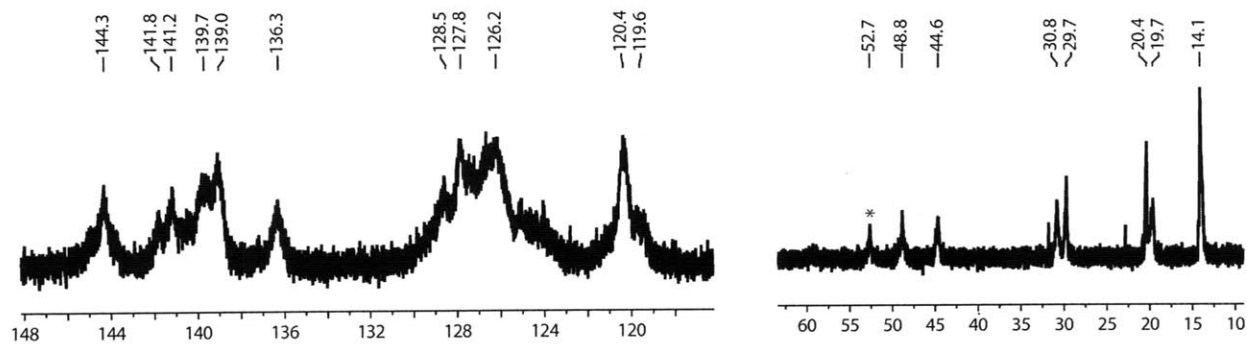


P1b NMR Spectrum

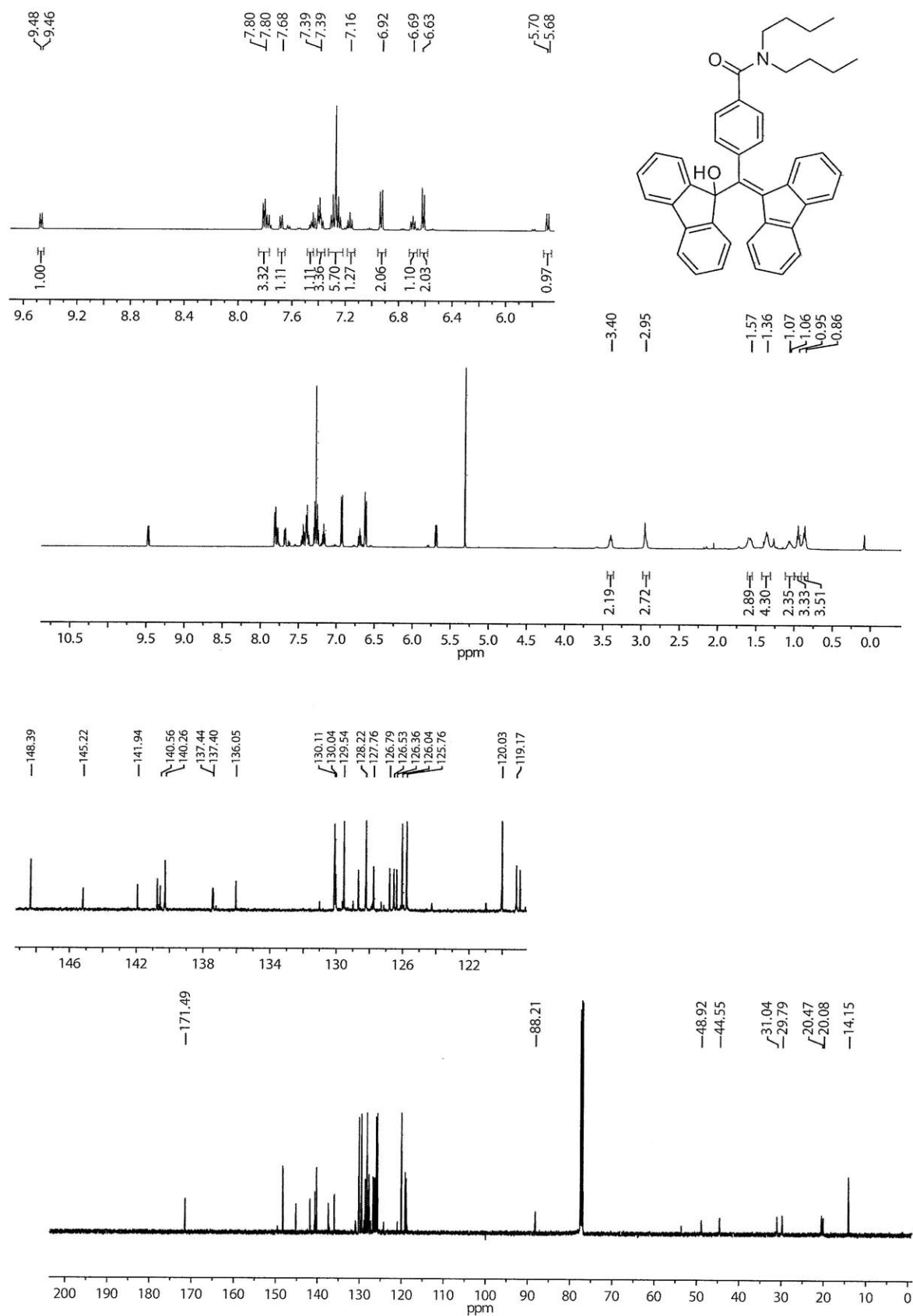
¹H-NMR, CDCl₃
500 MHz



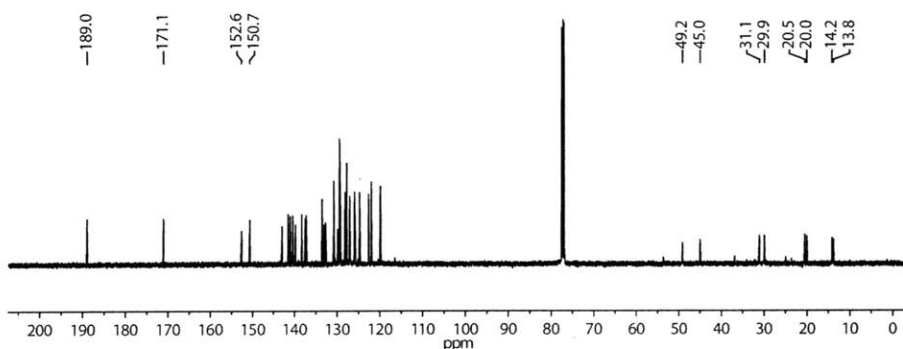
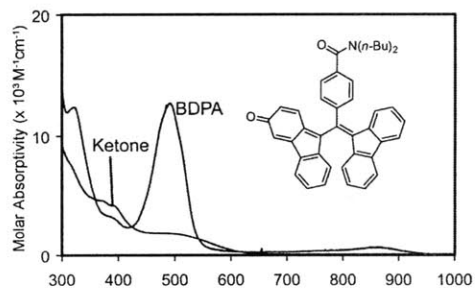
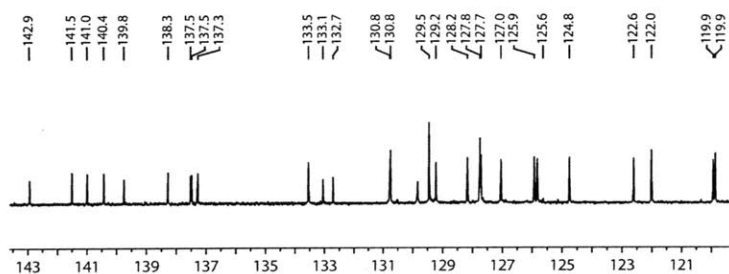
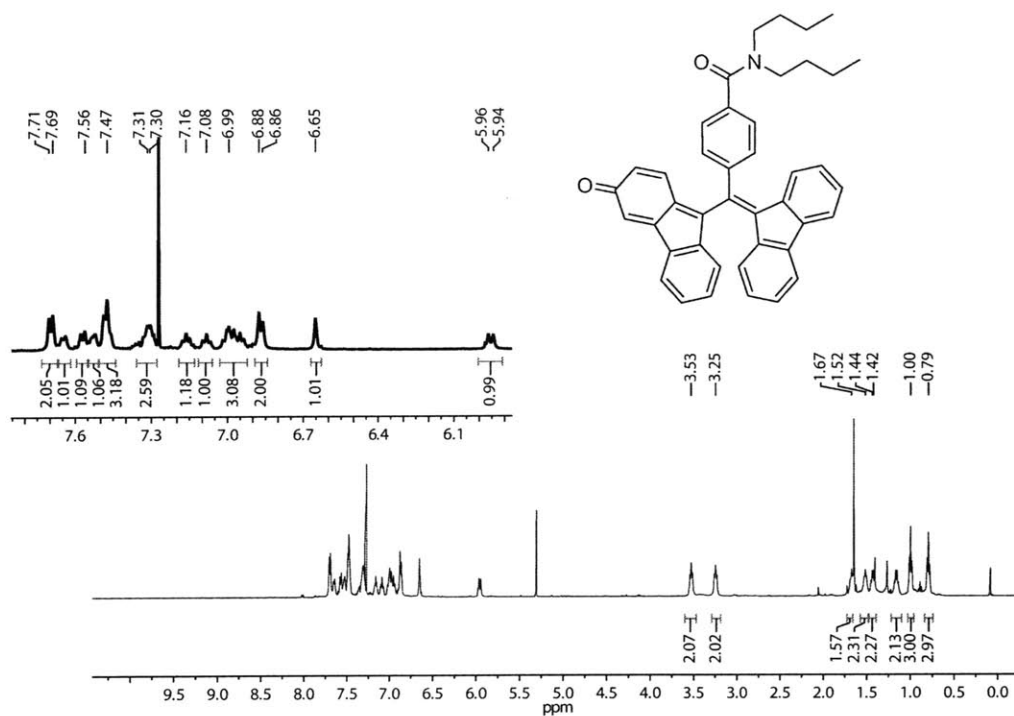
¹³C-NMR, CDCl₃
126 MHz



2c Alcohol Decomposition Product (isolated by chromatography)



2c Ketone Decomposition Product (isolated by chromatography)



Eric L. Dane

Organic Materials Chemist

30 Chester St. #14
Somerville, MA 02144

Office: 617-258-6537
Mobile: 617-755-7755
Email: edane@mit.edu

EDUCATION AND RESEARCH EXPERIENCE

- Graduate Student (Ph.D.)** Massachusetts Institute of Technology (MIT), Dept. of Chemistry
2005-present GPA: (4.9/5) Expected graduation date: September 2010
Thesis Advisor: Timothy M. Swager (tswager@mit.edu)
- Undergraduate Student** Michigan State University, Chemistry BA with High Honors East Lansing, MI
1998-2001 Advisor: James E. Jackson (jackso65@msu.edu)
Overall GPA 3.94; GPA in Major 4.00

PUBLICATIONS/PATENTS

- Dane, E. L.; Maly, T.; Debelouchina, G. T.; Griffin, R. G.; Swager, T. M. "Synthesis of a BDPA-TEMPO Biradical" *Org. Lett.* **2009**, *11* (9), 1871–1874.
- Dane, E. L.; King, S. B.; Swager, T. M. "Conjugated Polymers that Respond to Oxidation with Increased Emission" *J. Am. Chem. Soc.* **2010**, *132*, 7758.
- Dane, E. L.; Swager, T. M. "Synthesis of a Water-Soluble BDPA Radical" *J. Org. Chem.* **2010**, *75*, 3533.
- Griffin, R. G.; Hu, K.-N.; Swager, T. M.; Song, C.; Dane, E. L. "Biradical Polarizing Agents for Dynamic Nuclear Polarization" *US Patent Application* 60/747,102 (12/05/2006).

Assistant Editor Synfacts – Synthesis of Materials and Unnatural Products Section.
2006-2008

As an assistant editor, I selected from the literature articles that described important advances in the field of synthetic organic materials chemistry, and then summarized and discussed the importance of the work in a "Synfact".

TEACHING EXPERIENCE

- Teaching Assistant** General Chemistry and Organic Chemistry Laboratory Cambridge, MA
2005-2006 MIT
- Secondary Teacher** 10th-grade Chemistry, 9th-grade Biology, Anatomy and Physiology Port Huron, MI
2002-2005 Port Huron Northern High School
- Teaching Intern** 11th-grade Chemistry, 10th-grade Biology Fowlerville, MI
2001-2002 Fowlerville High School

CONFERENCES/WORKSHOPS

- MIT-Europe Workshop at BASF: "Sustainable Chemistry - A Challenge for the Future" October 4 - 7, 2006 BASF Ludwigshafen, Germany.
- American Chemical Society National Meeting, Boston, MA, August 2007, oral presentation.
- MIT Materials Day, October 2009, poster presentation.
- MIT Graduate Organic Chemistry Research Symposium, February 2009, oral presentation.

ACKNOWLEDGEMENTS

I would like to thank Tim Swager for providing interesting scientific problems, experimental advice, and a research environment that is supportive of personal creativity and initiative. I thank Rick Danheiser for acting as my thesis committee chair and Bob Griffin for being a member of my thesis committee and supporting the collaboration that is described in Chapters 1-4.

I thank all members of the Swager Group, both past and present, for their help. In particular, I would like to acknowledge the help provided by: Sarah B. King in synthesizing and characterizing the thioether-containing polymers described in Chapter 5, David Chenoweth for helpful conversations, Trisha Andrew for helpful conversations and advice on fluorescence spectroscopy, William Collins for help proofing Chapters 1 and 2, Birgit Esser for help with DFT calculations, Shuang Liu for help proofing Chapter 5, and Olesya Haze for help proofing Chapter 3. I also worked with several members of the Griffin Group and would like to thank Thorsten Maly and Galia Debelouchina for helpful discussions and their work related to high field EPR and DNP.

Finally, I would like to thank my friends and family for their support during my time in graduate school.